School of Chemical and Petroleum Engineering

Department of Chemical Engineering

Combined Adsorption and Oxidation Technique for Waste Water Treatment:

Potential Application in Permeable Reactive Barrier

Pradeep Shukla

This thesis is presented for the degree of

Doctor of Philosophy

of

Curtin University of Technology

March 2010

Declaration

To the best of my knowledge and belief this thesis contains no material previously published by any other person except where due acknowledgment has been made.

This thesis contains no material which has been accepted for the award of any other degree or diploma in any university.

Signature:……

Date:……

This thesis is dedicated in the loving memory to my grandparents

Acknowledgement

First of all, I wish to express my deepest gratitude to my supervisor, **Dr Shaobin Wang** for his guidance, encouragement and patience throughout the journey. His acceptance and faith in my ideas, irrespective of them being good or bad and his enormous support made my research an enjoyable experience.

I am thankful to my co-supervisor **Professor Ming Ang** for his personal and professional support. Despite his busy schedule as a Department Head, I never had to seek an appointment to meet him. His doors were always open for me. I am also grateful to him to give me the opportunity to tutor and lecture the courses ChE227, Mass and Energy Balance and tutor the course of ChE325 Chemical Reaction Engineering. I also express my sincere thanks to **Prof Moses Tade** for constant motivation and guidance.

I would like to thank Prof Ravi Naidu, Managing Director, CRC for Contaminant Assessment and Remediation of the Environment (CRC-CARE) and Chemical Engineering Department, Curtin University of Technology for providing me with scholarship to complete this research.

I express my sincere thanks to Dr. Kailash Singh for his support in Modeling and Simulation. My special heartfelt thanks to Ms. Karen Haynes for her enormous support despite her hectic schedule. I am also thankful to Ann and Zheno for their help in the lab.

I am thankful to Mr. Michael Boddy, Department of Pharmacy for not only providing me the training for using HPLC but also to allow me to use his instrument for almost 1 year.

I wish to thanks Ms. Nancy Hanna, Manager, (Particle Analysis Services CSIRO) for helping me with the characterization of several samples. I am thankful to Dr. Rob Hart and Ms Elaine Miller, Department of Imaging and Applied Physics for training me with XRD and Imaging instruments. I also wish to thank Mr. Ming Lim at Department of Imaging and Applied Physics for his kind help in analyzing the light spectra of my UV lamps. I am also thankful to Mr. Geoff Chidlow and Mr. Peter Chapman, Department of Applied Chemistry, for their help and support on GC and FT-Raman.

I am very lucky to have very close friends to take the stress out of life. I am thankful to Faye, Neha, Sameer, Divyamaan, Tahir, Chirayu, Imran, Santu, Dewi, Roy, Paresh and Rahul for all their love and support. I would like to acknowledge the support of my lab mates Shariff, Nurul, Iwan, Hussian, Rakpong, Yash, Ruh, Yanwu, Huihua, Yun and Syaifullah for creating an enjoyable environment in the lab.

I am grateful to all my graduate students Regina, Devina, Sandy, Garry, Maharindo, Zhaoying, Sheron, Luckman, Lan, Adrian and Oliver for your help in the lab. Working with you all was the best experience I had during my research.

I wish to thank my friend Jens Adria for sketching most of the graphic images found in this thesis.

I express my sincere gratitude to my father, mother, sister, brother, teachers and friends for their moral support to complete this work. Finally, my genuine thanks to all those who helped me knowingly or unknowingly for completing this project.

Pradeep Shukla

Summary

This dissertation explores a combined adsorption and advanced oxidation technology for trapping and destruction of organic pollutants in waste water. The adsorbed/ immobilized pollutant onto the surface of metal supported catalyst is oxidized via advanced oxidation technology. The advanced oxidation process is carried out using $Co^{2+}/KHSO_5$ *(Cobalt/peroxymonosulphate)* reagent to generate highly active sulphate radical (SO_4^{*}), which can readily attack and oxidize the organic pollutants in waste water. The reaction mechanism of $Co^{2+}/KHSO_5$ reagent follows similarly to the Fenton reagent (Fe^{2+}/H_2O_2) which is used to generate hydroxyl radical (OH^{*}). $Co^{2+}/KHSO_5$ reagent has been successfully utilized for bleaching applications and oxidation of organic contaminants. Compared to hydroxyl radical, the sulphate radical is highly potent to oxidize contaminants even at basic pH. However the biggest disadvantage of using $Co^{2+}/KHSO_5$ reagent is the dissolution of Co^{2+} ion into the water which poses a severe environmental hazard. In the current study, cobalt ion is incorporated into supporting media and utilized for advanced oxidation. Very few studies have so far explored the heterogeneous oxidation technology based on $Co^{2+}/KHSO_5$ for the treatment of organic contaminants in water. With this research focus, various support media have been utilized to load cobalt ions, which included Zeolite A, Zeolite X, ZSM-5, SBA-15, Silica and Activated Carbon. Cobalt metal was incorporated into commercial Zeolites by ion exchange technique whereas in-situ cobalt loading was carried out during the synthesis of SBA-15. Cobalt loading was done into Silica and Activated Carbon by conventional impregnation technique. The choice of cobalt loading technique inherently determines the oxidation state of cobalt species loaded into the sample which in turn determines the oxidation efficiency. Furthermore, the choice of cobalt precursor significantly affects the metal-support bonding which has been investigated by loading on silica support with different types of cobalt precursor such as cobalt chloride, cobalt acetate and cobalt nitrate. Many of these supports such as Zeolite ZSM-5 and Activated Carbon have never been tested before for cobalt loading and oxidation via sulphate based oxidant and demonstrate efficient oxidation of phenolic pollutants.

The investigation of organic oxidation using sulphate based oxidants was further extended into photocatalytic reactions. Photo degradation was carried out using artificial solar light and germicidal UV radiation in the presence of ZnO and oxidants such as peroxymonosulphate, peroxidisulphate and hydrogen peroxide. The

comparison of photochemical and photocatalytic oxidation was carried out and their synergy of combination was explored.

The thesis provides a thorough exploration of heterogeneous oxidation via sulphate based oxidant for the treatment of organic pollutants. The supported catalysts investigated here can be further improved and utilized as a PRB media for groundwater remediation. A final chapter discusses about the mathematical modeling of a column test to mimic a lab scale PRB in order to investigate the process parameters affecting the PRB design. The column modeling also directs towards a development of a novel “Reactive Adsorber” for the treatment of industrial waste by combined adsorption and oxidation.

Publications by the author

Referred Journals:

Pradeep Shukla, Shaobin Wang, H. M. Ang, M.O. Tadé, *Synthesis, Characterisation, and Adsorption Evaluation of Carbon-Natural-Zeolite Composites*, Advanced Powder Technology, 2009, 20, 245-250.

Pradeep Shukla, Shaobin Wang, H. M. Ang, M.O. Tade, *Heterogeneous photocatalytic oxidation of phenol using zinc oxide and sulphate radicals under artificial solar light*, Separation and Purification Technology, 2010, 30, 338-344

Pradeep Shukla, Is Fatimah, Shaobin Wang, Ming Ang, Moses Tade *Photocatalytic generation of sulphate radical using zinc oxide to oxidize phenolic contaminants in Waste water: Effect of Different Oxidants.* Catalysis Today, *In press, doi:10.1016/j.cattod.2010.04.015*

Pradeep Shukla, Shaobin Wang, Kailash Singh, H. M. Ang, M.O. Tade, *Investigation of stable cobalt-exchanged zeolite for wet oxidation of phenolic contaminants in the presence of peroxymonosulphate,* Applied Catalysis B: Environmental, In press, doi:10.1016/j.apcatb.2010.06.013

Pradeep Shukla, Rakpong Peampermpool, Shaobin Wang, H. M. Ang, M.O. Tade, *Excellent Performance of Co/AC in Heterogeneous Generation of Sulphate Radicals for Phenol Degradation*, Submitted to Applied catalysis B

Pradeep Shukla, Shaobin Wang, H. M. Ang, M.O. Tade, *Cobalt impregnated silica catalyst for oxidation of phenolic contaminants, Submitted to Catalysis Today*

I.Fatimah, P.R.Shukla, F.Kooli, *Combined Photo-catalytic and Fenton oxidation of Methyl Orange Dye using Iron Exchanged Titanium Pillared Montmorillonite,* Journal of Applied Science Vol 9, (20), 3715-3722, 2009.

Referred conference presentations:

Pradeep Shukla, Shaobin Wang, H. M. Ang, M.O. Tadé, *Synthesis of carbon-natural zeolite composites with controlled amount of carbon and evaluation of their adsorption properties*, Proceedings of CHEMECA-08, Newcastle-Aus. 2008

Pradeep Shukla, Kailash Singh, Shaobin Wang, H. M. Ang and M. O. Tadé, *Mmodeling and simulation of reactive adsorber for environmental remediation*, CHEMCON, Chandigarh-India, 2008

Pradeep Shukla, Shaobin Wang, H. M. Ang, M.O. Tadé, *Synthesis and characterization of silica and SBA-15 supported cobalt catalysts for oxidation of phenolic contaminants*, proceedings of World Congress of Chemical Engineering, Montreal-Canada, 2009

Pradeep Shukla, Is Fatimah, Shaobin Wang, H. M. Ang, M.O. Tadé, *Photo catalytic activation of sulphate based oxidants using zinc-oxide to oxidize phenolic contaminants in waste water***,** proceedings of World Congress on Oxidation Catalysis, Lille-France, 2009

Pradeep Shukla, Shaobin Wang, H. M. Ang, M.O. Tadé, *Oxidation of organic contaminants by combined adsorption and oxidation on cobalt impregnated Activated carbon,* proceedings of CHEMECA 2009, Perth, Australia

Pradeep Shukla, Hongqi Sun, Shaobin Wang, H.M. Ang, M.O.Tade, *Heterogeneous Activation of Sulphate based oxidant by Cobalt and Silver Exchanged ZSM-5 for Phenol Degradation in Aqueous Solution*, Submitted to 16th International Zeolite conference, Sorrento, Italy 2010.

Contents

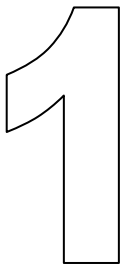

1 -Introduction

1.1 Motivation

Providing fresh water for drinking and sanitation for every individual has been a key challenge for the modern community, demanding persistent efforts by the government and industrialists to conserve this vital resource before it is too late. Despite enormous efforts by the World Health Organization (WHO) in the last few decades to supply potable water to every person, around 13% of world population still consumes water from unprotected sources which could contain harmful, toxic organic and/or chemical matters. Around 2.5 billion people in the world lack proper sanitation facilities and out of those almost 1.2 billion have no sanitation facility at all [1]. Even in large developing countries like India and China around 10-15% of the region faces severe water shortages. On the other hand enormous utilization of water for industrial application has added excessive pressure on the water supply bodies for supplying a sustainable amount of water to every person. With the increasing demand for clean and potable water for the domestic use, various countries have implemented regulations to cap the water utilization by the industries. This makes it more imperative to develop technologies for treatment and reutilization of the waste water.

In order to understand the issues concerning clean water and waste water around the world we would divide them into three categories based on the economic capacity and living conditions, the issues of clean water and waste water in the under-developed nations, in the developing nations and finally in the developed nations. This classification is not only an indication of individual nation's economical capacity, but interestingly also shows a trend which gives an insight about its water and environmental scenario.

1.1.1 The water and waste water scenario in underdeveloped nations

The major issue related to water in underdeveloped countries is the availability of fresh water for drinking and house-hold purpose. Water shortages or consumption of impure water in underdeveloped countries is mainly an issue of non uniform water distribution in the community, poverty and an uneducated population. The regions are generally not industrialized thereby protecting them from pollution due to anthropogenic activity. Nevertheless, the consumption of unprotected water and poor sanitation due to non availability of sufficient water results in the spread of several diseases such as diarrhoea, malaria, schistosomiasis, filariasis and Japanese

encephalitis. As per the estimate of UNICEF, Sub-Sahara African and South Asian countries share the largest burden of water borne diseases [1]. In 2002, almost 1.8 and 1.3 million deaths were due to diarrhoea and malaria respectively and sadly were almost entirely children under the age of 5. Most of the water borne diseases can be prevented by providing access to safe drinking water, proper sanitation and adequate water management system. There is an urgent requirement of primary water treatment system such as simple household cloth filtration, chlorination, boiling etc.

1.1.2 The water and waste water scenario in developing nations

In developing countries, the rapid development and industrialization results in the consumption of huge quantity of freshwater thus adding excessive pressure on the surface and ground water. Apart from consuming vast quantities of pure water for the processing of products, the industrial units are also responsible for polluting the surface water resulted from its toxic discharge. Despite the issues the desire of rapid economical growth results in overlooking of the damaging natural resource by most of the governments. The lack of availability of pure water from the surface has resulted in higher dependence on groundwater. In most of the developed and developing nations the abstraction of groundwater is as high as 50% of its annual recharge raising alarms over the sustainability of the underground resource [2, 3]. As per a prediction of WHO there will be almost 50% increase in water withdrawal by the developing nations as compared to 18% by the developed nations [3]. Additionally, the decreasing water table results in lower productivity of farms leading to food shortages, increased salinity of soils etc.

1.1.3 The water and waste water scenario in developed nations

The issue associated with water resource is entirely different in developed nations, mostly arising from the industrial action done in the past. Unplanned dumping of toxic waste in landfills has over the years leached into the ground thereby polluting the aquifer. The remediation of these polluted lands and aquifer would require enormous financial and energy resource. The number of potentially contaminated sites in North America, runs into the thousands and as many as 35,000 have been reported to the Environmental Protection Agency. In Australia around 30,000 sites have been identified as potentially contaminated [4].

The issues faced by the developed nations today would be seen by the developing nations tomorrow unless appropriate steps are taken to prevent the pollution of surface and ground water by the industrial actions. Additionally, it is also essential to take actions for remediating the already polluted land and surface and groundwater bodies.

The presence of toxic materials in surface or groundwater poses a grave threat to aquatic life. Hazardous compounds such as pesticides, herbicides, chlorinated aromatics, polycyclic aromatic hydrocarbons etc cause detrimental health effects even when present in minute quantity. The majority of the pollutants are released in the waste stream of petroleum and petrochemical industries, petroleum refineries, wood processing industries, coal conversion and phenol processing industries etc are classified as severely harmful [5]. However, these pollutants under appropriate conditions can be easily oxidized to harmless end products like CO_2 and water. Various techniques like thermal destruction, wet air oxidation, catalytic oxidation (both homogeneous and heterogeneous oxidation), ozonation etc. have been researched and employed. Among all the available oxidation techniques, heterogeneous catalytic oxidation has several advantages over others in terms of energy efficiency, given the fact that it is carried out at ambient temperature and pressure [6]. Affordable catalysts which can also be regenerated can certainly over-shadow other techniques. Furthermore, given the problem of harmful intermediates, a well designed system can assure complete oxidation of the pollutants. The technique of chemical oxidation though highly popular also faces a few drawbacks in terms of non selectivity, excessive usage of chemicals, slower rate of oxidation at low concentration etc.

1.2 Aim and Scope of the Present Work

The research objective is to devise a wastewater treatment technique based on Combined Adsorption and Advanced Oxidation technology for the pollutant removal. Further, the technique can be adapted in developing a Permeable Reactive Barrier (PRB) to remediate groundwater. In this technique, the pollutants are continuously adsorbed onto the adsorbent bed which is loaded with a catalyst for simultaneous oxidation of the pollutants. The technology of the combined Adsorption and Oxidation tends to reap the advantages of Adsorption such as pollutant selectivity, minimal dependence on temperature and higher efficiency even at low pollutant

concentration. It also offers the advantage of Oxidation such as complete destruction of pollutants. Additionally; in the combined Adsorption and Oxidation technique the pollutants are continuously oxidized as it gets adsorbed in the bed thus eliminating the need of frequent regeneration of the adsorbent.

To meet this research goal the following objectives are defined

I. Investigation of adsorption capacity of popular adsorbents
II. Development of catalyst loaded adsorbents for combined Adsorption and Oxidation
III. Carrying out the kinetic test to determine the degradation kinetics for a model pollutant using the catalyst loaded adsorbent
IV. Numerical modeling and simulation of the “Reactive Adsorber” to mimic a potential application of combined adsorption and oxidation for remediation of groundwater.
V. In addition, a chapter was also devoted to alternative technique of combined Photocatalytic and Photochemical oxidation for treatment of waste water.

1.3 Thesis organization

The thesis has been organized as a compilation of several researches carried out during the research period to achieve the above defined objectives. Every chapter provides its own objective and has a well defined Abstract and Conclusion. This format of the thesis makes it easier to read any chapter in between the thesis with minimal referral from the previous chapters. The following chapters are organized in the order of the objectives been defined above.

Chapter 2: The chapter briefly presents the overview of the various oxidation techniques for the treatment of waste water. The chapter also briefly describes the application of combined Adsorption and Oxidation technique in Permeable Reactive Barrier for Groundwater Treatment.

Chapter 3: This chapter reports the adsorption of phenolic contaminants in Activated Carbon. The major focus is on understanding the adsorption of contaminants in multicomponent system and investigates various competitive adsorption models.

Chapter 4: This chapter reports the investigation on the capacity of cobalt exchanged zeolites (Zeolite A, Zeolite X, ZSM-5) for catalytic oxidation of phenolic compounds. The study describes the stability of different zeolites for catalytic reaction. It also presents the kinetics of phenol oxidation on the surface of the catalyst via desorption controlled mechanism.

Chapter 5: This chapter is divided into 2 different parts. The first part of the chapter describes the synthesis of mesoporous SBA-15 and silica supported cobalt catalysts. The detailed kinetic tests were carried out for each of the developed material using phenol as a model pollutant.

The second part of the chapter is focused on the synthesis of cobalt impregnated activated carbon and its application for phenol degradation.

Chapter 6: This chapter is divided into two parts. The first part investigates photocatalytic degradation of phenol in the presence of zinc oxide and peroxidisulphate oxidant. The second part of the chapter is focused on understanding the combined photocatalytic and photochemical reaction in the presence of zinc oxide in different oxidants (Peroxydisulphate, Peroxymonosulphate and Hydrogen Peroxide). The synergetic effect of coupling photochemical and photocatalytic oxidation was investigated at low power UV radiation.

Chapter 7: This chapter discusses the application of combined adsorption and oxidation technique in Permeable Reactive Barrier (PRB) for groundwater remediation. A simple “Reactive Adsorber” system to mimic PRB is proposed. Further a mathematical model was developed to predict the efficiency of the system.

Chapter 8: This chapter provides the summary and future opportunities in this research area.

1.4 References

1. Unicef, *Progress on Drinking water and Sanitation*, A.V.M. Chan, Editor. 2008. p. 58.

2. Seckler, D., R. Barker, and U. Amarasinghe, *Water scarcity in the twenty-first century.* International Journal of Water Resources Development, 1999. **15**(1): p. 29-42.

3. Report, U., Water a shared responsibility: The United Nations World water Development Report 2. 2006. p. 52.

4. Burns R.Gm Rogers S, M., Remediation of inorganic and organics in industrial and urban contaminated soils, in Contaminants and the soil Environment in the Australia Pacific Region. 1996, Kulwer Academic Publisher: Netherlands. p. 361-410.

5. ATSDR, Toxicological Profile for Polycyclic Aromatic Hydrocarbons (PAHs). A.f.T.S.a.D. Registry, Editor. 2004.

6. Matatov-Meytal, Y.I. and M. Sheintuch, *Catalytic abatement of water pollutants.* Ind. Eng. Chem. Res, 1998. **37**(2): p. 309-326.

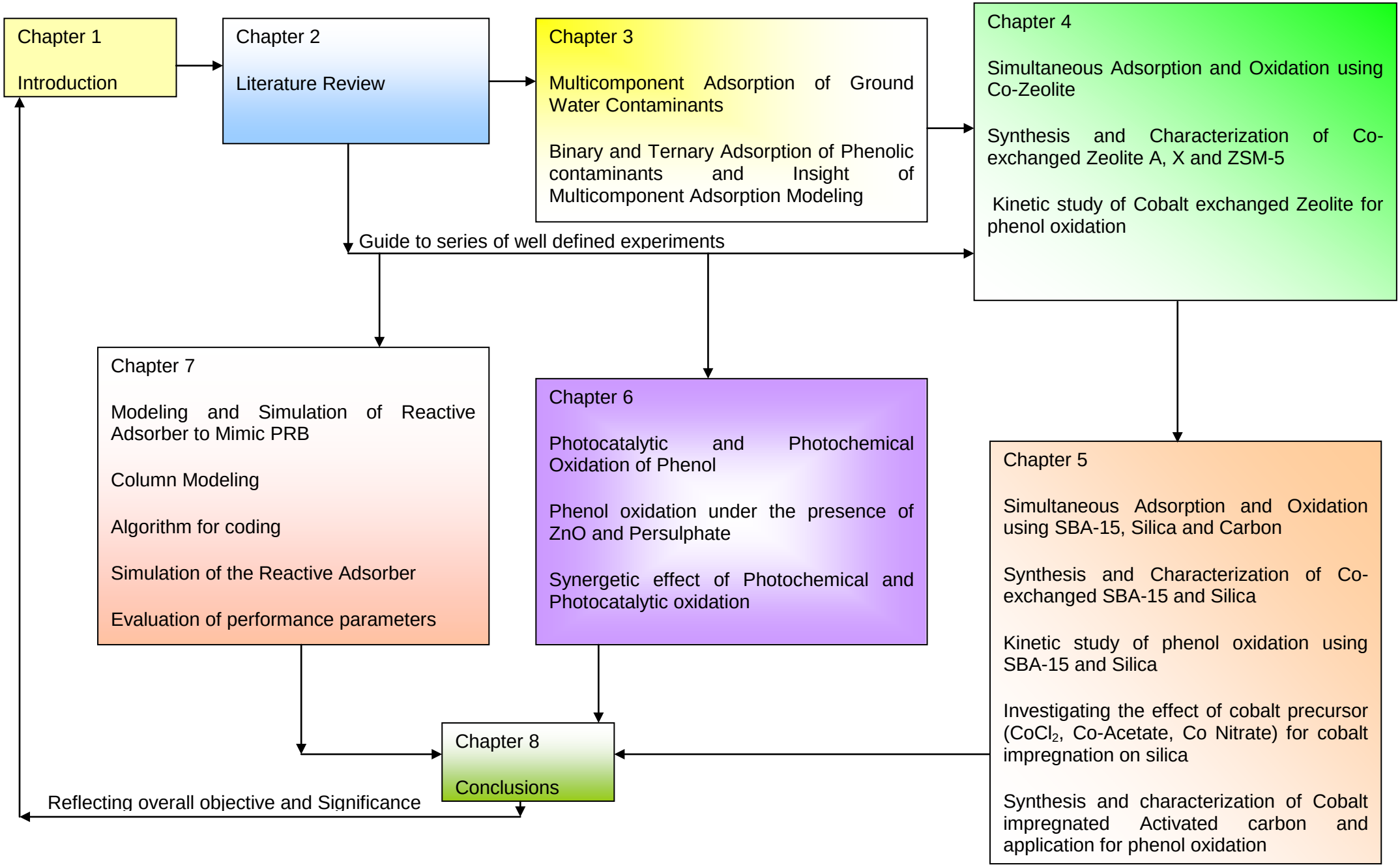
Chapter 1
Introduction
Chapter 2
Literature Review
Chapter 3
Multicomponent Adsorption of Ground Water Contaminants
Binary and Ternary Adsorption of Phenolic contaminants and Insight of Multicomponent Adsorption Modeling
Chapter 4
Simultaneous Adsorption and Oxidation using Co-Zeolite
Synthesis and Characterization of Co-exchanged Zeolite A, X and ZSM-5
Kinetic study of Cobalt exchanged Zeolite for phenol oxidation
Guide to series of well defined experiments
Chapter 7
Modeling and Simulation of Reactive Adsorber to Mimic PRB
Column Modeling
Algorithm for coding
Simulation of the Reactive Adsorber
Evaluation of performance parameters
Chapter 6
Photocatalytic and Photochemical Oxidation of Phenol
Phenol oxidation under the presence of ZnO and Persulphate
Synergetic effect of Photochemical and Photocatalytic oxidation
Chapter 5
Simultaneous Adsorption and Oxidation using SBA-15, Silica and Carbon
Synthesis and Characterization of Co-exchanged SBA-15 and Silica
Kinetic study of phenol oxidation using SBA-15 and Silica
Investigating the effect of cobalt precursor ($CoCl_2$, Co-Acetate, Co Nitrate) for cobalt impregnation on silica
Synthesis and characterization of Cobalt impregnated Activated carbon and application for phenol oxidation
Chapter 8
Conclusions
Reflecting overall objective and Significance

2 -Literature Review

Abstract

In-order to counter the rising issue of water pollution, several treatment techniques have been developed over the period. The treatment technique varies depending on the final objective such as trapping and removing the pollutants, transfer of the pollutants from one phase to other or complete destruction of the pollutant by oxidation. The current chapter focuses on the techniques for completely destroying the pollutants by oxidation. Several different techniques of pollutant oxidation have been outlined with their respective benefits and shortcomings. Finally the technique of combined adsorption and oxidation has been discussed for highly efficient pollutant removal.

2.1 Introduction

Wastewater treatment has become a critical factor partially governing the economical performance of the manufacturing unit since the beginning of 20th century. Despite significant developments in the processing facilities to reduce the waste and/or by-product, the concern of discharge stream treatment has always been on the rise. With the advancement of analytical technique making it possible to detect any organic or inorganic compounds at ppb level, there has been increasing demand by the regulatory bodies to reduce the pollutants to much lesser quantity. Stringent government regulations, awareness in the people (including the industrial management) for the environment protection have added excess responsibility on the manufacturing units to reduce the pollutant discharge below ppb level. Recent development in the concept of "**Zero Discharge**" has attracted great attention both in research and industry. In-order to achieve this target various strategies have been proposed by environmental managers worldwide, such as developing new technologies for minimal waste generation, water networking to use and reuse the water within the same industry or in the collective industrial estate to minimize the discharge of wastewater, improving the performance of the existing technology for environmental protection and finally adapting highly efficient wastewater treatment techniques to convert the wastewater into a usable resource.

2.1.1 Wastewater: A resource for reuse

Wastewater has become a valuable resource rather than a liability for most industries in the given context of water scarcity in various parts of the world. An efficient treatment system can convert the wastewater discharge stream leaving the plant into an added source of water which could be used for several purposes such as toilet and urinal flushing; agricultural irrigation; landscape irrigation; ornamental wastewater reuse that can be aesthetic such as decorative pools, decorative fountains, ponds, and lagoons etc.

The treatment of industrial waste is more component specific in contrast to the municipal waste, wherein the type and concentration of the pollutant determines the treatment technique. The treatment technique also depends on the application for which the water is proposed to be reused. In certain cases, the wastewater stream with low concentration of salts and organics which needs to be reused for toilet flushing or floor washing would require a simple primary or secondary treatment.

Treatment such as adsorption on carbon or clay, coagulation, air stripping would be feasible for transferring the pollutants from aqueous phase to solid or gaseous phase thereby reclaiming both water and the organic compounds. Transferring the aqueous pollutant to the gaseous phase by air stripping has also been a favorable technique for removal of volatile compounds from the contaminated water. However, the technique of pollutant transfer from water to solid or gas is environmentally and economically feasible only if the pollutants are further recovered and reused. If not, then the solid material ends up in the landfill site causing further harm to the land and underground water system. The biological treatment systems in the form of activated sludge systems, aerated lagoons, trickling bed filters and others have the potential to completely destroy the pollutants; however these processes are inherently slow and are unsuitable for the degradation of certain pollutants which are toxic to the micro-organism. For example, aromatic compounds like phenol are known to be toxic to the micro organism at concentration above 70 ppm [1]. Ammonia concentration above 300 ppm could make the biodegradation extremely slow [2], the presence of cyanides or cyanides producing substance even in a trace quantity can cause significant harmful effects to the biological treatment systems [2]. Additionally the biological treatment system results in generation of large quantity of sludge requiring disposal in landfill sites. The techniques such as membrane filtration and reverse osmosis are feasible only for treatment of pollutants if they are above a threshold concentration and purity so that the pollutant can be recovered and reused. The technique of "**Complete Destruction**" of the pollutants by oxidation has been highly favored over other techniques owing to its universal application for a wide range of pollutants. The choice of the oxidation technique generally depends on the concentration and characteristics of the pollutants. Techniques such as Wet Air Oxidation (WAO) (catalytic and non catalytic), Chemical Oxidation, Incineration and Advanced Oxidation Techniques (AOT) have been successful in complete removal of the pollutants resulting in minimal end products (sometime no end product). Figure 2.1-1 shows the suitability of different schemes of oxidation techniques depending on the extent of COD present in the wastewater. For the treatment of high waste with extremely high concentration of Total Organic Compounds (TOC), generally incineration is recommended followed by Wet Air Oxidation and AOT in the descending order. Techniques such as Incineration and Wet Air Oxidation, although have been reported to be tested for a wide range of pollutant concentrations, becomes economically feasible only above the certain threshold of COD. During the treatment of waste in the feasible range the exothermic energy released during the

combustion/oxidation makes the process self sustainable in terms of energy requirement. In fact, if the wastewater has a very high level of COD, the WAO process can even be an energy producing sector, by generating a net positive energy from the exothermic energy released from the reaction [3]. For wastewater stream having very small quantity of pollutants, the application of Incineration or WAO becomes highly uneconomical and the focus is shifted to alternative techniques such as AOT. In AOPT there are several techniques such as Fenton Oxidation, UV based technique and ozonation whose applicability is also determined by the pollutant concentration. At extremely low concentration of the pollutants, the application of popular Fenton oxidation is limited due to slow rate of reaction and uneconomical utilization of the oxidants due to self quenching. In order to oxidize the pollutants of extremely low concentration, there is a need of additional energy input in the form of UV or ozonation to achieve complete oxidation.

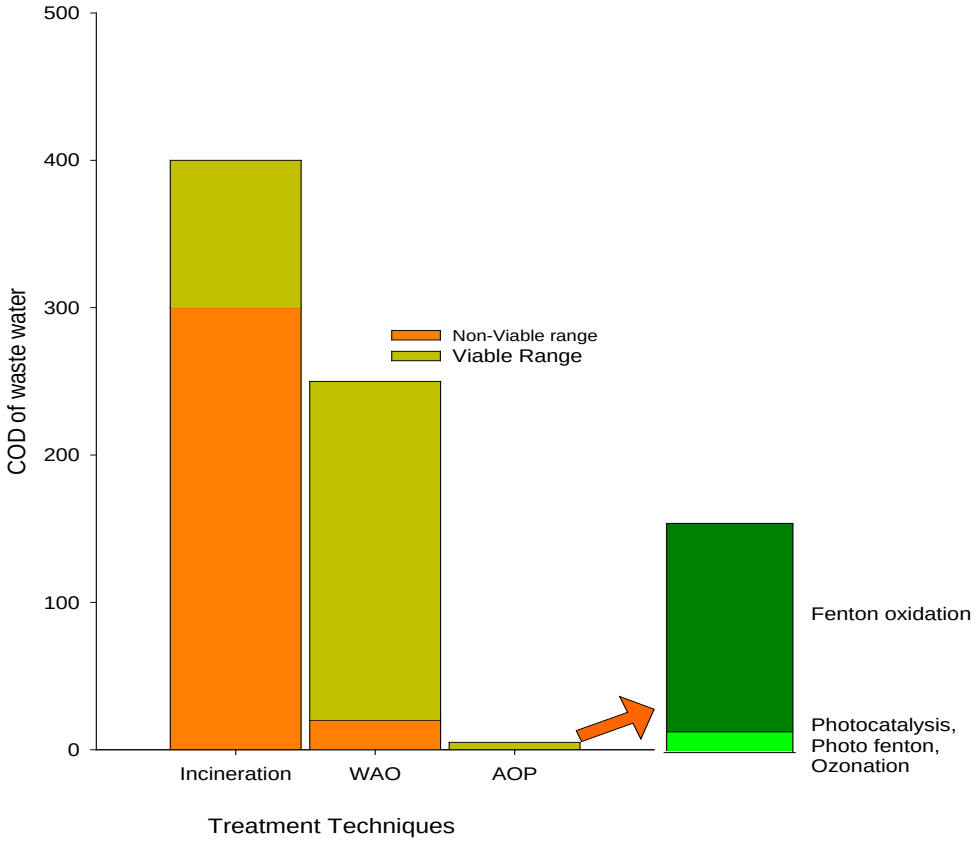

Figure 2.1-1 Application range of different waste oxidation technique for economical performance

2.2 Incineration

Incineration is a thermal degradation of organic compounds carried out by raising the temperature of waste stream to about 800 ^{0}C, ideally forming CO_2 and H_2O. The basic reactions involved in the process are given as follows [4]

$$R - H + O_2 \xrightarrow{\Delta} xCO_2 + yH_2O$$ Equation 2.2-1

$$R - Cl + O_2 \xrightarrow{\Delta} xCO_2 + yH_2O + HCl$$ Equation 2.2-2

$$R - N + O_2 \xrightarrow{\Delta} xCO_2 + yH_2O + NO_2$$ Equation 2.2-3

Various systems have been developed for carrying out waste incineration such as rotary kiln incineration (for solid waste), liquid injection incineration, fluidized bed incineration, high temperature fluid wall destruction-advanced electric reactor, infrared incineration, plasma arc pyrolysis, etc [4]. The incineration of toxic waste may result in the formation of undesired gaseous end products such as HCl, SO_x, NO_x and chlorine which need to be removed from the exit gas. Thus a well designed incinerator needs to incorporate air treatment systems such as wet or dry scrubbing. Although this technique has been one of the popular waste destruction techniques in the past, it has come under regulatory and economical pressure in recent years. The effect of incineration has posed several health problems to the people in the vicinity. The major pollutants released in and around the incineration units are fine particles, acidic gases and aerosols, metals and organic compounds. Studies suggest the release of small particles and metals such as lead, cadmium, mercury, chromium and arsenic are responsible for carcinogenic and non-carcinogenic health effects among the workers and the people in the neighborhood [5]. In the process of thermal incineration of tri-, tetra- and penta chlorophenol at around 500-600 ^{0}C significant amount of polychlorinated dibenzo-p-dioxins (PCDD) was observed in the gaseous outlet. The concentration of PCDD was found to reduce on increasing the temperature (800-900 ^{0}C) thus demanding a high energy input for complete destruction of pollutant [6]. Increased concentration of polychlorinated dibenzo-p-dioxins (PCDDs) and polychlorinated dibenzo-furans (PCDFs) have been reported among the workers working in municipal waste incinerators in South Korea [7]. Other organics found in the combustion product of municipal waste as reported by Ahling et al [6] are given in Table 2.2-1below

Table 2.2-1 Organic compound released from the Municipal Waste Incineration

Organic Products released during incineration at 680-1040 ^{o}C	Concentration µg/m^3
Formic Acids	500
Acetic Acid	2.5
Chlorophenols	48
Formaldehyde	500
Acetaldehyde	500
PAH (Poly-aromatic Hydrocarbons)	5
Chlorinated Benzenes	20
Dioxins	0.038

It could be clearly noticed from Table 2.2-1 that the concentration of the low molecular compounds such as formic acid and aldehydes, resulted from the breakdown of the large molecular weight compounds are in much higher concentration. Black liquor released from paper and pulp industry containing chlorinated compounds when treated by incineration was reported to generate chlorinated benzene as an end product [6]. Due to the significant financial implications arising from the toxic gas releases several incinerators in US have been forced to shut down in the past few years [4].

2.3 Reduction Technique: Zero Valent Iron Reduction

A reduction technique by its own does not achieve the target of complete destruction of organic compounds. Nevertheless it is a highly useful technique to reduce the toxicity of the target pollutants, thereby making the pollutants venerable for biological destruction. The most common pollutants treated by this technique are halogenated compounds. The reduction step of reductive dehalogenation is given as follows [4, 8-10]

$$R-X+H^{+}+e^{-}\rightarrow R-H+X^{-}$$ Equation 2.3-1

In recent years, there has been an increasing interest in the application of zero valent iron as a reducing agent for ground water detoxification. The major advantage of using iron is due to the abundance in the availability of Fe^0 in the form of scrap iron. Furthermore the spent by-product obtained from the reduction reaction (Fe^{2+}) is environmentally harmless. The chemical reaction of reductive dehalogenation using zero valent iron can be given as follows [4, 9]

$$Fe^o + R - X + H^+ \rightarrow Fe^{2+} + R - H + X^- \qquad \text{Equation 2.3-2}$$

Zero valent iron has been used in Permeable Reactive Barriers (PRB) for the treatment of chlorinated ethene, ethanes, methanes and propanes, chlorinated pesticides, ferons and nitrobenzenes. Currently there are 83 full scale and 37 pilot scale PRB installed worldwide employing zero valent Iron (ZVI) for the treatment of chlorinated compounds [8, 11].

Despite the spontaneous reactivity of halogenated compounds with Fe^0, several interferences within the reaction can hinder the economical feasibility of Permeable Reactive Barrier. The presence of nitrates tends to negatively impact the reaction rate by passivating the iron surface. Similarly, the presence of oxygen or other oxidizing agents results in the formation of oxyhydroxide [FeO(OH) or $Fe(OH)_3$] solid on the surface thereby clogging the reactive media [12, 13]. The formation of iron oxyhydroxide and carbonate precipitates also occurs in the presence of elevated HCO_3^- ions in SO_4^{2-}-containing water [14]. The presence of metals such as chromium, arsenic, uranium, lead and cadmium tends to compete with the organics for the active sites on the iron surface. The interaction of the ZVI with the contaminant plume results in increase of pH leading to the precipitate formation. The precipitates, generally carbonates and hydroxides of Fe, Ca and Mg cause the blockage of the permeable reactive barrier thereby reducing the hydraulic conductivity of the barrier [13]. An excellent review of the issues arising with the long term performance of ZVI based PRB recently analyzed by Henderson et al [12] adds more light on the matter.

2.4 Wet Air Oxidation

One of the most successful and highly investigated techniques for wastewater oxidation, Wet Air Oxidation (WAO) has drawn attention of thousands of scientists

and researchers. More than 60 review articles and number of research articles running in thousands have been published on this technique within the period of just 30 years [3, 15]. The first patent based on this technology was granted almost a century ago, in the year 1911 however the first commercial installation was done almost half a century later in 1958 by Borregaard in Norway for the treatment of sulphate liquor [3]. Wet Air Oxidation involves treatment of wastewater under high temperature and pressure which results in the oxidation of the water organic with the dissolved oxygen present in the water. During the oxidation process the high molecular compounds are generally broken down to low molecular weight compounds and further to CO_2 and H_2O. The general kinetic model for the waste oxidation proceeds by two mechanisms running in parallel as shown below [16, 17]

1) Direct oxidation to the end product

$$R - H + O_2 \xrightarrow{k_1} xCO_2 \qquad \text{Equation 2.4-1}$$

2) With the formation of intermediate product (carboxylic acid)

$$R - H + O_2 \xrightarrow{k_2} xCH_3COOH \xrightarrow{k_3} yCO_2 \qquad \text{Equation 2.4-2}$$

The net kinetic expression obtained from the above 2 steps is given as follow [17]

$$\frac{[R - H + CH_3COOH]}{[R - H + CH_3COOH]_0} = \frac{k_2}{k_1 + k_2 - k_3} e^{-k_3 t} + \frac{k_1 - k_3}{k_1 + k_2 - k_3} e^{-(k_1 + k_2)t} \qquad \text{Equation 2.4-3}$$

The reaction steps involved in the radical formation can be broken into 3 different steps involving Initiation, Propagation and Termination steps as seen from the equations below [18].

Initiation $R - H + O_2 \rightarrow R^{\bullet} + HO_2^{\bullet}$ Equation 2.4-4

Propagation $R^{\bullet} + O_2 \rightarrow RO_2^{\bullet}$ Equation 2.4-5

$R - H + RO_2^{\bullet} \rightarrow ROOH + R^{\bullet}$ Equation 2.4-6

Termination $RO_2^{\bullet} + RO_2^{\bullet} \rightarrow ROOR + O_2$ Equation 2.4-7

The oxidation of carboxylic acid is the reaction controlling step due to extremely slow rate of reaction. In WAO, the majority of the high molecular weight compounds are broken down to low molecular compounds like formic acid, acetic acid and some aldehydes. These intermediate compounds are highly resistant to oxidation and can be oxidized only at severe operating conditions

The treatment system consists of a simple feed pump, an air compressor (alternatively pure oxygen may also be used), a heat exchanger and a reactor. The brief flow diagram is shown in Figure 2.4-1. The wastewater is pumped continuously into the tank maintained at high pressure and temperature (approximately 0.5 MPa to 20 MPa and 200-300 ^{o}C). The high pressure enhances the partial pressure of oxygen which in turn enhances the solubility of the oxygen thereby increasing the rate of oxidation. The treated water coming out of the reactor can be used to preheat the incoming wastewater and/or to generate steam by passing through the heat exchanger. For the waste having COD more than 20000 ppm, the exothermic heat generated by the oxidation reaction would be enough to generate sufficient heat to produce steam for running a turbine and generating power in-order to make the process self sustainable [3, 19]. In certain cases hydrogen peroxide is added to the system in-order to generate active hydroxyl radical for quicker and efficient oxidation of the pollutants.

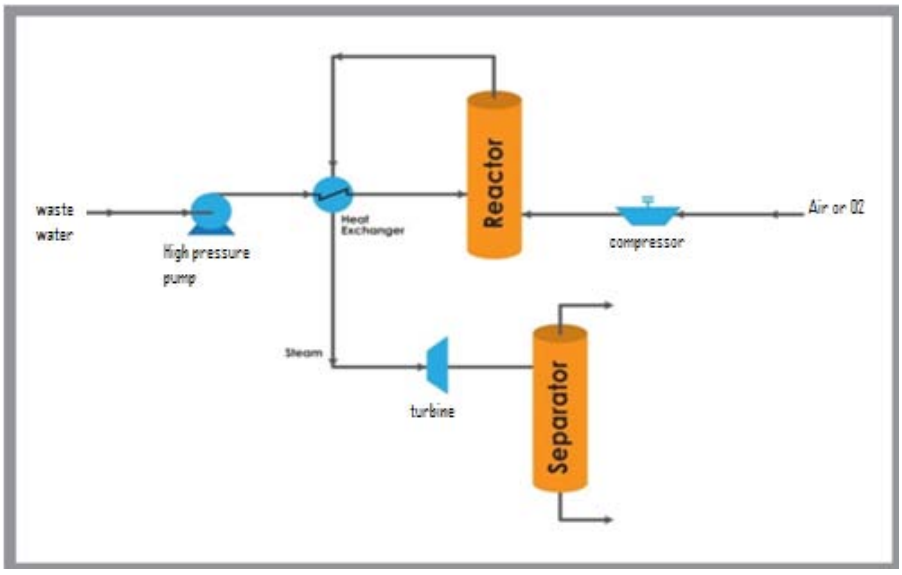

Figure 2.4-1: Wet Air Oxidation process (WAO)

The COD removal by wet air oxidation technique is limited in the range of 75 to 90% depending on the extent to which the intermediate compounds are oxidized [16]. An alternative technology but based on similar principle known as Supercritical Wet Air Oxidation (SWAO) promises a higher COD removal from the wastewater but the reaction takes place at supercritical conditions with the temperature higher than 500 ^{0}C and the pressure between 20-50 MPa [20]. The extent of oxidation in WAO rises with the increase in the reaction temperature. The pressure is accordingly adjusted with the temperature to maintain the water in liquid state. The extent of COD removal is also dependent on the type of waste. For instance in the case of oxidation of caustic scrubbing liquors almost 99.9% waste can be removed [3]. In certain cases pure oxygen can be introduced in contrast to air to enhance the degradation rate. A comparative study of air and pure oxygen based wet air oxidation reported by Prasad and Materi [21] concluded that pure oxygen based WAO shows higher efficiency and greater profitability. WAO has been successfully employed to treat a huge range of wastewater from having specific pollutant in spent pulp mill liquor to mixed pollutants arising from municipal sewage [3, 15]. The following Table 2.4-1 gives a summary of different pollutants that have been treated by WAO and their operating conditions, which has been selectively extracted from several published reviews [3, 15, 16, 22]

Table 2.4-1 Wet Air oxidation operating conditions of various pollutants

Pollutants	Operating Temp ^{0}C	Operating Pressure MPa
Phenol	180-210	5.5-15.2
Propionic Acid	232-287	1.72-5.17 (P-O_2)
Acetic Acid	270-300	2-20
Butyric Acid	237-257	6.8-13.6
Formic Acid	300	1
Oxalic Acid	227-288	2-20
2-Chlorophenol	204-260	3.9-7.1
P-Cresol	150-200	3.9-7.1

		($P\text{-}O_2$)
Acetonitrile	275-320	1
Nitrite acetic Acid	200-225	5-15.2
Glucose	177-260	10.9
n-butanol	160-200	6.8-13.6
Sec-butanol	160-200	6.8-13.6
Acetone	160-200	6.8-13.6
Tetrachloro ethylene	225	13.8
Morpholine	150-240	0.39-1.38 ($P\text{-}O_2$)
Diethanolamine	140-240	0.39-1.38 ($P\text{-}O_2$)
Real Distillery Waste	150-210	0.1-2.5 ($P\text{-}O_2$)
Black Liquor from Paper and Pulp unit	40-90	0.021 ($P\text{-}O_2$)
Sewage sludge from paper industry	250-300	13

2.5 Catalytic Wet Air Oxidation

The severe process conditions employed in homogeneous wet air oxidation demanding high energy input and incomplete or slower rate of reaction were the major driving forces to look towards catalytic oxidation technique. It allows substantial gain on process condition. Catalytic oxidation for the treatment of gaseous pollutants had established a strong hold in commercial processes in early nineteenth century. For the treatment of aqueous pollutants, the first patent on catalytic oxidation was filed by DuPont in the year 1950 [16] to claim a catalyst composition of Mn-Zr-Cr oxides to be used for catalytic WAO at the temperature of 120-200 ^{0}C. It paved the way for several investigations being carried out for oxidizing an array of pollutants by using several different catalysts. The catalysts employed for the oxidation can be classified into 3 types: metal, metal oxides and organo-metals. Homogeneous

catalytic oxidation employing metal salts are comparatively more efficient as compared to that of heterogeneous metal oxides; however such a system would require an additional separation unit in-order to remove that catalyst from the liquid. In many cases the separation of such catalyst maybe technically or economically unfeasible. Additionally, most of the dissolved metal catalysts are toxic to the environment. The heterogeneous catalytic oxidation overcomes these limitations but suffers a major drawback in terms of slow rate of reaction which is limited by mass transfer resistance, limited life expectancy and catalyst poisoning. For the heterogeneous catalytic reaction, generally 5 steps would determine the kinetic rate of degradation[23]

I. Diffusion of reactants on the surface
II. Adsorption of reactants to the surface
III. Reaction on the surface
IV. Desorption of product off the surface
V. Diffusion of products from the surface.

In the majority of catalytic reactions, the reaction kinetics is highly dependent on the molecular transport (diffusion and adsorption) rather than the reaction itself thus demanding enormous research on development and modification of catalyst. The important metal catalysts for catalytic waste oxidation, without exception, are noble metals including Ru, Pt, Rh, Ir, and Pd [23]. These noble metals are generally loaded onto other metal oxides or on an inert support which tends to enhance the reactivity and stability of the catalyst. In certain cases the metal catalysts are also supported onto the adsorbent materials such as activated carbon. The examples given in the current subsection are limited to the catalytic oxidation involving metal or metals supported onto metal oxide. The adsorbent supported metals are discussed in a later part of this chapter (section 2.8) which involves the influence of simultaneous or sequential adsorption of pollutants along with reaction.

The oxidation of the pollutants in the presence of catalyst would follow the redox mechanism as shown below [18]

$$ROOH + Me^{(n-1)+} \rightarrow RO^{\bullet} + Me^{n+} + OH^{-}$$ Equation 2.5-1

$$ROOH + Me^{n+} \rightarrow RO_2^{\bullet} + Me^{(n-1)+} + H^{+}$$ Equation 2.5-2

The efficiency of the catalyst is related to the redox potential of the $Me^{n+}/Me^{(n-1)+}$ couple [18].

The second type of WAO catalyst i.e. “Metal oxides” is characterized by high electron mobility and a positive oxidation state by the d-shell electronic configuration of the metals. The metal oxide catalysts are classified either by the stability of the oxides or their electrical conductivity. The most stable oxides in the high oxidation state are of the metals such as Ti, V, Cr, Mn, Zn and Al. Oxides with intermediate stability are those of Fe, Co, Ni and Pb and finally the least stable metal oxides are of Ru, Au and Ag [24]. In terms of electrical conductivity, they are classified as n-type metal oxides, p-type metal oxides and insulators. Among the three the p-type oxides are highly active for catalytic oxidation due to the electron deficient lattice. The n-type and insulators are mostly used as supports [2]. The noble metals are usually more active than that of metal oxide and their individual activity can be concluded from the ranking provided by Imamura et al (1988) based on the TOC conversion during the oxidation of polyethylene glycol at 200 ^{o}C [25]. The ranking was in the following order

$$Ru = Rh = Pt > Ir > Pd > MnO$$

In the case of metal oxide the ranking was provided by Kochetkova et.al 1992 [26] for the oxidation of phenol in the following order

$$CuO > CoO > Cr_2O_3 > NiO > MnO_2 > Fe_2O_3 > YO_2 > Cd_2O_3 > ZnO > TiO_2 > Bi_2O_3$$

The third type of catalyst based on organometallic complex has not been able to arouse significant interest, most probably due to the high cost of synthesis. Nevertheless, compared to other catalysts this has a specific but a significant advantage of lower toxicity if leached into the solution during oxidation. Metallophorphyrins and phthalocyanines are the two popular catalysts used in organic oxidation in aqueous solution. The immobilized organometals have been utilized in treatment of various pollutants. Amberlite-supported iron and manganese sulfonated phthalocyanines have been utilized for treatment of chlorinated phenols[27], Silica supported iron phthalocyanines was utilized for the oxidation of trichlorophenol [28], cobalt macrocycles supported on hectorite, silica and layered double hydroxides were utilized for de-chlorination of carbon tetrachloride polluted water [29], silica bonded cobalt(II) phthalocyanines was utilized for oxidation of aqueous sulphite solutions [30]. Table 2.5-1 gives a list of several different pollutants

oxidized with various catalysts which was extracted from various review articles [2, 3, 16, 23, 31].

Table 2.5-1 Catalytic Wet Air Oxidation of different pollutants

Pollutants	Operating condition	Catalyst
Phenols	200-390 ^{o}C & 10-241 atm	Ru/CeO_2; $Pt/\gamma\text{-}Al_2O_3$; Cr_2O_3;
Chlorophenols	150-190 ^{o}C using pure oxygen, 1-30 atm depending on Air or O_2	Mn, Ce, Pt, Pd, Ru, Pt-Pd, Pt-Pd-Ce supported on $\gamma\text{-}Al_2O_3$ or C; CuO-ZnO-CoO
Nitro-phenol	105-130 ^{o}C, 1.5-10 atm	$CuO\text{-}ZnO/Al_2O_3$; Mn-Ce composite oxide (temp 200-325 ^{o}C in air)
Trichlorophenol	20 ^{o}C, 1 atm in the presence of H_2O_2 or $KHSO_5$	Metallophthalocyanines
Acetonitrile	130-200 ^{o}C in O_2	$Ru\text{-}\gamma\ Al_2O_3$
Aniline, b-aniline, Ammonia	200-325 ^{o}C Air	Mn-Ce oxide composite
Succinic Acid	25^{o}C 1 atm in the presence of O_3	$Ru\text{-}CeO_2$
Dichlorobenzene	390 ^{o}C 241 atm	Cr_2O_3;$V_2O_5\text{-}Al_2O_3$
Pyridine	270 ^{o}C 10 atm	$CoO\text{-}Bi_2O_3$;$MnO_2\text{-}CeO_2$
Carboxylic Acid	1-4 atm 200^{o}C	Co_2O_3; $Ru\text{-}CeO_2$; $MnO_2\text{-}CeO_2$
Acetic Acid	200-400^{o}C depending on the catalyst	Pt; Fe_2O_3; TiO_2; $Ru\text{-}CeO_2$; Pt/Al_2O_3; $MnO_2\text{-}CeO_2$
Sulphides	30-40^{o}C	Ac fiber; Phtalocyanine; Metal Phtalocyanine; MoS_2

2.6 Chemical Oxidation Technique

Chemical oxidation is a simple technique which uses chemical oxidants to oxidize the harmful chemicals in wastewater to harmless compounds. This technique has recently become highly popular in remediation of soil and groundwater, mainly due to its ease of application and possibility of in-situ treatment. Some of the popular oxidants which have been used for chemical oxidation are shows in Table 2.6-1 along with their reduction potential [32].

Table 2.6-1 Oxidation Potential of different oxidants

Oxidants	Redox Potential E^o (eV)
Fluorine	3.03
Hydroxyl radical	2.70
Sulphate Radical	2.60
Atomic Oxygen	2.42
Ozone	2.07
Persulphate	2.01
Hydrogen Peroxide	1.78
Permanganate	1.68
Chlorine Dioxide	1.57
Hypochlorous Acid	1.49
Chlorine	1.36

Classical chemical oxidation process basically involves the addition of the above mentioned oxidizing agent into the wastewater to oxidize the contaminants. The following section briefly describes a few of the important oxidants used for wastewater oxidation.

2.6.1 Chlorination

History of the treatment of water by chemicals dates back to 1850 when chlorine was first used by John Snow [33] to disinfect the drinking water supply. Later, chlorine

found its application in treatment of sewer wastewater in-order to destroy the dangerous pathogenic organism. Chlorine is a good oxidant for the destruction of micro-organisms in water; however it's applicability for organic oxidation is generally limited by the selectivity and its requirement in a large quantity even for mild oxidation. Additionally, it renders ineffective in the oxidation of high molecular weight organic pollutants and also lead to the formation of hazardous intermediates [34].

2.6.2 Permanganate

Potassium permanganate is one of the most popular oxidant for the treatment of wastewater. It is utilized in drinking water for destroying organic compounds that causes color, taste and odor problems [35]. The dissolution of potassium permanganate in water generates more than one type of active radical which reacts with the organic converting it into harmless end products. The reactivity of permanganate is dependent on the type of the active radical being generated during the oxidation which is dictated by the reaction conditions. The solution pH is the most influential parameter during the oxidation with permanganate. Depending on the system pH, permanganate can form the following different reactive species.

$$MnO_4^- \xleftrightarrow{H^+} HMnO_4 \xleftrightarrow{H^+} H_2MnO_4^+ \xleftrightarrow{-H_2O} MnO_3^+$$

Based on the kinetic study of the oxidation of benzene and alkyl benzene with different permanganate species it has been reported that reaction with MnO_4^- dominates at pH greater than 2.5 whereas at pH less than 0.3 the reactivity of $HMnO_4$ dominates [36, 37].

The biggest disadvantage associated with this oxidant is the formation of magnesium oxide precipitate as the end product. The cost of the removal of this precipitate becomes the major controlling factor for insitu treatment systems [38].

2.6.3 Peroxide

Hydrogen peroxide has been widely known as a green oxidant due to the environmental friendly hydroxyl (OH^*) radical produced during the reaction. The oxidant has a combined capacity as a oxidizing and reducing agent. It is used as an oxidizing agent to carry out bleaching in textile industries, whereas it also has a capacity as a reducing agent by reducing permanganate to Mn^{2+}. In wastewater

treatment its oxidative capacity is harnessed to oxidize ferrous ion (Fe^{2+}) to ferric ion (Fe^{3+}) and in-turn forming active hydroxyl radical. This hydroxyl radical is a highly potent oxidant capable of oxidizing very high molecular weight and calcitrant compounds in wastewater. Such a technique of generation of hydroxyl radical is known as advanced oxidation technique which is to be discussed in detail in section 2.7.

2.6.4 Persulphate

Potassium peroxydisulphate or popularly known as persulphate is widely used in-situ in treatment of groundwater [39-41]. Similar to hydrogen peroxide, persulphate was primarily used as bleaching agent until its application was uncovered in environmental remediation. It has recently gained large popularity due to its higher oxidizing capacity than potassium permanganate and applicability in wider range of pH. At high temperature (around 40-99 ^{o}C), persulphate is known to generate highly active sulphate radical (SO_4) [42].

$$S_2O_8^- \xrightarrow{thermal} 2SO_4^{\bullet} \qquad \text{Equation 2.6-1}$$

The kinetic study of thermal activation of persulphate in aqueous medium was studied by Kolthoff and Miller (1951) [43] and Huang et al [44] who found its potential to degrade a large spectrum of organic molecules. The destruction of TCE and TCA pollutants in aqueous medium using persulphate was studied by Liang et al. [45]. Complete removal of TCE and TCA was observed at around 60 ^{o}C. The reaction was found to proceed as the first order at different temperature with the activation energy measured as 97.5 and 163.5 kJ/mol for TCE and TCA, respectively. The study was further extended for the oxidation of TCE and TCA in soil slurry. In the presence of sufficient quantity of divalent metal ions, serving as electron donor, persulphate ions can be catalytically generated at ambient temperature as per following reaction [46].

$$S_2O_8^- + Fe^{2+} \longrightarrow SO_4^{\bullet -} + Fe^{3+} + SO_4^{2-} \qquad \text{Equation 2.6-2}$$

2.6.5 Ozonation

Application of ozone for the oxidation, generally known as ozonation provides specific advantage of high reactivity as compared to other popular oxidizing agents such as H_2O_2 and persulphate and can react with several classes of compounds.

Similar to chlorine, ozone was initially utilized as a disinfectant until its capacity was harnessed for treatment of toxic and hazardous compounds. Direct ozonation is carried out by producing ozone from oxygen and bubbling it though the wastewater [47]. The solubility of ozone is 10-15 times higher than that of oxygen in the temperature range of 0-60 ^{o}C [48]. The oxidation by ozone may occurs directly by the ozone molecule or indirectly involving OH radical, the later belonging to advanced oxidation technique. Generally, direct ozonation occurs within acidic regime (pH < 4), combined direct and indirect ozonation occurring between the pH range of 4 to 9, and above that indirect ozonation prevails [49]. The direct oxidation of the organics by ozone occurs by the electrophilic attack on the atoms which have a negative charge density like N, P, O or nucleophilic carbon or to the double/triple bonds in the unsaturated carbon chain compounds [47].

The radical reaction involved in indirect ozonation can be simply described as follows.

$$3O_3 + OH^- + H^+ \rightarrow 2OH^\bullet + 4O_2$$ Equation 2.6-3

Ozonation has been investigated for the destruction of several pollutants such as carboxylic acids, alcohols, ethers, phenols, amino acids etc [50, 51]. It has also been found highly efficient in treatment of textile wastes and dyes [52-55].

2.7 Advanced Oxidation Technique [AOT]

AOT is broadly defined as the aqueous phase oxidation based on the reaction of dissolved organic contaminants with active radical (mainly hydroxyl radical) to mineralize the organic pollutants into water and CO_2 [56]. In the past several decades AOT has been almost completely associated with the utilization of hydroxyl radical generated from hydrogen peroxide due to its cheap availability and being environmentally benign. Recently, there has been considerable research involving several other oxidants, mostly sulphate based oxidants for the application in AOT. In comparison to other oxidative techniques, AOT is still an emerging technology and thus has a vast potential to be explored in several aspects such as the type of oxidants to be utilized, the type of catalyst used for activating the oxidants and the conditions that would favor the reaction etc. A cumulative R&D study conducted by Matatov and Sheintuch [2] describes the current status of various waste oxidation

technologies as shown in Figure 2.7-1. The figure shows the extent of research carried out on the abscissa with respect to the performance achieved by the technology on the ordinate. The WAO technique has been thoroughly explored and has almost reached the maturity. The recent studies carried out on WAO shows no major improvement in the process performance as evident from the flattening of its curve towards the end. On the other hand the SCWO curve shows a steep rise suggesting a significant improvement in the technology in the recent years. Lastly, the AOT technique has seen little improvement in the recent period and thus demands further investigations. Since the early 20th century focus has been diverted towards the development in AOT, mainly due its advantage in low energy requirements.

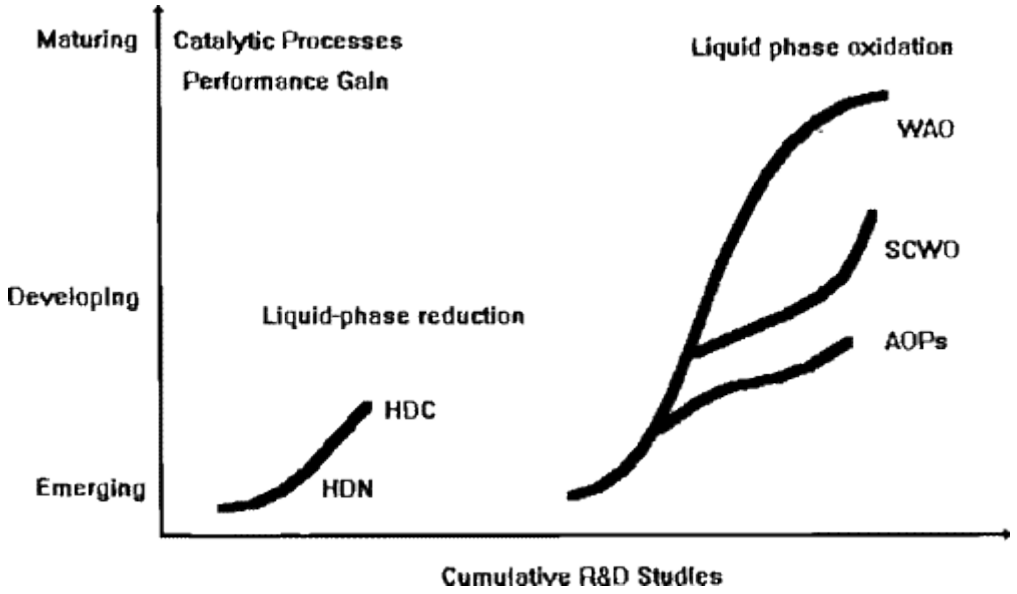

Figure 2.7-1 Current status of various waste oxidation technique *[Reprinted from publication mentioned in reference [2] with kind permission from Elsevier]*

The AOT generally includes but certainly not limited to Fenton reagent, UV/H_2O_2, modified Fenton reagent, UV/Ozone, Ozone/H_2O_2 also known as peroxone technique, TiO_2/UV, Co^{2+}/oxone and others. A few of these techniques are discussed in detail below.

2.7.1 Fenton and Modified Fenton based Oxidation techniques

Discovered in late eighteenth century by H.J. Fenton, this technique has aroused research interest of many scientists for several years. The mechanism of the reaction

involving hydroxyl radical was first proposed by Haber & Warris in 1934 [57]. Since then enormous contributions have been put forth to understand the hydroxyl radical related chemistry for the degradation of different organics. Fenton reagent based treatment involves the addition of hydrogen peroxide and salts of ferrous ions into the wastewater treatment system. The reaction involves generation of hydroxyl radical as per equation 2.7.1-2 which would then in turn oxidize the organics [58].

$$H_2O_2 + Fe^{2+} \longrightarrow OH^{\bullet} + OH^{-} + Fe^{3+}$$ Equation 2.7-1

$$RH + OH^{\bullet} \longrightarrow R^{\bullet} + H_2O$$ Equation 2.7-2

The Fenton reagent has been successful in oxidation of alcohol, ketones, phenols, chlorophenol, benzene, nitrobenzene, dichlorophenol and also poly aromatic hydrocarbons which are most difficult to treat with other conventional techniques [59-64]. The second order rate constant of the reaction of hydroxyl radical with several organics is given in Table 2.7-1 [49].

Table 2.7-1 Second order rate constant of organic degradation using hydroxyl radical

Compound	Reaction rate constant (k, L $mol^{-1}s^{-1}$)
Chlorinated Alkenes	10^9 to 10^{11}
Phenols	10^9 to 10^{10}
N-organics	10^8 to 10^{10}
Aromatics	10^8 to 10^{10}
Ketones	10^9 to 10^{10}
Alcohols	10^8 to 10^9

The radical reactions involved in the Fenton based treatment have been classified into 3 types; Initiation (formation of active radical), propagation (additional formation of the active radicals from the interaction of the in organics) and finally termination (quenching of the active radical). The series of radical reactions involved in the reaction proceed at different rates which are generally dictated by the type of the pollutant present. An example of the series of radical reactions involved in the degradation of chlorophenol by the Fenton reagent is presented in

Table 2.7-2 [65].

Table 2.7-2 Series of reaction involved in chlorophenol degradation via Fenton Reaction

Reaction	Rate constant (k $M^{-1}s^{-1}$
$Fe^{2+} + H_2O_2 \rightarrow Fe^{3+} + OH^{\bullet} + OH^-$	63
$Fe^{3+} + H_2O_2 \rightarrow Fe^{2+} + HO_2^{\bullet} + H^+$	0.01
$OH^{\bullet} + H_2O_2 \rightarrow HO_2^{\bullet} + H_2O$	$2.7*10^7$
$HO_2^{\bullet} \rightarrow O_2^{\bullet} + H^+$	$1.58*10^5$ s^{-1}
$O_2^{-\bullet} + H^+ \rightarrow HO_2^{\bullet}$	$1*10^{10}$
$OH^{\bullet} + Fe^{2+} \rightarrow Fe^{3+} + OH^-$	$3.2*10^8$
$HO_2^{\bullet} + Fe^{2+}(+H^+) \rightarrow Fe^{3+} + H_2O_2$	$1.2*10^6$
$HO_2^{\bullet} + Fe^{3+} \rightarrow Fe^{2+} + H^+ + O_2$	$3.1*10^5$
$O_2^{-\bullet} + Fe^{2+}(+H^+) \rightarrow Fe^{3+} + H_2O_2$	$1*10^7$
$O_2^{-\bullet} + Fe^{3+} \rightarrow Fe^{2+} + O_2$	$5*10^7$
$OH^{\bullet} + OH^{\bullet} \rightarrow H_2O_2$	$4.2*10^9$
$HO_2^{\bullet} + HO_2^{\bullet} \rightarrow H_2O_2 + O_2$	$8.3*10^5$
$HO^{\bullet} + HO_2^{\bullet} \rightarrow H_2O + O_2$	$1*10^{10}$
$HO^{\bullet} + O_2^{-\bullet} \rightarrow HO^- + O_2$	$1*10^{10}$
$HO_2^{\bullet} + O_2^{-\bullet}(+H^+) \rightarrow H_2O_2 + O_2$	$9.7*10^7$
$OH^{\bullet} + p-chlorophenol \rightarrow (Cl)DHCD^{\bullet}$	~
$(Cl)DHCD^{\bullet} + Fe^{3+} \rightarrow Fe^{2+} + (Cl)benzendiols$	$2*10^{10}$
$OH^{\bullet} + (Cl)DHCD \rightarrow THB + Cl^{\bullet}$	~
$(Cl)benzenediols + Fe^{3+} \leftrightarrow Fe^{2+} + (Cl)semiquinones$	~
$THB + Fe^{3+} \rightarrow Fe^{2+} + (Cl)benzoquinones$	~
$THCD^{\bullet} + Fe^{3+} \rightarrow Fe^{2+} + THB$	$7*10^9$
$OH^{\bullet} + (Cl)benzoquinones \rightarrow MA^{\bullet}$	~

$OH^{\bullet} + THB \rightarrow (H)AA^{\bullet}$	~
$OH^{\bullet} + MA/(H)AA \rightarrow (H)AA^{\bullet}$	~
$MA^{\bullet}/(H)AA^{\bullet} + Fe^{3+} \rightarrow Fe^{2+} + MA/(H)AA$	$1.2*10^{9}$
$Fe^{3+} + \alpha(H)AA \rightarrow Fe^{3+} - organiccomplex$	~

$(Cl)DHCD^{\bullet}$ - (chloro)dihydroxycyclohexadienyl radical

THB – trihydroxybenzene

THCD – trihydroxycyclohexadienyl

MA – cic muconic acid

(H)AA – (hydroxylated) aliphatic acid

2.7.2 Factors affecting the Fenton reaction

Despite high popularity of this technique both in research and industrial application, it also faces several limitations in terms of constrained process conditions.

Fe^{2+}/H_2O_2 ratio: Fenton reaction generally proceeds with the first order reaction kinetics with respect to hydroxyl radical and the pollutant concentration. The rate constant of hydroxyl radical are usually in the range of 10^{8}-10^{10} [49]. However apart from oxidizing the organics the active hydroxyl radical tends to react with the oxidant themselves thereby introducing an upper limit for the amount of oxidant to be beneficially added to the system. Studies conducted by Beltran et al[66] for Fenton oxidation suggests that the rate of oxidation increased on increasing the concentration of H_2O_2 from 10^{-4} to 10^{-3} M, further to which the rate of oxidation was found to decrease. In the same study a plateau was observed for the amount of iron added to the system above $7x10^{-5}$ M.

Low pH requirement: The biggest drawback for the Fenton system is the narrow range of pH required for the operation. A low pH of around 3 has been notably reported to be the best operating condition, thus necessitating highly acidic condition for the reaction. Moreover, the pH of the system tends to increase during the process thus requiring additional cost of pH control [67].

Quenching of the hydroxyl radical: The degradation of the organic contaminant is generally found to decrease with the presence of various anions found in the industrial wastewater systems. The degradation rate of dichlorous was found to reduce significantly in the presence of phosphate, chloride and nitrate ions [68, 69]. The suppression of the degradation rate was found to be the order $H_2PO_4^-$>Cl^->NO_3^-.

Precipitation: The precipitation of ferric ion is a major operational issue with the application. The precipitation generally occurs for an uncontrolled pH reaction system wherein Fe^{3+} ions tend to insolublize oxide-hydroxide complex. This also prevents the regeneration of the ferrous ions.

2.7.3 UV/Oxidant

Similar to the Fenton process, the disintegration of hydrogen peroxide (or any other oxidants) to obtain active hydroxyl/sulphate radical can be achieved by irradiating the solution with UV radiation. This advanced oxidation process generally known as “Photochemical Oxidation” has been widely used for oxidation of wastewater having low COD amount as seen in Figure 2.1-1.

The reaction mechanism is via three stages: initiation, propagation and termination as given below [70]

Initiation Reaction

$$H_2O_2 + h\nu \rightarrow 2OH^\bullet \qquad \text{Equation 2.7-3}$$

Propagation Reaction

$$H_2O_2 + OH^\bullet \rightarrow HO_2^\bullet + H_2O \qquad \text{Equation 2.7-4}$$

$$H_2O_2 + HO_2^\bullet \rightarrow OH^\bullet + H_2O + O_2 \qquad \text{Equation 2.7-5}$$

$$HO_2^- + HO_2^\bullet \rightarrow OH^\bullet + OH^- + O_2 \qquad \text{Equation 2.7-6}$$

Termination Reaction

$$OH^\bullet + HO_2^\bullet \rightarrow H_2O + O_2 \qquad \text{Equation 2.7-7}$$

$$OH^{\bullet} + OH^{\bullet} \rightarrow H_2O_2$$ Equation 2.7-8

Similar to the Fenton reaction the concentration of hydrogen peroxide needs to be properly selected in-order to achieve the maximum efficiency by reducing the scavenging effect of hydroxyl radical. Tanaka et.al [71, 72] have reported that optimum concentration of hydrogen peroxide as 0.01 M for the degradation of several organo-halide compounds, Similarly Beltran et al.[73] have reported a similar optimum concentration of hydrogen peroxide for the degradation of atrazine. During the treatment of industrial waste, the presence of high UV absorbing compounds such as humic acid would be a major factor to be considered [74]. Apart from oxidant concentration, the pH plays a crucial role in determining the treatment efficiency. Lowering the pH tends to nullify the effect of radical scavengers such as carbonate and bicarbonate ions [75].

The photochemical oxidation has been studied for the treatment of phenol, chlorophenol, dichlorophenol, nitro benzene, major groundwater pollutants such as PCE&TCE, hydroxyl phenyl acetic acid and even actual industrial wastewater [76-80].

In the study conducted by Anipsitakis et al [81] for the degradation of dichlorophenol under UV/Oxidant system, persulphate gave the highest efficiency followed by peroxymonosulphate and then hydrogen peroxide

$$UV/K_2S_2O_8 > UV/KHSO_5 > UV/H_2O_2$$

The trend is due to the higher oxidation potential of sulphate radical generated in comparison with that of the hydroxyl radical. In addition the molar amount of sulphate radical generated from the persulphate based oxidant is numerically twice that of peroxymonosulphate, suggesting a higher rate of degradation.

2.7.4 Photo Fenton Process

The UV/oxidant system has found profound applications in conjunction with other AOT. The best example would be photo Fenton reaction combining the benefits of both Fenton and UV/H_2O_2 system. The combination produces larger quantity of hydroxyl radical in comparison to conventional Fenton reaction and photochemical reaction, thus resulting in highly enhanced rate of reaction. Balcioglu et al.[82]

studied the degradation of textile dyes using photo Fenton reaction. Under the influence of UV light, the $Fe(OH)^{2+}$ ions obtained as the Fenton reaction end product, absorbs the radiation to reconvert into ferrous ions thereby enhancing the rate of oxidation [83].

In-order to further improve the process economy, solar light can be utilized instead of electrical powered lamp. Photo-Fenton reaction has been successfully used for the degradation of herbicides, nitro and di-nitro phenols, aniline, toluene, nitrotoluene, atrazine, effluent arising from dye industries, landfill leachate etc [62, 84-88].

Synergetic combination of three types of UV/Oxidant system i.e. UV/Peroxymonosulphate with cobalt ions, UV/Hydrogen peroxide with addition of ferrous and ferric ions and UV/Persulphate with addition of silver ion was reported for dichlorophenol degradation. It observed efficiency was in the following order.

$$UV/Fe^{3+}/H_2O_2 > UV/Fe^{2+}/H_2O_2 > UV/Cos^{2+}/KHSO_5 > UV/Ag^{+}/K_2S_2O_8.$$

The order is completely reverse of that found for UV/oxidant system reported in section 2.7.3 above, which is believed to be due to the photosensitivity of the Fe^{3+} as compared to cobalt and silver ions [81].

2.7.5 UV/Ozone:

Another popular oxidant used in conjunction with UV irradiation is ozone. UV/O_3 technique has been highly successful in treatment of agro-industrial wastewater, which offers an advantage of treatment at alkaline pH [89]. The technique involves saturation of the waste-water system with ozone and irradiation with the UV radiation. The rate of decay of O_3 is reportedly 1000 times higher than that of hydrogen peroxide thereby inducing higher rate of oxidation[90]. The radical pathway for UV/O_3 system is dependent on the wavelength of the incident light. For wavelength lower than 300 nm (under UV-C radiation), the generation of $OH^{\cdot}$ occurs as per the following equations.[91]

$$O_3 + H_2O \xrightarrow{h\nu} H_2O_2 + O_2 \qquad \text{Equation 2.7-9}$$

$$H_2O_2 \xrightarrow{h\nu} 2OH^{\bullet} \qquad \text{Equation 2.7-10}$$

For wavelength greater than 300nm, the ozone molecule would react with the in situ generated H_2O_2 as per the equation. [91]

$$O_3 + H_2O_2 \xrightarrow{h\nu} OH^{\bullet} + HO_2^{\bullet} + O_2$$ Equation 2.7-11

The technique has been investigated for the removal of caffeic, p-couric, syringic, vanallic acid, atrazine, nitrobenzene, di nitrotoluene, etc. in acidic and neutral medium [89, 92, 93], the degradation of actually textile waste was investigated by Moraes et al.[94] and found UV/O_3 system to be more favorable than UV/H_2O_2.

2.7.6 O_3/H_2O_2 (peroxone) and UV/O_3/H_2O_2

Peroxone technique or Ozonation combined with hydrogen peroxide has been favorably used for oxidation of a few organics resistant to ozonation. The method involves addition of hydrogen peroxide to the wastewater saturated with ozone. The organic oxidation in peroxone process would generally occur by 2 different processes [95]

1) Direct oxidation of the contaminants with the aqueous ozone
2) Radical initiated oxidation occurring due to hydroxyl radical generated within the system.

The addition of hydrogen peroxide accelerates the decomposition of the ozone resulting in additional generation of active hydroxyl radical. The production of hydroxyl radical is in equi- molar to the amount of ozone present in the solution. The important radical reactions taking place in the peroxone system are shown as follows [96].

$$O_3 + 2H^+ + 2e^- \rightarrow O_2 + H_2O$$ Equation 2.7-12

$$O_3 + H_2O + 2e^- \rightarrow O_2 + OH^{\bullet}$$ Equation 2.7-13

$$H_2O_2 + OH^{\bullet} \rightarrow HO_2^{\bullet} + H_2O$$ Equation 2.7-14

$$O_3 + OH^{\bullet} \rightarrow HO_2^{\bullet} + O_2$$ Equation 2.7-15

$$H_2O_2 + OH^{\bullet} \rightarrow HO_2^{\bullet} + O_2$$ Equation 2.7-16

Peroxone system has been effective in treatment of halogenated-aromatic such as 1,1-dichloropropene (DCPE), TCE, 1-chloropentane (CPA), and 1,2-dichloroethane (DCA) etc [97-99]. The major limitation faced in the technique is the optimum utilization of hydrogen peroxide. Similar to the situation in Fenton reaction, the generation of excess amount of hydroxyl radical act as a quencher to the exiting oxidant, thereby forming an upper limit to the extent of oxidation. In case of degradation of 4-chlorophenol reported by chamarro et al, an optimum ratio for H_2O_2/O_3 of 0.601 was established. In the case of TCE and PCE degradation in ground water an optimum ratio of 0.5 was established [98]. Given the limitation of existing peroxone system for increase in the rate of oxidation, it has been proposed to combine peroxone with UV irradiation system. The major beneficial outcome of $UV/O_3/H_2O_2$ technique is in the reduction of TOC of the wastewater. The study conducted for the degradation of nitrophenol in the combined $UV/O_3/H_2O_2$ system showed much higher efficiency as compared to individual ozonation or UV/O_3 system [100].

2.7.7 UV/Photocatalyst

UV/Photocatalyst treatment system, also known as “Photocatalytic treatment” is an excellent technique for degradation of highly refractory compounds and gives an advantage of higher TOC removal when compared to the conventional treatment methods. The technique is based on addition of photocatalyst in wastewater under the illumination of UV radiation.

The reaction mechanism is based on the generation of active electron-hole pair on the photo-catalyst. When the semiconductor is illuminated by UV radiation, the light photon promotes the electrons from the valance band to the conduction band, resulting in the generation of an oxidative hole in the valance band as seen in Figure 2.7-2. The amount of energy required for the electrons to move from the valance to the conduction band is equal or more than the band gap energy of the photocatalyst. The contaminant molecules which are adsorbed on the catalyst surface then get oxidized with the valance band hole by the election transfer.

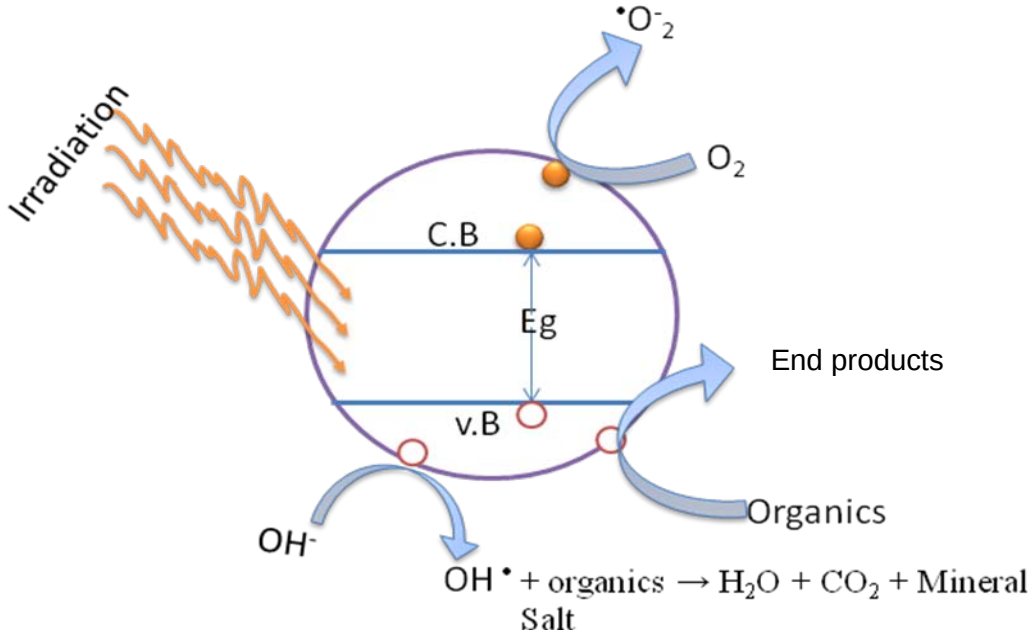

Figure 2.7-2: Organic oxidation mechanism on the photocatalyst surface

Various halogenated compounds such as chlorophenols, nitrophenols, trichloroethylene, and toluene have been shown to be completely degraded in both UV and combined photocatalyst/UV system [101-103]. Acids like salicyclic & t-cinnamic, dyes, and various biocalcitrant pesticides could also be successfully treated under photocatalytic systems [104, 105]. There has also been a marked rise in the research involving photo catalytic degradation of actual industrial effluents and mixed pollutants.

To date, titanium dioxide has been the most extensively used photocatalyst. Studies have also been conducted using ZnO, ZrO_2, SrO_2, CdS etc [106]. As an alternative to TiO_2, zinc oxide has been reported as an efficient catalyst, which has a similar band gap of 3.2 eV. Few investigations have supported the assertion of ZnO being a better photocatalyst than TiO_2, especially for chlorinated compounds [107]. It has been tested for the oxidation of dyes, phenolic compounds and also for the treatment of groundwater pollutants [108-111].

In further developments of photo catalytic efficiency, it has been observed that addition of small quantities of oxidants such as hydrogen peroxide results in enhanced formation of the hydroxyl radicals. The addition of the oxidants into the system not only prevents the electron-hole recombination on the photocatalyst

surface but also provides additional organic degradation via photochemical reaction. Thus the oxidation takes place via combined photocatalytic and photochemical oxidation. The combination of oxidants with photocatalyst has the capability of oxidizing several highly refractory compounds. Doong et al [112] has reported the oxidation of several pesticides with the combined H_2O_2/TiO_2/UV system. Hydrogen peroxide is more potent to undergo photo dissociation by the photo catalytic activated TiO_2 surface, thereby enhancing the rate of the reaction. On similar lines, bubbling ozone or oxygen has also been reported to intensify the degradation rate. A comprehensive review on the combine ozonation and photocatalysis have been reported by Augustina et.al [113]. Apart from H_2O_2 and O_3, few studies have reported the application of sulphate based oxidants such as persulphate and peroxymonosulphate. Dhanalakshmi et al [114] have tested the application of peroxymonosulphate and peroxydisulphate in conjunction with TiO_2 and have reported beneficial influence of addition of oxidants. They have observed peroxymonosulphate as having a higher oxidizing capability as compared to persulphate for dye degradation. Malato et al. [115] has investigated the degradation of PCP under the influence of hydrogen peroxide, peroxymonosulphate and peroxidisulphate along with TiO_2. They have found peroxydisulphate in combination with TiO_2 to maximize the rate of degradation.

In contrast to the enhancement of oxidation efficiency by addition of oxidants, there are a few reports showing a non synergetic effect of combining oxidant with photocatalytic oxidation. Wang and Hong [116] have compared the effect of three different types of oxidants viz, peroxide, persulphate and periodate and have found that the effect of addition of oxidant for combined photochemical oxidation along with UV and TiO_2 have a negative effect on the oxidation efficiency, except for persulphate, wherein the rate of reaction under the presence of UV/Oxidant was faster than the rate of reaction in the presence of UV/TiO_2/oxidant. In the case of persulphate based oxidant, the rate of reaction in UV/TiO_2/persulphate was found to be similar to that of UV/persulphate system. Further details of the combined photochemical and photocatalytic oxidation is discussed in Chapter 6.

2.7.8 Cobalt/Peroxymonosulphate based Advanced Oxidation

Until recently, Fenton reagent was the most popular AOT based on radical generated from hydrogen peroxide in the presence of metal ion. Although, the Fenton reagent is one of the most popular advanced oxidation technique and is used in several

industrial applications for the treatment of industrial discharged streams, it faces several limitations such as requirement of low pH, formation of precipitate, limited total organic carbon removal, quenching of hydroxyl radical by the carbonate species present in the system etc. In the last decade there has been the development of an alternative technology to a Fenton reagent for degradation of various organic contaminants. The oxidation process involves the utilization of peroxymonosulphate based oxidant in the presence of cobalt ions to generate active sulphate based oxidants.

Peroxymonosulphate (PMS) (molecular formula $KHSO_5$) is a component of a triple salt $2KHSO_5.KHSO_4.K_2SO_4$ which is available under the commercial name “Oxone”. The investigation of PMS decomposition in the presence of Co^{2+} ion has been first reported by Ball and Edward in 1956 [117]. They studies the decomposition of PMS as a function of pH and reported the second order law for the decomposition at the pH between 6-8 when HSO_5 is the major species

$$2HSO_5^- \rightarrow 2SO_4^{2-} + 2H^+ + O_2 \qquad \text{Equation 2.7-17}$$

$$-\frac{dHSO_5^-}{dt} = k_a \frac{[HSO_5^-]^2}{H^+} \qquad \text{Equation 2.7-18}$$

It is critical to point out here that the commercial preparation of PMS as a solid state triple salt has been made available much later, Ball and Edward had used a solution of PMS which they made by themselves which contained half sulphuric acid and a small amount of hydrogen peroxide. The application of PMS gained significant attention in pulp and paper industry after the availability of hydrogen peroxide free solid form of PMS under the commercial name oxone. Bouchard et al [118] have reported the application of salt of PMS (oxone) for insitu synthesis of dimethyldioxirane which is further use for bleaching of Kraft pulp. PMS have also been utilized in a chemiluminescence system for the detection of fluorescent organic compounds [119].

The application of peroxymonosulphate as an oxidant for waste water treatment has received attention in past few years. The application of this reagent has been proposed by Anipsitakis at.el [120] for the degradation of dichlorophenol, naphthalene and atrazine. The system includes cobalt mediated decomposition of PMS to generate sulphate radical which can further oxidize the organic pollutants as per the following equation

$$Co^{2+} + HSO_5^- \rightarrow Co^{3+} + SO_4^{\cdot} + OH^-$$ Equation 2.7-19

$$SO_4^{\cdot} + R - H(organic\ pollutants) \rightarrow R^{\bullet} + SO_4^{2-} + H^+ \xleftarrow{Several\ steps} xCO_2 + yH_2O$$ Equation 2.7-20

The technology is similar to that of Fenton reaction; however it employs sulphate radical for the degradation of organic pollutants in contrast to that of hydroxyl radical. The degradation efficiency of Co/PMS system was observed to be higher than Fenton reagent for pollutants such as Dichlorophenol and Atrazine. For naphthalene, Fenton reagent was found to be more efficient at acidic pH, however the Co/PMS system was found to have better efficiency at higher pH [121]. Francis et al. [122] have investigated the decomposition of PMS using various transition metals such as Mg, Fe, Cu, Ni, V and Co. It has been reported PMS is insensitive in the presence of Mg, Fe, V & Ni except in the case of Cu at basic pH and Co above a certain concentration limit.

The type of active radical produces depends on the transition metal used as the catalyst as well as it oxidation state.

$$HSO_5^- + e^- \rightarrow SO_4^{\cdot} + OH^-$$ Equation 2.7-21

$$HSO_5^- + e^- \rightarrow SO_4^{2-} + OH^{\cdot}$$ Equation 2.7-22

$$HSO_5^- \rightarrow SO_5^{-\cdot} + H^+ + e^-$$ Equation 2.7-23

A small quantity of peroxymonosulphate and hydroxyl radical formation have been reported however the activity is considerably less than that of sulphate radical. For the Co/PMS system the quenching study conducted suggests that the major radical reaction proceeds as per Equation 2.7-22 with the formation of sulphate radical [120].

Co/PMS system has been extensively utilized for detoxification and mineralization of azo dye. Fernandez et al. [123] have investigated the bleaching, photo-bleaching and mineralization of Azo dye Orange II in Co/PMS system. Most recently the kinetic degradation of Acid red has been reported by Madhavan et al [124]. In both the cases a typical zero order kinetic of dye degradation was reported. The major radical reaction involved in the degradation is composed of initiation, propagation and termination step as seen from equations below [123].

$$Co^{2+} + H_2O \leftrightarrow CoOH^+ + H^+$$ K_1 Equation 2.7-24

$$CoOH^+ + HSO_5^- \rightarrow CoO^+ + H_2O + SO_4^{\cdot-}$$ k_2 Equation 2.7-25

$$CoO^+ + 2H^+ \leftrightarrow Co^{3+} + H_2O$$ K_3 Equation 2.7-26

$$Co^{2+} + SO_4^{\cdot-} \rightarrow Co^{3+} + SO_4^{2-}$$ k_4 Equation 2.7-27

$$RH + SO_4^{\cdot-} \rightarrow RH^+ + SO_4^{2-}$$ k_5 Equation 2.7-28

The rate of dye degradation from equation 2.7-26 can be given as

$$-\frac{d(RH)}{dt} = k_4[Rh][SO_4^{\cdot-}]$$ Equation 2.7-29

$$-\frac{d(SO_4^{\cdot-})}{dt} = k_2K_1[Co^{2+}]\frac{[HSO_5^-]}{H^+} - k_4[Co^{2+}][SO_4^{\cdot-}] - k_5[RH][SO_4^{\cdot-}]$$ Equation 2.7-30

At steady state assuming the rate of change of sulphate radical as zero thus

$$[SO_14^{\uparrow}(\cdot -)] = k_12\ K_11\ [Co^{\uparrow}(2+)\ ]\ \ ([HSO_15^{\uparrow}-])/H^{\uparrow} + * k_14\ [Co^{\uparrow}(2+)\ ] * k_15\ [RH]$$ Equation 2.7-31

which on substituting in equation 2.7-28 becomes

$$-\frac{d(RH)}{dt} = k_{co}[Co^{2+}]$$ Equation 2.7-32

where k_{co} is given as

$$k_{co} = k_5\frac{k_2K_1[HSO_5^-][RH]}{\{[H^+](k_4[Co^{2+}] + k_5[RH])\}}$$

A further more detailed reaction mechanism for PMS disintegration as reported by Kim and Edward [125] and represented as a cyclic view by Chen et al. [126] is shown in the figure below.

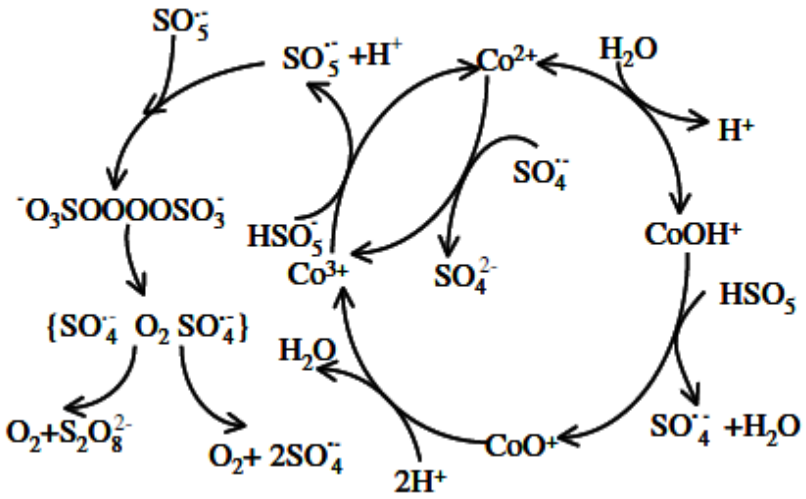

Figure 2.7-3: Mechanism of SO_4 chain reaction. *[Reprinted from publication mentioned in reference [126] with kind permission from Elsevier]*

The major limitation of Co/PMS based oxidation reaction is the dissolution of Co^{2+} ion in the system. Cobalt is a highly toxic heavy metal and its release in environment is highly undesirable. Apart from homogeneous organic degradation reaction, attempts have been made to utilize solid cobalt oxide particles as a catalyst to activate PMS thereby carrying out the reaction under heterogeneous mode. This helps in preventing the release of cobalt ions in the discharged stream. Anipsitakis et al [127] carried out the investigation of heterogeneous Co/PMS oxidation using two different types of cobalt oxides (CoO and Co_3O_4). It was reported that only Co_3O_4 showed true heterogeneous activation of PMS while considerable dissolution of CoO was observed, especially at low pH. At acidic pH a slight dissolution of Co_3O_4 ($CoO.Co_2O_3$) was reported which may be due to its CoO component. In another similar attempt, nano Co_3O_4 was developed and utilized for catalytic oxidation of Acid Orange 7 dye [128]. Once again, it was observed that at neutral pH, the heterogeneous reaction over Cobalt oxide prevails which was evident from extremely low amount of cobalt ions leached into the solution. The catalyst was found to be reusable even after 8 cycles.

In the current thesis further several attempts have been made to develop cobalt supported catalyst for carrying out organic oxidation in heterogeneous mode.

2.8 Combined Adsorption and Advanced Oxidation Technique

The techniques discussed so far suggests that the prospective technique for complete removal of pollutants are mainly restricted to oxidation, “Advanced oxidation” to be specific. Enormous research has been carried out in this area and several of them have been applied in practice. However in all the techniques there are several shortcomings or limitations. If limitation is not the proper term to describe, still it is certainly bounded by the process limitations for an economical application.

The major issues which have been faced in all the oxidation technologies are:

The generation of intermediates: This is one of the most important issues faced by any oxidation technique if the process is tried to be controlled by mole economy. In order to ascertain complete removal, either the oxidant is added 4-5 times more than the theoretical requirement or additional techniques are applied in conjunction with oxidation such as ozonation or UV application. Such a method can be termed as “Hybrid Technology”.

Upper limit of feed concentration: This limitation is evident from Figure 2.1-1 which indicates that for any oxidative technique to suit the operation, the concentration has to be below a certain level. This limitation although is highly case dependent, but is certainly a problem faced by many industries. Even if the industry has the concentration of discharged pollutants within the applicability limit of the desired oxidative techniques there are times when sudden pulse of high concentration pollutants are generated, especially during the startup and shutdown of the system or during the accidental release. In order to account for such uncertainties it is generally recommended to over design the waste treatment system which further hampers the process economics. One way to reduce the concentration of the discharged pollutants is to dilute it with large quantity of water prior to sending it to the treatment facility. But such a technique is highly unadvisable and undesirable due to the large volume of water treatment required. Additionally, polluting fresh water by using it for dilution is not a viable solution.

Application difficulties: The application of chemical oxidation for the remediation of groundwater aquifer added further difficulties. The performance of the treatment system is dominated by the physical and chemical heterogeneities at the remediation

sites, such as the improper mixing of the oxidant in the soil and pollutants in the pore, poor transport of the oxidant in the polluted groundwater zone, presence of geochemical minerals affecting the reaction kinetics of the oxidant etc

In order to address these and many other limitations of advanced oxidation, a “Hybrid technology” based on combined adsorption and advanced oxidation has been proposed and investigated in the past several years. The combination of adsorption prior-to or along with oxidation provides a specific advantage of trapping the pollutants in-order to maximize the oxidation efficiency. This technology should not be mixed with solid catalytic oxidation discussed earlier. In this technique the support has a specific function of immobilizing the pollutants in-order to give an advantage of high concentration of pollutants in a localized place near the catalyst for efficient reaction and thus demands the high adsorption capacity for the catalyst support.

A potential system design for combined adsorption and oxidation technique is shown in Figure 2.8-1.The steps involve filling the column with the catalytic materials having the potential to adsorb and oxidize the contaminants. The wastewater and the dilute oxidant are pumped through wastewater pump and oxidant pump, respectively. Alternatively, the oxidant can be dissolved into the wastewater directly and the mixture is pumped by a single pump into the column.

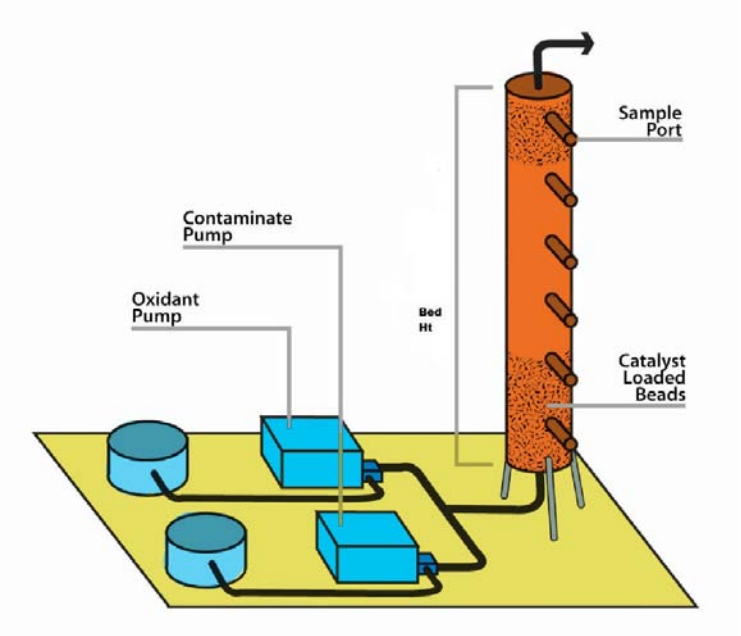

Figure 2.8-1 Combined Adsorption and Oxidation experimental Setup

A combined adsorption and oxidation technique can be basically classified into two types

Sequential Adsorption and Oxidation Technique

Simultaneous Adsorption and Oxidation Technique

2.8.1 Sequential Adsorption and Oxidation Technique

This technique involves primarily an adsorption step to immobilize the pollutants onto the adsorbent particles followed by the regeneration of the adsorbent by oxidation techniques. Sequential Adsorption and Oxidation can be further divided into two types. The first type is the adsorption of pollutants onto the adsorbent surface followed by desorption to remove and collect the concentrated pollutants into another system which is oxidized separately. The second type is the adsorption of pollutants onto the surface of the adsorbent followed by insitu oxidation of the pollutants inside the adsorption column. The first process is generally uneconomical since it involves several different steps and units, however for certain cases it is impeccable. Especially if the pollutants need to be separated from the process stream before oxidation, or if the pollutant is too dilute and needs to be concentrated prior to oxidation. This technique is, however, beyond the scope of this discussion.

The second type which is termed here as Sequential Adsorption and Oxidation was first studied by Turk et al in 1975 for a gas phase contaminant system using activated carbon impregnated with Cr_2O_3, CuO, WO_3 etc [129]. Benzene and xylene adsorbed on metal oxide impregnated activated carbon were catalytically oxidized at a temperature range of 150-240 ^oC. Similar technique for liquid phase sequential adsorption and oxidation for treatment of phenolic and surfactant based wastewater using Fe_2O_3, CuO and Al_2O_3 impregnated carbon was studies by Koganovskii and others [130]. The process was carried out in a single column wherein the column after getting saturated was heated at around 280-330 ^oC under the flow of 5% O_2 in N_2. However, the high temperature regeneration tends to result in carbon loss due to burnoff. Almost 2-3% carbon was reported to be lost per regeneration cycle. A similar study conducted by Sheintuch et al. [131] for phenol adsorption in 5 wt% Fe_2O_3:CuO:Cr_2O_3 in activated carbon followed by regeneration carried out under 5-20% oxygen showed excellent regeneration of the carbon even after 10 cycles. They observed that the catalytic loading of carbon favored the phenol adsorption; however

it also caused the lowering of the ignition temperature of carbon, thus putting an upper limit on the regeneration temperature. The nominal temperature for the catalytic regeneration was reported to be in the range of 220-240 ^{o}C.

As an alternative to activated carbon, the usage of Al_2O_3 has also been reported for sequential adsorption and oxidation. The adsorbent consisted of PtO, MnO, Fe_2O_3 and CaO supported on Al_2O_3. The study reported that the best adsorption of phenol was obtained on 0.5% PtO, 4.5% MnO, 1.9% Fe_2O_3 and 2,4% CaO on Al_2O_3. The adsorption stage was followed by oxidation of the adsorbed contaminants using 6% steam at 240 ^{o}C. The sorbent performance was found unaffected even after 5 rounds of regeneration indicating the high stability of the catalyst [132].

In an interesting alternative to catalyst supported activated carbon, Delmas et al. [133] reported the application of pure activated carbon for combined adsorption and oxidation. The adsorbed phenol on the surface of AC within the column was further regenerated by the oxidation carried out at 140 ^{o}C under a pressure of 40 bar. It was reported that the activated carbon can itself act as a catalyst at the given conditions.

The sequential adsorption oxidation study reported so far employed catalytic oxidation step carried out at high temperature. For adsorbents such as activated carbon, such a treatment is highly detrimental as it causes carbon loss due to burn off. As discussed earlier, almost 2-3% carbon loss was reported per regeneration cycle. An alternative approach to carry out the oxidative regeneration of the adsorbent bed is by using the Fenton reagent at normal temperature. The contaminants adsorbed on the surface of Iron oxide impregnated activated carbon were further oxidized by the addition of H_2O_2 at different concentrations. Successful removal of 2-CP for the wastewater was obtained by the sequential adsorption and oxidation using the Fenton reagent [134, 135]. The performance of the column remained essentially similar after multiple usage without showing any sign of decline in the adsorption capacity [136]. In a similar approach, the MTBE saturated activated carbon was treated by passing a solution of Fe^{2+} and H_2O_2 through the column bed to oxidized the adsorbed pollutants. The sequential adsorption and oxidation technique using the Fenton reagent has been utilized for a series of pollutants including dimethyl phthalate, TCE, 2-CP, chlorobenzene, chloroform, tetra chloroethylene and MTBE [137-142]. Fe-ZSM-5 was used for combined Adsorption and Oxidation study by Doocey and Sharatt [143], however they employed the technique for sequential adsorption and oxidation of 2-DCP from wastewater. The loading of Fe certainly

enhances the oxidative regeneration but simultaneously offsets the adsorption capacity of AC. The optimum Fe loading of around 500 mg/kg was recommended for efficient treatment of MTBE contaminated water [144].

2.8.2 Simultaneous Adsorption and Oxidation

This process involves continuous adsorption of the pollutants from the water and its immediate oxidation with the help of highly oxidative radicals generated Insitu. This technique was initially well utilized in gas phase system.

The simultaneous adsorption and oxidation gives a better edge than sequential adsorption and oxidation in terms of treatment time required, however the latter technique gives more operation freedom for adjusting the optimum reaction conditions [e.g. pH]. Simultaneous adsorption and oxidation of Fe supported catalyst in the presence of H_2O_2 has been investigated on several supported media such as clay, activated carbon, and zeolite. The combined adsorption and oxidation of phenol reported by Fajerwerg et al [145] suggests Fe-ZSM and Fe-aerosil 200 as the promising catalyst compared to 15 other supported catalyst containing Fe, Cu, Mn or Ti as the active metal. The low leaching of Fe from Fe-ZSM-5 suggests the potential stability of the catalyst for multiple usages.

The combination of adsorption on impregnated carbon and simultaneous oxidation for the removal of azo dyes was recently investigated by Ramirez et al [146]. The finding suggests that the removal of dye is due to the process of adsorption and oxidation and the role of oxidation being more significant than adsorption. Among all, the most popular support employed for simultaneous adsorption and oxidation is carbon. The catalytic oxidation of phenol in the presence of Fe-AC has been reported by Zazo et al. [147]. In the given case complete removal of phenol and a high TOC removal of around 85% was observed for a stoichiometric input of H_2O_2 giving a clear indication of advantage of this technique over individual oxidation. The reaction mechanism of simultaneous adsorption and oxidation is rather debatable in terms of reaction taking place in either heterogeneous or homogeneous mode. The two possible mechanisms is discussed as follows.

1) Oxidation reaction taking place in the homogeneous mode: This mechanism although defies the overall objective of simultaneous adsorption and oxidation has been observed for the degradation of TCE and MTBE using activated carbon as a

catalyst for the activation of hydrogen peroxide [148]. In the process, the active hydroxyl radical is generated on the surface of the AC and is then desorbed into the solution and then oxidized the pollutants present in the solution as depicted in Figure 2.8-2. Such a mechanism involved a heterogeneous surface reaction for the generation of active radical followed by a homogeneous reaction for oxidation of the contaminants.

2) Oxidation reaction taking place in the heterogeneous mode: This mechanism involves transportation of both oxidant and pollutant molecules onto the surface. The active radical generated on the adsorbent surface stays on the surface of and then reacts with the pollutant molecules which are concentrated onto the surface. The phenomenon is depicted in Figure 2.8-3. The oxidation of formate onto the surface of goethite in the presence of hydrogen peroxide reported by Kwan and Volker follows this assertion [149].

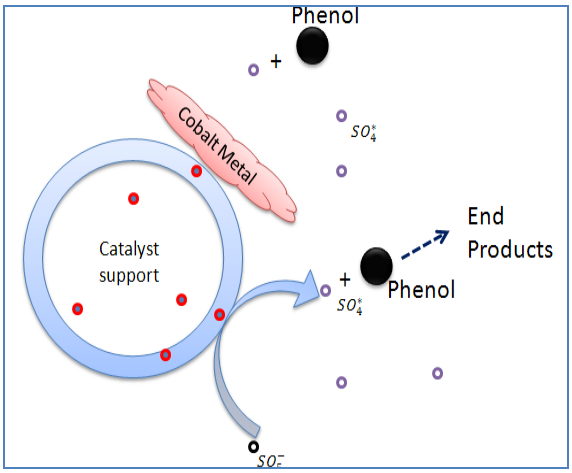

Figure 2.8-2: Formation of active radical on the surface followed by it's desorption into the solution resulting in phenol oxidation in liquid phase

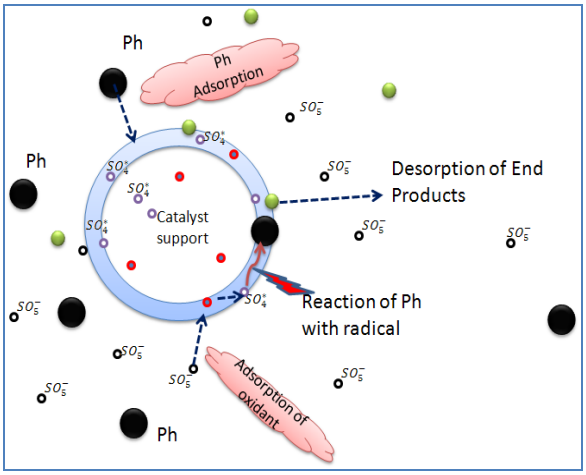

Figure 2.8-3: Formation of active radical on the surface along with simultaneous adsorption of phenol on the surface resulting in phenol oxidation in solid phase.

In the current research, we have investigated the technique of simultaneous adsorption and oxidation for the oxidation of phenolic pollutants. Several different adsorbents such as Zeolite A, Zeolite X, ZSM-5, SBA-15, silica and activated carbon have been utilized to support “Co” catalyst. The supported catalysts were utilized to perform the dual tasks of immobilizing the pollutants and also to generate active sulphate based radical from peroxymonosulphate based oxidant. Till date, little studies have been conducted on cobalt supported catalyst for activation of peroxymonosulphate, mostly directed to silica, titania, pervoskite and resin etc. To the best of my knowledge, no significant research has been reported on the family of zeolite, mesoporous silica and carbon loaded cobalt catalyst to activate peroxymonosulphate for oxidation of pollutants.

2.9 Reference

1. Metcalf, E. and H.P. Eddy, *Wastewater engineering: treatment, disposal and reuse.* McGraw-Hill New York 1991, 1991.

2. Matatov-Meytal, Y.I. and M. Sheintuch, *Catalytic abatement of water pollutants.* Ind. Eng. Chem. Res, 1998. **37**(2): p. 309-326.

3. Mishra, V.S., V.V. Mahajani, and J.B. Joshi, *Wet air oxidation.* Industrial & Engineering Chemistry Research, 1995. **34**(1): p. 2-48.

4. Laine, D.F. and I.F. Cheng, *The destruction of organic pollutants under mild reaction conditions: a review.* Microchemical Journal, 2007. **85**(2): p. 183-193.

5. Rushton, L., *Health hazards and waste management.* Br Med Bull, 2003. **68**(1): p. 183-197.

6. Ahling, B. and A. Lindskog, *Emission of chlorinated organic substances from combustion.* Chlorinated dioxins and related compounds: impact on the environment. Pergamon, Oxford, 1980: p. 215-225.

7. Kim, B.H., et al., *A case study of dioxin monitoring in and around an industrial waste incinerator in Korea.* Chemosphere, 2005. **58**(11): p. 1589-1599.

8. Team, T.I.T.R.C.P.R.B., *Permeable Reactive Barriers:Lessons Learned/New Directions.* Technical/Regulatory Guidelines www.itrcweb.org, 2005.

9. Puls, R.W., C.J. Paul, and R.M. Powell, *The application of in situ permeable reactive (zero-valent iron) barrier technology for the remediation of chromate-contaminated groundwater: a field test.* Applied Geochemistry, 1999. **14**(8): p. 989-1000.

10. Gavaskar, A.R., *Design and construction techniques for permeable reactive barriers.* Journal of hazardous materials, 1999. **68**(1-2): p. 41-71.

11. McMahon, P.B., K.F. Dennehy, and M.W. Sandstrom, *Hydraulic and geochemical performance of a permeable reactive barrier containing zero-valent iron, Denver Federal Center.* Ground Water, 1999. **37**(3): p. 396-404.

12. Henderson, A.D. and A.H. Demond, *Long-term performance of zero-valent iron permeable reactive barriers: a critical review.* Environmental Engineering Science, 2007. **24**(4): p. 401-423.

13. Thiruvenkatachari, R., S. Vigneswaran, and R. Naidu, *Permeable reactive barrier for groundwater remediation.* Journal of Industrial and Engineering Chemistry, 2008. **14**(2): p. 145-156.

14. Gu, B., et al., *Biogeochemical dynamics in zero-valent iron columns: Implications for permeable reactive barriers.* Environ. Sci. Technol, 1999. **33**(13): p. 2170-2177.

15. Bhargava, S.K., et al., *Wet Oxidation and Catalytic Wet Oxidation.* Industrial & Engineering Chemistry Research, 2006. **45**(4): p. 1221-1258.

16. Luck, F., *Wet air oxidation: past, present and future.* Catalysis today, 1999. **53**(1): p. 81-91.

17. Lixiong, L., C. Peishi, and F.G. Earnest, *Generalized kinetic model for wet oxidation of organic compounds.* AIChE Journal, 1991. **37**(11): p. 1687-1697.

18. Zhang, Q. and K.T. Chuang, *Alumina-Supported Noble Metal Catalysts for Destructive Oxidation of Organic Pollutants in Effluent from a Softwood Kraft Pulp Mill.* Industrial & Engineering Chemistry Research, 1998. **37**(8): p. 3343-3349.

19. Luck, F., *A review of industrial catalytic wet air oxidation processes.* Catalysis today, 1996. **27**(1-2): p. 195-202.

20. Kritzer, P. and E. Dinjus, *An assessment of supercritical water oxidation (SCWO) existing problems, possible solutions and new reactor concepts.* Chemical Engineering Journal, 2001. **83**(3): p. 207-214.

21. Prasad, J., et al. *Comparative Study of Air-and Oxygen-Based Wet Oxidation Systems*. in *Proc of 7th Natl Conf., Hazard waste Hazard mater.;*. 1990: Hazard Mater Res Control Inst; Silver spring MD.

22. Imamura, S., *Catalytic and noncatalytic wet oxidation.* Ind. Eng. Chem. Res, 1999. **38**(5): p. 1743-1753.

23. Pirkanniemi, K. and M. Sillanpää, *Heterogeneous water phase catalysis as an environmental application: a review.* Chemosphere, 2002. **48**(10): p. 1047-1060.

24. Golodets, G.I., *Heterogeneous catalytic reactions involving molecular oxygen*. 1983: Elsevier Science Pub. Co., Inc., New York, NY.

25. Imamura, S., I. Fukuda, and S. Ishida, *Wet oxidation catalyzed by ruthenium supported on cerium (IV) oxides.* Industrial & Engineering Chemistry Research, 1988. **27**(4): p. 718-721.

26. Kochetkova R P, B.A.F., Shiplevskaya L I, Shiplevskaya I P, Eppel S A, Smidt F K, *Liquid phase oxidation of Phenol.* Khim.Tekhnol.Topl.Masel, 1992. **4**(31): p. Chem Abstract 1992, 117, 156952.

27. Meunier, A.S.a.B., J. Chem. Soc., Chem. Commun, 1994: p. 1799 - 1800.

28. Meunier, B. and A. Sorokin, *Oxidation of Pollutants Catalyzed by Metallophthalocyanines.* Accounts of Chemical Research, 1997. **30**(11): p. 470-476.

29. Ukrainczyk, L., et al., *Reductive Dechlorination of Carbon Tetrachloride In Water Catalyzed by Mineral-Supported Biomimetic Cobalt Macrocycles.* Environmental Science & Technology, 2002. **29**(2): p. 439-445.

30. Holger, F., S.-E. Günter, and W. Dieter, *Oxidation of aqueous sulfide solutions by dioxygen Part II: Catalysis by soluble and immobilized cobalt(II) phthalocyanines.* Chemical Engineering & Technology, 1997. **20**(9): p. 624-632.

31. Stüber, F., et al., *Carbon materials and catalytic wet air oxidation of organic pollutants in wastewater.* Topics in Catalysis, 2005. **33**(1): p. 3-50.

32. Hunsberger, J.F., *Standard reduction potentials; in: R.C. Weast (Ed.),Handbook of Chemistry and Physics*. 58 ed. 1977, Ohio: CRC Press, Ohio.

33. Ashbolt, N.J., *Microbial contamination of drinking water and disease outcomes in developing regions.* Toxicology, 2004. **198**(1-3): p. 229-238.

34. Gallard, H. and U. von Gunten, *Chlorination of natural organic matter: kinetics of chlorination and of THM formation.* Water research, 2002. **36**(1): p. 65-74.

35. Vella, P.A., et al., *Treatment of Low Level Phenols (g/L) with Potassium Permanganate.* Research journal of the water pollution control federation, 1990: p. 907-914.

36. Yan, Y.E. and F.W. Schwartz, *Oxidative degradation and kinetics of chlorinated ethylenes by potassium permanganate.* Journal of Contaminant Hydrology, 1999. **37**(3-4): p. 343-365.

37. Waldemer, R.H. and P.G. Tratnyek, *Kinetics of contaminant degradation by permanganate.* Environ. Sci. Technol, 2006. **40**(3): p. 1055-1061.

38. Seol, Y., H. Zhang, and F.W. Schwartz, *A review of in situ chemical oxidation and heterogeneity.* Environmental and Engineering Geoscience, 2003. **9**(1): p. 37.

39. Huang, K.C., R.A. Couttenye, and G.E. Hoag, *Kinetics of heat-assisted persulfate oxidation of methyl tert-butyl ether (MTBE).* Chemosphere, 2002. **49**(4): p. 413-420.

40. Watts, R.J. and A.L. Teel, *Treatment of contaminated soils and groundwater using ISCO.* Practice Periodical of Hazardous, Toxic, and Radioactive Waste Management, 2006. **10**: p. 2.

41. Dahmani, M.A., K. Huang, and G.E. Hoag, *Sodium persulfate oxidation for the remediation of chlorinated solvents (USEPA superfund innovative technology evaluation program).* Water, Air, & Soil Pollution: Focus, 2006. **6**(1): p. 127-141.

42. Johnson, R.L., P.G. Tratnyek, and R.O.B. Johnson, *Persulfate Persistence under Thermal Activation Conditions.* Environmental Science & Technology, 2008. **42**(24): p. 9350-9356.

43. Kolthoff, I.M. and I.K. Miller, *The Chemistry of Persulfate. I. The Kinetics and Mechanism of the Decomposition of the Persulfate Ion in Aqueous Medium1.* Journal of the American Chemical Society, 1951. **73**(7): p. 3055-3059.

44. Huang, K.C., et al., *Degradation of volatile organic compounds with thermally activated persulfate oxidation.* Chemosphere, 2005. **61**(4): p. 551-560.

45. Liang, C., et al., *Persulfate oxidation for in situ remediation of TCE. II. Activated by chelated ferrous ion.* Chemosphere, 2004. **55**(9): p. 1225-1233.

46. Block, P.A., R.A. Brown, and D. Robinson. *Novel activation technologies for sodium persulfate in situ chemical oxidation*. in *Proceedings of 4th International Conference on the Remediation of chlorinated and Recalcitrant Compounds*. 2004.

47. Langlais, B., D.A. Reckhow, and D.R. Brink, *Ozone in water treatment: Application and engineering: Cooperative research report*. 1991: CRC Press.

48. Battino, R., T.R. Rettich, and T. Tominaga, *The solubility of oxygen and ozone in liquids.* J. Phys. Chem. Ref. Data, 1983. **12**(2): p. 164-177.

49. Munter, R., *Advanced oxidation processes—current status and prospects.* Proc. Estonian Acad. Sci. Chem, 2001. **50**(2): p. 59-80.

50. Masten, S.J. and S.H.R. Davies, *The Use of Ozonization to Degrade Organic Contaminants in Wastewaters.* Environmental Science & Technology, 1994. **28**(4): p. 180-185.

51. Hoigné, J. and H. Bader, *Rate Constants of Reactions of Ozone With Organic and Inorganic Compounds in Water--II. Dissociating Organic Compounds.* 1983.

52. Shu, H.Y. and C.R. Huang, *Degradation of commercial azo dyes in water using ozonation and UV enhanced ozonation process.* Chemosphere, 1995. **31**(8): p. 3813-3825.

53. Lin, S.H. and C.M. Lin, *Treatment of textile waste effluents by ozonation and chemical coagulation.* Water research(Oxford), 1993. **27**(12): p. 1743-1748.

54. Lin, S.H. and C. Lin, *Decolorization of textile waste effluents by ozonation.* Journal of Environmental Systems, 1991. **21**(2).

55. Rice, R.G., *Applications of ozone for industrial wastewater treatment-- a review.* Ozone: Science & Engineering, 1997. **18**(6): p. 477-515.

56. Glaze, W.H., J.W. Kang, and D.H. Chapin, *The chemistry of water treatment processes involving ozone, hydrogen peroxide and ultraviolet radiation.* Ozone: Science & Engineering, 1987. **9**(4): p. 335-352.

57. Haber, F. and J. Weiss, *The catalytic decomposition of hydrogen peroxide by iron salts.* Proceedings of the Royal Society of London. Series A, Mathematical and Physical Sciences, 1934. **147**(861): p. 332-351.

58. De Laat, J., G. Truong Le, and B. Legube, *A comparative study of the effects of chloride, sulfate and nitrate ions on the rates of decomposition of H2O2 and organic compounds by Fe (II)/H2O2 and Fe (III)/H2O2.* Chemosphere, 2004. **55**(5): p. 715-723.

59. Benitez, F.J., et al., *Oxidation of several chlorophenolic derivatives by UV irradiation and hydroxyl radicals.* Journal of Chemical Technology &# 38; Biotechnology, 2001. **76**(3): p. 312-320.

60. Huang, C.P., C. Dong, and Z. Tang, *Advanced chemical oxidation: its present role and potential future in hazardous waste treatment.* Waste management, 1993. **13**(5): p. 361-377.

61. Walling, C. and S. Kato, *Oxidation of alcohols by Fenton's reagent. Effect of copper ion.* Journal of the American Chemical Society, 1971. **93**(17): p. 4275-4281.

62. Li, Z.M., P.J. Shea, and S.D. Comfort, *Nitrotoluene destruction by UV-catalyzed Fenton oxidation.* Chemosphere, 1998. **36**(8): p. 1849-1865.

63. Kavitha, V. and K. Palanivelu, *Destruction of cresols by Fenton oxidation process.* Water Research, 2005. **39**(13): p. 3062-3072.

64. Potter, F.J. and J.A. Roth, *Oxidation of chlorinated phenols using Fenton's reagent.* Hazardous Waste and Hazardous Materials, 1993. **10**(2): p. 151-170.

65. Kang, N., D.S. Lee, and J. Yoon, *Kinetic modeling of Fenton oxidation of phenol and monochlorophenols.* Chemosphere, 2002. **47**(9): p. 915-924.

66. Beltran, F.J., et al., *Fenton reagent advanced oxidation of polynuclear aromatic hydrocarbons in water.* Water, Air, & Soil Pollution, 1998. **105**(3): p. 685-700.

67. Wadley, S. and T.D. Waite, *Fenton processes.* 2006.

68. Pignatello, J.J., *Dark and photoassisted iron (3+)-catalyzed degradation of chlorophenoxy herbicides by hydrogen peroxide.* Environmental Science & Technology, 1992. **26**(5): p. 944-951.

69. Lu, M.C., J.N. Chen, and C.P. Chang, *Effect of inorganic ions on the oxidation of dichlorvos insecticide with Fenton's reagent.* Chemosphere, 1997. **35**(10): p. 2285-2293.

70. Benitez, F.J., et al., *Rate constants for the reactions of ozone with chlorophenols in aqueous solutions.* Journal of hazardous materials, 2000. **79**(3): p. 271-285.

71. Tanaka, K., T. Hisanaga, and K. Harada, *Efficient photocatalytic degradation of chloral hydrate in aqueous semiconductor suspension.* Journal of photochemistry and photobiology. A, Chemistry, 1989. **48**(1): p. 155-159.

72. Tanaka, K., T. Hisanaga, and K. Harada, *Photocatalytic degradation of organohalide compounds in semiconductor suspension with added hydrogen peroxide.* New journal of chemistry(1987), 1989. **13**(1): p. 5-7.

73. Beltran, F.J., G. Ovejero, and B. Acedo, *Oxidation of atrazine in water by ultraviolet radiation combined with hydrogen peroxide.* Water research(Oxford), 1993. **27**(6): p. 1013-1021.

74. Ku, Y., L.S. Wang, and Y.S. Shen, *Decomposition of EDTA in aqueous solution by UV/H sub (2) O sub (2) process.* Journal of Hazardous Materials, 1998. **60**(1): p. 41-55.

75. Gogate, P.R. and A.B. Pandit, *A review of imperative technologies for wastewater treatment II: hybrid methods.* Advances in Environmental Research, 2004. **8**(3-4): p. 553-597.

76. Hirvonen, A., T. Tuhkanen, and P. Kalliokoski, *Formation of chlorinated acetic acid during UV/H 2 O 2 -oxidation of ground water contaminated with chlorinated ethylenes.* Chemosphere(Oxford), 1996. **32**(6): p. 1091-1102.

77. De, A.K., S. Bhattacharjee, and B.K. Dutta, *Kinetics of phenol photooxidation by hydrogen peroxide and ultraviolet radiation.* Ind. Eng. Chem. Res, 1997. **36**(9): p. 3607-3612.

78. Andreozzi, R., et al., *The oxidation of metol (N-methyl-p-aminophenol) in aqueous solution by UV/H2O2 photolysis.* Water Research, 2000. **34**(2): p. 463-472.

79. Benitez, F.J., et al., *The role of hydroxyl radicals for the decomposition of p-hydroxy phenylacetic acid in aqueous solutions.* Water Research, 2001. **35**(5): p. 1338-1343.

80. Hou, W.J., S. Tsuneda, and A. Hirata, *TOC removal of raw industrial wastewater from LSI photo-resist processing with H 2 O 2 /UV in a batch reactor.* Journal of chemical engineering of Japan, 2001. **34**(3): p. 444-447.

81. Anipsitakis, G.P. and D.D. Dionysiou, *Transition metal/UV-based advanced oxidation technologies for water decontamination.* Applied Catalysis B, Environmental, 2004. **54**(3): p. 155-163.

82. Balcioglu, I.A. and I. Arslan, *Treatment of textile industry wastewater by enhanced photocatalytic oxidation reaction.* Journal of Advanced Oxidation Technologies, 1999. **4**(2): p. 189-195.

83. Lee, C. and J. Yoon, *Determination of quantum yields for the photolysis of Fe (III)-hydroxo complexes in aqueous solution using a novel kinetic method.* Chemosphere, 2004. **57**(10): p. 1449-1458.

84. Kim, S.M. and A. Vogelpohl, *Degradation of organic pollutants by the photo-Fenton-process.* Chemical Engineering & Technology, 1998. **21**(2): p. 187-191.

85. Brand, N., G. Mailhot, and M. Bolte, *Degradation photoinduced by Fe (III): method of alkylphenol ethoxylates removal in water.* Environ. Sci. Technol, 1998. **32**(18): p. 2715-2720.

86. Huston, P.L. and J.J. Pignatello, *Degradation of selected pesticide active ingredients and commercial formulations in water by the photo-assisted Fenton reaction.* Water Research, 1999. **33**(5): p. 1238-1246.

87. Arslan, I., I. Akmehmet Balcioglu, and T. Tuhkanen, *Oxidative treatment of simulated dyehouse effluent by UV and near-UV light assisted Fenton's reagent.* Chemosphere, 1999. **39**(15): p. 2767-2783.

88. Engwall, M.A., J.J. Pignatello, and D. Grasso, *Degradation and detoxification of the wood preservatives creosote and pentachlorophenol in water by the photo-Fenton reaction.* Water Research, 1999. **33**(5): p. 1151-1158.

89. Benitez, F.J., et al., *Simultaneous photodegradation and ozonation plus UV radiation of phenolic acids-major pollutants in agro-industrial wastewaters.* Journal of Chemical Technology and Biotechnology, 1997. **70**(3): p. 253-260.

90. Guittonneau, S., et al., *Characterization of natural water for potential to oxidize organic pollutants with ozone.* Ozone: Science & Engineering, 1992. **14**(3): p. 185-196.

91. Peyton, G.R., *Oxidative treatment methods for removal of organic compounds from drinking water supplies.* Significance and Treatment of Volatile Organic Compounds in Water Supplies, 1990: p. 313-362.

92. Beltran, F.J., J.F. Garcia-Araya, and B. Acedo, *Advanced oxidation of atrazine in water--II. Ozonation combined with UV vis irradiation.* Water research, 1994. **28**(10): p. 2165-.

93. Beltran, F.J., J.M. Encinar, and M.A. Alonso, *Nitroaromatic hydrocarbon ozonation in water. 2. Combined ozonation with hydrogen peroxide or UV radiation.* Ind. Eng. Chem. Res, 1998. **37**(1): p. 32-40.

94. Gomes de Moraes, S., R. Sanches Freire, and N. Durán, *Degradation and toxicity reduction of textile effluent by combined photocatalytic and ozonation processes.* Chemosphere, 2000. **40**(4): p. 369-373.

95. Hoigne, J. and H. Bader, *The role of hydroxyl radical reactions in ozonation processes in aqueous solutions.* WATER RESEARCH, VOL. 10, NO. 5, P 377-386, 1976. 4 FIG, 10 TAB, 45 REF., 1976.

96. Hong, A., et al., *Modeling kinetics of illuminated and dark advanced oxidation processes.* Journal of Environmental Engineering, 1996. **122**: p. 58.

97. Aieta, E.M., et al., *Advanced oxidation processes for treating groundwater contaminated with TCE and PCE: Pilot-scale evaluations.* Journal American Water Works Association, 1988. **88**(5): p. 64-72.

98. Glaze, W.H. and J.W. Kang, *Advanced oxidation processes for treating groundwater contaminated with TCE and PCE: laboratory studies.* Journal-American Water Works Association, 1988. **80**(5): p. 57-63.

99. Masten, S.J. and J. Hoigné, *Comparison of ozone and hydroxyl radical-induced oxidation of chlorinated hydrocarbons in water.* Ozone: Science and Engineering OZSEDS, 1992. **14**(3).

100. Trapido, M., Y. Veressinina, and J. Kallas, *Degradation of aqueous nitrophenols by ozone combined with UV-radiation and hydrogen peroxide.* Ozone: Science & Engineering, 2001. **23**(4): p. 333-342.

101. Wang, K.H., et al., *Photocatalytic degradation of 2-chloro and 2-nitrophenol by titanium dioxide suspensions in aqueous solution.* Applied Catalysis B, Environmental, 1999. **21**(1): p. 1-8.

102. Luo, Y. and D.F. Ollis, *Heterogeneous Photocatalytic Oxidation of Trichloroethylene and Toluene Mixtures in Air: Kinetic Promotion and Inhibition, Time-Dependent Catalyst Activity.* Journal of Catalysis, 1996. **163**(1): p. 1-11.

103. Crittenden, J.C., et al., *Photocatalytic oxidation of chlorinated hydrocarbons in water.* Water Research, 1997. **31**(3): p. 429-438.

104. Farré, M.J., et al., *Degradation of some biorecalcitrant pesticides by homogeneous and heterogeneous photocatalytic ozonation.* Chemosphere, 2005. **58**(8): p. 1127-1133.

105. Ranjit, K.T., et al., *Lanthanide Oxide Doped Titanium Dioxide Photocatalysts: Effective Photocatalysts for the Enhanced Degradation of Salicylic Acid and t-Cinnamic Acid.* Journal of Catalysis, 2001. **204**(2): p. 305-313.

106. Serpone, N., et al., *Exploiting the interparticle electron transfer process in the photocatalysed oxidation of phenol, 2-chlorophenol and pentachlorophenol: chemical evidence for electron and hole transfer between coupled semiconductors.* Journal of Photochemistry & Photobiology, A: Chemistry, 1995. **85**(3): p. 247-255.

107. Shukla, P., et al., *Photocatalytic oxidation of phenolic compounds using zinc oxide and sulphate radicals under artificial solar light.* Separation and Purification Technology, 2009.

108. Villasen8or, J., P. Reyes, and G. Pecchi, *Photodegradation of Pentachlorophenol on ZnO.* J. Chem. T echnol. Biotechnol, 1998. **72**: p. 105È110.

109. Akyol, A., H.C. Yatmaz, and M. Bayramoglu, *Photocatalytic decolorization of Remazol Red RR in aqueous ZnO suspensions.* Applied Catalysis B, Environmental, 2004. **54**(1): p. 19-24.

110. Khodja, A.A., et al., *Photocatalytic degradation of 2-phenylphenol on TiO2 and ZnO in aqueous suspensions.* Journal of Photochemistry & Photobiology, A: Chemistry, 2001. **141**(2-3): p. 231-239.

111. Khalil, L.B., W.E. Mourad, and M.W. Rophael, *Photocatalytic reduction of environmental pollutant Cr (VI) over some semiconductors under UV/visible light illumination.* Applied Catalysis B, Environmental, 1998. **17**(3): p. 267-273.

112. Doong, R. and W. Chang, *Photoassisted titanium dioxide mediated degradation of organophosphorus pesticides by hydrogen peroxide.* Journal of Photochemistry & Photobiology, A: Chemistry, 1997. **107**(1-3): p. 239-244.

113. Agustina, T.E., H.M. Ang, and V.K. Vareek, *A review of synergistic effect of photocatalysis and ozonation on wastewater treatment.* Journal of Photochemistry & Photobiology, C: Photochemistry Reviews, 2005. **6**(4): p. 264-273.

114. Dhanalakshmi, K.B., et al., *Photocatalytic degradation of phenol over TiO2 powder: The influence of peroxomonosulphate and peroxodisulphate on the reaction rate.* Solar Energy Materials and Solar Cells, 2007.

115. Malato, S., et al., *Enhancement of the rate of solar photocatalytic mineralization of organic pollutants by inorganic oxidizing species.* Applied Catalysis B, Environmental, 1998. **17**(4): p. 347-356.

116. Wang, Y. and C. Hong, *Effect of hydrogen peroxide, periodate and persulfate on photocatalysis of 2-chlorobiphenyl in aqueous TiO2 suspensions.* Water Research, 1999. **33**(9): p. 2031-2036.

117. Ball, D. and J. Edwards, *The kinetics and mechanism of the decomposition of Caro's Acid. I.* Journal of the American Chemical Society, 1956. **78**(6): p. 1125-1129.

118. Bouchard, J., et al., *Kraft pulp bleaching using dimethyldioxirane: stability of the oxidants.* Canadian Journal of Chemistry, 1996. **74**(2): p. 232-237.

119. Tsukada, S., et al., *Chemiluminescence from fluorescent organic compounds induced by cobalt (II) catalyzed decomposition of peroxomonosulfate.* Analytica Chimica Acta, 1998. **371**(2-3): p. 163-170.

120. George, P.A. and D.D. Dionysiou, *Degradation of organic contaminants in water with sulfate radicals generated by the conjunction of peroxymonosulfate with cobalt.* Environ Sci Technol, 2003. **37**: p. 4790-4797.

121. George, P. and D. Dionysiou, *Degradation of organic contaminants in water with sulfate radicals generated by the conjunction of peroxymonosulfate with cobalt.* Environ Sci Technol, 2003. **37**: p. 4790-4797.

122. Francis, R., et al., *Alkali-and metal-induced decomposition of peroxymonosulfate, TAPPI JOURNAL, June 1994, Vol. 77 (6).* Tappi journal, 1994. **77**(6).

123. Fernandez, J., et al., *Bleaching and photobleaching of Orange II within seconds by the oxone/Co2+ reagent in Fenton-like processes.* Applied Catalysis B, Environmental, 2004. **49**(3): p. 207-215.

124. Madhavan, J., et al., *Kinetics of degradation of acid red 88 in the presence of Co2+-ion/peroxomonosulphate reagent.* Applied Catalysis A, General, 2009. **368**(1-2): p. 35-39.

125. Kim, J. and J. Edwards, *A study of cobalt catalysis and copper modification in the coupled decompositions of hydrogen peroxide and peroxomonosulfate ion.* Inorganica Chimica Acta, 1995. **235**(1-2): p. 9-13.

126. Chen, X., et al., *Kinetics of oxidative decolorization and mineralization of Acid Orange 7 by dark and photoassisted Co2+-catalyzed peroxymonosulfate system.* Chemosphere, 2007. **67**(4): p. 802-808.

127. ANIPSITAKIS, G., E. STATHATOS, and D. DIONYSIOU, *Heterogeneous activation of oxone using Co 3 O 4.* Journal of physical chemistry. B, Condensed matter, materials, surfaces, interfaces, & biophysical chemistry, 2005. **109**(27): p. 13052-13055.

128. Chen, X., et al., *Performance of nano-Co3O4/peroxymonosulfate system: kinetics and mechanism study using acid orange 7 as a model compound.* Applied Catalysis B, Environmental, 2008. **80**(1-2): p. 116-121.

129. Nwankwo, J. and A. Turk, *Rapid evaluation of oxidation catalysts supported on activated carbon.* Carbon, 1975. **13**(6): p. 495-499.

130. Prodan, L.N., A.M. Koganovskii, and V.I. Kofanov, *Catalytic regeneration of active carbon saturated with SAS, dye, and phenol.* Soviet Journal of Water Chemistry and Technology, 1988. **10**(3): p. 122-124.

131. Matatov-Meytal, Y.I. and M. Sheintuch, *Abatement of pollutants by adsorption and oxidative catalytic regeneration.* Ind. Eng. Chem. Res, 1997. **36**(10): p. 4374-4380.

132. Wang, Y.H., et al., *Adsorption Removal of Phenol in Water and Simultaneous Regeneration by Catalytic Oxidation.* Environmental Engineering Science, 2005. **22**(5): p. 608-614.

133. Polaert, I., A.M. Wilhelm, and H. Delmas, *Phenol wastewater treatment by a two-step adsorption-oxidation process on activated carbon.* Chemical Engineering Science, 2002. **57**(9): p. 1585-1590.

134. Huang, H.H., et al., *Catalytic decomposition of hydrogen peroxide and 4-chlorophenol in the presence of modified activated carbons.* Chemosphere, 2003. **51**(9): p. 935-943.

135. Huang, H.H., M.C. Lu, and J.N. Chen, *Catalytic decomposition of hydrogen peroxide and 2-chlorophenol with iron oxides.* Water Research, 2001. **35**(9): p. 2291-2299.

136. Huling, S.G., et al., *Fenton-driven chemical regeneration of MTBE-spent GAC.* Water Research, 2005. **39**(10): p. 2145-2153.

137. Huling, S.G., R.G. Arnold, and R.A. Sierka, *Contaminant adsorption and oxidation via the fenton reaction*. 2008, Google Patents.

138. Huling, S.G., et al., *Repeated reductive and oxidative treatments of granular activated carbon.* Journal of environmental engineering, 2005. **131**: p. 287.

139. Kan, E. and S.G. Huling, *Effects of temperature and acidic pre-treatment on Fenton-driven oxidation of MTBE-spent granular activated carbon.* Name: Environmental Science and Technology, 2009. **43**(5).

140. Huling, S.G., E. Kan, and C. Wingo, *Fenton-driven regeneration of MTBE-spent granular activated carbon—Effects of particle size and iron amendment procedures.* Applied Catalysis B, Environmental, 2009. **89**(3-4): p. 651-658.

141. Toledo, L.C., et al., *Application of Fenton's reagent to regenerate activated carbon saturated with organochloro compounds.* Chemosphere, 2003. **50**(8): p. 1049-1054.

142. Mourand, J.T., et al., *Regeneration of spent adsorbents using homogeneous advanced oxidation.* Water Environment Research, 1995: p. 355-363.

143. Doocey, D.J., et al., *Zeolite-Mediated Advanced Oxidation of Model Chlorinated Phenolic Aqueous Waste Part 2: Solid Phase Catalysis.* Process Safety and Environmental Protection, 2004. **82**(5): p. 359-364.

144. Huling, S.G., P.K. Jones, and T.R. Lee, *Iron optimization for Fenton-driven oxidation of MTBE-spent granular activated carbon.* Environmental science & technology, 2007. **41**(11): p. 4090-4096.

145. Fajerwerg, K. and H. Debellefontaine, *Wet oxidation of phenol by hydrogen peroxide using heterogeneous catalysis Fe-ZSM-5: a promising catalyst.* Applied Catalysis B, Environmental, 1996. **10**(4): p. 229-235.

146. Ramirez, J.H., et al., *Azo-dye Orange II degradation by heterogeneous Fenton-like reaction using carbon-Fe catalysts.* Applied Catalysis B, Environmental, 2007. **75**(3-4): p. 312-323.

147. Zazo, J.A., et al., *Catalytic wet peroxide oxidation of phenol with a Fe/active carbon catalyst.* Applied Catalysis B, Environmental, 2006. **65**(3-4): p. 261-268.

148. Georgi, A. and F.D. Kopinke, *Interaction of adsorption and catalytic reactions in water decontamination processes Part I. Oxidation of organic contaminants with hydrogen peroxide catalyzed by activated carbon.* Applied Catalysis B, Environmental, 2005. **58**(1-2): p. 9-18.

149. Kwan, W.P. and B.M. Voelker, *Influence of electrostatics on the oxidation rates of organic compounds in heterogeneous Fenton systems.* Environ. Sci. Technol, 2004. **38**(12): p. 3425-3431.

3

3 - Adsorption of Phenolic Contaminants from Water: An Insight into Multicomponent Adsorption Isotherms

Abstract

The chapter focuses on the multicomponent adsorption of phenolic compounds from solution onto an activated carbon. The effects of competitive sorption in batch systems were comprehensively studied at higher concentration of the competing adsorbate. The observed adsorption isotherms were correlated using some known multicomponent adsorption isotherm equations. An improved adsorption isotherm based on the Butler and Ockrent multicomponent adsorption model was proposed and it provided good correlations with the experimental data. This model proposes that the maximum monolayer capacity of any adsorbate in a multicomponent system is variable and depends on the concentration of the competing adsorbate. The model employs a correction factor to integrate the change in the monolayer capacity due to the adsorption of the competing adsorbate.

3.1 Introduction

Adsorption processes for treating industrial wastewater, as well as contaminated surface and groundwater, are attracting significant attention. However, applications of adsorption for environmental remediation differ considerably from the adsorption processes used in process industries. The latter generally involves a known contaminant and usually seeks to recover a particular component from solution, but in environmental remediation the type of contaminant is generally unknown and the number of adsorbate is certainly more than one. In general, contaminated groundwater and surface water have a variety of pollutants arising either from a source or from the conversion of parent contaminants via biochemical reactions.

Activated carbon shows a great potential for use in water treatment due to its efficiency in adsorbing several groups of organic pollutants over a wide range of concentration. Enormous research has been conducted on the use of activated carbon for removing phenol from water, but most of those studies are focused on single-component adsorption. An excellent study of single-component phenolic pollutant adsorption on activated carbon has been reported by Hamdaoui and Naffrechoux [1]. They critically analyzed the adsorption isotherms obtained from two- and three-parameter model equations. However, the parameters obtained from single-component adsorption may not successfully represent adsorption equilibrium in multicomponent systems. The variation is more prominent in liquid adsorption than in gaseous adsorption because of interactions between adsorbate and the solvent (generally water). This has motivated the development of various modified equations to estimate the equilibrium in multicomponent systems.

Among earlier work, the Langmuir competitive adsorption model proposed by Butler and Ockrent [2] and the model proposed by Fritz and Schluender [3] have been used successfully for phenol and nitrophenols. A modified Freundlich model has been proposed by Sheindorf et al. [4] for a multicomponent system of bromophenol and nitrophenol in an aqueous medium. Jain and Snoeyink [5] proposed a model for adsorption of competing anionic species; the model was also successfully applied to adsorption of substituted phenols [6]. Most of these models are based on the equilibrium between rates of adsorption and desorption of components in the system. However, the ideal adsorption solution theory (IAST) proposed by Radke and Prausnitz [7] is based on the thermodynamic equivalence of the spreading pressure

of the adsorbed species and that of each component in a standard state; the model has been used to analyze the multicomponent adsorption of resorcinol and phenol. Due to its sound thermodynamic basis, this model has gained wide popularity; however, the model equations are complex and cumbersome to solve. This motivated LeVan and Vermeulen [8] to propose an analytical solution using the Langmuir and Freundlich isotherms. The IAST model has been further improved by Costa to incorporate the nonideality of the solution, resulting in a real adsorption solution theory (RAST) that has been applied to multicomponent gaseous adsorption [9].

Most single-component models and a few multicomponent models were initially developed for gaseous adsorption, and later they were modified to apply to liquid adsorption. Unfortunately these models fail to take into account the effects of adsorbate-adsorbate interactions, adsorbate-water interactions, and surface defects (which act as a sink with a high potential for adsorption). Such interactions are important in multicomponent systems, where each component has different molecular partial charges and thus interacts differently. To consider the effects of surface heterogeneity, Hoory and Prausnitz [10] incorporated the energy distribution at different sites of adsorbent in the IAST and proposed a heterogeneous ideal adsorption solution theory (HIAST). In a further development, Hu and Do [9] have shown that the HIAST is better than IAST for predicting adsorption in multicomponent systems.

Nitta et al. [11] have proposed an adsorption model for both homogeneous and heterogeneous adsorbent surfaces based on the theory of equipotential between surface and adsorbed molecules. These isotherms take into account the reduced chemical potential of the adsorbate due to its interaction with the neighboring adsorbate in a multicomponent system. A more conventional adsorption model has also been proposed for surface heterogeneity [12]. Jovenic modified conventional adsorption models to account for surface heterogeneity, which was further extended to multicomponent systems [12]. Recently, Ho and McKay [13] proposed a modified Butler and Ockrent isotherm, wherein they incorporated the effects of adsorbate interactions in multicomponent systems. The model has been successfully employed to predict multicomponent adsorption of heavy metals from water; they observed that the interaction coefficient depends on the surface coverage of the adsorbent. In a similar approach Yonge and Keinath [14] have suggested an improvement in the

simplified IAST model to account for nonideality in the mixture and adsorbent heterogeneity.

The present study focused on single and multicomponent adsorption on activated carbon. The adsorbates are phenol and its halo substitutes. Phenol and its analogues are recognized as priority pollutants by several environmental agencies including the USEPA. Phenols are mostly released by petroleum and petrochemical industries, petroleum refineries, wood-processing industries, coal conversion plants, and phenol-processing industries. Apart from these industrial sources, chlorophenols have also been found in a few contaminated sites due to the degradation of larger molecules like hexachlorocyclohexanes [15, 16]. Phenols are strong skin irritants and consumption of water containing these compounds leads to severe pain, vomiting, and capillary damage. Toxic effects occur in the brain, lungs, kidney, liver, pancreas, and spleen [17]. Some phenolic compounds are recognized carcinogens.

The study investigated the applicability of existing adsorption models to multicomponent systems containing a liquid phase with high concentrations of a competing adsorbate. Most previous studies of multicomponent systems have focused on small ranges of concentration but in the current research, significantly larger ranges of concentration were studied, and various models were analyzed and compared. Finally, an empirical model was proposed and correlated with experimental observations. This model is based on the assumption that the monolayer capacity of the adsorbent for any particular adsorbate is not fixed, as has been assumed in the past; rather, the capacity changes (a) in the presence of a competing adsorbate and (b) with the concentration of the competing adsorbate. The model has the advantage of requiring simple calculations compared to those required by older, more complex models.

3.2 Materials and Methods

3.2.1 Adsorbent and Reagents

A granular activated carbon obtained from Picacarb having the surface area of 944 m^2/gm was used as the adsorbent. The adsorbent was initially ground to a particle size of 250 μm and then washed several times with distilled water and dried in an oven. Diluted solutions of phenol (Ph), 2-chlorophenol (CP), 2,4-dichlorophenol

(DCP), and 2,4,6-trichlorophenol (TCP) were used as adsorbates. All chemicals were purchased from Biolabs with purities greater than 99.5%. The test solution was prepared using ultra high purity water (resistance greater than 16 μΩ). The properties of the adsorbates are shown in Table 3.2-1.

Table 3.2-1 Properties of Adsorbates

	Phenol	Chlorophenol	Di-Chlorophenol	Tri-Chlorophenol
Molecular Formula	C_6H_5OH	C_6H_5OCl	$C_6H_4OCl_2$	$C_6H_3OCl_3$
Molar Mass	94.11	128.56	163.01	197.45
Density	1.07	1.262	1.383	1.675
Solubility (g/l)	83.0	26	4.5	0.85
pKa	9.95	9.2	7.7	6.1

3.2.2 Equilibrium Tests

3.2.2.1 Single-Component Adsorption Analysis

Adsorption tests were carried out in 30 ml bottles, wherein a fixed amount of adsorbent (approx 0.01 g) was added to phenolic solutions of varying concentrations. Adsorbate concentrations ranged from 50 to 500 ppm. The upper limit of concentration was selected at less than 50% of the solubility of trichlorophenol (the least soluble phenolic compound under consideration) to prevent over flooding of the solution and ensure that the solute was well-dissolved in water. The solutions were filled exactly to the tops of the sample bottles, and the tops were sealed properly to prevent any loss by evaporation. The bottles were kept in an incubator shaker, set at 25°C and 200 rpm, for three days to achieve equilibrium. To prevent any competition for adsorption from a buffer reagent, no buffer was added to control the pH. Thus, adsorption would be assumed to occur by combined molecular and ionic species. A one ml sample was acquired from the sample bottles using a syringe filter and analyzed on a HPLC having a UV detector at a fixed wavelength of 270 nm. The mobile phase used for transporting the sample in the column was a 30% acetonitrile-water mixture flowing at 1.50 ml/min. To ensure no loss in the filter, the syringe filters were flushed with the samples twice before taking the one ml sample for analysis. Blank samples without any adsorbent were also kept with the experimental samples

to monitor any change in concentration due to evaporation or precipitation; analyses of the blanks showed negligible losses of phenols.

3.2.2.2 Multicomponent Adsorption Analysis

Multicomponent Adsorption study have been conducted by two different schemes

Scheme A: The procedure for studying multicomponent adsorption was similar to that for single-component systems, except that the solutions were prepared with the desired numbers of adsorbates and concentrations. Again, the upper limit in concentration was selected at less than 50% of the solubility of trichlorophenol. The initial mixture for the binary adsorption study was carried out for these six adsorbate combinations: Ph-CP, Ph-DCP, Ph-TCP, CP-Ph, CP-DCP, and CP-TCP. In all six cases, the adsorption equilibrium was studied by varying the feed concentration of the first component from 50-500 ppm whereas the feed concentration of 2^{nd} component was fixed at 100 ppm.

Scheme B: In this experiments we conducted for the binary adsorption equilibrium of Ph-CP and Ph-DCP and Ph-TCP. In this scheme, the adsorption equilibrium was studied by varying the feed concentration of both components equally from 50-500 ppm.

Due to the complexity of the systems in the presence of competing adsorbates at high concentrations and the heterogeneity of the adsorbent sample, it was not surprising that the results varied between 1% and 10% over different runs; in contrast, results from the single-component systems were much more consistent. All experiments were conducted in duplicate and multicomponent adsorption samples were run in triplicate; the resulting mean values were used in calculations.

3.3 Single-Component Isotherms

Most multicomponent models are predictive models; i.e., the model predicts adsorption isotherms based on the parameters estimated from single-component isotherms. Thus, single-component adsorption modeling was performed prior to multicomponent analyses; two- and three-parameter isotherms were obtained from the Langmuir, Freundlich, Sipps, Dual Sorption Model (DSM), Nitta, and Fowler and

Guggenheim models. The resulting isotherm parameters were then utilized in the respective multicomponent isotherm analyses.

3.3.1 Langmuir Model

The Langmuir equation is one of the premier isotherm models and is derived based on the equality achieved by adsorption and desorption of an adsorbate on adsorbent [18]. The model equation is

$$q = \frac{q_m bc}{1 + bc}$$ Equation 3.3-1

This model can be easily converted into an explicit form to obtain the constant q_m, which represents the monolayer capacity, and the adsorption constant b.

3.3.2 Freundlich Model

The Freundlich equation is

$$q = K_F c^{1/n}$$ Equation 3.3-2

Although this model was initially proposed empirically, it can be justified on a theoretical basis. The constant n is related to the favorability for adsorption and the constant K_F is symptomatic of an adsorbent's adsorption capacity.

3.3.3 The Dual Sorption Model (DSM)

Initially proposed by Vieth and Sladek [19], this model assumes that adsorption equilibrium is a two-step equilibration process in which some solute dissolves in the partition medium and the remaining is adsorbed onto adsorption sites. This is basically a combination of Henry's law and the Langmuir model [20] and is written as

$$q = Kc + \frac{q_m bc}{1 + bc}$$ Equation 3.3-3

The constants q_m and b are obtained from the Langmuir equilibrium model, and K is the film rate transfer constant.

3.3.4 Sipps Model

A three-parameter model is expected to give a better fit to experimental data due to the presence of a third degree of freedom. In the Sipps equation the effects of kinetic equality in adsorption and desorption are combined with an exponential increment in the surface concentration of the adsorbate. The equation is

$$q = \frac{q_m b c^{1/n}}{1 + b c^{1/n}} \qquad \text{Equation 3.3-4}$$

The nomenclature is as defined in the previous models.

3.3.5 Nitta et al. Model

The models discussed so far, although derived by simple kinetic-thermodynamic equilibrium, tend to overlook surface heterogeneity and adsorbate-adsorbate interactions. However, a new generation of model, such as that from Nitta et al., takes nonidealities into account. The equation accounting for adsorbate-adsorbate interactions is [11]

$$nK_n c = \frac{\theta}{(1-\theta)^n} \exp[-n\alpha\theta] \qquad \text{Equation 3.3-5}$$

Here, the parameter *n* accounts for the number of sites occupied by each adsorbate, θ is the relative adsorption with respect to the maximum single-component adsorption, and α accounts for adsorbate interactions. The factor α depends on molecular interactions, Boltzmann's constant, and temperature. The model reduces to the Langmuir model for n = 1 and α = 1. The model reduces to the Fowler isotherm if a molecule is assumed to occupy only one site in the adsorbent (n = 1):

$$Kc = \frac{\theta}{(1-\theta)} \exp[\gamma\theta] \qquad \text{Equation 3.3-6}$$

Here γ is the adsorbate interaction constant and is a function of temperature [21].

3.4 Multicomponent Adsorption Isotherms

3.4.1 Butler and Ockrent Model

This model extends the Langmuir model to multicomponent systems. The equation is derived on the Langmuirian assumption that adsorption equilibrium is achieved when adsorption and desorption reach kinetic equilibrium. The adsorption rate of each component is proportional to (a) the concentration of that component in solution and (b) the fraction of unoccupied surface on the adsorbent. The desorption rate of each component is proportional to the amount of adsorption of that component. For components *j* = 1, 2, 3, …, the isotherm is given by

$$q_j = \frac{q_{mj} b_j c_j}{1 + b_1 c_1 + b_2 c_2 + ...}$$

Equation 3.4-1

The major limitation of this model is that it is based on the kinetic equilibrium of adsorption and desorption for every component, irrespective of the effects of the presence of the neighboring adsorbate. More importantly, the model is thermodynamically limited for the adsorbates having similar maximum monolayer adsorption capacities. The nomenclature is as defined in the previous models.

3.4.2 Competitive Dual Sorption Model (CDSM) Theory

The DSM model has been extended to multicomponent systems by Koros as referenced by Song et al. [22]. The multicomponent version of the model makes the same assumptions as the single-component DSM model. For any number of component *j*, the Competitive Dual Sorption Model is

$$q_i = K_i c_i + \frac{q_{mi} b_i c_i}{1 + \sum_{j=1}^{n} b_j c_j}$$

Equation 3.4-2

Values for the parameters are determined from single-solute adsorption isotherms.

3.4.3 IAS Theory

This theory was initially proposed by Radke and Prausnitz [23] and is based on the thermodynamics of multicomponent adsorption. The theory assumes equivalent

spreading pressures between the mixture and species in a standard state. A simple algorithm has been proposed for applying the model to gaseous systems; that approach can be easily modified for liquid-phase adsorption and is given below [18].

An Algorithm for estimating the adsorption using IAST

Step 1: Obtain the equilibrium concentration of each component in the liquid phase. Obtain the single component adsorption isotherm parameters.

Step 2: Predict an initial value of spreading pressure. The following equation can be used to get a good initial estimate

$$z = \sum_{1}^{n} \int_{0}^{c} \frac{q_i}{c_i} dc_i \quad , \qquad \text{Equation 3.4-3}$$

wherein qi can be substituted by the single component isotherm, such as the Langmuir, Freundlich, Sipps etc. In the current work, it was observed that Freundlich model fails to predict the single component isotherm, hence IAS theory based on Langmuir and Sipps model was used for prediction. Using the Langmuir and Sipps Isotherm the above equation can be simplified as:

For Langmuir isotherm

$$z = q_{avg} \ln\left(1 + \sum_{i}^{n} b_i c_i\right) \qquad \text{Equation 3.4-4}$$

For Sipps isotherm

$$z = n q_{avg} \ln\left(1 + \sum_{i}^{n} (b_i c_i)^{1/n}\right) \qquad \text{Equation 3.4-5}$$

where q_{avg} is the mean of the maximum adsorption capacity of each component.

Step 3: Estimate the hypothetical pure component concentration which gives the same spreading pressure as that of the mixture, as per the relations given below

For Langmuir isotherm

$$c_i^0 = \frac{1}{b_i}\left[\exp\left(\frac{z}{q_{mi}}\right) - 1\right]$$

Equation 3.4-6

For Sipps isotherm

$$c_i^0 = \frac{1}{b_i}\left[\exp\left(\frac{z}{n_i q_{mi}}\right) - 1\right]^{n_i}$$

Equation 3.4-7

Step 4: Knowing the hypothetical pure component concentration, estimate the new value of Z from the following relations given below,

$$z^{k+1} = z^k - \frac{F(z^k)}{F^{!}(Z^k)}$$

Equation3.4-8

Where the function and the first derivative of Z is given as

$$F(z^k) = \sum_1^n \frac{c_i}{c_i^0} - 1$$

Equation 3.4-9

$$F^1(z^k) = \left[-\sum_1^n \frac{c_i}{c_i^0 q_i^0}\right]$$

Equation 3.4-10

where q_i^0 is obtained from the single component adsorption isotherm equation with concentration as c_i^0.

Step 5: Knowing the new value of Z, go back to step 3 to estimate a new value of hypothetical pure component concentration, further moving to step 4. Keep iterating until the change in value of z is negligible.

Step 6: Knowing the value of c_i^0, estimate the value of $x_{i,}$ from the relation,

$$c_i = x_i c_i^0$$

Equation 3.4-11

And then estimate the total equilibrium adsorption as

$$\frac{1}{q_t} = \sum_1^n \frac{x_i}{q_i^0}$$

Equation 3.4-12

And the individual adsorption of each component is as

$$q_i = x_i q_t \qquad \text{Equation 3.4-13}$$

For the purpose of application, the above algorithm was coded in MATLAB and used for the calculation.

Although this model is thermodynamically sound, it requires cumbersome calculations; therefore, LeVan and Vermeulen [8] proposed a simplified analytical solution for the IAS theory for two- and three-component adsorption. In terms of liquid concentrations, this simplified theory is

$$q_i = \frac{\overline{Q} c_i}{1 + c_1 + c_2} + \Delta_{L2} \qquad \text{for two-component systems} \qquad \text{Equation 3.4-14}$$

$$q_i = \frac{\overline{Q} c_i}{1 + c_1 + c_2} + \Delta_{L2}\left(1 + \Delta_{L3}\right) \qquad \text{for three-component system} \qquad \text{Equation 3.4-15}$$

Here, Δ_{L2} and Δ_{L3} are concentration related factors.

3.4.4 Fowler-Guggenheim Model (F-G)

Similar to single-component models, the above multicomponent models are based on a kinetic or thermodynamic balance of adsorption equilibrium on a homogeneous surface. Unfortunately, every adsorbent has a heterogeneous surface with defects and potential sinks at different locations. Thus, the assumption of uniform surface adsorption is invalid. Nitta's model and its simplified version, the Fowler-Guggenheim model, incorporate parameters to account for those nonidealities. The generalized model can be written as

$$K_1 c_1 = \frac{\theta_1}{(1 - \theta_1 - \theta_2)} \exp\left[-\gamma_1 \theta_1 - \gamma_{12} \theta_2\right] \qquad \text{Equation 3.4-16}$$

Here γ_1 refers to the interaction of the first molecule and γ_{12} refers to the cross interaction between two molecules.

3.4.5 Modified Butler and Ockrent Theory

The Butler and Ockrent theory was an extension of the Langmuir theory to a multicomponent system; however, it fails to consider adsorbate-adsorbate interactions. The model was modified by Ho and McKay to include the mutual adsorbate interaction through a factor η [13]. Unlike the Nitta and Fowler model, the interaction factor in this model has not been derived from molecular interaction properties; instead, it is correlated with the relative adsorption of each component. For components *i* = 1, 2, 3, …, the modified model is

$$q_i = \frac{q_{mi} b_i \eta_i c_i}{1 + b_1 \eta_1 c_1 + b_2 \eta_2 c_2 + ...}$$

Equation 3.4-17

Although this model was proposed empirically, it can be easily derived by a slight modification of the Butler and Ockrent equations as shown below.

3.4.5.1 Derivation of Modified Butler and Ockrent Theory

Assuming η is the refinement of the interaction factor b. This can be considered as the factor affecting the movement or the adsorption of molecules onto the surface. Desorption is generally dependent only on the amount of molecules adsorbed and seldom gets affected by the type and concentration in the liquid phase. Thus, assuming that the rate of adsorption depends on the concentration of the adsorbate, the fraction of unoccupied surface and the extent of interaction between the adsorbate molecules, the rate of adsorption suggested by Butler and Ockrent can be modified as

$$r_{a_1} = \eta_1 k_a c_1 \left(1 - \theta_1 - \theta_2\right)$$

Equation 3.4-18

(Assuming γ as total adsorption in the adsorbent for a given component)

And the rate of desorption can be written as

$$r_{d_1} = k_d \left(\theta_1\right)$$

Equation 3.4-19

This at equilibrium becomes

$\eta_1 b_1 c_1 (1-\theta_1-\theta_2) = (\theta_1)$ **component 1** Equation 3.4-20

$\eta_2 b_2 c_2 (1-\theta_1-\theta_2) = (\theta_2)$ **component 2** Equation 3.4-21

(where $b = k_a/k_d$)

On further solving the above two equations simultaneously results in the modified Butler and Ockrent Model.

The interaction factor η has been observed to be related to the component concentration in the solid,

$$\eta = \eta_0 \left(\frac{q_i}{q_m} \right)^n \qquad \text{Equation 3.4-22}$$

The biggest disadvantage of this model is that it is not predictive: the interaction factor η must be obtained from the equilibrium concentration on the adsorbent.

3.4.6 Empirical Model

The two popular multicomponent adsorption isotherms, viz the Butler and Ockrent Theory and the Modified Butler and Ockrent theory, tends to neglect the change in the monolayer capacity of the adsorbent for the compound under consideration in the presence of the competing adsorbate. In both models the maximum monolayer capacity 'q_m' is considered equal to the single component maximum monolayer capacity of the component under focus. Thus for the adsorption of phenol on activated carbon from the mixture of phenol and chlorophenol, the maximum monolayer capacity in the Butler and Ockrent theory is to be equal to that of the pure component maximum monolayer capacity of phenol. Thus unfortunately makes the model thermodynamically inconsistent. In-order to overcome this limitation, Do [18] proposed to replace the 'q_m' in the multicomponent system as the average of the pure component monolayer capacity of phenol and chlorophenol as follows

$$q_m = \frac{q_{mPh} + q_{mCP}}{2} \qquad \text{Equation 3.4-23}$$

However, the above equation is still an approximation to the actual monolayer capacity in a multicomponent system.

As discussed briefly in Appendix A, the Butler and Ockrent theory is based on a simple kinetic balance of adsorption and desorption occurring on occupied and unoccupied sites of an adsorbent surface. In quantitative terms the total adsorption of an individual component is the product of the fraction of sites and the maximum monolayer capacity. Thus quantitatively, the total adsorption in a multicomponent system would be affected not only by the reduced number of sites, due to competition with other molecules, but also by the change in the total maximum adsorption capacity of that molecule in the competitive environment.

It has been observed that the maximum monolayer adsorption capacity of an adsorbent in a single-component system differs from that in a multicomponent system. In a multicomponent system, the maximum adsorption capacity of the adsorbent for an individual adsorbate generally decreases due to the presence of competing adsorbates, so fewer adsorption sites are available. However, in a few multicomponent systems, the maximum adsorption capacities of certain components are enhanced relative to those in single-component systems. This is generally observed for the adsorption of preferentially adsorbed components over weakly adsorbed components. A similar observation has been reported by Çeçen [24].

In spite of several observations of the change in the maximum adsorption capacity of the adsorbent, few attempts have been made to include mathematical representations of the phenomenon in models. To account for the changes in the maximum monolayer adsorption capacity of the adsorbent, we propose adding a correction factor to the Butler and Ockrent theory. The correction factor is a lumped parameter that tends to refine the value of q_m for any component. Furthermore, since the change in the maximum adsorption capacity is influenced by the competing adsorbate, it is proposed that the correction factor should be a function of the concentration of the competent adsorbate. Therefore, for components j = 1, 2, 3, …, the resulting model equation is

$$q_j = \frac{[f(c)_j q_{mj}]b_j c_j}{1 + b_1 c_1 + b_2 c_2 + ...}$$

Equation 3.4-24

3.5 Model Fitting and Error Analysis

Regressions of experimental data for both single-component and multicomponent isotherms were performed using the Levenberg-Marquardt algorithm implemented in Polymath software. The adsorption parameters obtained from single-component isotherms were utilized in regression of multicomponent systems. The implicit non-linear equations were solved using the Newton-Raphson algorithm coded in MATLAB.

Model predictions tend to deviate from experimental results, and the deviations are more severe for multicomponent adsorption. For some models the predictions deviate by more than 40% from the experimental results; similar observations have been reported by other authors [25, 26]. Thus, to obtain a numerical expression for the reliability of model prediction, goodness of fit was measured by the correlation coefficient R^2, which was computed by

$$R^2 = \frac{\sum q_i^2 - \sum \left(q_i - q_{m,i}\right)^2}{\sum q_{m,i}^2} \qquad \text{Equation 3.5-1}$$

where *i* stands for the component.

Apart from the correlation coefficient, the average relative error (ARE) and Marquardt's percent standard deviation (MPSD) were estimated by

$$\text{ARE(\%)} = \frac{100}{N}\sum_{i=1}^{N}\left(1-\frac{q_{i,m}}{q_i}\right) \qquad \text{Equation 3.5-2}$$

and

$$\text{MPSD} = 100\sqrt{\frac{1}{N-P}\sum_{i=1}^{N}\left(1-\frac{q_{i,m}}{q_i}\right)^2} \qquad \text{Equation 3.5-3}$$

In these equations, *N* is the number of experimental points and *P* is the number of parameters in the model equation.

3.6 Results and Discussion

3.6.1 Single-Component Adsorption Analysis

3.6.1.1 Experimental Results

Adsorption isotherms for single-component adsorption of various phenolic compounds are presented in

Figure 3.6-1 - 3.6-5.

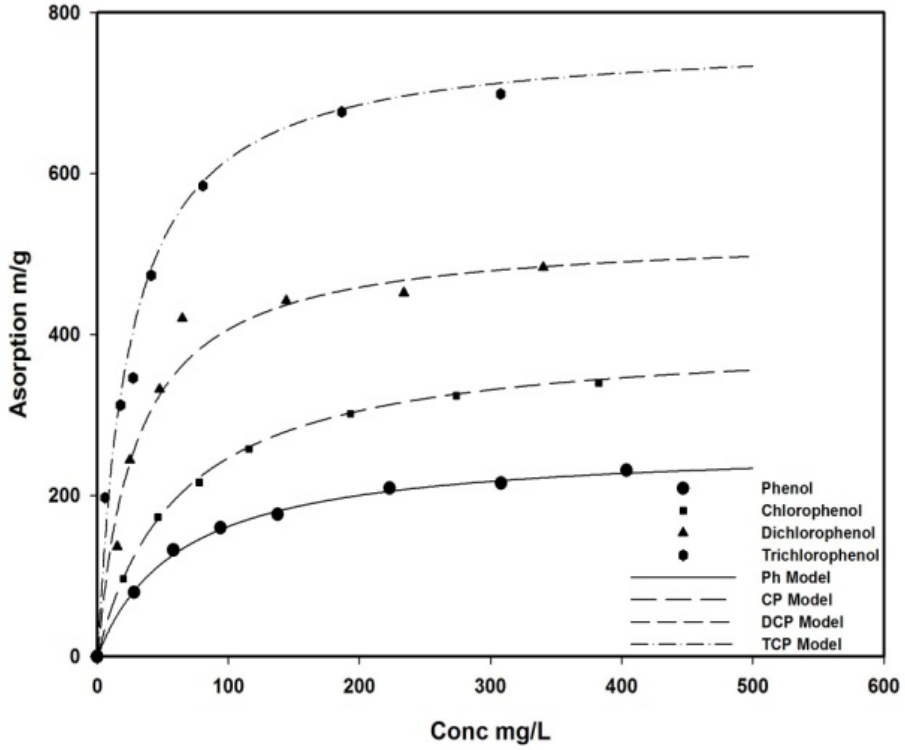

Figure 3.6-1 Single component adsorption and Langmuir modeling

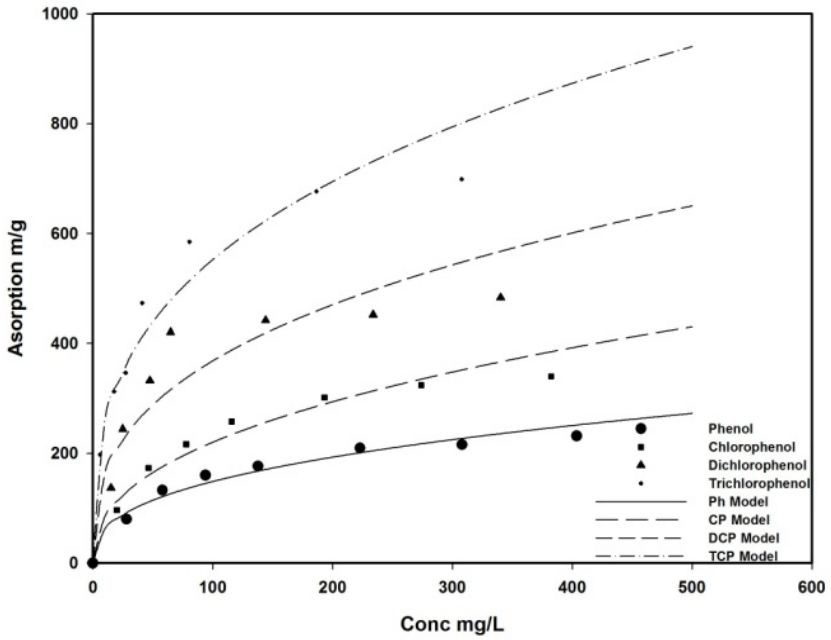

Figure 3.6-2 Single component adsorption and Freundlich modelling

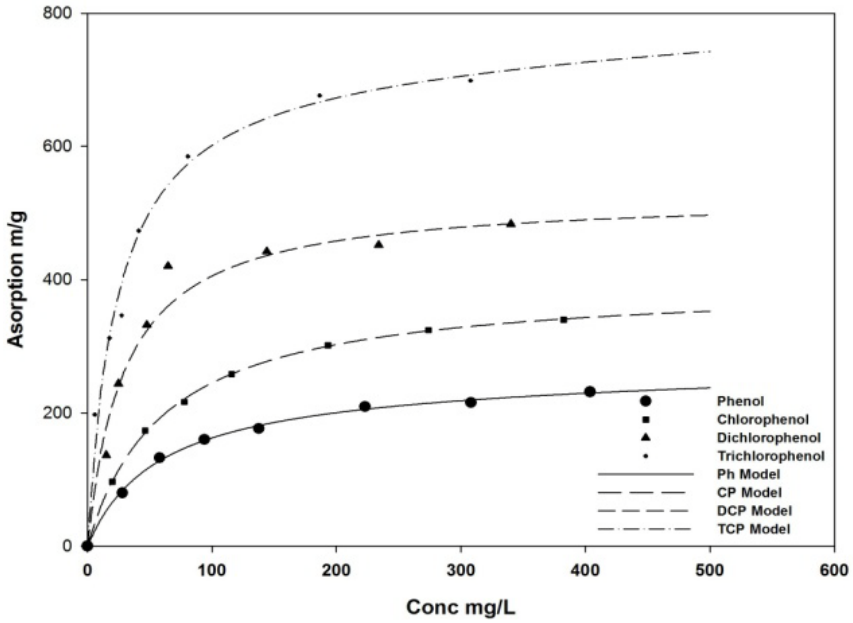

Figure 3.6-3 Single component adsorption and DSM modeling

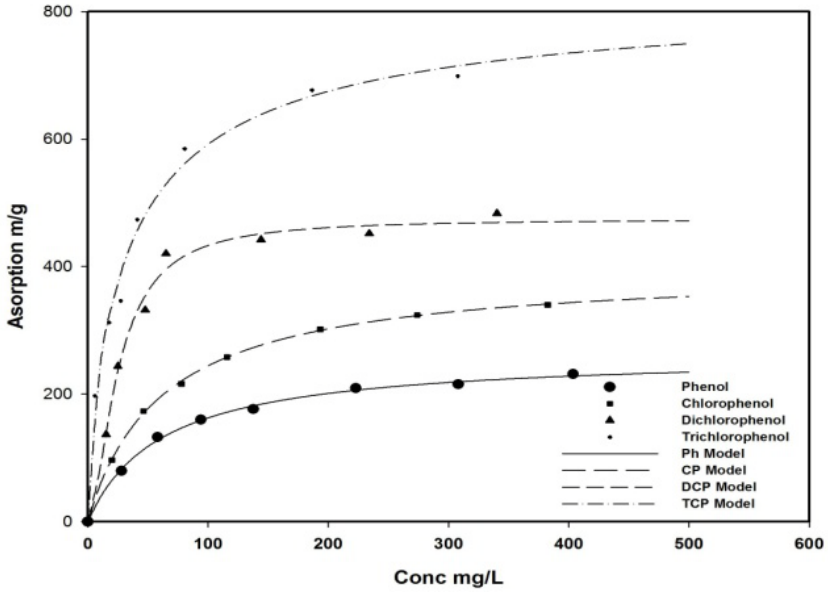

Figure 3.6-4 Single component adsorption and Sipps modelling

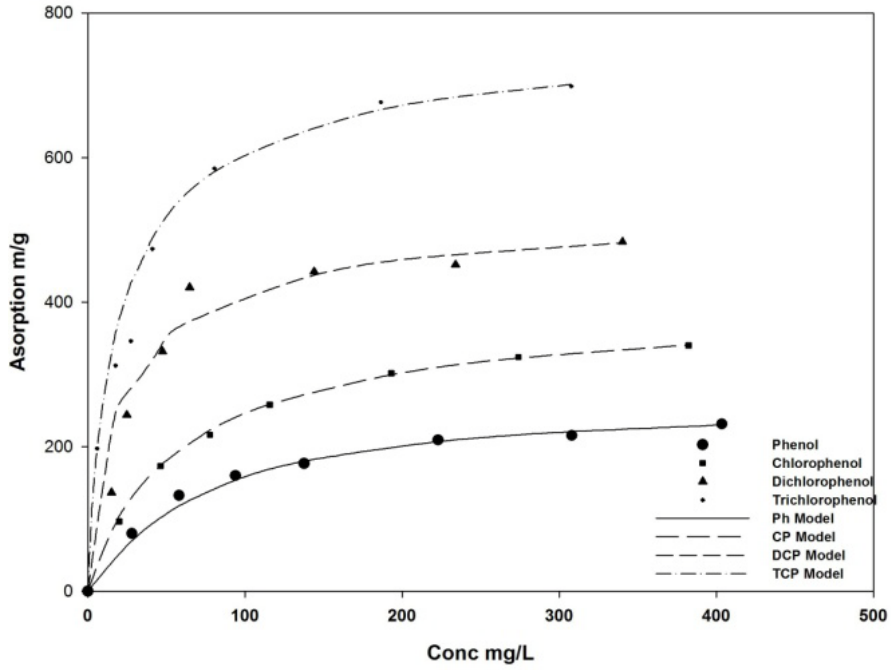

Figure 3.6-5 Single component adsorption and F-G modelling

The figures show an increase in adsorption capacity of activated carbon for phenolic compounds with higher halogenations. All the isotherms show a sharp rise in adsorption at low concentrations, reaching a plateau at higher equilibrium

concentrations. Adsorption increases with more chlorine on the adsorbate molecules: maximum capacities were found to be 263 mg/g for phenol, 400 mg/g for chlorophenol, 526 mg/g for dichlorophenol, and 769 mg/g for trichlorophenol. This trend has been attributed to various adsorbate properties, such as solubility, molecular weight, and molecular cross-sectional area [27] [1].

The adsorption mechanism of aromatic compounds on activated carbon is generally known to occur by an electron acceptor-donor mechanism. The functional groups (generally carboxyl group) present on the adsorbent tend to bond with the aromatic ring of phenols by electron transfer [28, 29]. In the case of substituted phenols, chlorine as an electron donor tends to reduce the electron density around the aromatic ring of the adsorbate; this results in enhanced adsorption as the number of halogen group is increased on the adsorbate. However, another theory describes the adsorbate-adsorbent interaction as a π interaction between the aromatic rings of the adsorbates and adsorbent, with the adsorbate molecules being arranged flat over the carbon surface [27]. Then, the presence of functional groups on the adsorbate (as in the case of chlorophenols) would reduce the electron density around the adsorbate, implying that a smaller electron density is available for the π interaction, resulting in less adsorption.

Given the contrasting observations of these two theories, the final adsorption capacity should depend on the number of functional groups present on activated carbon. If the adsorbent has an ample number of surface functional groups, the interaction between the functional groups and the aromatic ring of adsorbate dominates the π interaction between the aromatic rings of the adsorbent and adsorbate. The adsorbent with more functional groups would have higher electron transfer and thus increased adsorption, in spite of lower electron density in the aromatic ring of the adsorbate. Furthermore, given the choice of attracting several different adsorbate molecules, the molecules with higher electron negativity would have higher electron transfer between the functional group of adsorbate and adsorbent, resulting in higher adsorption.

3.6.1.2 Tests of the Models

The adsorption equilibrium data were modeled using five different isotherm models: Langmuir, Freundlich, DSM, Sipps, and F-G. The resulting parameter values are shown in Table 3.6-1. As observed in

Figure 3.6-1, the results from the Langmuir model were in reasonable agreement with the experiments, having R^2 = 0.988. In contrast, Figure 3.6-2 shows that the Freundlich model gives reasonably good predictions for low chlorinated compounds like phenol, but the predictions are not as good for higher chlorinated compounds. Generally, at high equilibrium concentrations, the Freundlich model over predicts the experimental data.

The three-parameter models proposed by Sipps and DSM better fit the observed data, with higher values of R^2, as shown in Table 3.6-2. The Sipps model gives a better correlation coefficient than the Langmuir and Freundlich models. The DSM model shows that the fraction of solute dissolved in the partition medium with respect to the solute immobilized on the surface decreases for higher chlorinated compounds; this suggests that the attractive force is higher for more chlorinated compounds like chlorophenol and dichlorophenol. However, this observation does not hold for trichlorophenol. The DSM model does predict a higher adsorption capacity for trichlorophenol, but it also predicts a significantly larger amount of solute in the partition medium.

Figure 3.6-5 compares the experimental data to the results from the Fowler model assuming a homogeneous surface but including the adsorbate-adsorbate interaction parameterγ. The model gives a suitable fit to the observed data for the similar kinds of adsorbates given in Table 3.6-1. Note that the value of the interaction parameter γ for phenol is positive whereas for the other three adsorbates it is negative. The sign of the parameter γ indicates whether the force among adsorbate molecules is attractive or repulsive. The value of the equilibrium constant *K* increases from phenol to trichlorophenol.

Table 3.6-1 Modelling parameters of single component adsorption

Adsorbate	Langmuir	Freundlich	DSM	Sipps	Fowler
Phenol	q_m: 263.2	K_f: 26.1	K: 0.0244	Q: 264.0	K: 0.0113
	b: 0.0158	n: 0.377	q_m: 4.40	b: 0.0161	γ: 0.481
			b: 0.0175	n: 0.993	
Chlorophenol	q_m: 400	K_f: 32.2	K: 0.0011	Q: 398.7	K: 0.0186
	b: 0.0160	n: 0.417	q_m: 6.42	b: 0.0159	γ: -0.250
			b: 0.0162	n: 0.985	
Dichlorophenol	q_m: 526.1	K_f: 72.1	K: 1.48×10^{-11}	Q: 474.7	K: 0.066
	b: 0.0338	n: 0.354	q_m: 17.63	b: 0.0396	γ: -0.792
			b: 0.0335	n: 1.70	
Trichlorophenol	q_m: 769.2	K_f: 120.5	K: 0.083	Q: 837.9	K: 0.073
	b: 0.0407	n: 0.331	q_m: 30.78	b: 0.0306	γ: -0.857
			b: 0.0419	n: 0.784	

Table 3.6-2 Error analysis of single component adsorption modelling.

Adsorbate	Model	R^2	ARE	MPSD
Phenol	Langmuir	0.988	0.482	2.577
	Freundlich	0.981	0.319	9.469
	DSM	0.999	0.153	2.610
	Sipps	0.998	0.287	2.768
	Fowler	0.998	3.019	7.071
Chlorophenol	Langmuir	0.983	0.607	1.479
	Freundlich	0.967	0.387	10.70
	DSM	0.999	0.026	1.246
	Sipps	0.999	0.019	1.232
	Fowler	0.992	1.259	3.146
Dichlorophenol	Langmuir	0.964	1.883	13.76
	Freundlich	0.969	1.071	19.03
	DSM	0.961	0.190	4.485
	Sipps	0.995	1.646	13.55
	Fowler	0.967	8.426	25.88
Trichlorophenol	Langmuir	0.957	0.093	12.37
	Freundlich	0.966	0.384	10.31
	DSM	0.997	0.458	7.634
	Sipps	0.995	1.857	12.17
	Fowler	0.946	4.843	11.20

3.6.2 Multicomponent Adsorption Analysis

3.6.2.1 Effects of the Presence of Competing Adsorbates

The competitive binary adsorption isotherms for phenol and chlorophenols in the presence of competing adsorbate obtained by multicomponent adsorption test are given in Figure 3.6-6 and Figure 3.6-7, respectively. Each molecule in the solution competes to occupy an adsorption site available on the surface, resulting in a reduced number of adsorption sites available to individual adsorbate molecules when compared with single-component adsorption. Moreover, adsorbate molecules do not tend to share the available sites equally, due to differences in adsorption capacity compared to single-component systems. The adsorbate having the higher tendency to adsorb (preferentially adsorbed component) suppresses the competing adsorbate (weakly adsorbed component) even more. Further, the adsorbate-adsorbate interaction between dissimilar molecules is much higher compared to that of similar molecules in single-component adsorption, resulting in a further decrease in adsorption capacity for the weakly adsorbed component as compared to the preferentially adsorbed component.

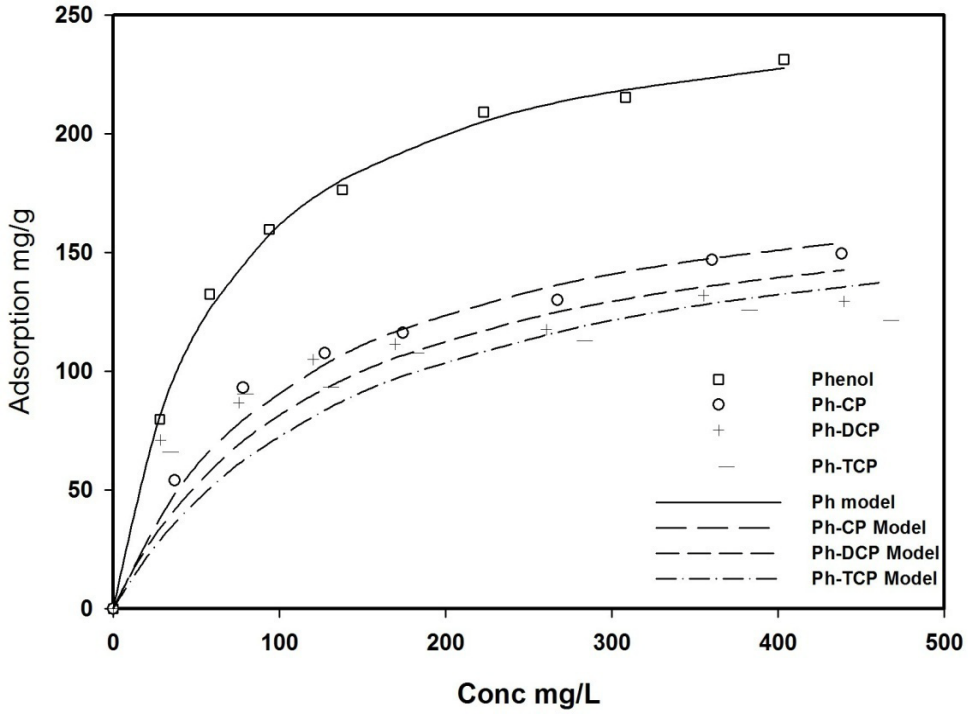

Figure 3.6-6 Adsorption isotherm of phenol in binary system conducted as per multicomponent adsorption test scheme 1.

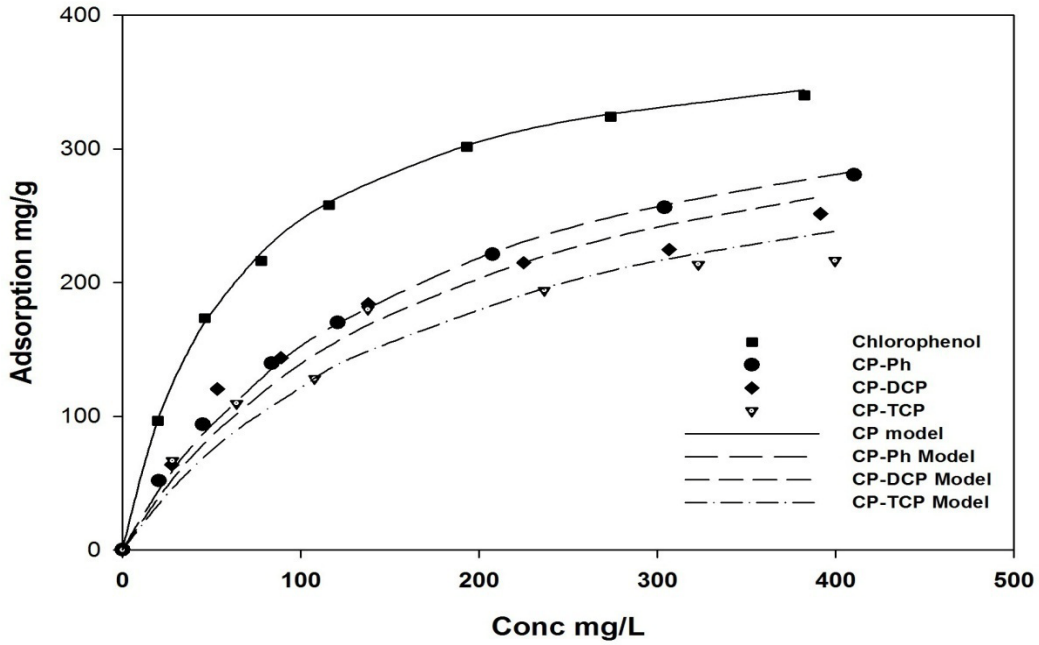

Figure 3.6-7 Adsorption isotherm of chlorophenol in binary system conducted as per multicomponent adsorption test scheme 1.

As observed in Figure 3.6-6, the adsorption of phenol seems to get progressively lower in the presence of chlorophenol, dichlorophenol, and trichlorophenol. The influence of competition between adsorbates is observed to be comparatively smaller with chlorophenol than with phenol. When compared with single-component adsorption, the uptake of phenol for the initial concentration of 500 ppm is reduced by 35% in the presence of chlorophenol, 45% in dichlorophenol, and 51% in trichlorophenol. Comparing Figure 3.6-6 and Figure 3.6-7 it is observed that the loss in the uptake of the chlorophenol in the presence of phenol is significantly lesser than the loss of uptake of phenol in the presence of chlorophenol. The uptake of chlorophenol is slightly reduced in the presence of dichlorophenol, and it is significantly reduced (by 30%) in the presence of trichlorophenol. The significant decrease in the adsorption capacity of phenol in presence of chlorophenol, dichlorophenol, and trichlorophenol suggests that phenol is weakly adsorbed compared to the other three compounds; however, chlorophenol is preferentially adsorbed compared to phenol and weakly adsorbed compared to dichlorophenol and trichlorophenol.

3.6.2.2 Comparisons of Model Predictions

Figure 3.6-8 and Figure 3.6-9 present phenol and chlorophenol adsorption isotherms in Ph-CP binary systems along with predictions using various multicomponent models. The adsorption isotherms and model results for other binary systems (Ph-DCP, Ph-TCP, CP-DCP, and CP-TCP) are presented in Appendix **B**, Figures B1-B4.

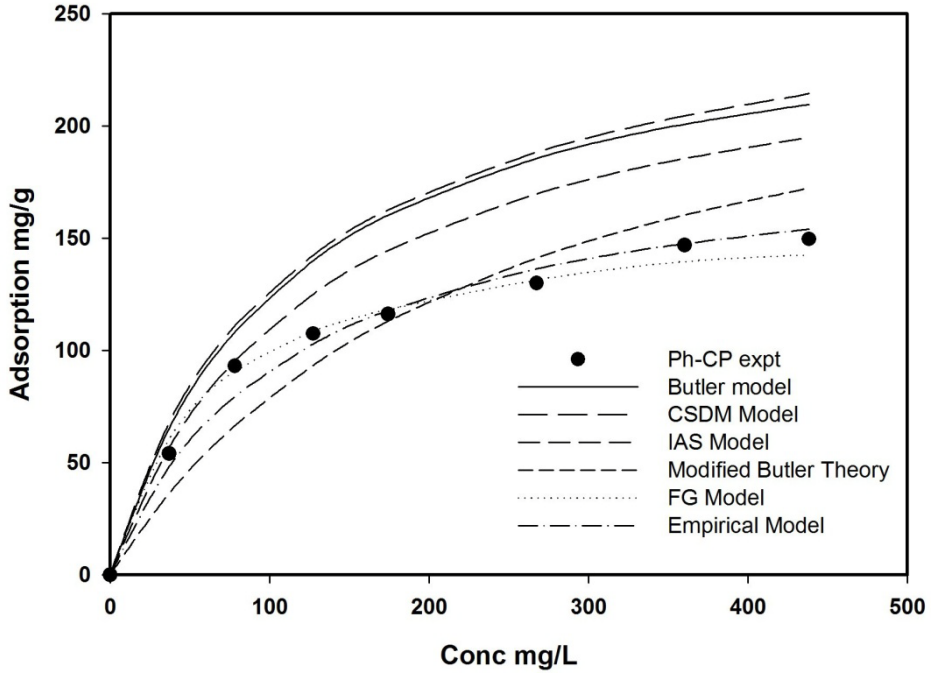

Figure 3.6-8 Modelling the binary adsorption of phenol in the presence of chlorophenol conducted as per multicomponent adsorption test scheme 1.

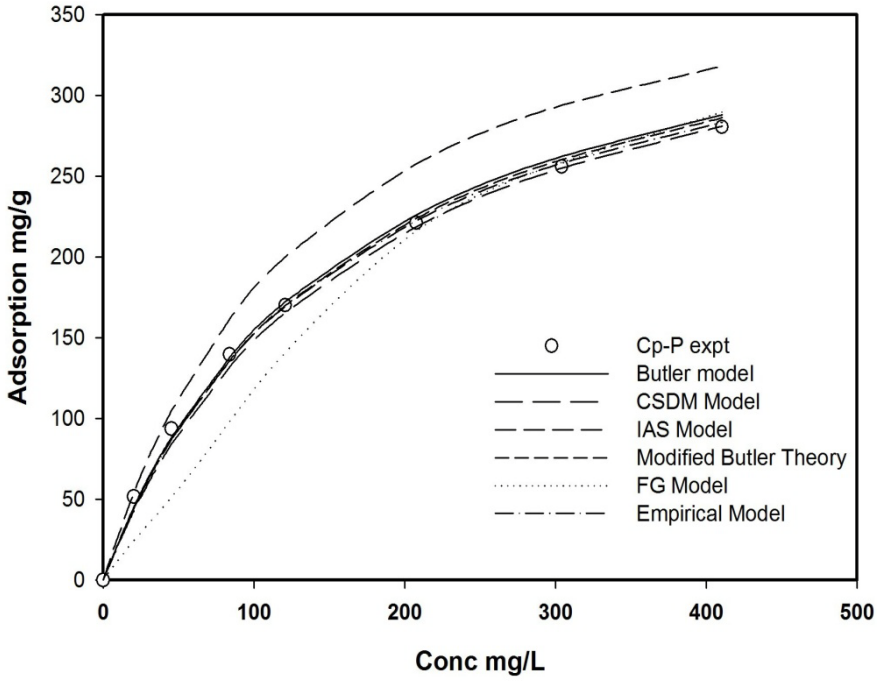

Figure 3.6-9 Modelling the binary adsorption isotherm of CP in presence of phenol conducted as per multicomponent adsorption test scheme 1.

For phenol adsorption, Figure 3.6-8 shows that the Butler and Ockrent theory over predicts the experimental data by 25%. This model is based on the single-component adsorption capacity and does not account for the suppressed adsorption occurring due to adsorbate interactions. For chlorophenol adsorption, wherein the competing adsorbate is phenol, whose adsorption capacity is much less than that of chlorophenol and provides minimal resistance to the chlorophenol adsorption, Figure 3.6-8 shows the prediction to be much better. For both phenol and chlorophenol adsorption, Figure 3.6-8 and Figure 3.6-9 show that the CSDM model is less reliable than the Butler and Ockrent theory; it gives a poor R^2 value of 0.443. Mathematically, the CSDM model simply distributes deviations between the partition and the sorption sections of the model.

Table 3.6-3 Error analysis of modelling of binary component adsorption. The first component is the adsorbate in consideration with varying concentration whereas the second adsorbate is competing adsorbate with fixed concentration.

Adsorbate	Model	R^2	ARE	MPSD
Ph-CP	Butler and Ockrent	0.469	28.13	39.63

	CDSM	0.442	30.55	47.68
	IAS	0.607	16.89	26.24
	Fowler and Guggenheim	0.972	0.46	6.31
	Modified Butler and Ockrent	0.930	5.50	28.73
	Empirical	0.993	2.54	8.07
Ph-DCP	Butler and Ockrent	0.390	26.60	50.28
	CDSM	0.357	29.69	59.72
	IAS	0.710	2.58	33.45
	Fowler and Guggenheim	0.861	13.37	29.34
	Modified Butler and Ockrent	0.890	9.83	49.35
	Empirical	0.942	8.88	24.47
Ph-TCP	Butler and Ockrent	0.382	24.31	54.81
	CDSM	0.349	27.10	64.69
	IAS	0.58	29.14	51.18
	Fowler and Guggenheim	0.90	16.70	40.51
	Modified Butler and Ockrent	0.87	10.68	56.90
	Empirical	0.893	10.23	30.41
CP-Ph	Butler and Ockrent	0.967	1.38	6.46
	CDSM	0.987	4.67	10.55
	IAS	0.74	11.76	16.61
	Fowler and Guggenheim	0.93	17.85	34.69

	Modified Butler and Ockrent	0.98	2.43	9.49
	Empirical	0.998	2.77	6.53
CP-DCP	Butler and Ockrent	0.912	2.46	14.63
	CDSM	0.919	2.03	16.06
	IAS	0.842	13.50	23.55
	Fowler and Guggenheim	0.955	8.78	0.19
	Modified Butler and Ockrent	0.942	4.33	20.46
	Empirical	0.982	6.19	14.59
CP-TCP	Butler and Ockrent	0.744	5.40	20.14
	CDSM	0.768	4.02	21.75
	IAS	0.438	27.66	41.52
	Fowler and Guggenheim	0.984	13.38	0.35
	Modified Butler and Ockrent	0.938	6.15	28.55
	Empirical	0.975	6.46	16.94

IAS theory is one of the most successful theories for explaining gas-phase multicomponent adsorption. In the current work, this model gives better predictions than the earlier models, as observed in Figure 3.6-8. The ARP and MPSD values are shown in Table 3.6-3. The simplified analytical solution of the IAS model, proposed by LeVan based on the Langmuir and Freundlich isotherm (not shown here), give similar predictions. The main factors affecting absolute accuracy in predictions from the IAS model are the heterogeneity of the adsorbent surface and interactions between adsorbates (which are generally higher in liquid systems than in gaseous systems); these are not taken into account in the model. In contrast, these effects are included in the models proposed by Fowler and Guggenheim, Nitta, and Ho and McKay, and others.

The interaction parameters of the Fowler and Guggenheim model, estimated from the binary isotherms, are presented in Table 3.6-4. The absolute value of the adsorbate interaction for Ph-CP, Ph-DCP, and Ph-TCP increases subsequently, suggesting higher interactions between compounds that have greater partial charges on the molecules. On a similar approach, the modified Butler and Ockrent theory incorporates an interaction factor, which is based on the extent of relative adsorption.

Table 3.6-4 Modelling parameters of binary component adsorption. The first component is the adsorbate in consideration with varying concentration whereas the second adsorbate is competing adsorbate with fixed concentration.

Adsorbate	F-G Model	Modified Butler and Ockrent	Empirical correction factor F(c)
Ph-CP	γ_{12}: 0.81	η_1: 0.0077	0.799
		η_2: 0.0016	
Ph-DCP	γ_{12}: -0.96	η_1: 0.00056	0.780
		η_2:0.00016	
Ph-TCP	γ_{12}: -3.47	η_1: 0.0123	0.711
		η_2: 0.0033	
CP-Ph	γ_{12}: -5.19	η_1: 0.0067	0.984
		η_2: 0.0040	
CP-DCP	γ_{12}: -2.27	η_1: 0.0114	0.956
		η_2: 0.0071	
CP-TCP	γ_{12}: -5.47	η_1: 0.0121	0.872
		η_2: 0.0064	

Table 3.6-4 suggests that the Butler and Ockrent theory gives extremely poor estimates of multicomponent adsorption with very low values for the correlation coefficient R^2. Results are much better from the modified Butler and Ockrent model and the Fowler and Guggenheim model, with R^2 in the range 0.85–0.90.

The Butler and Ockrent model was originally based on independent kinetic equilibrium between each adsorbate in the system, as shown in Appendix B. The model generally is valid for the systems having equal monolayer capacities for each component; however, this is never observed in practice. To apply the model to systems having components with different monolayer capacities, it was proposed to employ a mean maximum monolayer capacity of each component [18]. Several researchers have utilized the theory by employing the maximum monolayer capacity obtained from single-component isotherms to predict the adsorption capacity in multicomponent systems. This approach leads to a certain degree of error because, in practice, the monolayer capacity parameter (q_m) changes considerably from a single-component system to a multicomponent system. In general, the presence of the competing adsorbate tends to reduce the number of sites available for adsorption, thereby reducing its maximum monolayer adsorption capacity. However, in certain cases, the presence of a competing adsorbate may enhance the adsorption of the main adsorbate in comparison to that in single-component adsorption. This has been observed for the adsorption of a component that has a higher adsorption affinity (preferentially adsorbed) in the presence of a competing adsorbate with a lower adsorption affinity (weakly adsorbed). Such observations have been previously reported by other investigators [24]. To account for such changes, it is essential to re-estimate the monolayer capacity obtained from a single-component system, if it is to be successfully employed in multicomponent systems. Furthermore, in multicomponent systems, the monolayer capacity is not a fixed quantity, as it is in single-component systems; rather, the capacity changes with the type and concentration of competing adsorbate.

In the empirical model proposed here, a correction factor *f* is added to the Butler and Ockrent theory to refine the maximum monolayer adsorption capacity obtained from single-component systems. The correction factor accounts for an increase or decrease in adsorption, and thereby represents the influence of the competing adsorbate on the equilibrium of the adsorbate under consideration. On applying the correction factor *f* to change the monolayer capacity, the model takes the form shown in equation 3.6-1.

Figure 3.6-8 shows that the empirical model gives a satisfactory representation of the experimental observations for the adsorption of phenol and chlorophenol in the presence of competing adsorbates. The values for R^2 and ARE in Table 3.6-3 are

quite satisfactory, compared to other models. But note that, for simplicity at this stage, the correction factor *f* in the table is an average value; in reality, the correction factor should change with changes in the equilibrium-adsorbed concentration of the competitive adsorbate. This is discussed in the following section.

3.6.3 Effects of Concentration of Competing Adsorbates

To determine how the concentration of competing adsorbate affects the correction factor *f* in 3.6-1, experiments were performed on the binary systems Ph-CP, Ph-DCP, and Ph-TCP and the concentrations of both the components were varied in equal ratios as per multicomponent adsorption test scheme 2. As shown in Figures 3.10–3.12, the adsorption of phenol, in each case, tends to decrease as the concentration of the competing adsorbate increases; however, adsorption of chlorophenol, dichlorophenol, and trichlorophenol continues to increase, despite the rising concentration of the competing phenol. This suggests preferential adsorption of chlorophenol, dichlorophenol, and trichlorophenol over phenol. The contrasting behavior of phenol implies that the adsorption of the weakly adsorbed component in a multicomponent system is highly suppressed by the competing adsorbate, whereas the adsorption isotherm of the preferentially adsorbed component follows a rising trend, similar to what is observed in the case of single-component systems. The final results also show that the ratios of the two-component concentrations, which were initially equal, changed after adsorption to approximately 1.3 for Ph-CP, 1.6 for Ph-DCP, and 2.3 for Ph-TCP. The various values of the correction factor, obtained by fitting the observed adsorption isotherms, were correlated with the concentration of the competing adsorbate. The values were well-described by an exponential function of the competing adsorbate,

$$f(c) = a^{c} \qquad \text{Equation 3.6-1}$$

Here *c* is the concentration of the competing component at equilibrium and values for the correlation constant '*a'* are given in Table 3.6-5.

Isotherms predicted by the empirical model tend to follow the trends shown in Figure 3.6-10, Figure 3.6-11 and

Figure 3.6-12, confirming the dependence of the correction factor *f* on competitive adsorbate concentration. As the concentration of the competing adsorbate

decreases, the correction factor moves closer to one, thereby approaching the Butler and Ockrent model. This implies that the basic theory proposed earlier by Butler and Ockrent holds for low concentrations of the competing adsorbate. Furthermore, in the absence of the competing component, the empirical equation reduces to the Langmuir model. The correlation equation for *f* (*c*) is derived purely from the present experimental observations and should not be used as a generalized relation for every adsorbate. A more fundamental correlation equation should be developed to predict the influence of competing adsorbates and to place the proposed model on a sound theoretical basis. The biggest advantage of this model is that it provides an explicit prediction of adsorption isotherm which can be easily utilized for column design.

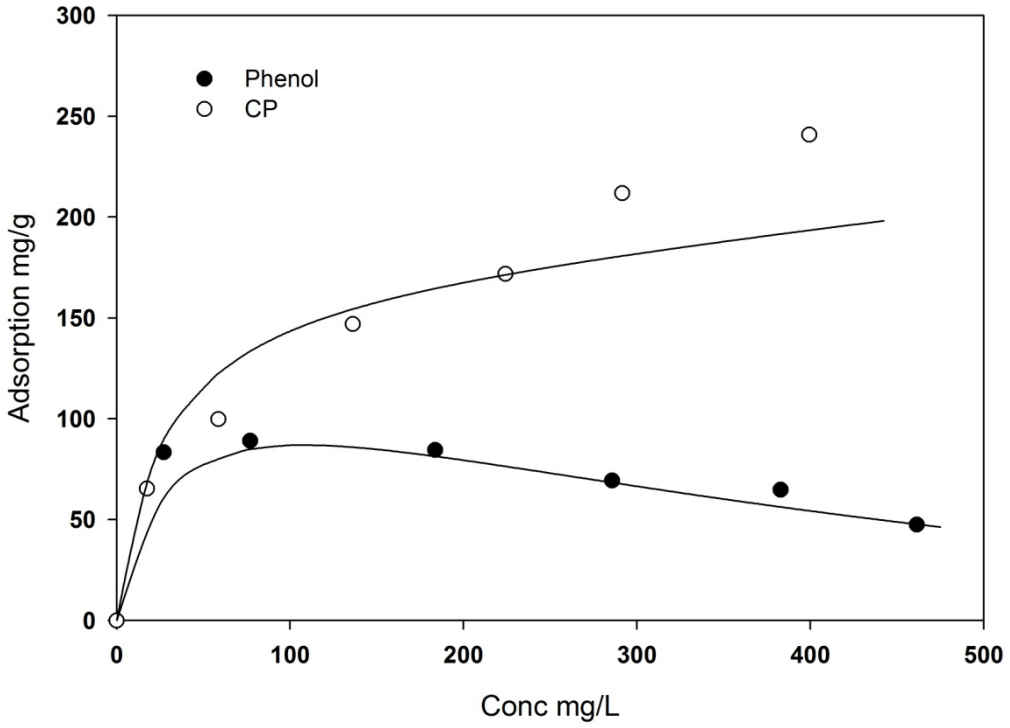

Figure 3.6-10 Adsorption Isotherm of phenol and chlorophenol conducted as per multicomponent adsorption test scheme 2.

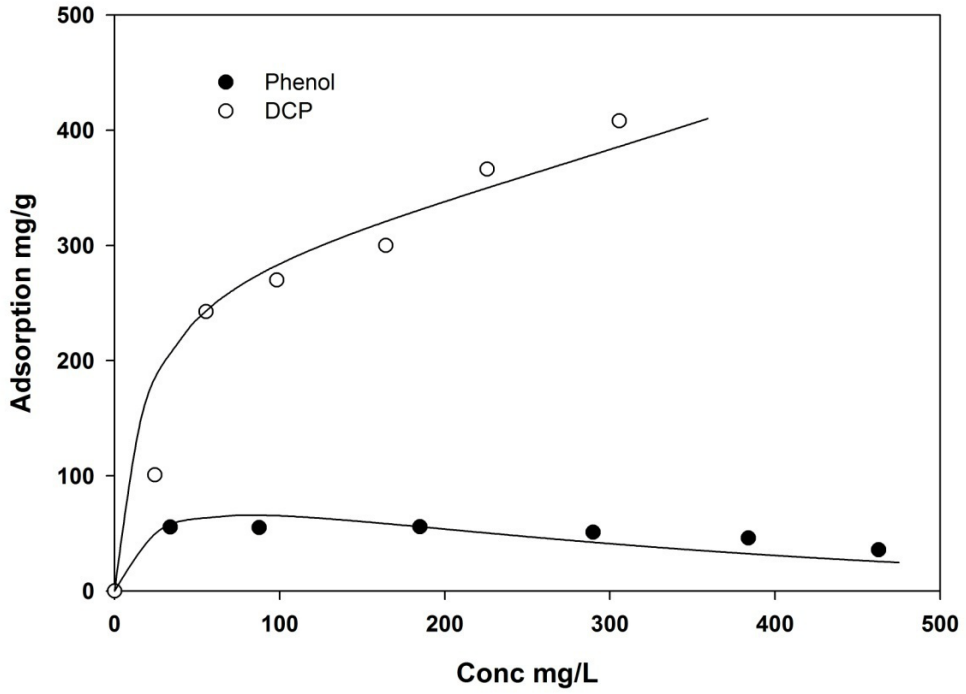

Figure 3.6-11 Adsorption isotherm of phenol and dichlorophenol conducted as per multicomponent adsorption test scheme 2.

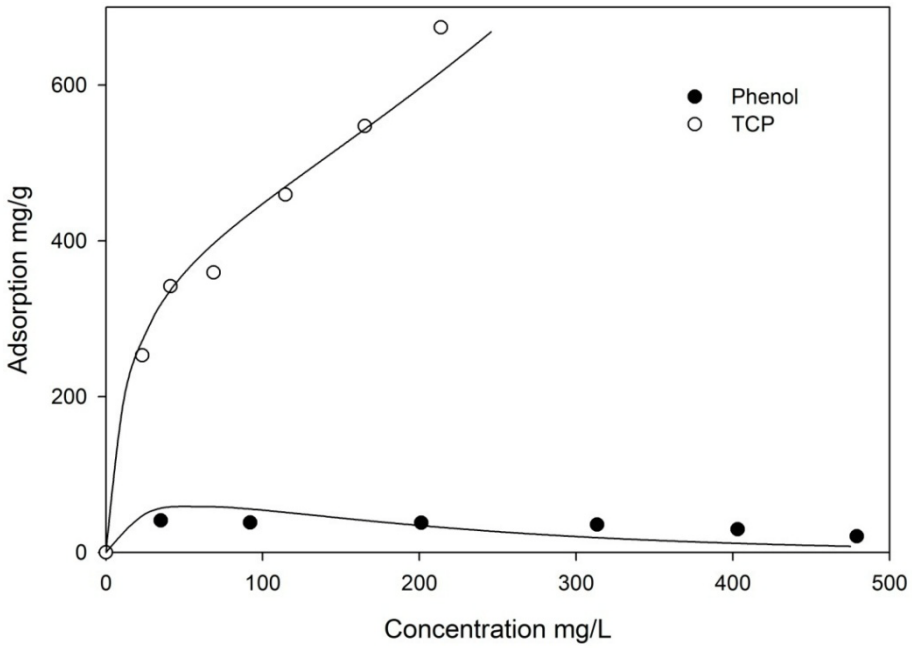

Figure 3.6-12 Adsorption isotherm of phenol and trichlorophenol conducted as per multicomponent adsorption test scheme 2.

Table 3.6-5 Exponential factor of the correction factor for the system wherein the concentration of both the component is varying.

Adsorbate	Competing Adsorbate	Exponential Factor (a)	Concentration Range (ppm)
Ph-CP	Chlorophenol	0.9970	0-300
Ph-DCP	Dichlorophenol	0.9950	0-400
Ph-TCP	Trichlorophenol	0.9865	0-500
Ph-CP	Phenol	1.0003	0-500
Ph-DCP	Phenol	1.0006	0-500
Ph-TCP	Phenol	1.0009	0-500

3.7 Conclusion

A comprehensive study of multicomponent adsorption of several phenolic compounds on activated carbon revealed the complexities of interactions occurring between different adsorbate species. Additionally, a mathematical derivation was proposed for the modified Butler and Ockrent theory. Analyses of previously reported models indicate that model predictions deviate considerably from experimentally measured adsorption. These deviations increase with increases in the concentration of the competing adsorbate and with increases in the number of the competing adsorbates. Most previous models ignore the effects of adsorbent heterogeneity and adsorbate interactions. The modified Butler and Ockrent model tends to provide better predictions, compared to other models, but it still fails for compounds at high concentrations and for compounds having high monolayer adsorption capacities.

To account for the changes in monolayer adsorption capacities, a new empirical model, incorporating a lumped correction factor into the original Butler and Ockrent theory, has been proposed. The correction factor showed an exponential dependence on the competing adsorbate concentration. Future work will be directed toward more detailed studies of the correction factor, such as its use for various types of adsorbates and development of a generalized correlation that will predict values for the factor in many different multicomponent systems.

3.8 References

[1] O. Hamdaoui and E. Naffrechoux, Modelling of adsorption isotherms of phenol and chlorophenols onto granular activated carbon Part I. Two-parameter

models and equations allowing determination of thermodynamic parameters, J. Hazard. Mater. 147(2007) 381-394.

[2] J.A.V. Butler and C. Ockrent, Studies in electro capillarity. III, J. Phys. Chem. 34 (1930) 2841-2859.

[3] W. Fritz and E.U. Schluender, Simultaneous adsorption equilibria of organic solutes in dilute aqueous solutions on activated carbon, Chem. Eng. Sci. 29 (1974) 1282.

[4] C. Sheindorf, M. Rebhun, and M. Sheintuch, A Freundlich-type multicomponent isotherm, J. Colloid Interf. Sci. 79 (1981) 136-142.

[5] J.S. Jain and V.L. Snoeyink, Adsorption from bisolute systems on active carbon, J. Water Poll. Control Fed. 45 (1973) 2463-2479.

[6] S.K. Srivastava and R. Tyagi, Competitive adsorption of substituted phenols by activated carbon developed from the fertilizer waste slurry, Water Res. 29 (1995) 483-488.

[7] C.J. Radke and J.M. Prausnitz, Thermodynamics of multi-solute adsorption from dilute liquid solutions, Heat Mass Transf. 9 **(**1966) 1089.

[8] M.D. LeVan and T. Vermeulen, Binary Langmuir and Freundlich isotherms for ideal adsorbed solutions, J. Phys. Chem. 85 (1981) 3247-3250.

[9] X. Hu and D.D. Do, Comparing various multicomponent adsorption equilibrium models, AIChE J. 41 (1995)1585-1592.

[10] S.E. Hoory and J.M. Prausnitz, Monolayer adsorption of gas mixture on homogeneous and heterogeneous solids, Chem. Eng. Sci. 22 (1967)1025-1033.

[11] T. Nitta, et al., An adsorption isotherm of multi-site occupancy model for homogeneous surface, J. Chem. Eng. Jpn. 17 (1984) 39-45.

[12] I. Quiñones and G. Guiochon, Extension of a Jovanovic–Freundlich isotherm model to multicomponent adsorption on heterogeneous surfaces, J. Chromatogr. A. 796 (1998) 15-40.

[13] Y.S. Ho and M. G. McKay, Competitive sorption of copper and nickel ions from aqueous solutions using peat, Adsorption. 5 (1999) 409-417.

[14] D. Yonge and T. Keinath, The effect of non ideal competition on multi component adsorption equilibrium, J. Water Poll. Control Fed. (1986) 77-81.

[15] C.C. Wang, C.M. Lee, and C.H. Kuan, Removal of 2, 4-dichlorophenol by suspended and immobilized Bacillus insolitus, Chemosphere. 41 (2000) 447-452.

[16] O. Hamdaoui, et al., Ultrasonic desorption of p-chlorophenol from granular activated carbon, Chemical Engineering Journal. 106 (2005) 153-161.

[17] (ATSDR), A.f.T.S.a.D.R., Public Health Statement: Phenol, D.o.H.a.H. Services, Editor. 2006.

[18] D.D. Do, Adsorption analysis: equilibria and kinetics, Imperial College Press, London, 1998.

[19] W.R. Vieth and K.J. Sladek, A model for diffusion in a glassy polymer, J. Colloid Sci. 20 (1965)1014-1033.

[20] K.J. Sladek, W.R.V.a.K.J., A model for diffusion in a glassy polymer Journal of Colloid Science. 20 (1965) 1014-1033.

[21] B. P. Russell and M.D. LeVan, Group-contribution theory for adsorption of gas mixtures on solid surfaces, Chem. Eng. Sci. 51 (1996) 4025-4038.

[22] J.K. Huh, D.I. Song, and Y.W. Jeon, Sorption of phenol and alkyl phenols from aqueous solution onto organically modified montmorillonite and applications of dual-mode sorption model, Separ. Sci. Technol. 35 (2000) 243-259.

[23] C.J. Radke and J.M. Prausnitz, Thermodynamics of multi-solute adsorption from dilute liquid solutions, AIChE J. 18 (1972) 761-768.

[24] Ö.A.a.F. Çeçen, Competitive adsorption and desorption of a bi-solute mixture: effect of activated carbon type, Adsorption. 13 (2007) 159-169.

[25] A. Leitão and R. Serrão, Adsorption of phenolic compounds from Water on activated carbon: prediction of multicomponent equilibrium isotherms using single-component data, Adsorption. 11 (2005) 167-179.

[26] A.R. Khan, T.A. Al-Bahri, and A. Al-Haddad, Adsorption of phenol based organic pollutants on activated carbon from multi-component dilute aqueous solutions, Water Res. 31 (1997) 2102-2112.

[27] E.G. Furuya, et al., A fundamental analysis of the isotherm for the adsorption of phenolic compounds on activated carbon, Sep. Purif. Technol. 11 (1997) 69-78.

[28] J.F. Garcia-Araya, et al., Activated carbon adsorption of some phenolic compounds present in agroindustrial wastewater, Adsorption. 9 (2003) 107-115.

[29] J.A. Mattson, et al., Surface chemistry of active carbon: specific adsorption of phenols, J. Colloid Interf. Sci. 31 (1969) 116-130.

4 - Cobalt exchanged zeolites for catalytic oxidation of phenol in the presence of peroxymonosulphate

Abstract

The chapter describes the application of cobalt exchanged zeolites for heterogeneous catalytic oxidation of phenol in the presence of sulphate radical. Several Co ion exchanged zeolite catalysts based on ZSM5, zeolite-A, and zeolite-X were prepared and utilized for catalytic oxidation of phenol in the presence of various oxidants such as H_2O_2, persulphate, and peroxymonosulphate. It is found that Co-ZSM5 is highly effective in activation of peroxymonosulphate to produce sulphate radicals for organic oxidation in water. The phenol oxidation rate was observed to be much faster in the presence of Co-zeolite A and Co-zeolite X, however, the potential application is limited due to instantaneous decomposition of the catalyst and leaching of Co ions in solution. Unlike Co-zeolite-A and -X, Co-ZSM5 presents stable performance in activation of peroxymonosulphate for phenol degradation. The phenol degradation depends on catalyst loading, phenol concentration, oxidant concentration and temperature. Kinetic studies indicate that phenol degradation follows zero order kinetics and activation energy is estimated as 69.7 kJ/mol.

4.1 Introduction

Zeolites are crystalline alumino-silicate compounds consisting of well defined micropores and channels. The structure of zeolite is a 3 dimensional framework structure composed of SiO_4 and Al_2O_3 tetrahedrons as the building block. These building blocks are connected with one another by sharing an oxygen atom thereby forming a unit crystal structure which poses a 3 dimensional pore network. The access to these porous channels is through the molecular window which permits the passage of a molecule under a specified size. Additionally, most of zeolites contain extra framework cations in the cavities to balance the anionic charge in the framework [1, 2]. The general formula of a typical zeolite can be expressed as follows.

$$M_{2/n}O.Al_2O_3.xSiO_2.yH_2O$$

Where, M is the exchangeable cation with the valency 'n'. The value of 'x' is greater or equal to 2, since Al^{3+} doesn't occupy adjacent tetrahedral sites. Lastly, 'y' is the number of water molecules adsorbed in a unit cell.

The framework charge-balancing cations are generally alkaline or alkaline earth metals which are capable of getting exchanged with several transition metals such as iron, cobalt, ruthenium, magnesium, copper etc. It is this property of zeolite to strongly dock a catalytic transition metal which makes it an excellent catalytic support. Enormous research has been done in the past on transition metal exchanged zeolite as a catalyst. Silver exchanged zeolite Y was reported to activate the dimerization of alkanes under UV irradiation [3], zeolite containing Ag, Cu, Co, Mg and Ni ion has been reported to be useful for NO_x reduction in the emission from diesel and petrol vehicles [4, 5]. One of the most important applications of transition metal exchanged zeolite is in petrochemical industries. Co-exchanged ZSM-5 has been successfully utilized as a efficient catalyst for the Fischer-Tropsch reaction [6, 7], hydroisomerization using platinum exchanged zeolites [8], Pt and Pd exchanged zeolites have been used for hydrocracking [9, 10]. The list is exhaustive; however the discussion is beyond the scope of this work.

In waste water treatment, the application has been most limited to iron exchanged zeolite for heterogeneous Fenton or Fenton like reaction. Certain metal oxides have

been supported on zeolite for Catalytic Wet Air Oxidation but with limited success. Co, Cr, Mg exchanged zeolite Y have been utilized for catalytic oxidation of chlorinated hydrocarbons [11]. Fe exchanged ZSM-5 has been utilized to carry out heterogeneous Fenton reaction for oxidation of phenolic pollutants [12], Similarly, Fe exchanged zeolite Y was utilized for dye degradation via heterogeneous Fenton reaction [13]. In the current research we propose the application of Co-exchanged zeolite as a potential catalyst to generate sulphate radical for heterogeneous oxidation of phenol. Prior to discussing the application of Co-exchanged zeolite, it is worthwhile to briefly discuss the crystal structure and properties of the three zeolites under consideration.

4.1.1 Zeolite A (NaA)

Zeolite A is a synthetic zeolite, most popularly utilized for natural gas sweetening or dehydration of ethanol [14, 15]. It is a low silica zeolite having the silica to alumina ratio as 1. It has a unique cubical structure with the principal building block being the Silica and Alumina tetrahedral structure. These tetrahedras are interconnected with each other to form a sodalite cage which appears as truncated octahedra which forms the secondary building block as seen in Figure 4.1-1. The truncated octahedra are also known as beta cage or cuboctahedra. The sodalite cages are joined together at 4-rings by four bridging oxygen atom, resulting in a cubical structure (O4 in Figure 4.1-1). Several sodalite cages are interconnected with this O4 structure to represent a cubical structure (Figure 4.1-1). The assembly of the sodalite cage results in a creation of a central cage by an 8-ring opening which has a diameter of 6.6 A.

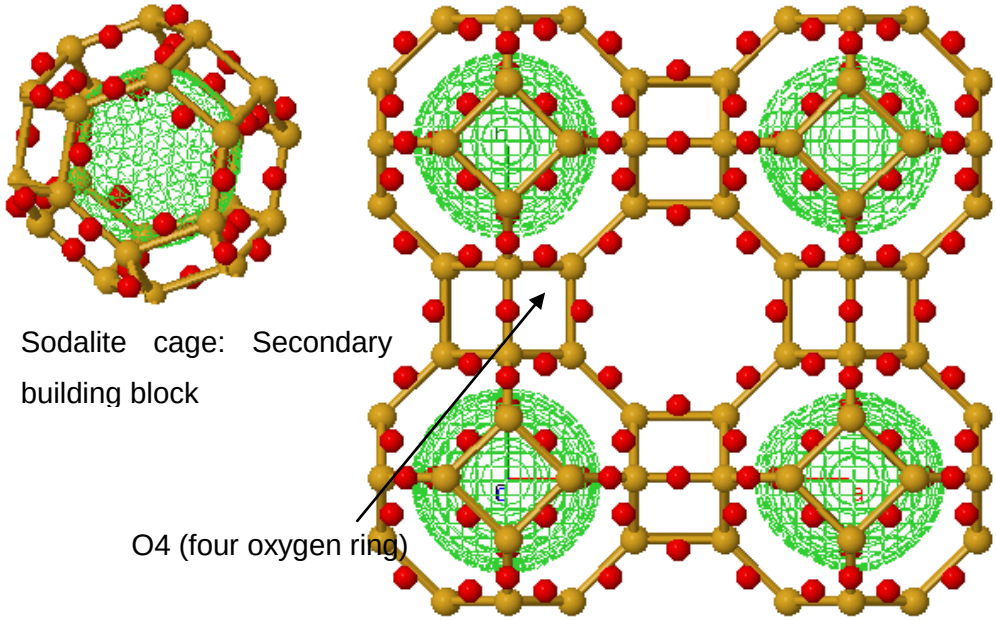

Figure 4.1-1: Zeolite A structure

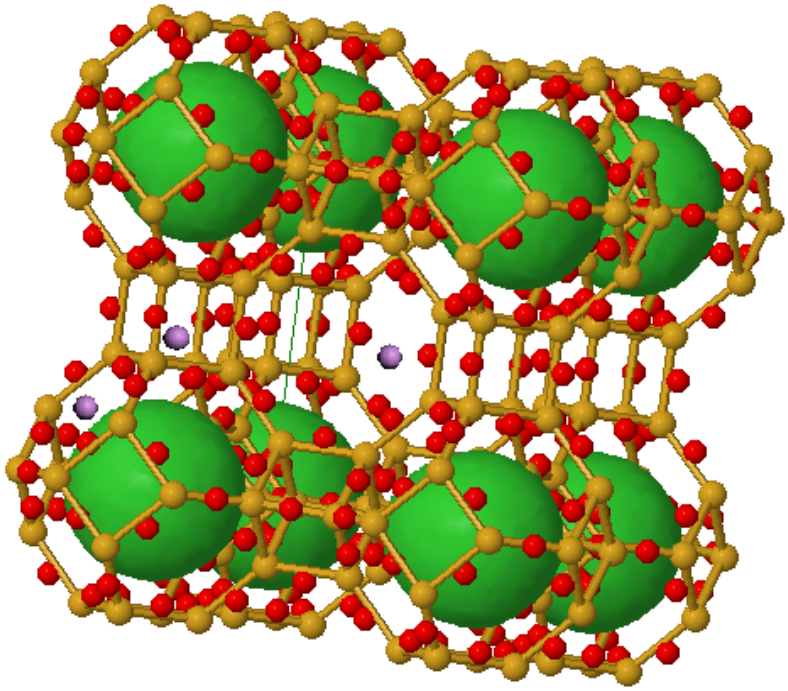

Figure 4.1-2: 3D picture of Zeolite A

There are 12 negative charges within a single crystal which are balanced by cations. For Na-A type zeolite, 8 Na^+ ions are located at site I at the centre of 6 member ring, 3 at site II at the eight member aperture and finally 1 at site III near the four member ring inside the cavity as shown by the purple atom in Figure 4.1-2 [16, 17]. This

position of the cation is unique not only for the zeolite type but also for the cation depending on its charge and atomic size. On exchanging the Na^+ with another cation, the location of the cation position would change in the unit cell to achieve minimal potential energy. The ion exchange of Na-A (sodium zeolite A) with cobalt would result in exchange of 2 monovalent sodium atom with 1 divalent cobalt atom. Complete exchange of cobalt with sodium ion is extremely difficult and would result in a damage to the crystalline structure as will be shown later in this chapter. In a partially cobalt exchanged NaA (8 atom of Na^+ replaced with 4 atom of Co^{2+}), the cobalt ion is located at 2 different sites. One cobalt ion located within the sodalite cage and the remaining 3 cobalt ions are located on unit cell three fold axes [16].

4.1.2 Zeolite X (NaX)

Zeolite X is a synthetic silica rich zeolite having the silica to alumina ratio as 1.25 thus having lesser number of exchangeable cations per mole as compared to zeolite A. It belongs to Faujasite type zeolite. Similar to zeolite A, zeolite X also has the sodalite cage as the secondary building block. However the sodalite cages are connected tetrahedrally at 6 rings by bridging oxygen in contrast to 4 rings in the case of zeolite A, thus resulting in a hexagonal structure (O6 in Figure 4.1-3). Several sodalite cages are interconnected with this O6 structure to represent a hexagonal structure. The assembly of the sodalite cage results in the creation of a central cage by a 12-ring window opening (Figure 4.1-3).

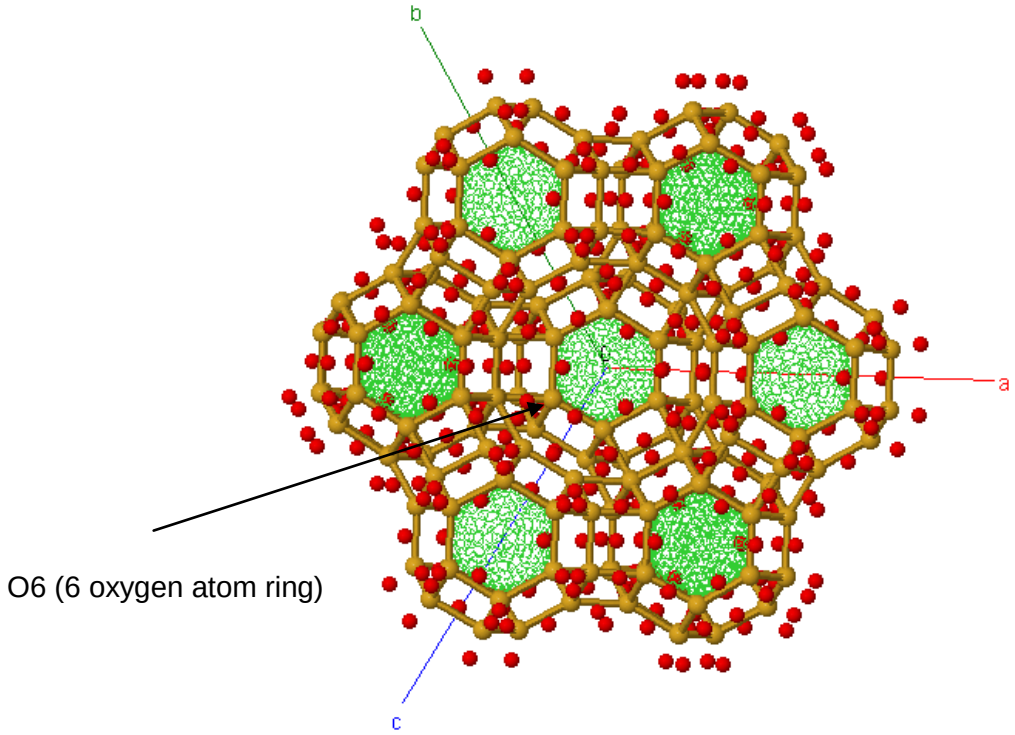

Figure 4.1-3 : Zeolite X

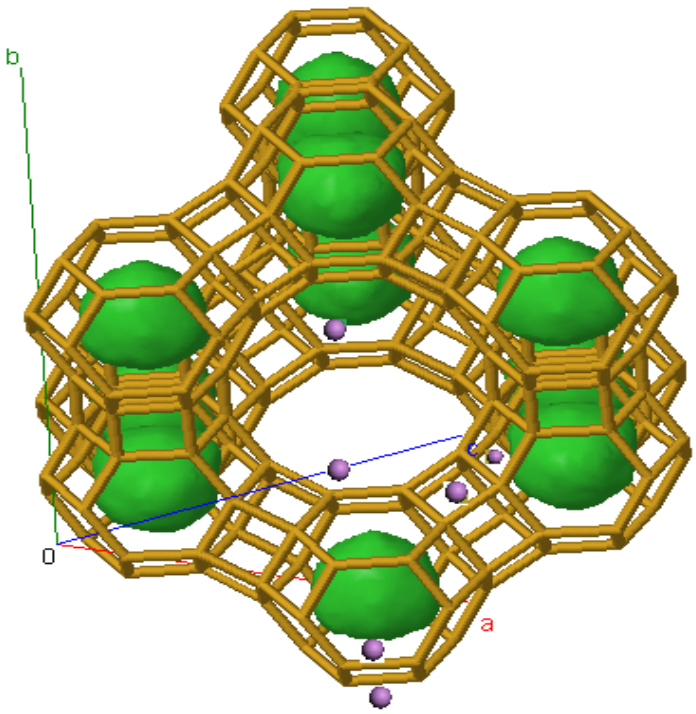

Figure 4.1-4: 3D image of Zeolite X

The exchangeable Na^+ ions are located at 6 different sites as shown by the purple atoms in Figure 4.1-4. One cation is located inside the O6 hexagonal prism (site I) followed by an adjacent cation located at the mirror plane just outside the prism and inside the sodalite cage (site II). Another cation is located inside the sodalite cavity close to the 6 ring structure (site III) followed by an adjacent cation located at the mirror plane just outside the 6 ring structure of the sodalite cage (site IV). Finally, a cation is located inside the super-cage which is opposite the 4 ring if seen from the top view and between the two 12 rings (one in front and other on side) if seen from the front (site V) followed by its mirror image plane at site VI [18]. Similar to zeolite A, it is highly difficult to achieve complete exchange of Na^+ with Co^{2+}. Upon exchanging with cobalt, the cobalt ions get coordinated with OH^- and Na^+ which upon hydration result in hydrolysis to generate H_3O^+ and $CoOH^+$. The location of cobalt ion was reported to be on site II, III and VI. However, the location of cobalt is strongly dependent on the temperature of ion exchange [18].

4.1.3 ZSM-5

ZSM-5 type zeolites are highly silicious zeolites belonging to MFI type structure family containing very high silica to alumina ratio (>25). The primary building block is similar to the earlier two forms of zeolite i.e. SiO_2 and Al_2O_3 tetrahedral. However, the secondary building block in this case is a structure consisting of 12 primary building units arranged in a pair of 5 ring structure with an additional stick protruding out as seen in Figure 4.1-5. Two 5-1 rings structure is combined to give a composite building block (MFI). The composite unit is further combined to generate a periodic building unit by rotating the MFI block in Z-axis. The periodic buildings are connected to result in formation of 10 ring pore structure perpendicular to the plane of the periodic building blocks to give a unit cell structure (Figure 4.1-6).

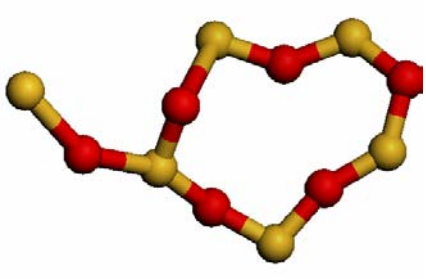

Figure 4.1-5: Secondary building block of ZSM-5

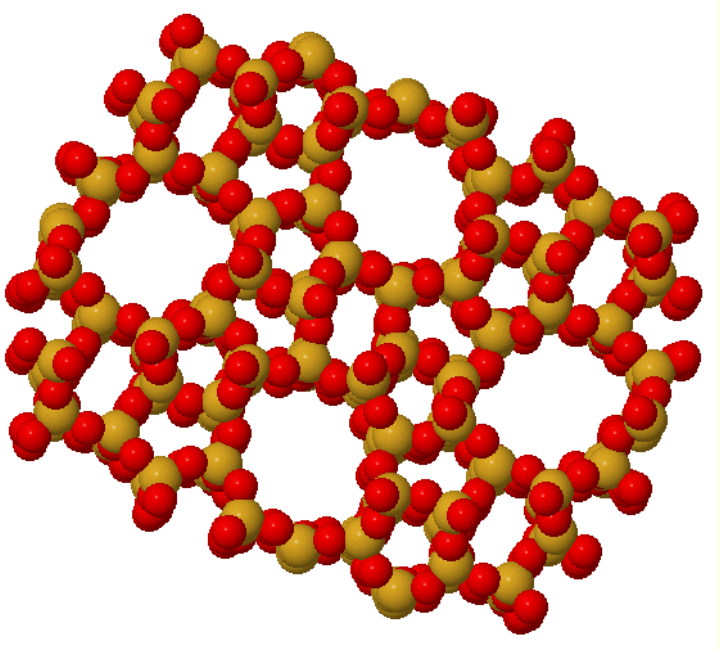

Figure 4.1-6: ZSM-5 crystal structure

In contrast to zeolites A and X wherein the cobalt ion is generally in the exchangeable form, ZSM-5 type of zeolite docks the cobalt in two different forms i.e. Co^{2+} ions in the exchangeable form or as an oxide form of CoO [19]. The CoO or the oxide like structure is formed due to the interaction of Co^{2+} with the intra-structural water molecules, which also play an important role in conserving the structure of ZSM-5 under high acidity as discussed later in the chapter.

4.2 Heterogeneous Catalytic Oxidation Using Sulphate Radical

Catalytic oxidation of organic pollutants using hydrogen peroxide to generate active hydroxyl radical has been used extensively for phenolic contaminant degradation. Iron has been found to be highly effective in reacting with peroxide to generate active hydroxyl radicals which is highly active for oxidizing the organic contaminants [20]. Similar to hydrogen peroxide, recently peroxymonosulphate (PMS) has been proposed as an alternative oxidant. In the presence of cobalt catalyst, the peroxymonosulphate breaks up to generate active sulphate radical which in turn helps in oxidizing pollutants as shown below [21, 22]. More details of Co/PMS based oxidation are available in section 2.7.8.

$$Co^{2+} + HSO_5^{\bullet} \rightarrow Co^{3+} + SO_4^{-\bullet} + OH^-$$

Equation 4.2-1

$$SO_4^{\bullet-} + C_6H_5OH \rightarrow C_6H_5OH - SO_4^{\bullet-} \xrightarrow{-SO_4^{2-}} C_6H_5OH^{\bullet+} \xrightarrow{several.steps} CO_2 + H_2O$$

Equation 4.2-2

Sulphate radical has a higher oxidation potential [1.75 eV] as compared to the hydroxyl radical [1.7 eV], thereby promising to be an efficient oxidant. However, in spite of being highly active and faster oxidation of pollutants, the reaction under homogeneous system with cobalt and peroxymonosulphate has profound disadvantage in terms of cobalt loss. The loss of cobalt in discharge stream renders it toxic as cobalt is recognized as a priority metal pollutant. It leads to several health problems such as asthma, pneumonia and other lung problems [23]. In order to make the technology commercially feasible, it is essential to prevent the loss of cobalt species. In the past few years, several attempts have been made in developing a supported cobalt based catalyst thereby carrying out the oxidation in a heterogeneous system. Dionysiou et al. [24] have reported the application of solid cobalt oxide for treatment of dichlorophenol. Although it was found that heterogeneous cobalt oxide (Co_2O_3) was capable of activating peroxymonosulphate, a considerable leaching of cobalt was observed. Further attempts to immobilize cobalt onto various supports such as SiO_2, Al_2O_3 and TiO_2 have shown promising outcomes [25, 26]. In all the cases, various cobalt precursors were loaded onto the support by wet impregnation followed by calcination. In spite of concluding the catalyst preparation by high temperature calcination, the cobalt leaching couldn't be completely prevented, rendering the catalyst unusable after twice or more use.

In the search of stable cobalt supported catalyst, attention was given to micro porous zeolite. Various types of zeolites have been used as adsorbents, catalyst supports, and catalysts. However, this type of material has not yet been tested as heterogeneous catalyst in generation of sulphate radicals for organic oxidation in aqueous solution. Co-zeolite has been successfully synthesized in the past by various techniques such as ion exchange or impregnation [27] and used successfully for various applications such as Fischer-Tropsch reaction, epoxidation of styrene, catalytic reduction of NO_x etc as discussed in the beginning of the chapter. In current study, cobalt-zeolite was synthesized by ion-exchange technique, wherein the ionic bonding between the cobalt cation and the anionic zeolite framework would hold the cobalt more strongly and prevents leaching as far as the framework structure

remains stable. Apart from retaining the cobalt ions on the surface, the cobalt species via ion exchange can also maintain cobalt oxidation state. In contrast to ion exchange, wet impregnation of cobalt results in cobalt species at various oxidation states generally Co_2O_3 depending on synthesis conditions [27-29].

In this study three different types of zeolites (A, X and ZSM-5) were exchanged with cobalt and the reaction kinetics for oxidation of phenol with sulphate radical and Co-zeolite were studied.

4.3 Experimental

4.3.1 Materials

Powdered zeolite-A, zeolite-X, and ZSM-5 were supplied by Zeolite and Allied Products, Mumbai, India. Cobalt chloride ($CoCl_2.6H_2O$) purchased from Aldrich was used as a precursor for cobalt ion exchange. Peroxymonosulphate which is available as a triple salt of sulphate commercially known as oxone ($2KHSO_5{\cdot}KHSO_4{\cdot}K_2SO_4$) was used as an oxidant. Pure methanol was used as a quenching reagent to stop the reaction in the sample bottle before HPLC analysis and sodium nitrile was used for quenching the reaction before the TOC analysis. The properties of the zeolite samples are given in Table 4.3-1

Table 4.3-1 Typical properties and cobalt loading in zeolite

	Molecular formula	Co after Ion exchange from XRF (g/kg)	Co after Reaction from XRF
zeolite A	$\left[Na_{12}^{+}\left(H_2O\right)_{27}\right]_8\left[Al_{12}Si_{12}O_{45}\right]_8$	142.019	N/A
Zeolite X	$\left[Na_{58}^{+}\left(H_2O\right)_{240}\right]\left[Al_{58}Si_{134}O_{384}\right]$	110.566	89.800
ZSM-5	$\left[Na_{n}^{+}\left(H_2O\right)_{16}\right]\left[Al_{n}Si_{96-n}O_{129}\right]$	18.329	15.371

4.3.2 Cobalt ion exchange on zeolites

Cobalt ion was loaded on zeolite samples following a conventional ion-exchange technique from an aqueous cobalt chloride solution. The concentration of cobalt ion

in the liquid was almost twice the maximum moles of cobalt capable of being exchanged into the zeolite. A fixed amount of zeolite samples were added to cobalt chloride solution in solid to liquid ratio of 1:60 and stirred under reflux condition for 6 h at 75 ºC. The solution was filtered and washed with warm distilled water for almost 8-10 times to ensure that the solid is free from chloride ions. The presence of chloride ion was tested with silver nitrate solution. The procedure was repeated 3 times to ensure the maximum exchange of the ions. Finally the samples were dried at 75 ºC and stored in a desiccator until use.

4.3.3 Characterization of catalyst.

The crystallinity of various zeolite samples were studied using XRD. The spectra were obtained on a Simens XRD instrument, using filtered Cu Kα radiation with accelerating voltage of 40 kV, current 30 mA and scanned at 2θ from 5 to 70^0. The crystallinity of the samples was calculated based on the intensity ratio of five major peaks as per equation below [30]. XRD pattern of sodium exchanged zeolite was used as the reference.

$$\%\text{crystallinity} = \frac{\text{sum of peak intensities of sample}}{\text{sum of peak intensities of reference}} \times 100 \quad \text{Equation 4.3-1}$$

The texture and morphology of the prepared samples were observed using scanning electron microscope (SEM). For analysis, the samples were sputtered gold coated in order to make the sample conducting and to easily distribute the charge. The analysis was done mostly with a secondary electron detector in order to focus on the particle's surface features. The quantitative analysis of cobalt content in the zeolite was done using X-ray fluorescence. Diffuse reflectance spectroscopic (DRS) studies were carried out using Jasco V-570 equipped with an integrating sphere at the room temperature in air. $BaSO_4$ was used as the reference material. The spectra were recorded in the wavelength range of 200 to 800 nm.

4.3.4 Kinetic study of phenol oxidation using oxone.

The catalytic oxidation of phenol was carried out in a 500 ml reactor filled with phenol solution of varying concentrations. The reactor was partially immersed in a water bath fitted with a temperature controller. The reaction mixture was stirred with a plastic coated stirrer to maintain homogeneous solution. Before the reaction, a known

amount of oxidant peroxymonosulphate (available as a triple salt and sold under commercial name as “oxone”) was added to the mixture and was allowed to dissolve. Later a fixed quantity of catalyst (Co-zeolite) depending on the predefined reaction parameter was added to start the reaction. The reaction was carried out for 6 h, and during a fixed interval, 0.5 ml of sample was withdrawn using a syringe filter into a HPLC vial to which 0.5 ml high purity methanol was added to quench the reaction. A few tests were carried out with different oxidants wherein the oxone was replaced with H_2O_2 and peroxydisulphate (PDS).

The phenol concentration was analyzed using a Varian HPLC with a UV detector at wavelength of 270 nm. The C-18 column was used to separate the organics while the mobile phase consisting of 30% CH_3CN and 70% water was used as the transport medium. For a few selected experiments, total organic content was also determined using a Shimadzu TOC-5000 CE analyzer. For the measurement of TOC, 5 ml sample was extracted at an interval of 1 h and quenched with 5 ml of 3M sodium nitrile solution and then analyzed on the TOC analyzer. The concentration of peroxymonosulphate was analyzed by a titration method. In brief, 5 ml of reaction mixture containing oxone was mixed with 2 g of KI and was shaken vigorously. 0.2 g of Vitrx indicator was added and left for 15 min. Finally 1 ml of glacial acetic acid was mixed into the solution and shaken well. The resultant mixture was titrated with sodium thiosulphate.

Lastly the radical quenching studies were carried out to determine the type of active radical formed in the reaction. Two different kinds of quenching reagent, *viz.*, ethanol and tertiary butanol were used for the study.

4.3.5 Catalyst Regeneration

The spent catalyst was recovered from the reaction mixture by filtration and washed thoroughly with distilled water and dried at 70 ºC.

4.4 Results and Discussion

4.4.1 Physiochemical characterization of supported catalysts

The ion-exchange of sodium ion present in the zeolite with the cobalt ions yielded a pinkish-red color powder with the intensity of coloration being the highest for zeolite X>zeolite A>ZSM-5 as evident from the visual inspection of the samples shown in

Figure 4.4-1.

1: Na-zeolite A

2: Na-zeolite X

3: Na-ZSM-5

4: Co-zeolite A

5: Co-zeolite X

6: Co-ZSM-5

7: Co-zeolite X Post Reaction

8: Co-ZSM-5 Post reaction

Figure 4.4-1 Na and Co exchanged zeolite samples

Figure 4.4-2 displays the diffuse reflectance spectroscopy (DRS) spectra of three Co exchange zeolites. In the given three cobalt exchanged zeolite samples, the spectral minima appear around 530 nm in the visible region and 240 nm in the UV region. These absorptions are assigned to the transitions of the octahedral $[Co(H_2O)_6]^{2+}$ complex formed due to the octahedral coordination of the exchanged cobalt ions located in the centre of the sodalite cage with 6 water molecules. This complex is also responsible for the hydrolysis and dissolution of zeolites especially with low Al/Si ratio which is discussed later. Additionally, in the case of zeolite-A a small peak observed at 640 nm is attributed to the cobalt ions present in unit cell body which confers to the tetragonal co-ordination with the framework oxygen.

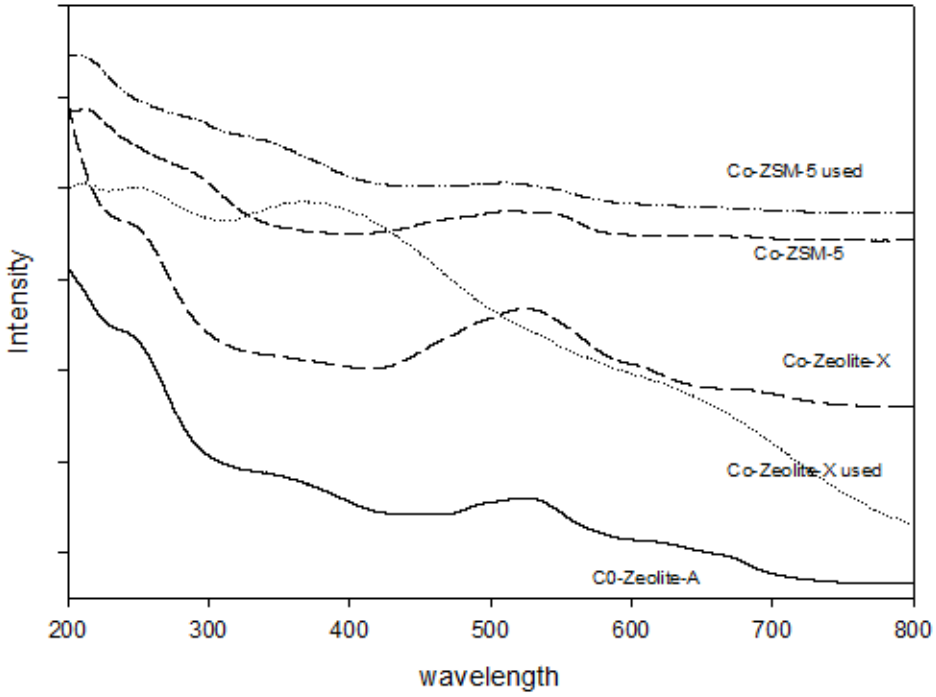

Figure 4.4-2 Diffuse UV-Viz spectra of Co-zeolite pre and post reaction

The capacity of the zeolites to retain the cobalt ion in the framework during the catalytic reaction mostly depends on the stability of the structure after the exchange of the metal ion. Figure 4.4-3 shows the XRD spectra of the zeolite samples after cobalt exchange. It is observed that Co-ZSM5 maintains the absolute crystalline structure of ZSM5 without any changes. Co-zeolite X still keeps the major crystal structure but the intensities of its representative peaks are significantly reduced, suggesting a partial loss of crystallinity and its transformation to amorphous phase, whereas the diffraction peaks for Co-zeolite A have disappeared suggesting the complete loss of crystallinity. Table 4.4-1 shows the crystallinity of the zeolite post and pre ion exchange. The crystallinity of Na-zeolite was taken as a reference with its crystallinity assigned to 100%.

Table 4.4-1 Crystallinity of Na and co exchanged zeolites

	% Crystallinity of Na form (reference)	% Crystallinity after Ion Exchange	% crystallinity after reaction
Zeolite A	100	Amorphous	Sample dissolved
Zeolite X	100	17.04	Amorphous
ZSM-5	100	83.80	39.86

The structural damage of zeolite after cobalt exchange is attributed to the excessive formation of the hydronium ions. The hydrated Co^{2+} is acidic and thus will result in the formation of H_3O^+ ion and $CoOH^+$ in the exchange solution, which are capable of being exchanged with Na^+ ion in the crystal along with the Co^{2+} ions. This hydronium ion tends to attack the zeolite framework causing the dissolution of the Al^{3+} ions resulting in the loss of crystallinity [31].

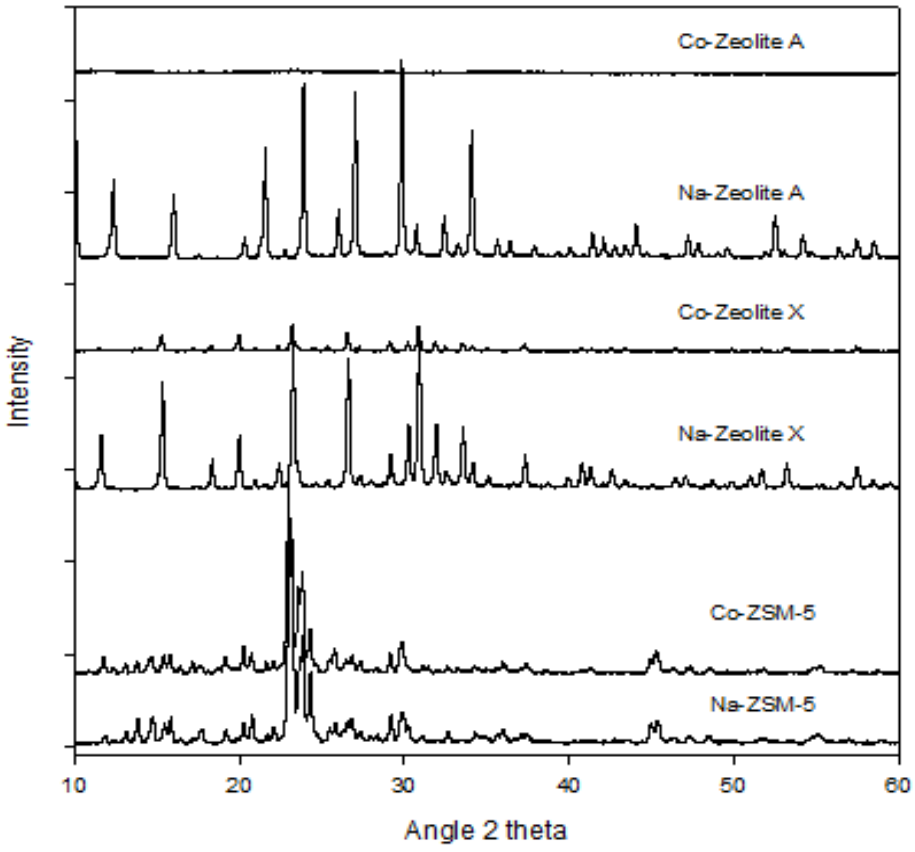

Figure 4.4-3 XRD spectra of Na and Co exchanged zeolites

Although the structures of both zeolites A and X were considerably lost, the SEM image showed a little change in the particle morphology (Figure 4.4-4). Both the Na and Co exchanged zeolite A and X showed rectangular shaped particles with sharp edges with the particle size in the range of 0.5-1 micron.

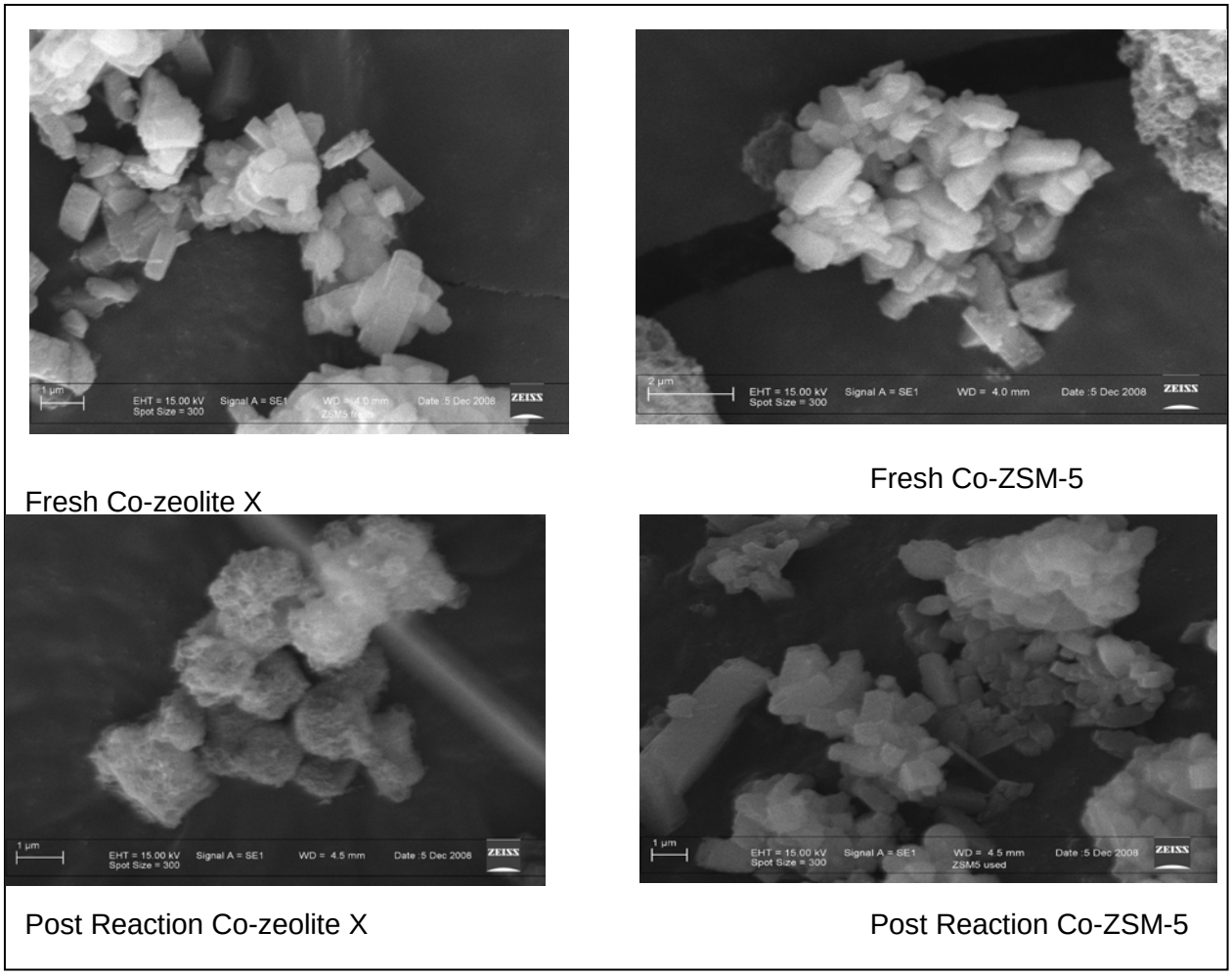

Figure 4.4-4 SEM images of fresh and used Co-zeolite samples

4.4.2 Catalytic activity and structural stability of Co-zeolite

Preliminary experiments of phenol oxidation were carried out in the presence of each Co-zeolite catalyst to test their efficiency and stability. Figure 4.4-5 shows the degradation profile of phenol in the presence of oxone and Co-zeolite catalyst. It is observed that the rate of oxidation with zeolite A and X is extremely fast with phenol degradation getting completed in less than 30 min whereas it takes around 6 h for complete phenol degradation in the presence of Co-ZSM-5. Interestingly, the rate of oxidation in the presence of Co-zeolite A and X is much similar to homogeneous oxidation of phenol in the presence of $CoCl_2$ and oxone. The extremely fast rate of oxidation observed in the presence of cobalt zeolite A and X is due to the homogeneous reaction between the oxone and cobalt ion which is leached into the solution occurring because of the collapse and dissolution of the zeolite structure. This phenomenon was visibly evident in the case of zeolite A, as the catalyst shows

strong dissolution in the solution and recovery of the catalyst by filtration yielded negligible amount of catalyst solid. Zeolite A is known to consume acid (H^+) ions via hydrolysis and proton ion-exchange at acidic pH. During the oxidation reaction, the pH of the solution was around 3-3.5. It is suggested that, the acid consumption of zeolite A is significantly high at low pH, which is attributed to the increase of aluminium oxidation state to +3 ions, resulting in dissolution of zeolite A [Cook et al.].

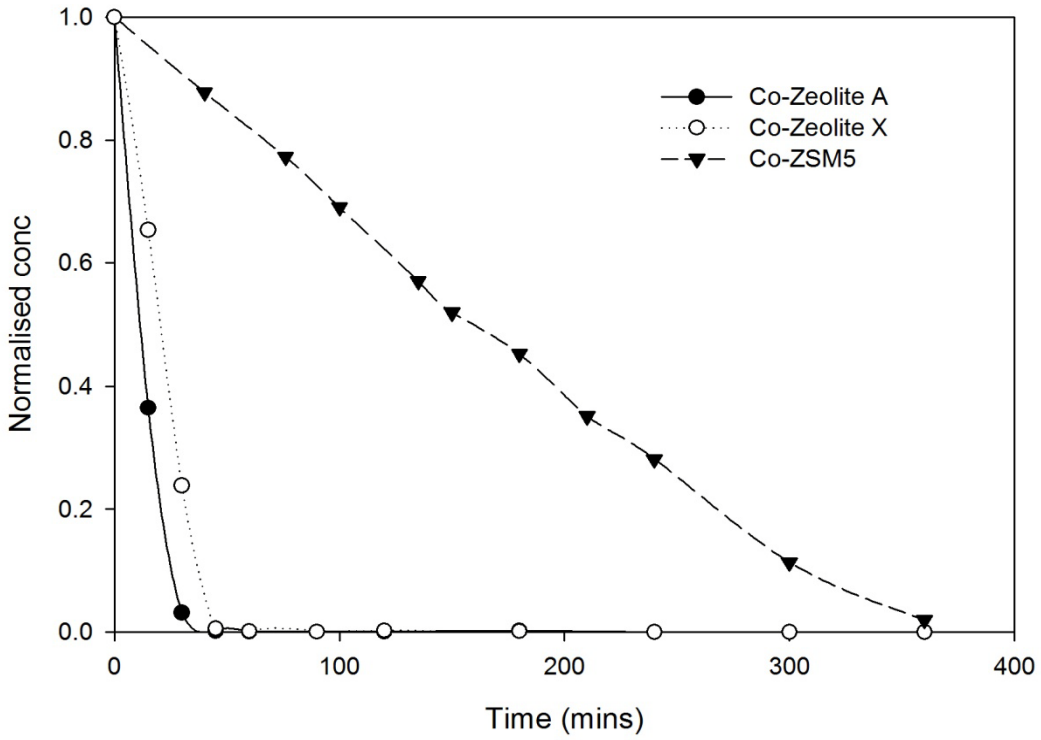

Figure 4.4-5 Phenol degradation kinetics using different cobalt exchanged zeolites [0.4 g/l catalyst, 2g/l oxone, 25 ppm Phenol and 25 ^{0}C]

Similar to zeolite A, zeolite X also gave a very fast reaction suggesting the major leaching of cobalt ion due to structural loss and dissolution. However, unlike zeolite A, only partial dissolution was observed in zeolite X and partial recovery of catalyst was possible by filtering the solution after the reaction. It was observed that the catalyst has turned from pinkish to grey as seen in Figure 4.4-1. XRD analysis of the spent catalyst obtained after the reaction is shown in Figure 4.4-6 shows a complete loss of the crystallinity. The structural loss of zeolite X is also due to formation of excess hydronium ion as discussed above resulting in loss of aluminium from the structure.

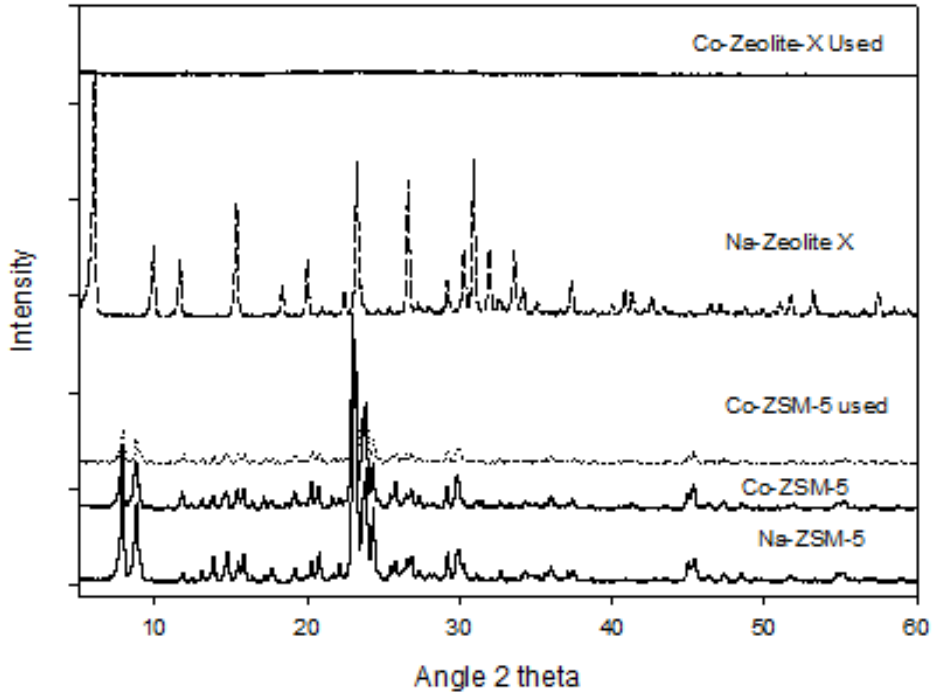

Figure 4.4-6 Post reaction XRD of Co exchanged zeolites

Additionally, the diffusive UV-Vis spectra of used Co-X as seen in Figure 4.4-2, showed no representative peak of octahedral $[Co(H_2O)_6]^{2+}$ complex as seen in the case of Co-zeolite X. For ZSM-5, a post reaction diffusive UV-Vis spectrum is almost same but with a slight decrease in the intensity of the representative peak of the octahedral complex. Among the three types of catalyst, ZSM-5 shows a comparative stable structural and catalytic property, thus confirming that the reaction is indeed taking place in the heterogeneous mode. The XRD spectra of the recovered ZSM-5 sample shows 40 % loss of crystallinity, with complete recovery of the catalyst post reaction. It has been earlier proposed that the cobalt exchanged into ZSM-5 is present in 3 different forms (Co^{2+} Co_3O_4 or $CoAl_2O_4$) depending on the Si/Al ration of the zeolite. The zeolite with the lower Si/Al ratio generally contains Co^{2+} ions present as an exchangeable ion. These ions are highly active for reaction with peroxymonosulphate, however during the reaction; it gets raised to a higher oxidation state probably causing the detoriation of the structure and getting leached out, as observed in the case of zeolite A and X. However apart from Co^{2+} ions, ZSM-5 also contains cobalt in the oxide form (generally as CoO, Co_3O_4 or $CoAl_2O_4$ [19]. The

oxides of Co are much more stable while reacting with peroxymonosulphate due to quick oxidation-reduction as per following reaction:

$$HSO_5^- \xrightarrow{Co^{2+} \rightarrow Co^{3+}} SO_4^{-\bullet} + OH^- \qquad \text{Equation 4.4-1}$$

$$HSO_5^- \xrightarrow{Co^{3+} \rightarrow Co^{2+}} SO_5^{-\bullet} + H^+ \qquad \text{Equation 4.4-2}$$

Thereby, it allows the Co-ZSM-5 based catalyst to remain partially stable for multiple usages. Furthermore, the amount of cobalt present as exchangeable ion or as an oxide form depends significantly on the Si/Al ratio. ZSM-5 having Si/Al = 15 would contains cobalt mostly in the exchangeable form as Co^{2+} whereas ZSM-5 having Si/AL=40 would contains cobalt mostly in the oxide form [19]. In the current case the Si/Al ratio of the ZSM-5 used was 25, thus even if a linear co-relation is assumed, it can be approximated that almost 50% of the cobalt was present in the ionic form and remaining as an oxide form. The 40% loss in crystallinity of ZSM-5 after reaction also implies toward the damage of the crystalline structure due to the exchangeable cation. Based on the observation, it can be proposed that the stability of the Co-ZSM-5 for the reaction would be better for higher Si/Al ratio, as it would have majority of the cobalt in the oxide form. However, this hypothesis has not been verified in this project and will be a focus of interest in our near future.

4.4.3 Catalytic activity of ZSM5 and Co-ZSM5

Figure 4.4-7 shows the dynamic variation of phenol concentration under various reaction conditions. A control experiment of phenol oxidation with Co-exchanged ZSM-5 but without any oxidant shows a negligible change in the concentration, suggesting a minimal adsorption of phenol on Co-ZSM5. Another control experiment of phenol oxidation in the presence of Na-ZSM5 with oxone also reveals a negligible rate of phenol oxidation, suggesting that Na-ZSM5 cannot activate peroxymonosulphate to generate sulphate radical. The reaction in the presence of peroxymonosulphate and Co-ZSM-5 catalysts resulted in complete degradation of phenol in less than 6 h. The phenol degradation in the presence of other two oxidants, H_2O_2 and persulphate, with Co-ZSM5 is shown in Figure 4.4-8. It is observed that phenol degradation is quite small, less than 10% in 6 h, indicating that Co-ZSM5 could not effectively activate H_2O_2 and persulphate as much as it can do for the peroxymonosulphate to produce hydroxyl and sulphate radicals, respectively.

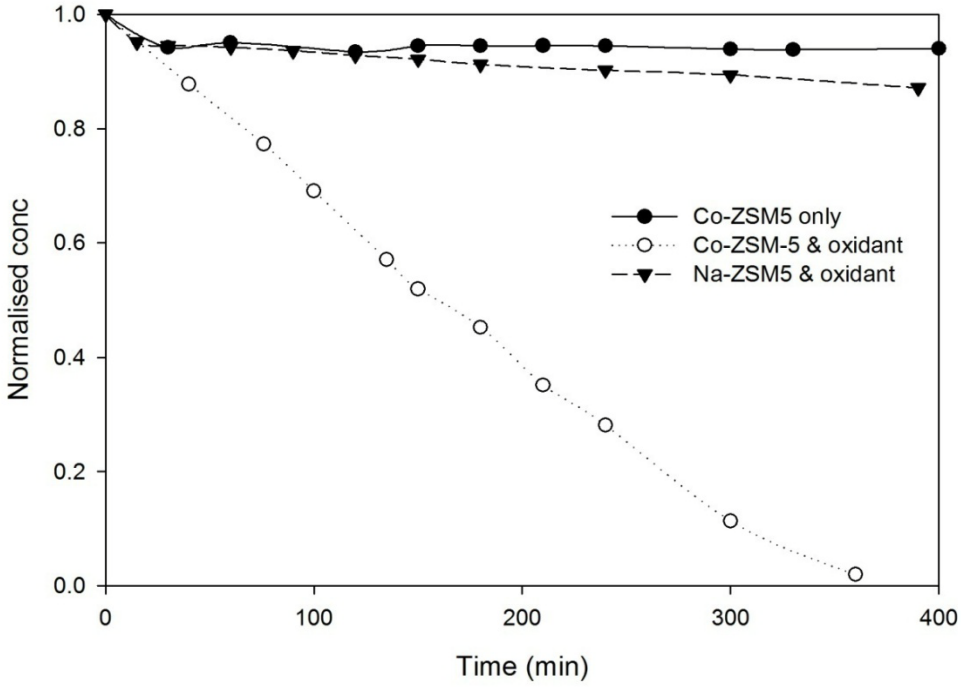

Figure 4.4-7 Preliminary study of Phenol degradation using Co-ZSM-5 [0.4 g/l catalyst, 2g/l oxone, 25 ppm Phenol and 25 ^{0}C]

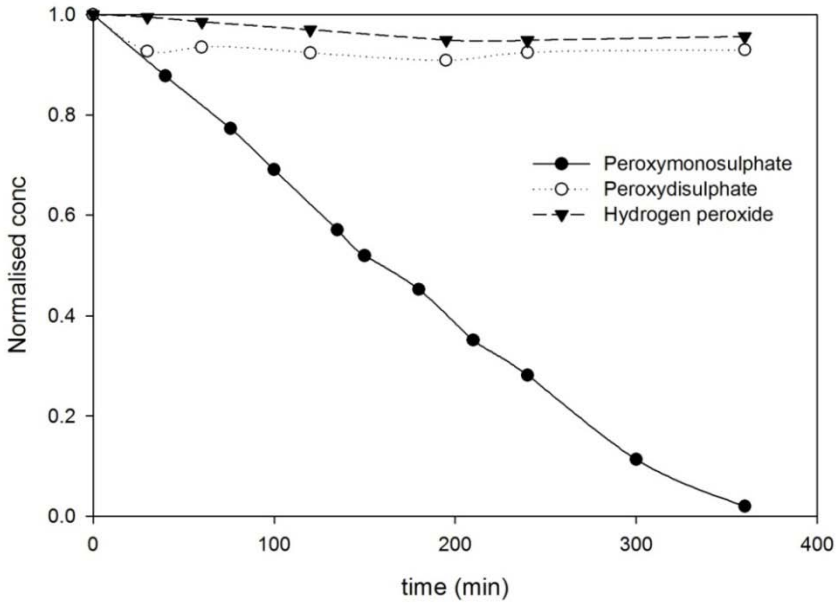

Figure 4.4-8 Oxidation of Phenol under the presence of different oxidants [0.4 g/l catalyst, 25 ppm Phenol and 25 ^{0}C]

4.4.4 Degradation kinetics of phenol in the presence of Co-ZSM-5

Figure 4.4-9 shows phenol degradation profiles at different initial concentrations. It is seen that phenol degradation efficiency changes with initial phenol concentration. At the concentration of 12.5 ppm, phenol degradation is fast and achieves 100% degradation within 4 hours, whereas at the concentration of 50 ppm, the degradation rate is slower and will achieve only 60% degradation within 6 hours. It is noted that the rate of phenol degradation rate seems to remain constant throughout the reaction, resulting in a linear degradation rate profile for each of the 3 initial concentrations.

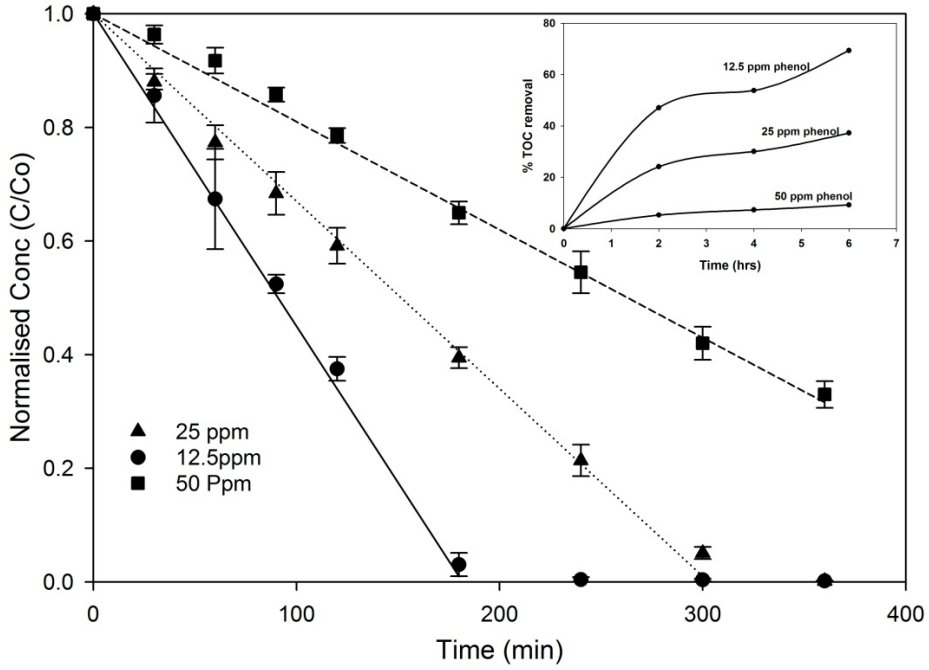

Figure 4.4-9 Phenol degradation kinetics at different initial concentration of Phenol [0.4 g/l catalyst, 2g/l oxone, and 25 ^{0}C]

The change in TOC was found to be very small with just 40% removal of organic carbon in the time period of 6 hours for the initial phenol concentration of 25ppm, suggesting that the majority of the degradation product still remains in water. However a few runs were carried out overnight and the TOC measurement showed a major 75-90 % removal depending on the amount of catalyst present. The extent of TOC removal varies with the initial concentration with the highest TOC removal observed for the lowest initial concentration of phenol. An interesting observation was made in regards to the change in the oxone concentration. As observed in Figure

4.4-10, only 25% oxone was consumed during the reaction having 25 ppm of phenol, however the similar test in the absence of phenolic contaminant in the solution shows 80% conversion of oxone. This is possibly due to the self consumption of oxone by the generated sulphate radical.

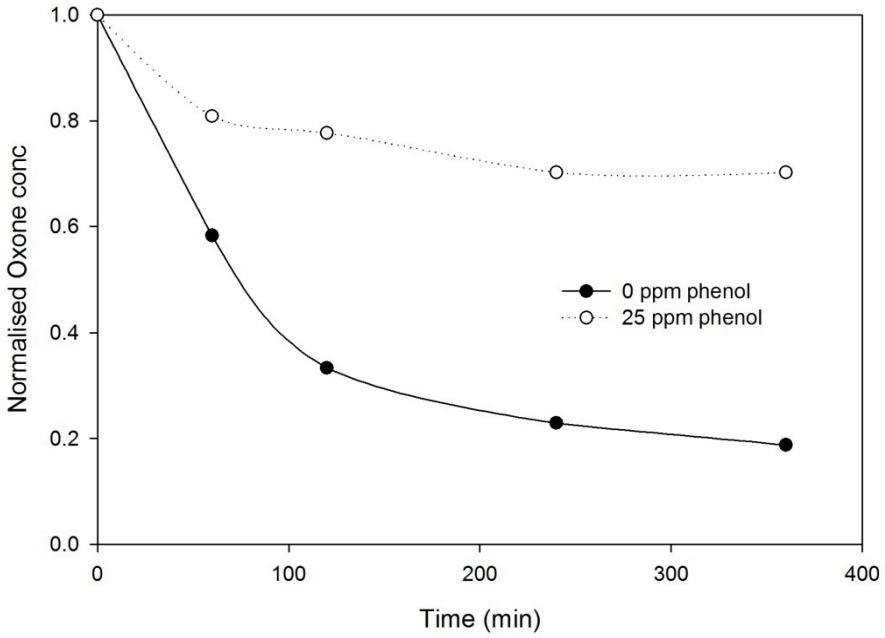

Figure 4.4-10 Oxone consumption with in the presence and absence of phenol.

The linear rate of phenol removal from the solution infers that the limiting step in the given case is not the phenol degradation by the active sulphate radical but the generation of the sulphate radical on the catalyst surface themselves.

The mechanism of sulphate radical formation and phenol degradation can be represented by the steps of initiation, propagation and termination as described by the equations below

Initiation

The reaction of cobalt ion in the zeolite structure with the inter-crystalline or adsorbed water molecule

$$Co^{2+} + H_2O \rightarrow CoOH^+ + H^+$$

$$CoOH^+ + HSO_5^- \rightarrow CoO^+ + H_2O + SO_4^{\cdot-}$$

Propagation

$$CoO^+ + 2H^+ \rightarrow Co^{3+} + H_2O$$

$$Co^{2+}\ HSO_5^- \rightarrow Co^{3+} + OH^- + SO_4^{\cdot-}$$
$$Co^{3+} + HSO_5^- \rightarrow Co^{2+} + H^+ + SO_5^{\cdot-}$$

$$SO_4^{\cdot-} + OH^-(or H_2O) \rightarrow SO_4^{2-} + OH^{\cdot}(+H^+)$$

Termination

$$Co^{2+} + SO_4^{\cdot-} \rightarrow Co^{3+} + SO_4^{2-}$$

$$RH + SO_4^{\cdot-} \rightarrow RH^+ + SO_4^{2-}$$

Based on the above reaction scheme the steady state approximation results in the rate kinetic equation as per the following equation which is dependent only on cobalt concentration as per equation below. Detail discussion about the derivation is given in section 2.7.8

$$\frac{dC_{ph}}{dt} = k_{co}[Co^{2+}] \qquad \text{Equation 4.4-3}$$

In the current experiment of phenol degradation for a fixed amount of cobalt catalyst and assuming zero order kinetics of phenol removal, the mass balance on the batch reactor can be written as follows.

$$V\frac{dc_{ph}}{dt} = -(-r_{ph})W = -k_{co}W \qquad \text{Equation 4.4-4}$$

Where, C_{ph} is the phenol concentration at any instant 't', k_{co} is the apparent zero order rate constant, W is the mass of the catalyst and V is the volume of the reactor. Integration of the above equation results in the mathematical model of the degradation profile. The rate constant is depicted in Table 4.4-2.

Initial Ph Conc.	Rate constant *10^{-4} (min^{-1})
12.5 ppm	1.25
25 ppm	0.75
50 ppm	0.25

4.4.5 Effect of Reaction parameter on phenol degradation kinetics

4.4.5.1 Effect of catalyst Amount

The effect of catalyst concentration on the phenol degradation was studied by varying the cobalt loading from 0.1 to 0.3 g/l while keeping the other parameters fixed. The degradation kinetic at different cobalt loading and the respective profile of rate constant is shown in Figure 4.4-11. It can be noted from equation 4.4-3 that the rate of phenol degradation is linearly dependent on the cobalt concentration. In the present case upon increasing the catalyst, the concentration of cobalt ions available for the reaction increases. As seen, the rate of phenol degradation increases with the increase in catalyst amount from 0.1 to 0.6 g/l. The plot of rate constant with respect to catalyst amount results in a straight line.

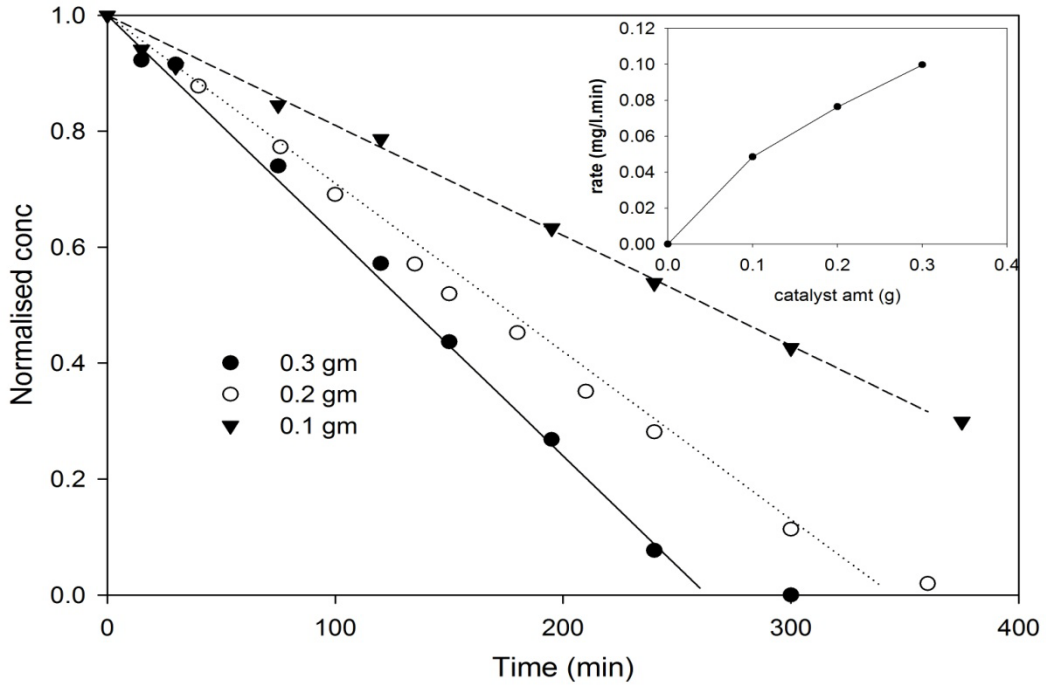

Figure 4.4-11 Effect of catalyst amount on the reaction rate [2g/l oxone, 25 ppm Phenol and 25 ^{0}C]

4.4.5.2 Effect of oxidant concentration

The effect of peroxymonosulphate concentration on phenol degradation is shown in Figure 4.4-12. As observed, the rate of phenol oxidation was improved by increasing

oxone concentration and a plateau was reached after 1 g, suggesting further increase in oxidant concentration will not affect the oxidation rate.

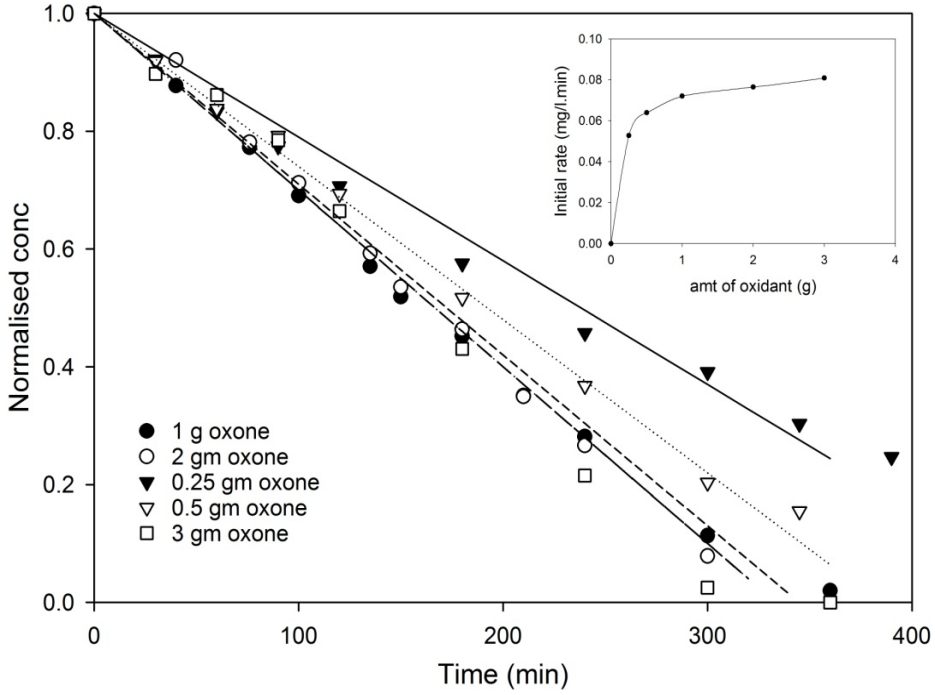

Figure 4.4-12: Phenol degradation at different amount of oxidant [0.4 g/l catalyst, 25 ppm Phenol and 25 ^{0}C]

4.4.5.3 Effect of reaction temperature

The temperature significantly affects the rate of reaction and the reaction rate constant increases exponentially with the increase in the temperature similar to that of the reaction rate constant following the Arrhenius correlation[32]. Figure 4.4-13 displays the variation of phenol concentration at varying temperatures. The relationship between reaction rate and temperature by the Arrhenius correlation was also presented. From the Figure, it is seen that phenol degradation is quite low at low temperature and will increase significantly with increasing temperature. At 15 ºC, phenol degradation efficiency was only 30% in 6 h, while it reached to 100% in 90 and 60 min, respectively at temperatures of 40 and 50 ºC. Based on zero-order kinetics, the relationship between phenol degradation rate and temperature follows the Arrhenius equation and gives the activation energy as 69.7 kJ/mol.

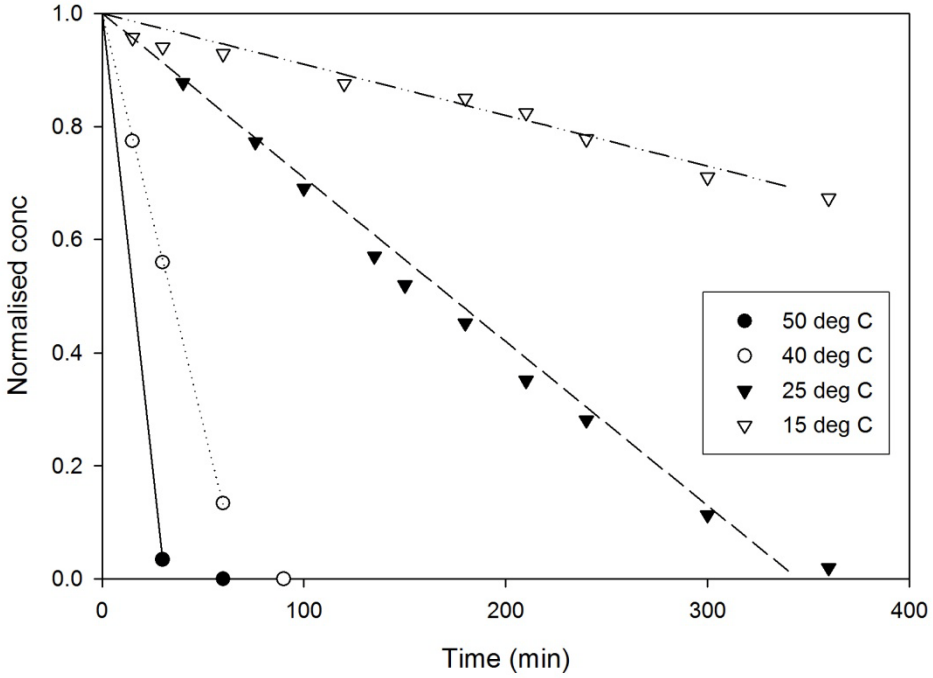

Figure 4.4-13 Temperature effect on the degradation rate of Phenol with Co-ZSM-5 [0.4 g/l catalyst, 2g/l oxone, 25 ppm Phenol]

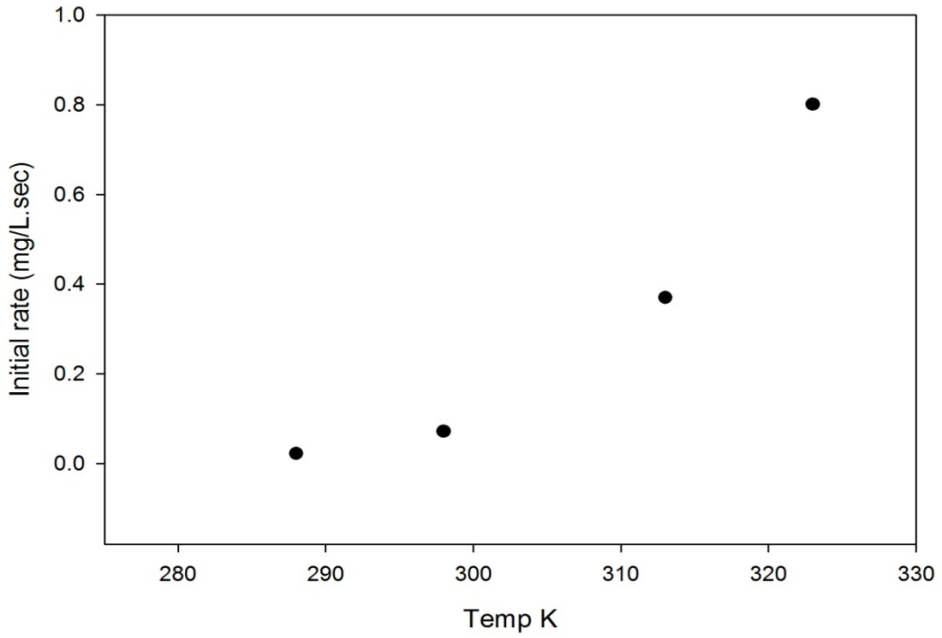

Figure 4.4-14 Effect of change in temperate on the rate kinetic for phenol oxidation with Co-ZSM-5

4.4.6 Validation of surface controlled reaction via quenching studies

So far we have assumed that the reaction takes place in the heterogeneous mode with the contaminant getting adsorbed and oxidized on the surface of zeolite. However, there could be a possibility of another mechanism wherein the active radical would get released from the surface and react with phenol in the homogeneous mode. In order to identify the mechanism, we conducted several experiments of phenol degradation in the presence of ethanol as the competing contaminant. The reactivity of ethanol with sulphate radical is extremely fast with the second order rate constant of $2x10^7$ $M^{-1}s^{-1}$ [33], and thus by spiking the solution with a small quantity of ethanol may highly affect the degradation kinetics of phenol.

However, the adsorption capacity between ethanol and phenol is reversed. Ethanol being highly hydrophilic as compared to phenol would have a poor adsorption tendency than phenol.

Figure 4.4-15 shows the phenol degradation kinetics in the presence of different ethanol concentration. It can be seen that the presence of equimolar amount of ethanol tends to have negligible effect on the phenol degradation kinetics. Had the reaction been taking place in the homogeneous mode, the degradation of phenol should have reduced considerably due to high reactivity of ethanol with SO_4^* radical. However, in the case of heterogeneous oxidation, since the adsorption capacity of phenol is significantly higher than that of ethanol, it would occupy the available position on the catalyst surface and get reacted without having any competition given by the ethanol molecules. Only at an extremely high concentration of ethanol (almost 1000 times that of phenol), there was a noticeable reduction in the phenol concentration. At extremely high concentration, the ethanol molecule would tend to give appreciable competition to phenol for occupying the active surface and thus result in the decrease of the phenol kinetics.

Lastly, the quenching test was also helpful in further justifying the generation of active sulphate radical from the peroxymonosulphate oxidant. Peroxymonosulphate oxidant can produce both sulphate and hydroxyl radical and also a small amount of peroxymonosulphate radical [34]. In order to identity the actual oxidizing radical present in the system, the quenching studies were carried out with ethanol and tertiary butanol. Ethanol is capable of quenching both sulphate and hydroxyl as it has

a high reactivity towards both radicals, whereas tertiary butanol mainly reacts with hydroxyl radical and much slowly with that of sulphate radical [33, 35].

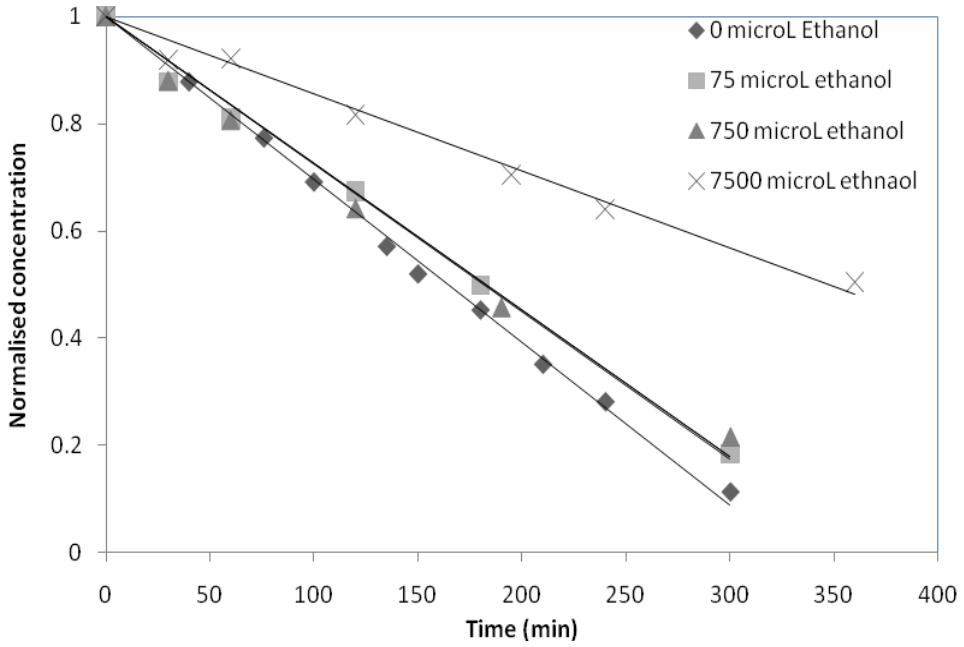

Figure 4.4-15: Reaction quenching with different amount of ethanol [0.4 g/l catalyst, 2g/l oxone, 25 ppm phenol and 25 ^{0}C]

Figure 4.4-16 shows the rate of phenol oxidation under the influence of both quenching reagents. It is observed that the rate of reaction is negligibly affected at lower concentration of ethanol (150 microL) despite the fact that ethanol is a strong quencher of both the sulphate and peroxide radicals. On further increase in the concentration of ethanol to 7.5 ml, the rate of phenol oxidation was found to decrease significantly, showing only 50% oxidation in the reaction period of 6 hrs.

The reaction carried out under the similar concentration of TBA, shows a minimal effect on the rate of phenol oxidation, thereby suggesting that major radical formed in the given reaction is sulphate, however, a presence of small amount of hydroxyl radical is also possible due to the slight reduction in the rate of phenol on addition of TBA.

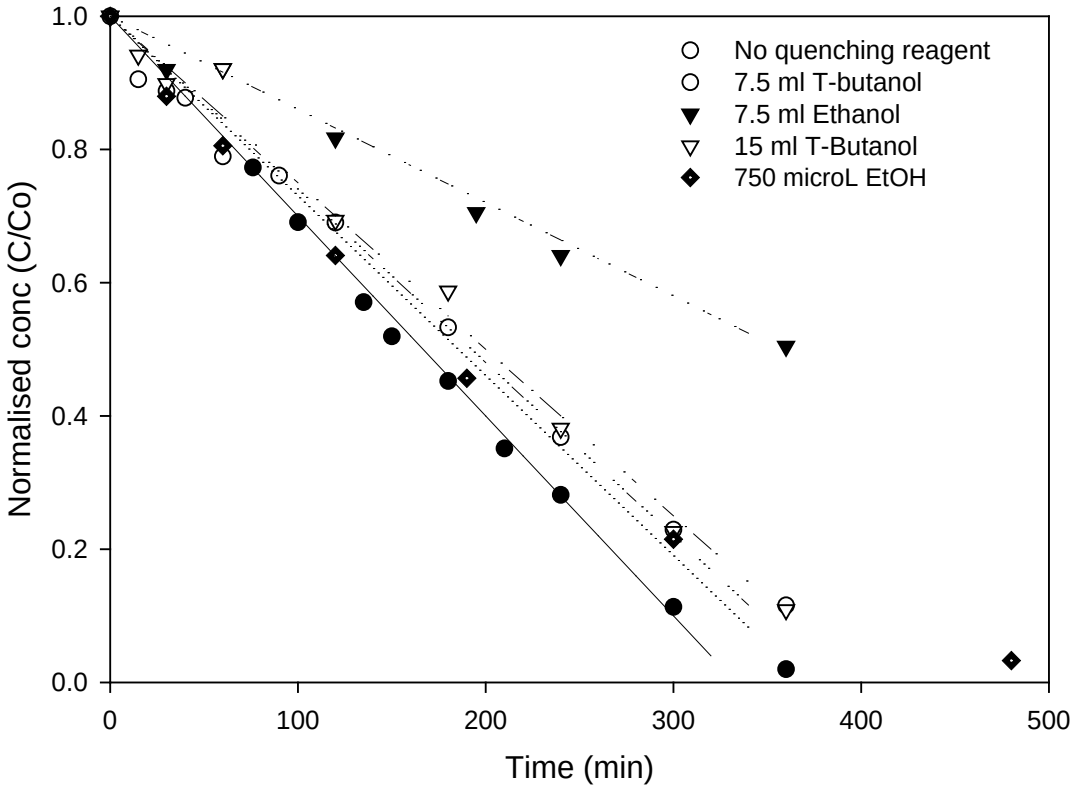

Figure 4.4-16 Reaction quenching of Phenol oxidation with Co-ZMS-5 in the presence of Ethanol and Tert Butanol. [0.4 g/l catalyst, 2g/l oxone, 25 ppm Phenol and 25 ^{0}C]

4.4.7 Reactivity of the spent catalyst and catalyst reusability

Figure 4.4-17 shows catalytic activity of recycled Co-ZSM5 for phenol degradation. As seen, the catalyst activity remained unaffected in the second round reuse and decreased slightly in the third test. The analysis of the solution using AAS shows a negligible presence of Co ion in the second test and 0.2 ppm Co ion leaching in the third recycled test. This suggests that the cobalt ion was bonded strongly in ZSM-5 framework, thus gives quite stable performance in the reaction.

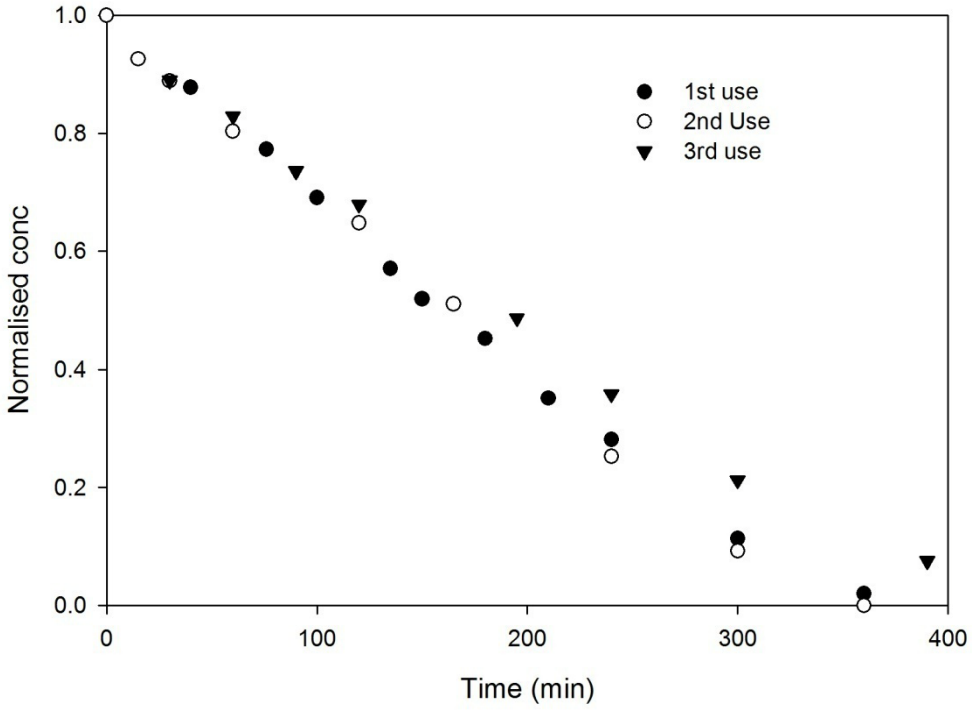

Figure 4.4-17 Phenol degradation carried out by repeated use of the Co-ZSM-5 catalyst. [0.4 g/l catalyst, 2g/l oxone, 25 ppm Phenol and 25 ^{0}C]

4.5 Conclusions

Cobalt exchanged zeolite was utilized for the activation of peroxymonosulphate to generate active sulphate radical for the oxidation of phenolic compounds. Among the three different types of zeolite, ZSM-5 was found to be the stable support to dock cobalt ions and catalyze the reaction. The rate of phenol oxidation is found to follow the zero order reaction. The rate of reaction was observed to be significantly enhanced with increase in the amount of catalyst and the reaction temperature. Based on quenching studies, it was confirmed that sulphate radical was the active radical taking part in the reaction. Apart from peroxymonosulphate, other oxidants such as hydrogen peroxide and persulphate showed negligible activity toward oxidation. Finally, the extent of TOC removal was observed to be comparatively slow with respect to phenol removal due to the slow degradation of the intermediates, however with the longer run of more than 24 hrs, appreciable removal of TOC resulted, implying the potential application of the catalyst for industrial waste water treatment.

4.6 References

1. Breck, D.W., *Zeolite molecular sieves*. 1974: Wiley New York.

2. Barrer, R.M., *Zeolites and their synthesis.* Zeolites, 1981. **1**(3): p. 130-140.

3. Ozin, G.A. and F. Hugues, Selective photo activation of carbon-hydrogen bonds in paraffinic hydrocarbons. Dimerization of alkanes. The Journal of Physical Chemistry, 2002. **86**(26): p. 5174-5179.

4. Li, Y. and J.N. Armor, *Selective catalytic reduction of NOx with methane over metal exchange zeolites.* Applied Catalysis B: Environmental, 1993. **2**(2-3): p. 239-256.

5. Johan, A.M., et al., NAbatement in Exhaust from Lean-Burn Combustion Engines by Reduction over Silver-Containing Zeolite Catalysts. Angewandte Chemie International Edition, 1998. **37**(13-14): p. 1901-1903.

6. Dry, M.E., *Present and future applications of the Fischer–Tropsch process.* Applied Catalysis A, General, 2004. **276**(1-2): p. 1-3.

7. Pierella, L.B., et al., Co-ZSM-5 Zeolites: Characterization and Magnetic Properties.

8. Froment, G.F., Kinetics of the hydroisomerization and hydrocracking of paraffins on a platinum containing bifunctional Y-zeolite. Catalysis Today, 1987. **1**(4): p. 455-473.

9. Sugioka, M., et al., *Hydrodesulfurization over noble metals supported on ZSM-5 zeolites.* Catalysis Today, 1998. **45**(1-4): p. 327-334.

10. Maxwell, I.E., *Zeolite catalysis in hydroprocessing technology.* Catalysis Today, 1987. **1**(4): p. 385-413.

11. Chatterjee, S., H.L. Greene, and Y.J. Park, Comparison of modified transition metal-exchanged zeolite catalysts for oxidation of chlorinated hydrocarbons. Journal of Catalysis, 1992. **138**(1): p. 179-194.

12. Fajerwerg, K. and H. Debellefontaine, Wet oxidation of phenol by hydrogen peroxide using heterogeneous catalysis Fe-ZSM-5: a promising catalyst. Applied Catalysis B, Environmental, 1996. **10**(4): p. 229-235.

13. Neamt u, M., et al., Fe-exchanged Y zeolite as catalyst for wet peroxide oxidation of reactive azo dye Procion Marine H-EXL. Applied Catalysis B, Environmental, 2004. **48**(4): p. 287-294.

14. Carmo, M.J. and J.C. Gubulin, *Ethanol-water separation in the PSA process.* Adsorption, 2002. **8**(3): p. 235-248.

15. Flanigen, E.M., *Molecular sieve zeolite technology—the first twenty-five years.* Zeolites--science and technology, 1984: p. 3.

16. Riley, P.E. and K. Seff, Crystallographic evidence for hydrolysis in zeolites. Structure of hydrated partially cobalt (II)-exchanged zeolite A. The Journal of Physical Chemistry, 1975. **79**(15): p. 1594-1601.

17. Park, J.Y., A Study on the Structure and Thermal Property of Co2+-Exchanged Zeolite A.

18. Bae, D. and K. Seff, *Structures of cobalt (II)-exchanged zeolite X.* Microporous and Mesoporous Materials, 1999. **33**(1-3): p. 265-280.

19. Michal, K. and S.J. Datka, *An IR spectroscopy study of Co sites in zeolites CoZSM-5.* Applied Catalysis. A, General, 2007: p. 330.

20. Wadley, S. and T.D. Waite, *Fenton processes.* 2006.

21. Anipsitakis, G.P. and D.D. Dionysiou, Degradation of organic contaminants in water with sulfate radicals generated by the conjunction of peroxymonosulfate with cobalt. Environ. Sci. Technol, 2003. **37**(20): p. 4790-4797.

22. Chen, X., et al., Kinetics of oxidative decolorization and mineralization of Acid Orange 7 by dark and photoassisted Co2+-catalyzed peroxymonosulfate system. Chemosphere, 2007. **67**(4): p. 802-808.

23. Lison, D., Human toxicity of cobalt-containing dust and experimental studies on the mechanism of interstitial lung disease (hard metal disease). CRC Critical Reviews in Toxicology, 1996. **26**(6): p. 585-616.

24. Anipsitakis, G.P., E. Stathatos, and D.D. Dionysiou, *Heterogeneous activation of oxone using Co3O4.* J. Phys. Chem. B, 2005. **109**(27): p. 13052-13055.

25. Yang, Q., H. Choi, and D.D. Dionysiou, Nanocrystalline cobalt oxide immobilized on titanium dioxide nanoparticles for the heterogeneous activation of peroxymonosulfate. Applied Catalysis B, Environmental, 2007. **74**(1-2): p. 170-178.

26. Yang, Q., et al., Heterogeneous activation of peroxymonosulfate by supported cobalt catalysts for the degradation of 2, 4-dichlorophenol in water: The effect of support, cobalt precursor, and UV radiation. Applied Catalysis B, Environmental, 2008. **77**(3-4): p. 300-307.

27. Pierella, L.B., et al., Catalytic activity and magnetic properties of Co–ZSM-5 zeolites prepared by different methods. Applied Catalysis A, General, 2008. **347**(1): p. 55-61.

28. Pierella, L.B., et al., Occluded cobalt species over ZSM-5 matrix: Design, preparation, characterization and magnetic behavior. Materials Research Bulletin, 2008. **43**(8-9): p. 2026-2035.

29. Verberckmoes, A.A., B.M. Weckhuysen, and R.A. Schoonheydt, *Spectroscopy and coordination chemistry of cobalt in molecular sieves.* Microporous and Mesoporous Materials, 1998. **22**(1-3): p. 165-178.

30. ASTM, Standard Test Method for Determination of Realtive Crystallinity of Zeolite ZSM-5 by X-Ray Diffraction, D. 5758-01, Editor. 2001.

31. Cook, T.E., et al., *Zeolite A hydrolysis and degradation.* Environmental Science and Technology, 1982. **16**(6): p. 344-350.

32. IUPAC, Compendium of Chemical Terminology. 2007.

33. Jameton, R.A., J.G. Muller, and C.J. Burrows, *Oxidative DNA damage from sulfite autoxidation catalyzed by manganese(III).* Comptes Rendus Chimie, 2002. **5**(5): p. 461-466.

34. McLachlan, G.A., et al., Metal-mediated oxidation of guanines in DNA and RNA: a comparison of cobalt(II), nickel(II) and copper(II) complexes. Inorganica Chimica Acta. **251**(1-2): p. 193-199.

35. Muller, J.G., et al., DNA and RNA Modification Promoted by [Co(H2O)6]Cl2 and KHSO5: Guanine Selectivity, Temperature Dependence, and Mechanism. Journal of the American Chemical Society, 1996. **118**(10): p. 2320-2325.

5 - Cobalt impregnated solid catalysts for combined adsorption and oxidation of phenolic waste water

Abstract

As seen in the previous chapter, cobalt exchanged ZSM-5 demonstrates significant capacity for catalytic oxidation of phenol, however, the rate of reaction is limited on the extent of amount of cobalt ion being exchanged into the structure. In the current chapter cobalt loading via impregnation technique into some support materials has been investigated. Two different support materials viz silica and SBA-15 were utilized. In-situ cobalt loading was carried out in SBA-15 support whereas impregnation technique was utilized for loading of cobalt in silica. In comparison to Co-Silica, Co-SBA-15 showed better cobalt-substrate bonding strength as evidence from lesser extent of cobalt leaching in the later case as compared to the former. Additionally, in-order to investigate the effect of cobalt precursor, three different types of cobalt precursor viz cobalt chloride, cobalt acetate and cobalt nitrate was utilized for loading cobalt on silica via impregnation technique. Co-Silica catalyst prepared using cobalt nitrate based precursor was found to be better in terms of metal-substrate bonding strength as evidence from minimal leaching and better catalyst reusability. The last part of this chapter is focused on a novel cobalt-activated carbon catalyst. Unlike silica, activated carbon based catalyst shows high rate of phenol removal. Several reaction parameters such as effect of catalyst loading, oxidant amount and temperature were investigated.

Part A: Cobalt impregnated silica catalyst

5.1 Introduction

The narrow pore opening within the micro-porous structures like those of zeolites tends to provide a specific hindrance to the transport of the reactant molecules from approaching the catalyst inside the solid pores and thus affects the reaction kinetics. Additionally, the catalytic activity of cobalt exchanged ZSM-5 is limited due to the upper limit on the moles on cobalt ions being exchanged into the ZSM-5 structure. It was observed in the previous chapter that the heterogeneous phenol oxidation occurs at extremely slow rate in the case of Co-ZSM-5. In the current chapter, two different types of catalyst support were investigated, a) commercial amorphous silica and b) In-house synthesized mesoporous silica (SBA-15) which poses larger pore diameter in comparison to commercial amorphous silica. Apart from the structural difference, there is another major difference in both catalysts. Cobalt was loaded into a commercial silica by impregnation technique, whereas cobalt ion was loaded into SBA-15 during the catalyst synthesis process (In-situ loading) as discussed in the later part of the chapter.

5.1.1 Mesoporous SBA-15

In order to overcome the resistance to the molecular transport within a catalyst, there has been increasing demand for the development of highly porous material with substantially thermal and acid stability. The development of MCM (*Mobil Corporation Mesoporous materials*) in the early 90's was one such an attempt in this direction. MCM's are highly ordered mesoporous silica based materials which pose very high surface area (<1000 m^2/g). MCM-41 belonging to this family is one popular mesoporous material which has been utilized for adsorption and storage for hydrogen [1], CO_2 [2], hydrodesulphurization of petroleum residue [3] and even for waste water oxidation [4]. However these materials had a limited success in waste water oxidative catalysis due to its poor thermal stability. The application of mesoporous materials in catalysis received a vital boost with the discovery of a family of SBA based silica material by Zhao et al. in Santa Barbara [5] thus making the material namesake of its place of origin (Santa Barbara Amorphous material). Unlike MCM, these mesoporous materials showed excellent thermal stability. SBA-15 belonging to the SBA family poses a two dimensional arrangement of hexagonal

tubes of silica. The wall thickness of the channels ranges from 3.1 to 6.4 nm [5]. Most interestingly, SBA-15 contains both micro and meso pores within the particles. A typical longitudinal section of a channel if enlarged would look as shown in Figure 5.1-1.

Figure 5.1-1: Section of meso-porous SBA-15

The hexagonal tubes of SBA-15 are hollow having meso-pores which would be advantageous for molecules to move freely. Additionally the micro pores present in the wall of the tubes would provide active sites for docking the catalyst particles. Due to its exceptional properties, SBA-15 has received substantial attention in supported metal catalysis [6, 7], adsorption of heavy metals [8], docking of enzymes and other biomaterials [9-11], and also providing efficient housing for synthesis of nano materials [12].

5.1.2 Production Technique of SBA-15

The synthesis of SBA-15 is generally carried out by a sol-gel technique which would follow 5 main steps: 1) Dissolution of a structure directing agent (a surfactant) in an aqueous solution resulting in self assembly of the surfactants to provide a framework for the deposition of silica. 2) Formation of silica monomer Si-O-Si from the precursor (generally TEOS) and deposition around the surfactant framework. 3) Polymerization

of the monomer surrounding the surfactant framework 4) Agglomeration of the surfactant covered silicate particles forming a hexagonal structure, the process also known as ageing 5) and finally calcining the agglomerated particles to remove the template resulting in the formation of highly organized mesoporous silica structure.

The detailed discussion of the steps is as follows.

5.1.2.1 Formation of structure directing framework

The most common structure directing agent (template) used for SBA synthesis is amphiphilic triblock copolymer, (Pluronic-123) chemically known as poly(ethylene oxide)-b-poly(propylene oxide)-b-poly(ethylene oxide) as seen in Figure 5.1-2a. As the name suggests the block molecule consists of a hydrophobic poly propylene oxide molecule surrounded by two hydrophilic poly ethylene molecules. Once dissolving these molecules in aqueous solutions, they tend to bend to form a “V” shaped structure with hydrophobic polypropylene oxide at the centre and two hydrophilic polyethylene oxide molecules forming the outer two ends. Several of these molecules come together to form a micelle surface (framework) for deposition of silica as seen in Figure 5.1-2b below.

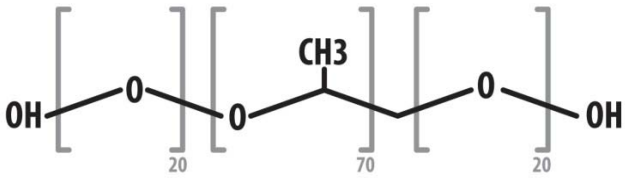

Figure 5.2.1 a: Molecular structure of surfactant P123

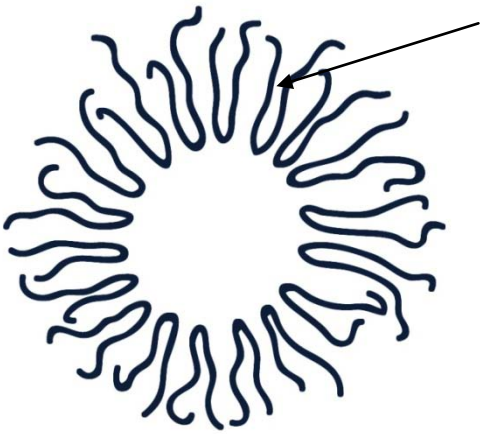

Figure 5.1-2b: Micelle structure of the dissolved surfactants

5.1.2.2 Formation of silica monomer and deposition on the framework

Following the dissolution of the surfactant, a silica precursor is added drop by drop into the solution. The common silica precursors used are TEOS (Tetra ethyl ortho silicate), TMOS (tetra methyl ortho silicate) or sodium silicate. We take the example of TEOS here; the other precursors would follow the same mechanism. The slow addition of TEOS in the aqueous solution results in the hydrolysis reaction thereby forming silanol group (Si-OH), which upon condensation and polymerization results in the formation of siloxane (Si-O-Si). Both these structure formation would be discussed in section 5.4.2 of this chapter while discussing the FTIR spectra of the sample. The siloxane would then polymerize to form silicate species which then tends to chemically bond to surfactant framework as seen in Figure 5.1-3.

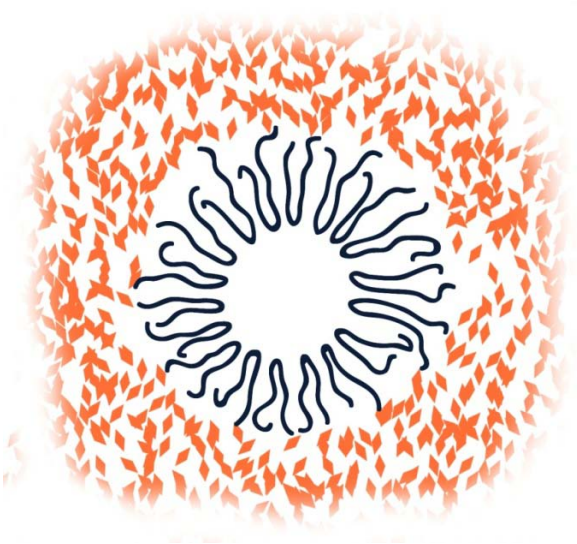

Figure 5.1-3: Polymerisation of siloxane around the micelle framework

5.1.2.3 Agglomeration of the surfactant covered silicate particles (Ageing)

The mixture thus obtained is allowed to age for 1-2 days which helps in the formation of hexagonal network due to the agglomeration of the particles.

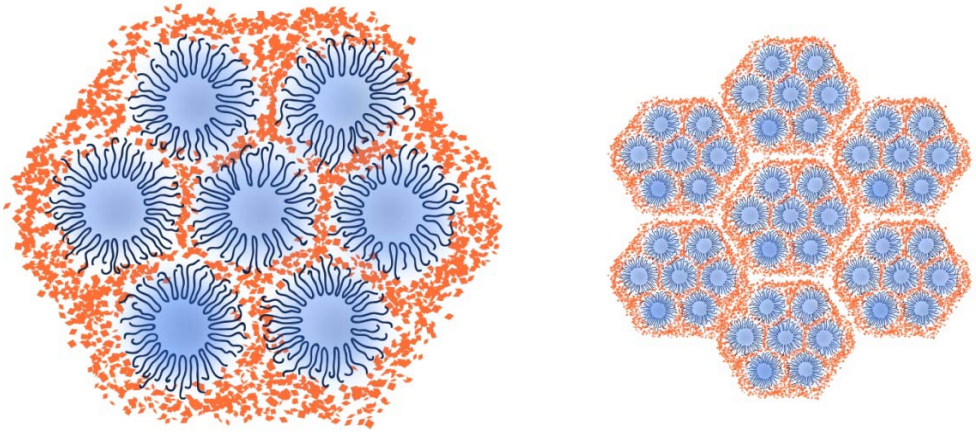

Figure 5.1-4: Agglomeration of particles

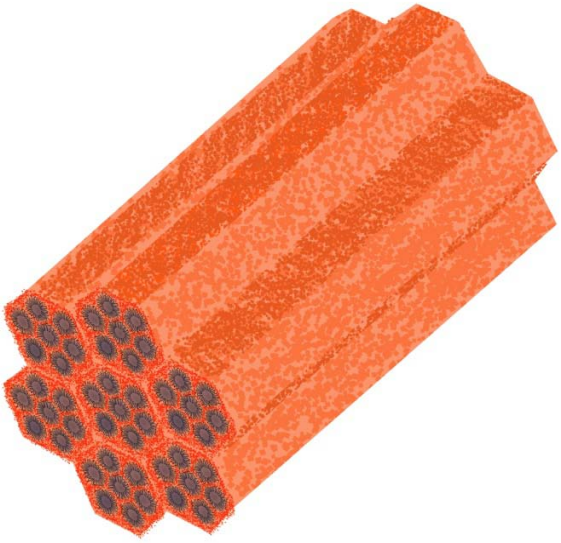

Figure 5.1-5: 3D structure of the siloxane tubes.

5.1.2.4 Removal of Template

This is the final stage of SBA synthesis which involves the removal of the template to expose the meso and micro pores within the structure. The most common technique of template removal is calcination carried out at around 500 ^{o}C under air. Alternatively solvent extraction or microwave digestion can also be employed to remove the template.

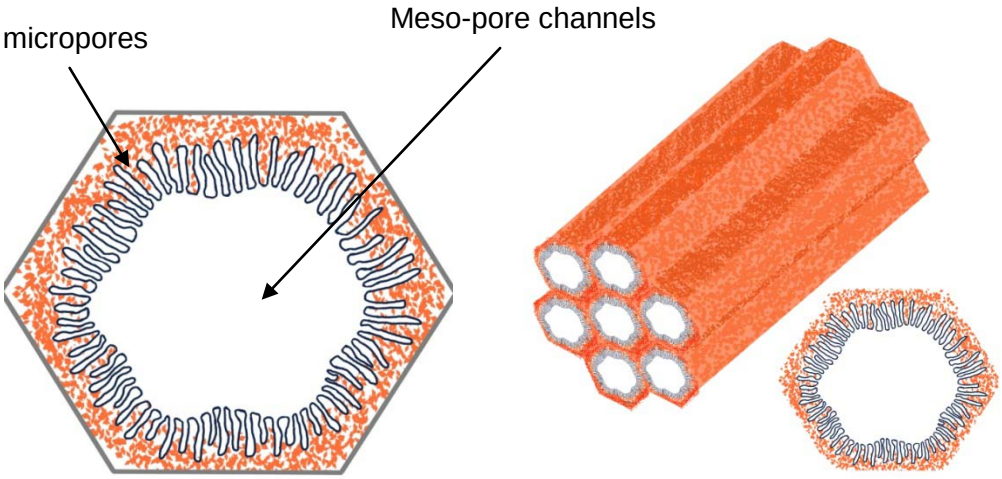

Figure 5.1-6: Meso-porous SBA-15 after removal of the template.

5.1.3 Catalysis loading in SBA-15

The pores within the channels of SBA-15 provide attractive sites to dock the catalyst for catalytic reaction. The most common technique to prepare a catalyst loaded SBA-15 is in-situ loading of the metal ions. In the process the desired amount of metal precursor is added in the surfactant solution prior to the addition of silica precursor. This technique has been employed for loading of Fe, Co, Cu and many others. Ti and Fe loaded SBA-15 has been employed as a catalyst for oxidation of phenol in the presence of H_2O_2. Cobalt loaded SBA-15 was utilized as a Fischer-Tropes catalyst [7, 13], Aluminum impregnated SBA for enhanced adsorption of phosphates [14]. SBA-15 has also been utilized to immobilize enzymes such as alpha-amylase for starch hydrolysis [15].

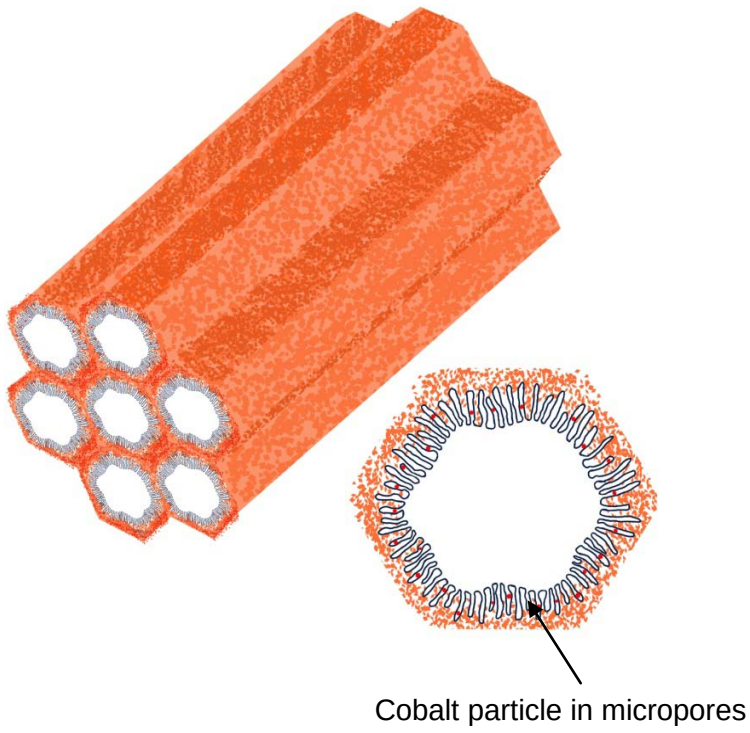

Figure 5.1-7 : Cobalt loaded SBA-15

5.2 Objective of this work

The main objective of this work was to test the efficiency of two different types of silica loaded catalyst for carrying out the heterogeneous advanced catalytic oxidation of phenol contaminated waste water. Phenol contaminated waste water was selected due to its harmful health effect when released into the environment. The phenol is present in the waste discharged stream of several industries such as pharmaceutical, petrochemical and others. The two different types of silica based supports selected were, a mesoporous SBA-15 having well defined pore structure and amorphous silica. The mesoporous SBA-15 provides meso-pores for efficient transport of the cobalt metal to penetrate deep inside the particle during the synthesis and possibly getting trapped in the microporous walls before converting to cobalt oxide, thus potentially having a higher metal-support interaction. The kinetic study was carried out to determine the rate of phenol degradation. The efficiency of the catalysts was estimated by measuring the total organic carbon removed by the catalytic reaction. The influences of catalyst type (SBA-15 or silica), catalyst amount, oxidant amount, reaction temperature and the type of cobalt precursor on the catalytic advanced oxidation reaction were studies.

5.3 Experimental

5.3.1 Synthesis of SBA-15 and Co-SBA-15

SBA-15 was synthesized, following the procedure previously described by Zhao et al. [5] with an intermediate step of addition of a cobalt precursor to incorporate the cobalt ions in the support. The method involved, mixing a known amount of tri-block copolymer P123 (obtained from BASF Corp.) into 2M HCl solution and stirring for 1-2 hrs at approx 35 ^{o}C, followed by an addition of silica precursor and cobalt precursor (TEOS and $COCl_2$ fixed to obtain 5 wt% cobalt in silica) drop-wise with constant stirring. The mixture was then allowed stirred continuously for 24 hrs at 35 ^{0}C. The mixture was transferred to a Teflon lined autoclave to keep the solution under hydrothermal condition at 90^{o}C for 2 days. The product was recovered by filtration and washed several times with deionized water, and dried at room temperature. The template was removed by calcination at 500^{o}C for 6 hrs with a slow ramp of 2 ^{o}C/min. The catalyst was then stored in a desiccator until further used. Pure SBA-15 sample was also synthesized following the same procedure without addition of cobalt precursor for a comparison.

5.3.2 Loading of Co^{2+} in Amorphous Silica

Amorphous silica was purchased from Sigma, which was directly used for cobalt loading without any treatment. A wet impregnation technique for loading of cobalt was utilized. In brief the method involves dissolving a fixed amount of cobalt precursor (cobalt chloride) in water. A fixed amount of SiO_2 (99% Aldrich) was added to the solution in order to obtain 5 wt% cobalt in silica. The suspension was stirred for 24 hrs for impregnation and proper distribution of the cobalt precursor in the support material (SiO_2). At the end of 24 hrs, the water was slowly evaporated using a rotary evaporator at 40 ^oC under vacuum. The recovered solid was calcined in a programmable furnace at 500 ^oC for 6 hrs with the slow ramp of 2 ^oC/min. After calcination, the catalysts were washed with milli-Q water to remove the loosely bonded cobalt. The catalyst was stored in a desiccator until further use.

5.3.3 Characterization of catalysts.

The cobalt analysis was done to estimate the amount of cobalt loaded in the support. In the process a fixed amount of the synthesized catalyst was dissolved in concentrated hydrofluoric acid. For a few silica samples, the mixture was slowly heated to enhance the dissolution. 1 ml of the solution was carefully extracted and diluted in milli-Q water (18 micro ohms). The concentration of cobalt in the sample was analyzed using an AAS. The texture and morphology of the SBA-15 sample were observed using transmission electron microscope (TEM). For analysis, the samples were dispersed in ethanol and then settled on the film by evaporating the solvent. The structural feature and the mineralogy of the samples were studied using XRD (Simens XRD instrument, using filtered Cu Kα radiation, with accelerating voltage of 40 kV, current 30 mA and scanned at 2θ from 5 to 70^0). Small angle XRD was used to measure the diffraction from SBA-15 due to larger diffracting distance. The FTIR spectroscopic analysis was done to determine the functional groups of the samples by a Bruker instrument using a KBr pellet technique at room temperature. The dried KBr was homogenized with the samples in a mortar. The disks with radius 1 cm and thickness 0.1 cm were then prepared using a hydraulic press. All the spectra were recorded over 4000-400 cm^{-1} at a resolution of 4 cm^{-1}. The samples for the FT-Raman analysis were prepared by pressing the powder using a hydraulic press and carefully placed on the slide for analysis.

5.3.4 Kinetic study of phenol oxidation with oxidant and catalyst

The catalytic oxidation of phenol was carried out in a 500 ml reactor containing 25 ppm of phenolic solution. The reactor was attached to a stand and dipped in a temperature regulated water bath to control the temperature. The reaction mixture was stirred with a plastic coated stirrer at around 400 rpm to maintain uniform mixing. Before the beginning of the reaction a known amount of oxidant; peroxymonosulphate (PMS) was added to the mixture and allowed to dissolve. Later a fixed quantity of catalyst depending on the predefined reaction parameter was added to start the reaction. The reaction was carried out for 6 hrs, and during a fixed interval, 0.5 ml of sample was withdrawn using a syringe filter into an HPLC vial. 5 ml of pure methanol was quickly added to quench the reaction. Methanol is known as an efficient compound to quench both sulphate and hydroxyl radical.

5.3.5 Chemical analysis

The reaction samples were analyzed for TOC (Total Organic Carbon), phenol concentration, cobalt ion concentration and pH. The phenol concentration was analyzed using a HPLC with a UV detector at wavelength of 270 nm. C-18 column was used to separate the compounds in the sample. The sample was transported within the column using the mobile phase consisting of 30% CH_3CN and 70% water. TOC was measured to estimate the percentage of organic compound converted to CO_2 which is the final product to ensure clean water permissible to be discharged into the river or sea. The TOC analysis was carried out using a Shimadzu TOC analyzer. In the process, a small quantity of sample was injected into a furnace filled with platinum catalyst to catalytically oxidize the organic compound into CO_2 which was measured using an infrared detector. Finally, the cobalt ions were measured in the solution using a Varian AAS to estimate the leaching of the heavy metal from the catalyst. The leaching of cobalt from the catalyst support not only affects the reusability of the catalyst but also ends up polluting the water due with highly cobalt ions.

5.4 Result and Discussion

5.4.1 Structural analysis of SBA-15 and silica based catalysts

Pure SBA-15 is a mesoporous material giving a Bragg reflection at small angles. The small angle X-Ray scattering as shown in Figure 5.4-1, shows three distinct peaks

below 2º, which is in good agreement with the reported literature [16]. These peaks are typical for mesoporous silica, representing the planes of (100), (110) and (200), respectively. The full scan of the pure SiO_2 and SBA-15 sample from 10-70º shown in Figure 5.4-2 suggests the amorphous nature of the sample. A slight hump at around 20 ^{0}C is generally observed from the water absorption of the amorphous materials.

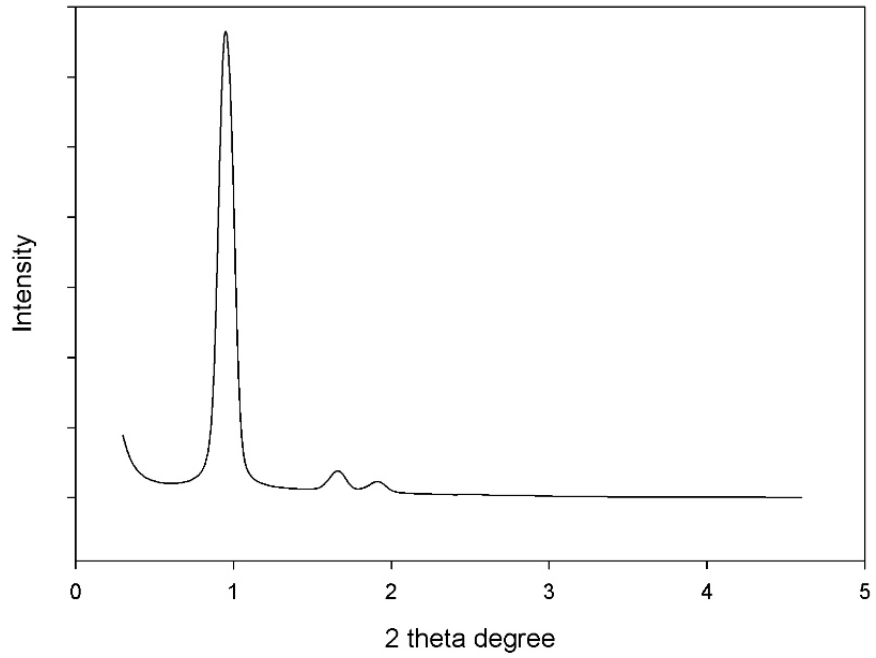

Figure 5.4-1 Small Angle scattering of the mesoporous SBA-15

The XRD spectra of Co-SiO_2 had distinct peaks of cobalt oxide crystallites which match closely to the first 5 major peaks of pure cobalt oxide (Co_3O_4). In the case of Co-SBA-15, the peaks at 37.96º and 64.54º suggest the presence of cobalt-oxide. A large ghost peak found at 43.96º suggests a presence of any impurity or probably could be a result of ordered alignment during sample preparation. The lowered intensity of the cobalt oxide peaks in the case of Co-SBA-15 when compared to Co-SiO_2 suggests that the cobalt oxide particles within the SBA-15 samples are well uniformly distributed and incorporated into the pores of SBA-15 as very small cluster. In the case of SiO_2 based support, the cobalt-oxide particles are highly aggregated and clustered resulting in higher diffraction of the incident X-ray beams. This observation is further validated by the FTIR spectra discussed further. The clustering of Co-oxide particles was also evident from the SEM image of Co-SiO_2 catalyst showing specks of bright cobalt particles within the samples.

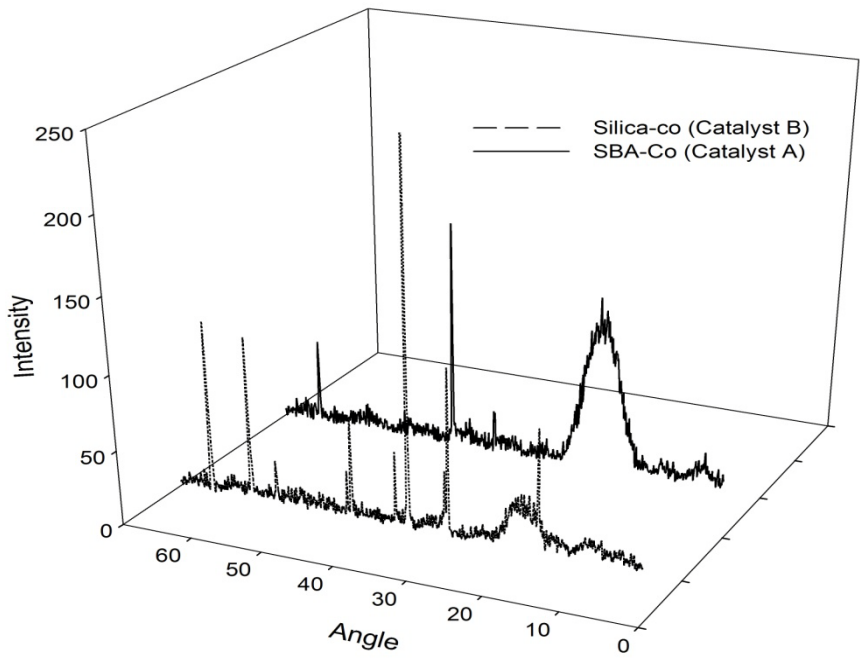

Figure 5.4-2 XRD spectra of Co-Silica and Co-SBA-15

The morphology of SBA-15 and cobalt loaded sample was analyzed using SEM and TEM imaging as observed in Figure 5.4-3 and Figure 5.4-4. The SBA particles are observed to be rod like cylindrical beads with the particle size with the range of 2-5 microns. TEM image confirms the well ordered channels in both SBA-15 and Co loaded SBA-15. The well organized channels provide sufficient opening for loading of the cobalt crystallites; however, several attempts to locate the specks of cobalt oxide crystallites yielded a negative result, suggesting the possibility of the formation of highly small and dispersed cobalt oxide particles which are well assimilated within the matrix. Never the less, the presence of cobalt in the sample was confirmed using EDX. The meso-porous channel width within the particle was measured to be approximately 20 nm. In contrast to the SBA-15 based support, silica particles were much smaller and lacked any organized matrix. The SEM image of silica particles shown in Figure 5.4-5 suggests hexagonal shaped particles of extremely small size.

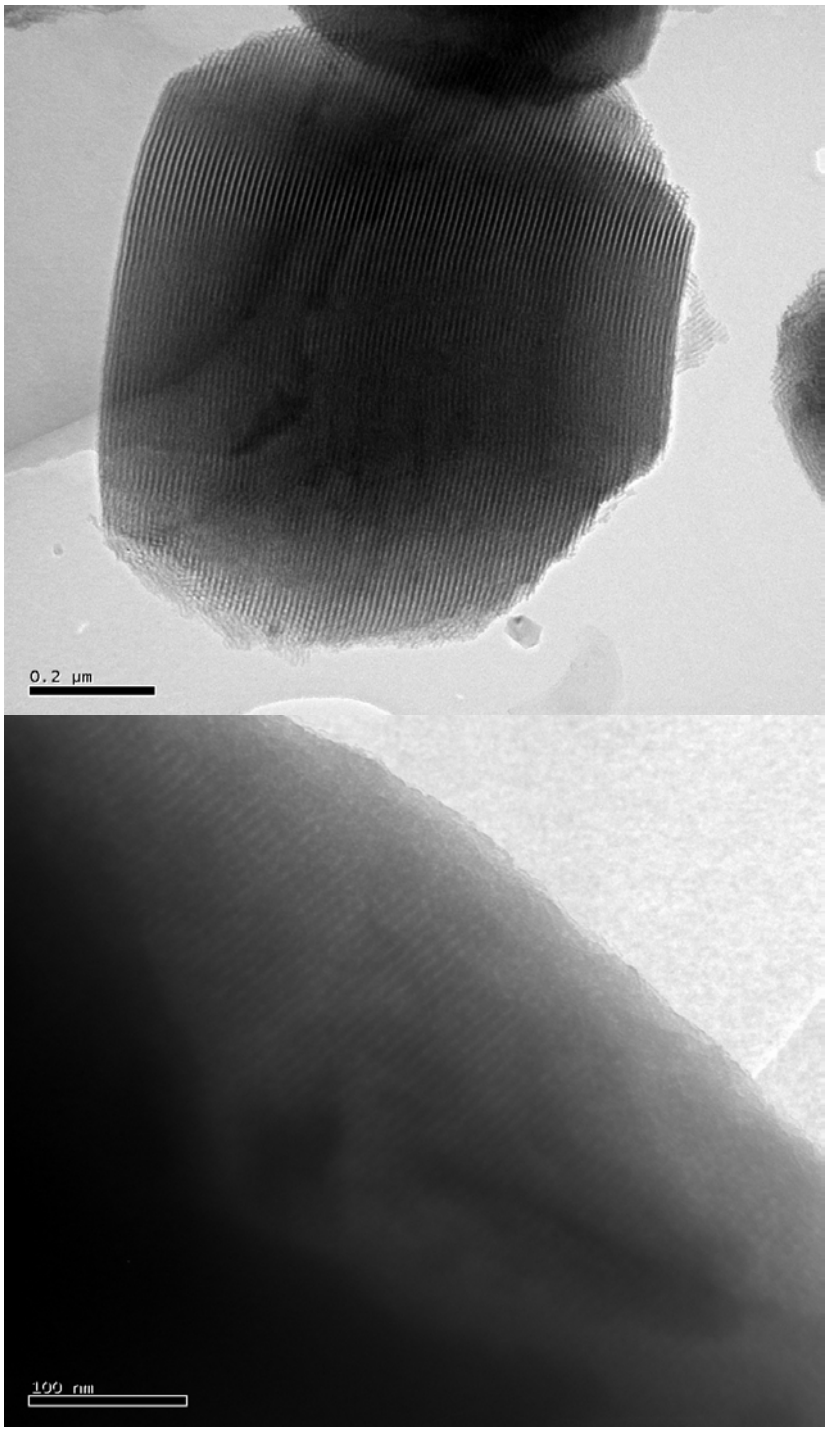

Figure 5.4-3 TEM showing the ordered mesoporous channels in SBA-15 (above) and Co-SBA-15 (below)

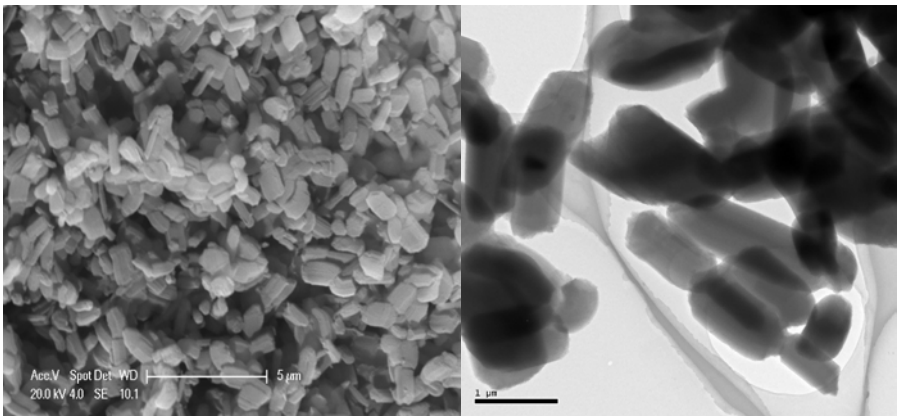

Figure 5.4-4 SEM (a) and TEM (b) showing the particle morphology of SBA-15

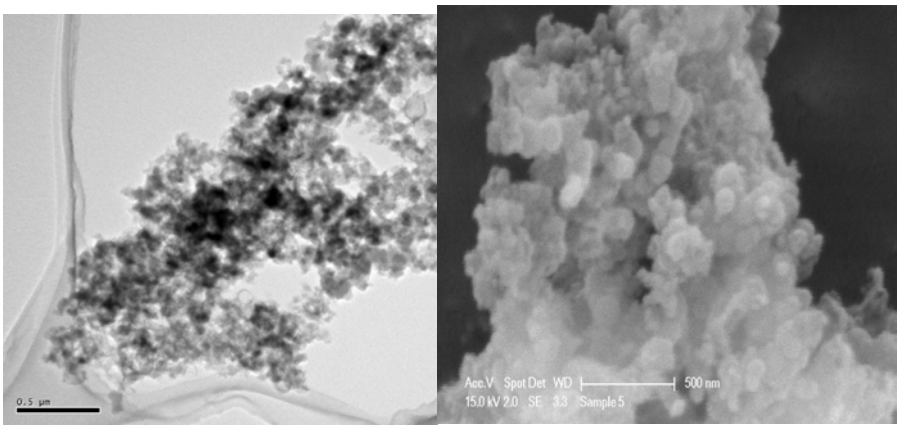

Figure 5.4-5 TEM (a) and SEM (b) showing the particle morphology of Co-silica

5.4.2 Spectroscopic analysis of SBA-15 and silica supported catalysts

FTIR spectra of both catalyst samples are illustrated in Figure 5.4-6. For Co-SBA-15, major peak at 1066 cm^{-1} represents the IR absorption due to stretching of Si-O-Si. The peaks close to 450 and 750 cm^{-1} are observed due to the bending and asymmetric stretching of the silicon and oxygen bonds. A small peak observed at around 1600 cm^{-1} is due to the presence of silanol (Si-OH) group present in the sample. This functional group is formed during the hydrolysis reaction of TEOS in the aqueous solution. The broad peak at 3357 cm^{-1} represents the O-H vibrations, which could be due to the adsorbed moisture from the atmosphere.

The Co-SBA-15 sample also shows a very small shoulder around 568 cm^{-1}, which is the representative of spinal Co-O bonding, thus suggesting the presence of small quantity of cobalt oxide crystallites. In the case of Co-SiO_2 catalyst, the typical Si-O-

Si stretching, bending and asymmetric stretching vibrations are observed at 1066, 450 and 750 cm^{-1}. In comparison to Co-SBA-15, Co-SiO_2 catalyst shows much intense peak of Co-O at 568 cm^{-1}, confirming the presence of large quantity of aggregated Co_3O_4 particles, as also suggested by the XRD spectra above.

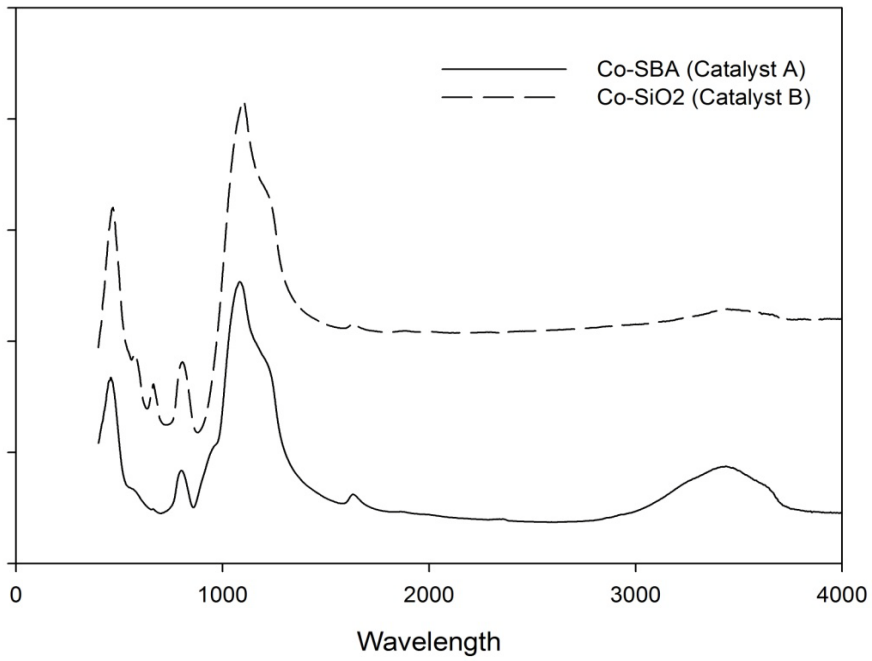

Figure 5.4-6 FTIR spectra of Co-SBA-15 and Co-Silica

5.4.3 Kinetic study of phenol oxidation

With the aim to test the potential of Co-SBA-15 and Co-SiO_2 to react with PMS for generating sulphate radicals, preliminary experiments were done and the results are shown in Figure 5.4-7.

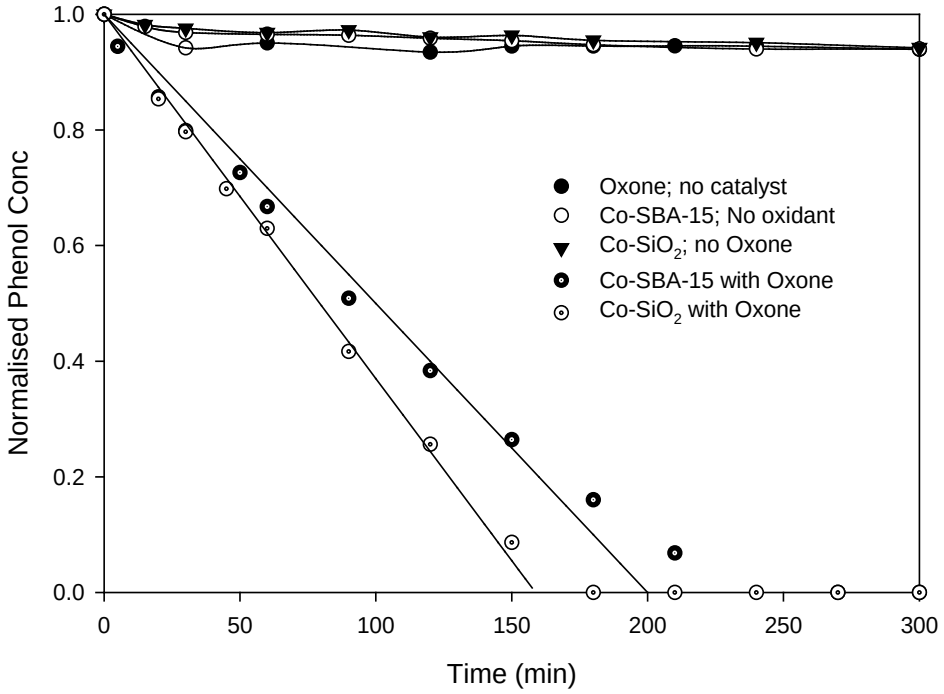

Figure 5.4-7 Preliminary test to examine phenol degradation using Co-silica and Co-SBA catalyst [C_{ph}-25 ppm, 25 ^{o}C, 0.2 g/l catalyst, 2 g/l oxone]

The control experiments to observe phenol degradation in the presence of catalyst and PMS individually showed negligible change in the phenol concentration. The reaction in the presence of catalysts along with 2 g/l oxone showed a complete degradation of phenol in less than 5 hrs. Under similar conditions, Co-SiO_2 with oxone showed a slightly higher rate of reaction as compared to Co-SBA-15 with oxone. The phenol degradation reaction was observed to follow zero order kinetics; indicating that the generation of sulphate radical is the rate controlling mechanism. Adapting the zero order kinetics, the rate constant measured is shown in Table 5.4-1.

Table 5.4-1 Kinetic parameter of Co-SBA and Co-SiO_2 catalyst

Catalyst	Mass of Catalyst (mg)	Mass of Oxidant (g)	Temperature ^{o}C	Rate constant (mg.min^{-1}l^{-1})
SBA-15-Co	100	1	25	0.005
SiO_2-Co	100	1	25	0.0063

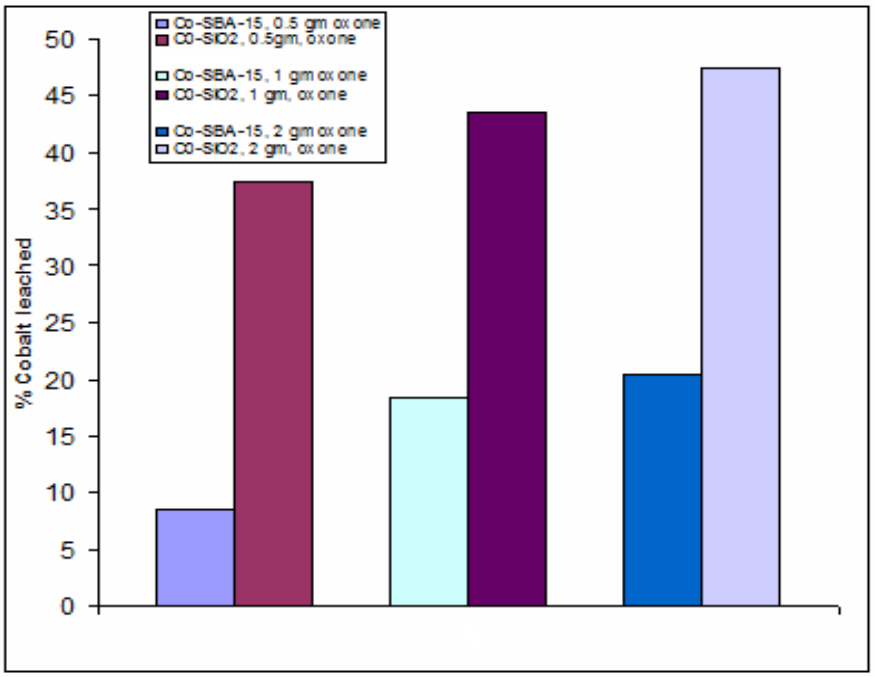

Figure 5.4-8 Cobalt leaching from Co-SBA and Co-Silica catalyst

Figure 5.4-8 showing the cobalt leaching from catalyst samples suggests a higher extent of cobalt leaching from Co-SiO_2 as compared to Co-SBA-15. SBA-15 support was finely engineered in-order to provide efficient transport of the pollutant (phenol) molecules within the mesoporous particle and thus provide efficient catalyst and reactant contact, which would enhance the rate of reaction and thus would prove better than SiO_2 based support. Regardless of this fact, the actual observation was contradictory. The enhanced rate of reaction in the case of Co-SiO_2 is attributed to the leached cobalt ions into the solution which contributes to phenol degradation from simultaneous homogeneous reaction. The effect of cobalt leaching also shows its impact on the catalyst reusability. Elevated leaching observed for Co-SiO_2 as compared to Co-SBA-15 results in decreased activity of the Co-SiO_2 during the reuse of the catalyst as seen from Figure 5.4-9 and Figure 5.4-10. After 6 hours of reaction, the silica based catalysts showed around 32% degradation of phenol as compared to 58% on Co-SBA-15. The better catalyst and support bonding and the uniform distribution of cobalt in Co-SBA-15 are primarily due to the *in-situ* loading of cobalt precursor into SBA-15 during the synthesis.

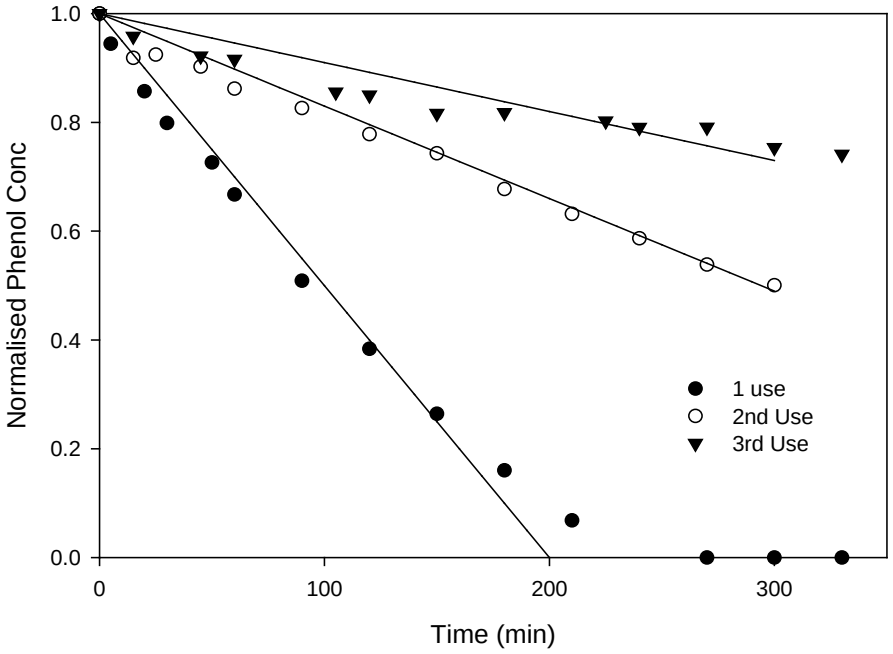

Figure 5.4-9 Co-SBA-15 reusability for phenol degradation [C_{ph}-25 ppm, 25 ^{o}C, 0.2 g/l catalyst, 2g/l g oxone]

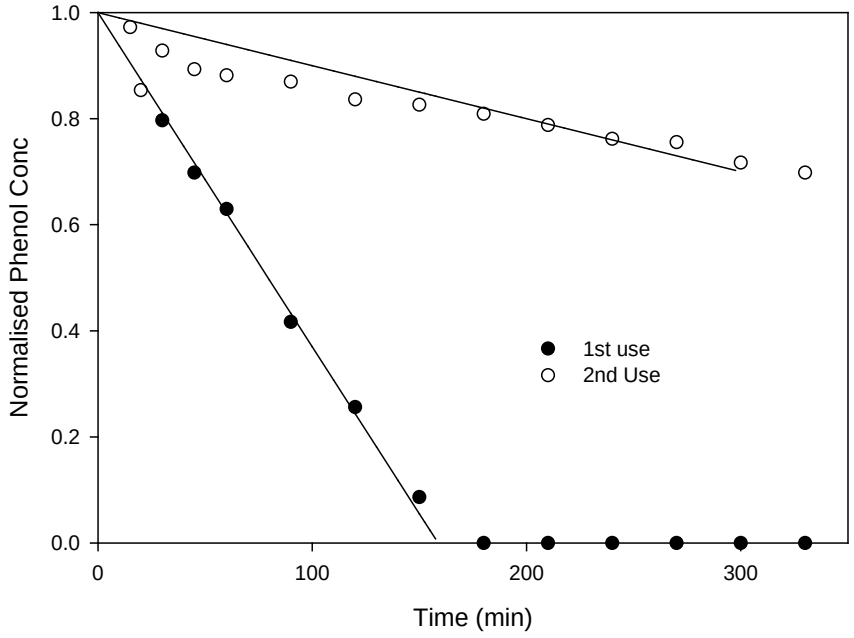

Figure 5.4-10 Co-Silica reusability for phenol degradation [C_{ph}-25 ppm, 25 ^{o}C, 0.2 g/l catalyst, 2/l g oxone]

5.4.4 TOC removal

The trend of TOC removal by either catalyst was observed to follow the similar pattern as seen for phenol removal. The extent of TOC removal for Co-SiO_2 was higher than that of Co-SBA-15. But the rate at which TOC was removed from the solution gives an entirely different picture. Both catalysts showed appreciable removal of phenol; however the rate of phenol oxidation of Co-SiO_2 was better as compared to Co-SBA-15 by a small margin. The rate constant of phenol removal by Co-SiO_2 and Co-SBA-15 differing by just 1.52×10^{-5} mol phenol/min. However, in the case of TOC removal, Co-SiO_2 catalyst showed twice as fast removal of TOC as compared to Co-SBA-15. The highly enhanced removal of TOC in the case of Co-SiO_2 is attributed to the excessive cobalt leached into the solution which accelerates the decomposition of intermediate molecules. The decomposition of intermediate is faster in homogeneous mode rather than the heterogeneous system due to poor adsorption on the catalyst surface.

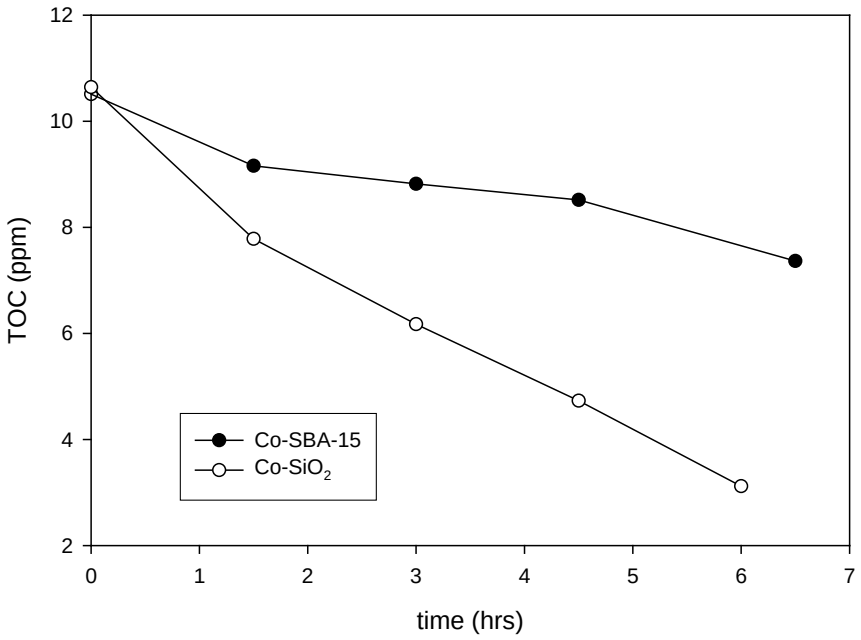

Figure 5.4-11 Extent of TOC removal using Co-Silica and Co-SBA catalyst [C_{ph}-25 ppm, 25 ^{o}C, 0.2 g/l catalyst, 2 g/l oxone]

5.4.5 Effect of Reaction Parameters

5.4.5.1 Effect of oxidant concentration

According to the previous results, it can be affirmed that in the absence of oxidant, the degradation of phenol was negligible. In the current section, the effect of the amount of the oxidant in the reaction was studied. Further, several other reaction parameters such as catalyst concentration and temperature were investigated.

The oxidation kinetics was studied at oxidant to phenol mol ratios ranging from 0 to 60. The high concentration of oxidant was used to enhance the extent of complete mineralization of phenol. For the experiments using Co-SBA-15, Figure 5.4-12 shows that the rate of phenol degradation increases considerably by raising the oxidant concentration from 0.2 to 1 g/l of solution. Further increasing the concentration from 1 to 4 g/l however showed negligible effect on the rate of oxidation. For oxidant concentration less than 1 g/l the rate of reaction was extremely slow and ceased to result in complete phenol degradation whereas beyond the oxidant concentration of 1g/l, the rate follows linear profiles suggesting zero order reaction kinetics with respect to phenol concentration.

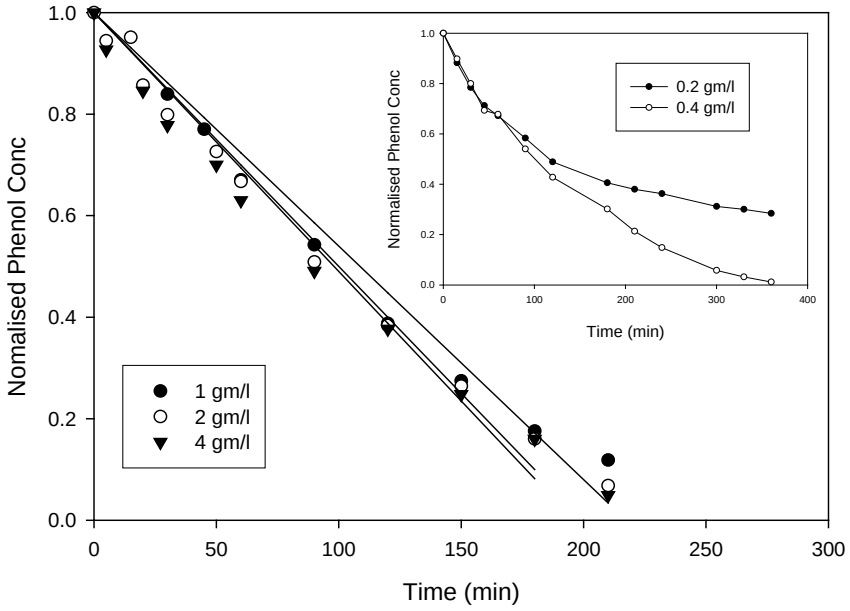

Figure 5.4-12 Phenol degradation in the presence of Co-SBA-15 at different concentration of oxone. [C_{ph}-25 ppm, 25 ^{o}C, 0.2 g/l catalyst]. Insert Figure: Degradation of phenol in the presence of extremely low concentration of oxidant

In the case of Co-SiO_2, the amount of oxidant was varied from 1 to 4 g/l. At lesser amount of oxidant the reaction was starved of sulphate radical. The results seen from Figure 5.4-13 show a minimal change in the rate of reaction with the increase in the oxidant amount. The extent of TOC removal however was found to be slightly better upon increasing the oxidant, thus pointing towards the predominance of homogeneous reaction for the degradation of the reaction intermediates.

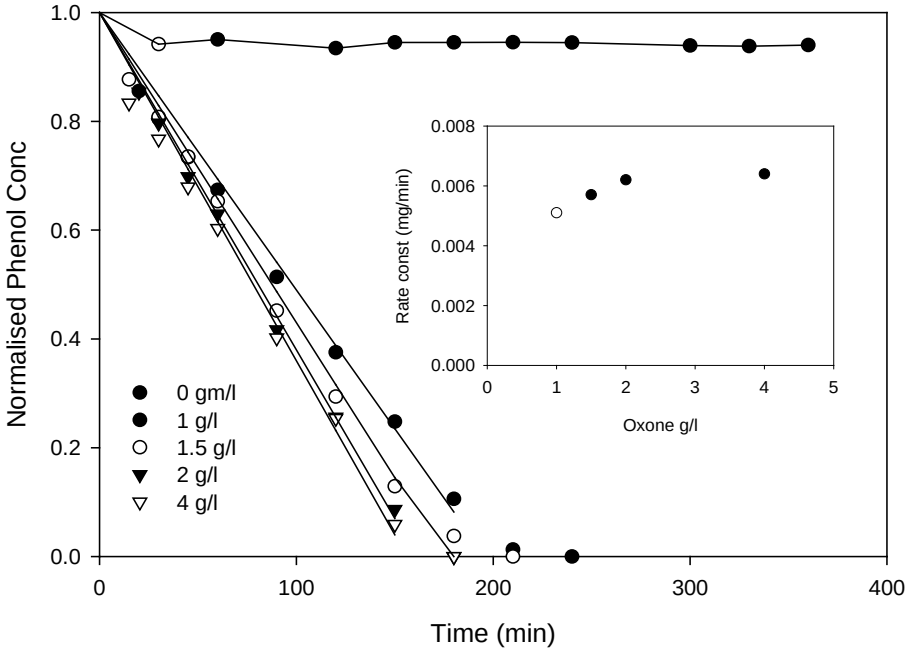

Figure 5.4-13 Phenol degradation in the presence of Co-SiO_2 at different concentration of Oxone. [C_{ph}-25 ppm, 25 ^oC, 0.2 g/l catalyst].

5.4.5.2 Effect of catalyst concentration

The variation in the amounts of catalyst produces a significant effect on the rate of reaction as observed in Figure 5.4-14 and Figure 5.4-15. Experiments carried out at various amount of catalyst concentration for a fixed amount of contaminant (25 ppm, phenol) and constant amount of oxidants showed a similar trend for both silica and SBA-15 based catalysts. Increasing the catalyst concentration from 0.1 to 0.4 g/l showed a significant increase in the oxidation rate with a complete degradation of phenol within 2 hrs. Increase in the amount of catalyst in the solution increases the available active site for the adsorption of both phenol and oxidants thereby increasing the rate of generation of oxidants and the degradation of phenol. The inserted graphs

in Figure 5.4-14 and Figure 5.4-15 show a linear dependence of the rate constant on the amount of catalyst.

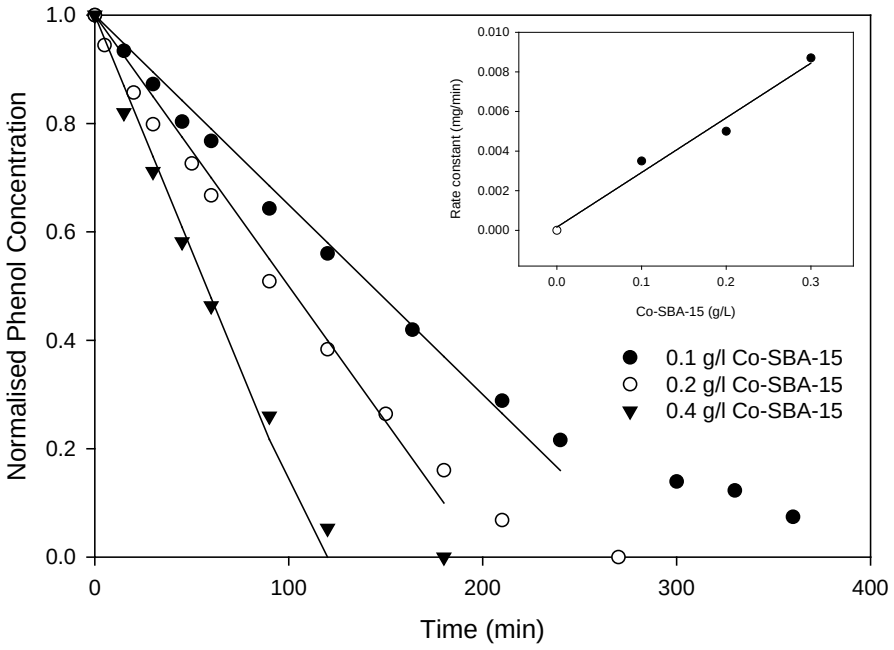

Figure 5.4-14 Phenol degradation in the presence of Co-SBA at different concentration of catalyst. [C_{ph}-25 ppm, 25 ^{o}C, 2 g/l oxone].

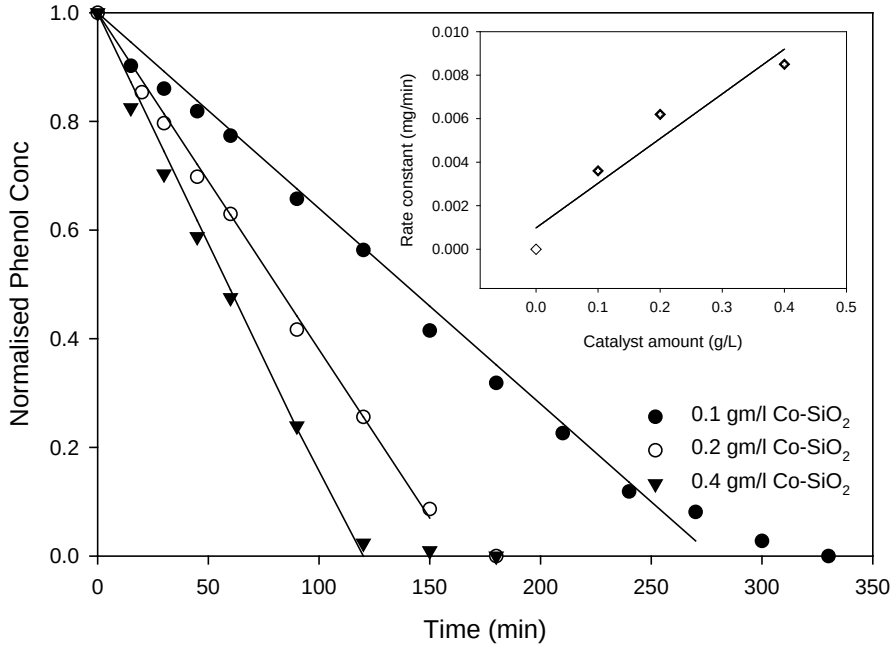

Figure 5.4-15 Phenol degradation in the presence of $Co\text{-}SiO_2$ at different concentration of catalyst. [C_{ph}-25 ppm, 25 ^oC, 2 g/l oxone].

5.4.5.3 Effect of reaction temperature

The temperature has a crucial effect on this reaction by enhancing the reaction kinetics, as it affects the rate constant of the reaction based on the Arrhenius law.

The effect of reaction temperature at 3 different levels is shown in Figure 5.4-16. In the presence of a catalyst, the oxidation rate increases with the increase in temperature. A similar effect was observed on both catalysts, with the change taking place in approximately the same ratio. At 10 ºC, phenol degradation efficiency is about 40% after 6 hours. At 25 ºC, a complete degradation of phenol would be achieved after 4 h. When the temperature is further increased to 40 ºC, 100% phenol degradation was observed within a period of 2h.

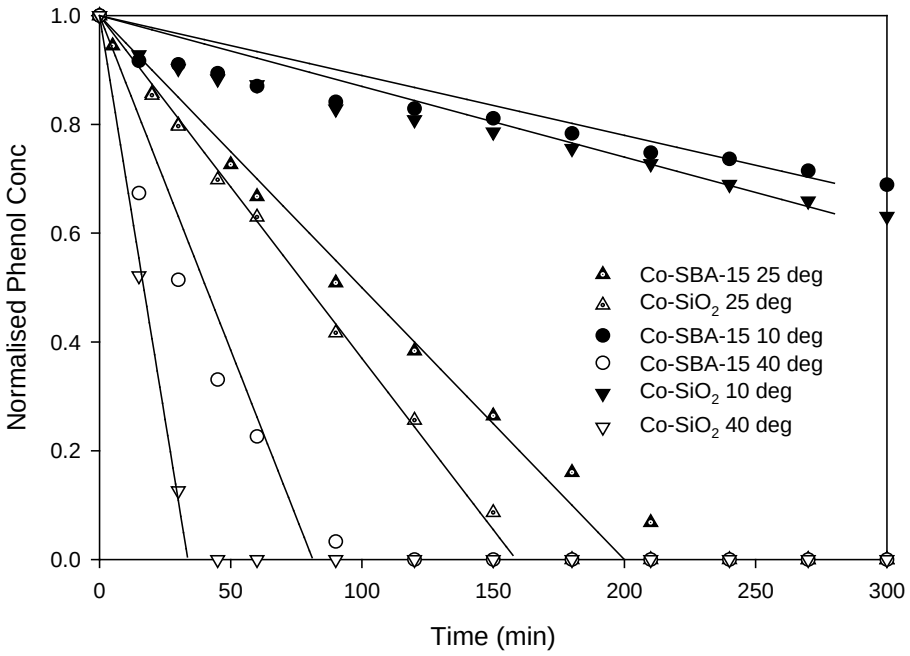

Figure 5.4-16 Phenol degradation in the presence of Co-SBA and Co-SiO_2 at different temperature [C_{ph}-25 ppm, 0.2 g/l catalyst, 2 g/l oxone].

5.5 Effect of cobalt ion precursor on the stability of Co-SiO_2 based catalyst

The results so far suggest the weak bonding between the cobalt and silica support posing a major hurdle in the utilization of Co-SiO_2 based catalyst for waste water treatment. The leached cobalt ion from the support renders the water toxic. In-order to enhance the metal support bonding strength, several catalysts was synthesized by utilizing different types of cobalt precursor.

Earlier research carried out by Yang et al [17] on cobalt impregnation on TiO_2 suggested a significant influence of the type of precursor used for the cobalt loading on the titania surface. They have analyzed the effect of 3 different precursors viz cobalt chloride, cobalt sulphate and cobalt nitrate. The heat treatment of the catalyst carried out at 500 ^oC resulted in complete removal of the nitrate ligand from cobalt nitrate precursor, whereas trace amounts of chloride and sulphate precursor were left on the surface of titanium, which tends to influence the bond between the cobalt and TiO_2. The presence of the ligand also tends to affect the crystallization of cobalt oxide. In the current study we have tried to investigate the effect of three types of

precursor for cobalt impregnation on silica. The effect of precursor on the rate of phenol oxidation was studied and compared.

5.5.1 Loading of Co^{2+} from different precursors in silica

The method was similar to that explained earlier, however 3 different types of cobalt precursor's viz cobalt chloride, cobalt acetate and cobalt nitrate were used in the given case. The amount of cobalt precursor used was calculated to ensure a fixed 5 wt% cobalt loading in the silica substrate. The three catalysts are represented as Co-SiO_2-Cl (Cobalt chloride based Co-SiO_2), Co-SiO_2-Ac (Cobalt Acetate based Co-SiO_2) and Co-SiO_2-Ni (Cobalt nitrate based Co-SiO_2). The samples were characterized using FTIR, XRD, SEM and EDS. The kinetic study was conducted in the similar way as explained previously in the Chapter, Section 5.3.4.

5.5.2 Characterization of three different Co-SiO_2 samples

All the three samples had a similar physical structure but with different colour. The sample colour is dictated by the types of cobalt precursor used for the synthesis. As seen in figure 5.5.1 cobalt impregnated silica prepared using cobalt chloride as a precursor was observed to be light blue whereas the sample prepared with cobalt acetate showed grey coloration while the sample prepared using cobalt nitrate was found to show intense dark coloration.

1: SiO_2

2: Co-SiO_2-Cl

3: Co-SiO_2-Ac

4: Co-SiO_2-Ni

Figure 5.5-1: Co-SiO_2 samples prepared using different cobalt precursors.

FTIR of the samples as illustrated in Figure 5.5-2 was similar as reported earlier in section 5.4.2. All the three samples showed the characteristic of silica peak observed from the silica oxygen bond vibrations. The three major peaks observed at 1072 cm^{-1}, 788 cm^{-1} and 455 cm^{-1} represents the IR absorption of Si-O-Si. The vibration observed at the lowest frequency (455 cm^{-1}) is due to the rocking mode corresponding to the out of Si-O-Si plane motion of the oxygen atom. The band observed at 788 cm^{-1} represents the bending vibration resulting from the oxygen atom motion between the Si-O-Si plane and along Si-O-Si angle bisector. Finally the largest band observed at 1072 cm^{-1} occurs from the vibration due to the stretching of the Si-O-Si bond.

The IR absorbance due to the spinal Co-O bond is observed at 663 cm^{-1} which corresponds to the Co_3O_4 crystallite formed within the silica support. Another weak absorbance at 568 cm^{-1} may be resulted from some CoO structure. During calcination, the cobalt precursor generally undergoes step decomposition to form silica composite structure containing CoO-Co_2O_3-Co_3O_4. Comparison of IR spectra of the three catalysts shows maximum Co-O bond absorbance peak intensity for Co-silica prepared using cobalt nitrate precursor and the minimum peak for Co-SiO_2 prepared using cobalt chloride *(on a fixed scale)*. The observation suggests that the well organized cobalt oxide crystallite formation in catalyst prepared using cobalt nitrate precursor. Among all the three precursors, the nitrate ion is the easiest precursor to be removed from the heat treatment resulting from the formation of nitrogen oxide. The cobalt oxide in Co-SiO_2-Ni sample was essentially free from any nitrate ion ligand due to the heat treatment and therefore it was crystalline and also strongly bonded with the support. In contrast, the acetate ligand is more difficult to be removed with the given heat treatment and thus a small extent of the ion tends to remain on the surface. This residual acetate ion prevents the crystallization of cobalt oxide and also weakens the metal-support interaction as evident from the leaching test to be discussed later. In comparison to nitrate and acetate ion, the chloride ion is most difficult to be removed and thus results in minimal crystallization of cobalt oxide and also shows the weakest metal-support interaction compared to the previous two catalysts.

The small peak around 1600 cm^{-1} observed in all the 3 samples is due to the presence of silanol (SiOH) group. Cobalt cations have a tendency to react with these hydrated silanol group (generally at pH less than 2 or higher then 5) to form cobalt

silicate. The Co-silica-nitrate sample showed a higher intensity of the silanol group as compared to the others. The lower amount of hydroxyl group found in Co-SiO_2-Ac and Co-SiO_2-Cl could be attributed to the reaction of chloride and acetate ligands with the hydroxyl group forming a complex. These complexes can further hinder the metal-cation bonding strength. In the case of Co-SiO_2-Ni, the presence of surface hydroxyl group (SiOH) helps in reaction of cobalt cation with the hydroxyl group to form cobalt silicate which is evident from the small peak around 1066 cm^{-1} found only on the Co-SiO_2-Ni sample which is assigned to Si-O-Co bond. Additionally the broad peak of Si-O-Si at 1072 cm^{-1} was observed to be much thinner in Co-silica-nitrate sample owing to the formation of cobalt silicate. Lastly the broad peak at 3400 cm^{-1} represents the O-H vibrations, which could be due to the presence of OH group of adsorbed water molecule.

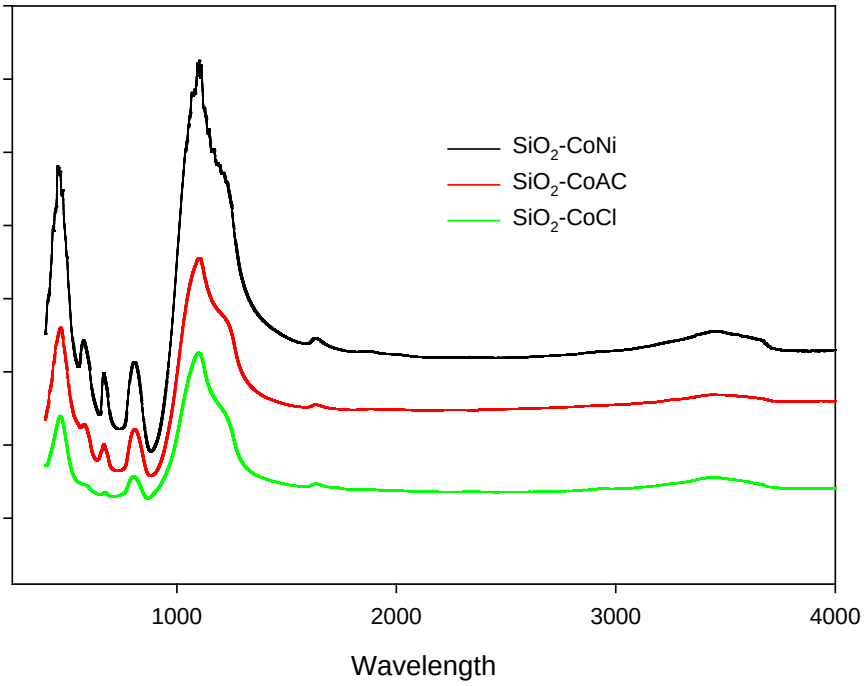

Figure 5.5-2 FTIR Spectra of Co-SiO_2 prepared with different precursors

Figure 5.5-3 shows the XRD spectra of the Co-silica catalysts prepared using the 3 different precursors. The result shows the presence of cobalt oxide crystallites in all the three samples with the major peaks found at 19°, 31°, 37°, 39°, 46°, 59° and 66°. A large hump observed at around 20 ^{0}C is commonly observed for highly small sized amorphous silica particle generally due to the adsorbed water on the surface.

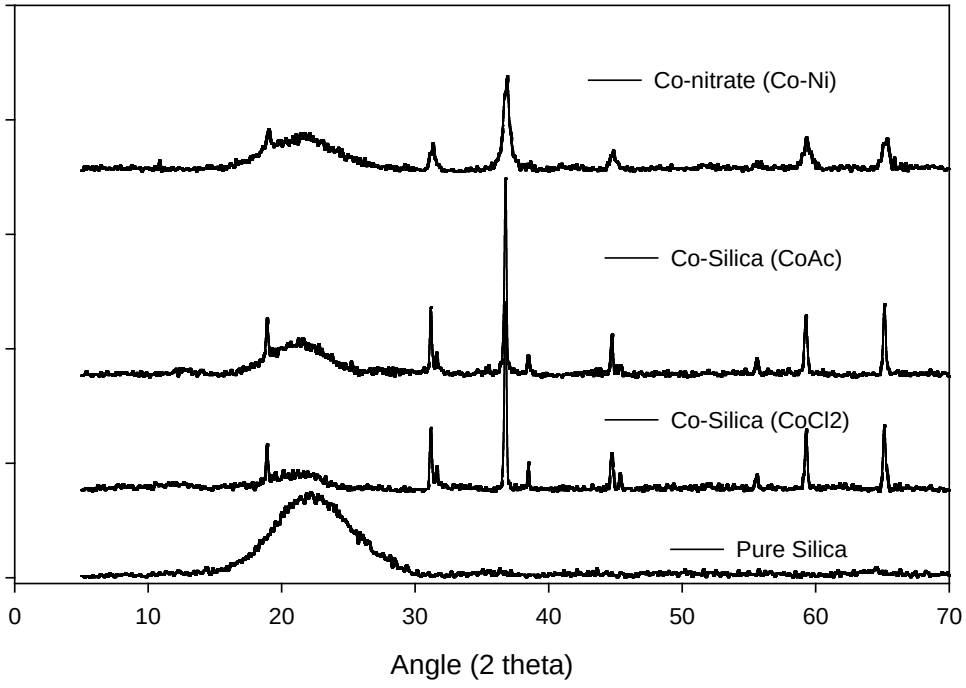

Figure 5.5-3 XRD spectra of Co-SiO_2 catalysts prepared with different precursors

Figure 5.5-4 shows the Raman spectra of all the three samples. Except SiO_2-CoNi, both the samples shows excessive fluoresce. All the three samples showed a Raman shift at 200, 480, and 700 cm^{-1} which is assigned to Co_3O_4. The results refer to the sample surface but agree with the results of the bulk material as shown by XRD. The intensity of the peak reduces in the order of SiO_2-Co-Nil> SiO_2-CoAc ~ SiO_2-CoCl, thus further justifying the influence of the cation on the formation of cobalt oxide crystallite.

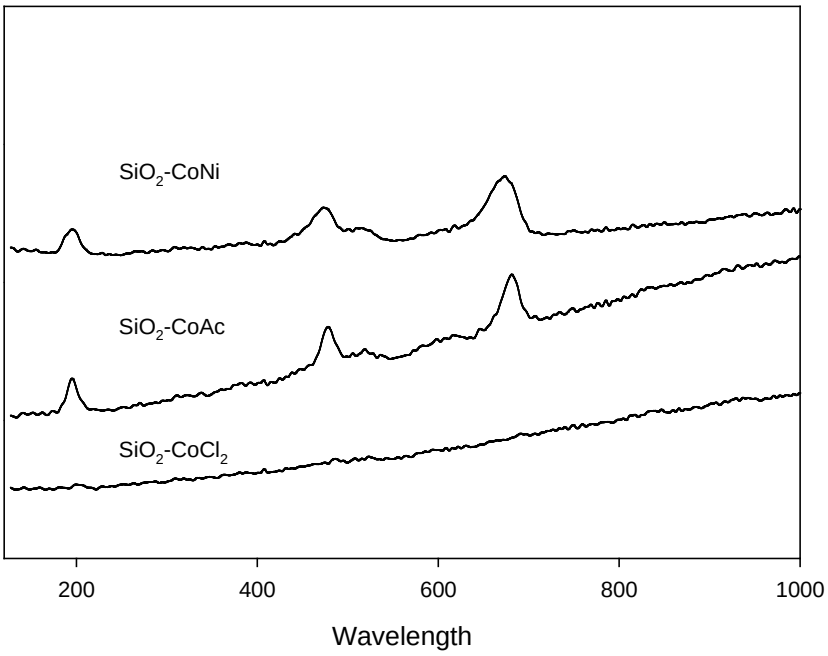

Figure 5.5-4 FT-Raman Spectra of Co-SiO_2 prepared with different precursors

The SEM images (Figure 5.5-5) show spherical silica particles in the nano size range. The cobalt crystallite is difficult to locate, possibly due to very small size and homogeneously distributed.

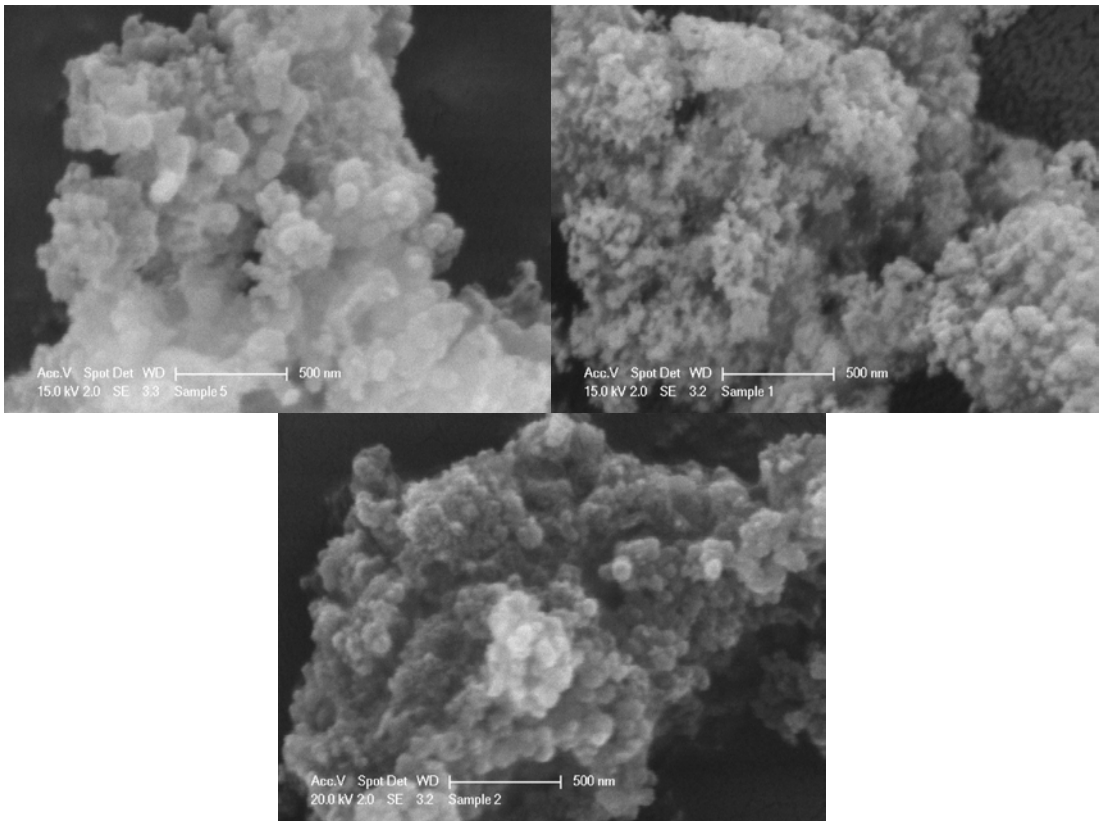

Figure 5.5-5 SEM image of Co-SiO_2 prepared with different precursors (from top to bottom : Co-SiO_2-Cl:Co-SiO_2-Ac:Co-SiO_2-Ni)

5.5.3 Effect of Cobalt Precursor on the Rate of Reaction and Cobalt Leaching

The precursor shows an influential effect on the metal-support bond strength which is directly related to the rate of organic oxidation and the catalyst reusability. Figure 5.5-6 shows the degradation trend of phenol carried out following the oxidation test in the presence of 0.1 g of the catalyst and 1 g of oxone. The rate of degradation was found to be in the order Co-SiO_2-Cl > Co-SiO_2-Ac > Co-SiO_2-Ni despite having a similar amount of initial cobalt loading.

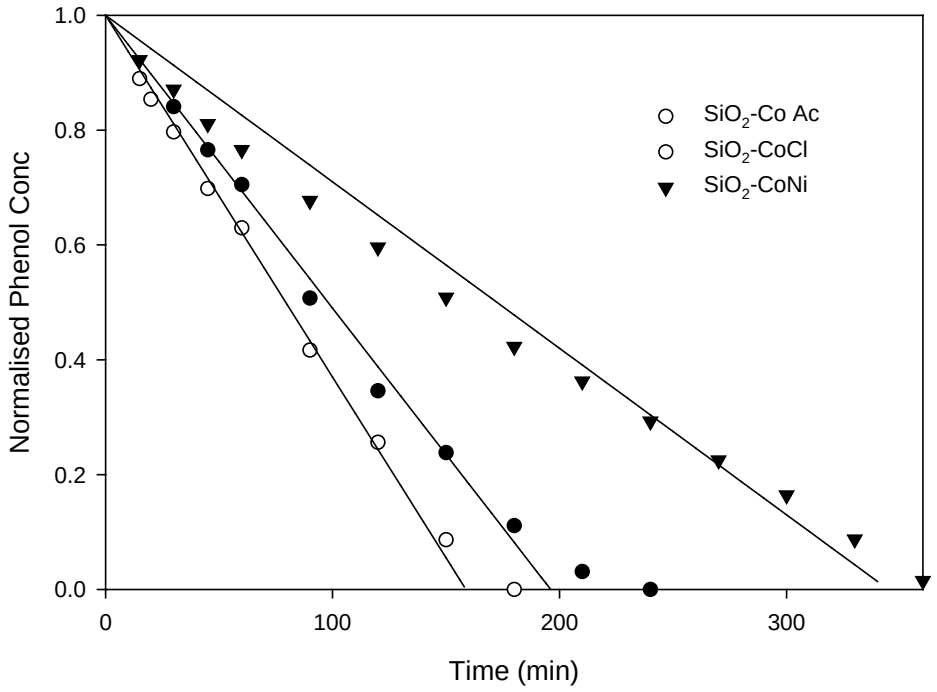

Figure 5.5-6 Phenol degradation with Co-SiO_2 catalyst prepared with different precursors [C_{ph} – 25 ppm, 2 g/l oxone, 0.2 g/l catalyst, 25 ^oC]

This trend is in accordance to the extent of cobalt leaching as seen in Figure 5.5-7, Co-SiO_2-Cl showing the maximum leaching followed by Co-SiO_2-Ac and Co-SiO_2-Ni. This suggests that the higher rate of reaction is influenced by the simultaneous homogeneous reaction taking place due to the leached cobalt ions. The Co-SiO_2-Ni having the strongest bonding between the metal and support is the best catalyst as seen from the reusability test in the following section.

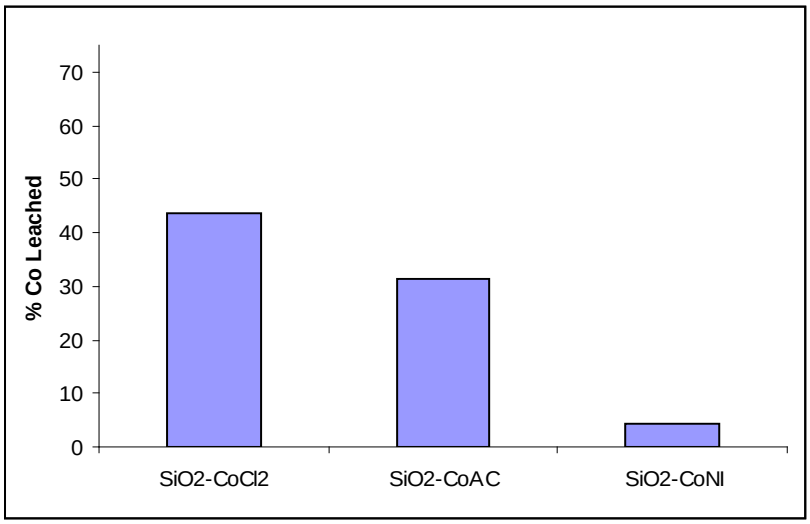

Figure 5.5-7 Cobalt leaching with the three Co-SiO_2 catalysts.

The cobalt leaching had a significant impact on the reusability of the catalyst. Figure 5.5-8, Figure 5.5-9 and Figure 5.5-10 show the reusability of the catalysts for phenol degradation. Co-SiO_2-Cl based catalyst has demonstrated to have the least metal support bond strength due to high amount of cobalt leaching. The reusability of this catalyst has been extremely poor with the extent of phenol degradation falling from 100% to just 20% when reusing in the time period of 200 min. Co-SiO_2-Ac is slightly better than Co-SiO_2-Cl. Among all, Co-SiO_2-Ni has been found to be a highly stable catalyst having a strong metal support interaction. The catalyst showed efficient removal of phenol even after repetitive usage. Additionally from the given observations, it can be further concluded that the rate of reaction is inversely related to the catalyst stability. The reaction in the catalyst having a very strong metal-support interaction would proceed via heterogeneous reaction mode which is much slower as compared to the homogeneous reaction.

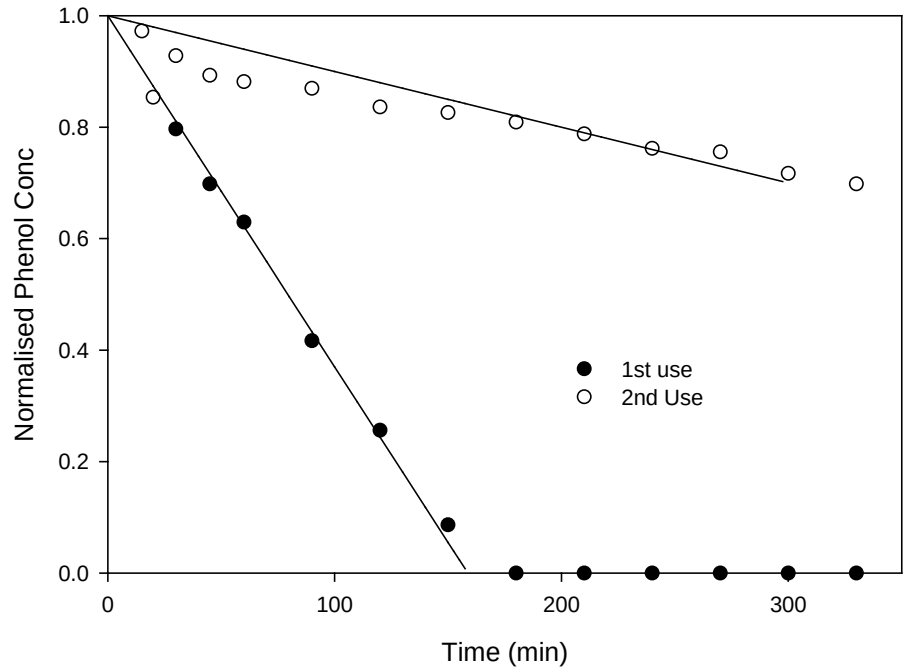

Figure 5.5-8 Co-SiO_2-Cl reusability for phenol degradation [C_{ph}-25 ppm, 25 ^oC, 0.2 g/l catalyst, 2/l g oxone]

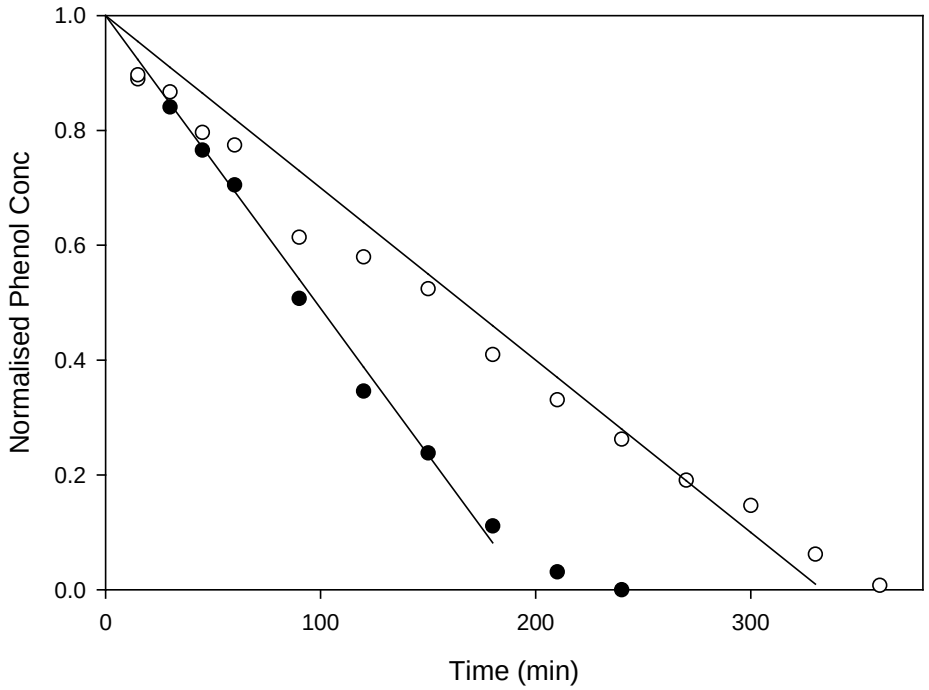

Figure 5.5-9 Co-SiO_2-AC reusability for phenol degradation [C_{ph}-25 ppm, 25 ^oC, 0.2 g/l catalyst, 2/l g oxone]

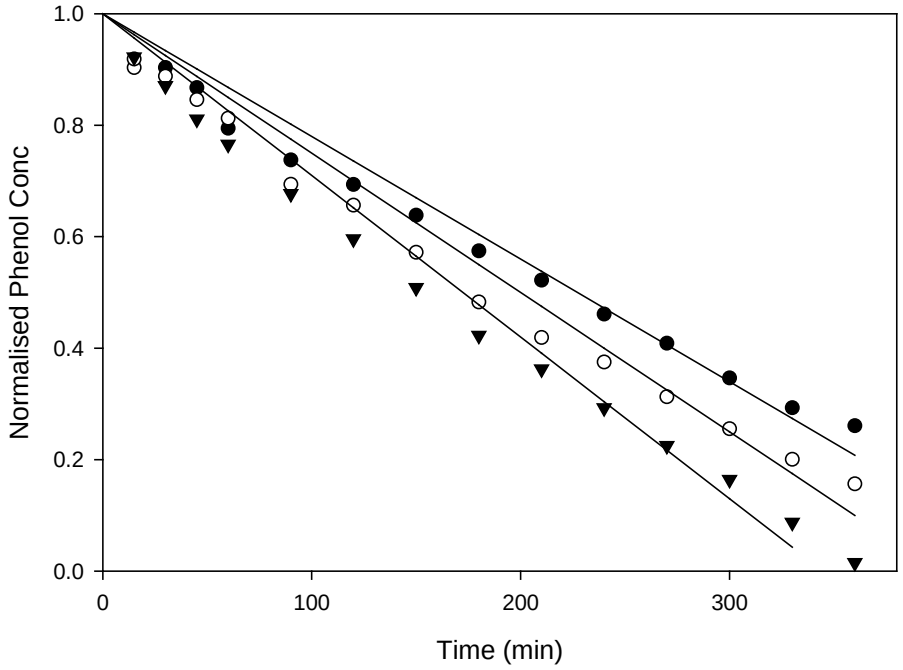

Figure 5.5-10 Co-SiO_2-Ni reusability for phenol degradation [C_{ph}-25 ppm, 25 ^oC, 0.2 g/l catalyst, 2/l g oxone]

Part B: Cobalt impregnated carbon catalysts

5.6 Introduction

The current section describes an application of activated carbon as a potential support for a cobalt catalyst. Activated carbon provides high specific surface area for enhanced adsorption of phenol. The trapped phenol can then further react with the sulphate radical generated on the surface. Earlier works using carbon supported catalysts to achieve the dual objectives of adsorption and oxidation have been mostly focused on activated carbon loaded with ferrous ions for simultaneous adsorption and Fenton oxidation. Ramired et al. [18] have reported the synergetic behavior between the adsorption and oxidation for the destruction of Azo-Dye Orange II from waste water. Similarly Zazo et al. [19] have reported the destruction of phenol with Fe-activated carbon. However, there has also been a report of non-synergetic behavior between carbon adsorption and Fenton oxidation. The research carried out by Georgi et al. [20] suggests that the adsorption of the contaminants by activated carbon tends to form an energy barrier around the molecules thereby preventing them from undergoing a reaction. The aim of this work is to investigate the synergy of combined adsorption and oxidation with cobalt loaded activated carbon. Although activated carbon has been widely used as a support, there hasn't been any work related to application of Co-activated carbon with sulphate based oxidant for organic degradation.

5.7 Experimental

5.7.1 Catalyst preparation

The catalysts were prepared using cobalt metal deposition on a commercially available activated carbon. Prior to the loading of metal, the activated carbon samples (AC) obtained from BDH Chemical was crushed and milled to obtain the particles in the size range from 500 to 100 micron. The powder was then washed several times with ultra-pure water to remove any loosely bonded impurities and dried in an oven at 30 ^{0}C. A wet impregnation technique was utilized for loading of cobalt in activated carbon. In brief, d a fixed amount of cobalt precursor (cobalt nitrate) was dissolved in water. Three different concentrations of cobalt nitrate were used to obtain the loading of 2.5, 5 and 10% by weight of cobalt in AC. The desired amount of AC was added to the solution and the suspension was stirred for 24 hrs.

Later, the water was slowly evaporated using a rotary evaporator set at the temperature of 50 ºC under vacuum. Finally, the recovered solid was calcined in a programmable furnace at 750 ºC for 6 hrs under the flow of argon in-order to remove the nitrate moiety from the sample. The sample was further calcined at 350 ºC under air to oxidize the metal to its oxide form. The samples obtained after calcination henceforth referred as Co-AC-x catalyst was washed several times with miliQ water to remove the loosely bonded cobalt. The term 'x' represents the weight % of the metal loaded on the support. The catalyst was then stored in a desiccator until used.

5.7.2 Characterisation of catalyst

The texture, morphology and semi quantitative analysis of the catalyst sample were done by SEM fitted with secondary and backscatter electrons detectors. Carbon being conductive does not require any gold coating for SEM analysis. The sample was sprinkled on the stub and directly analyzed. The elemental composition was determined using the Energy Dispersive X-ray Spectroscopy (EDS). The EDS analysis was carried out at several points in the region with different accelerating voltages and averaged to obtain the representative result. The structural features and the mineralogy of the samples were studied from X-ray diffraction patterns acquired by a Siemens XRD instrument, using filtered Cu Kα radiation with accelerating voltage of 40 kV and the current of 30 mA. The sample was scanned at 2θ from 5 to 70^{o}. The semi quantitative/relative amount of cobalt oxide on Co-AC catalysts was determined by burning the carbon under air and measuring the weight loss using a TG analyzer.

5.7.3 Kinetic study of phenol oxidation

The catalytic oxidation of phenol was carried out in a 500 ml reactor containing 25 ppm of phenol solution. The reactor was attached to a stand and dipped in a temperature regulated water bath to control the temperature. The reaction mixture was stirred with a plastic coated stirrer to maintain homogeneous solution. A known amount of peroxymonosulphate (obtained as a triple salt under the commercial name "Oxone") was added to the mixture and allowed to dissolve before starting the reaction. A fixed quantity of catalyst depending on the predefined reaction parameter was added to start the reaction. The reaction was carried on for 2 hr, and 0.5 ml samples were withdrawn at a fixed time interval into an HPLC vial using a syringe filter. 0.5 ml of methanol was immediately added to the acquired sample to quench

the reaction. The phenol concentration was analyzed using a HPLC fitted with a UV detector at the wavelength of 270 nm. For selected samples, total organic content was determined using a Shimadzu TOC-5000 CE analyzer. For the measurement of TOC, 5 ml sample was extracted at an interval of 1 h and quenched with 5 ml of 3M sodium nitrile solution and then analyzed on the TOC analyzer. The concentration of peroxymonosulphate was determined by titration against sodium thiosulphate. 5 ml of reaction mixture containing peroxymonosulphate was mixed with 2 g of KI and was shaken vigorously. 0.2 g of Vitrx indicator was added and left for 15 min. Finally 1 ml of glacial acetic acid was added to the solution and shaken well. The resultant mixture was titrated with sodium thiosulphate.

5.8 Result and discussion

5.8.1 Characterisation of cobalt-activated carbon catalyst

The metal distribution within the catalyst was studies using SEM whereas the oxidation state of the metal catalyst was examined using XRD. The XRD spectra of the impregnated carbon catalyst along with pure activated carbon are shown in Figure 5.8-1. The spectra of the cobalt impregnated catalyst shows distinct peaks of cobalt oxide crystallites (Co_3O_4). In addition, a few mini peaks obtained in the region between 40^o to 50^o are generally diffracted from the crystalline carbon samples. During the synthesis process, the catalyst underwent a thermal treatment up to a temperature of 750 ºC, which would result in a slight structural orientation of carbon. However, the bulk sample was found to be highly amorphous due to a large amount of noise found in the spectrum.

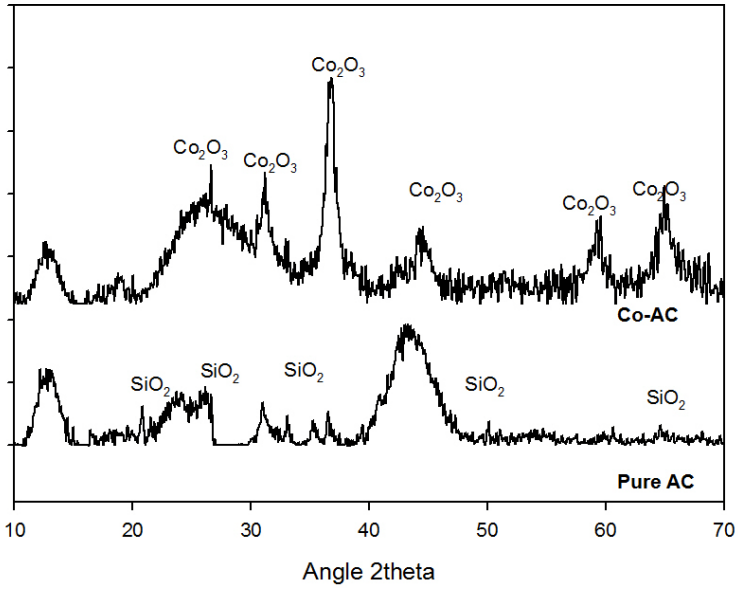

Figure 5.8-1 XRD spectra of AC and Co-AC.

The sample morphology of the cobalt and distribution within the activated carbon support were observed from SEM images. Figure 5.8-2 shows the SEM images obtained using the secondary electron detector. It is found that the milled sample has a diverse shape and size with a highly heterogeneous surface. The same region observed using the backscattered detector (Figure 5.8-2) shows the presence of cobalt particles as the brighter region in the large particles. Almost all the carbon particles are observed to be well coated with cobalt oxide crystallites.

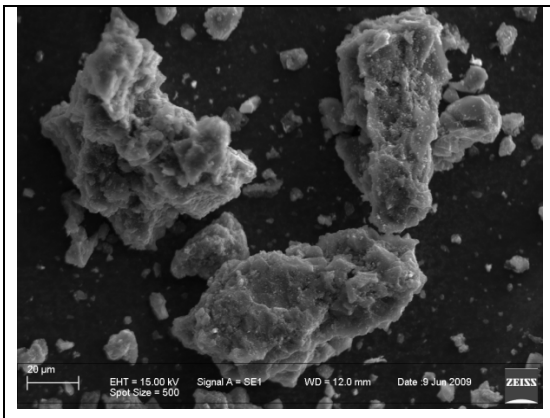

Figure 5.8-2 SEM image of Co-AC with SE detector

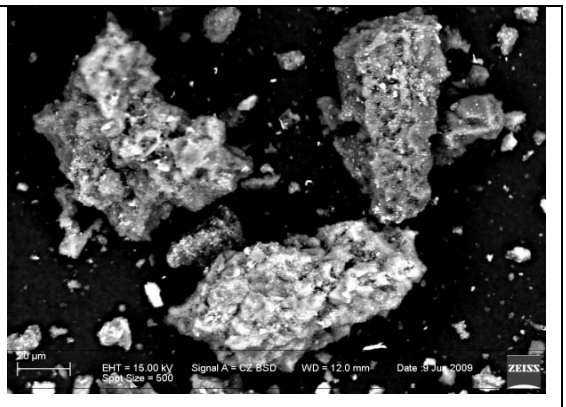

Figure 5.8-3: Same image as in Figure 5.8-4 but with BSE detector to observe cobalt crystallite as bring specks.

5.8.2 Adsorption analysis of AC and Co-AC samples

Prior to the oxidation tests, the adsorption capacity of Co-AC catalyst was measured and compared with pure AC at the fixed amount of adsorbent to liquid ratio of 0.2 g/l. The results are shown in Figure 5.8-5. The sorption uptake is quite fast due to the fast stirring of the mixture (approx 400 RPM), with more than 90% saturation occurring within first 40 min. The adsorption capacity of AC was found to be slightly higher than that of the catalyst. Given the fixed quantity of adsorbent used in both tests (0.2 g/L), the amount of activated carbon is higher in the case of pure AC as compared to that of catalyst which has 10 wt% cobalt, thereby resulting in lower sorption capacity.

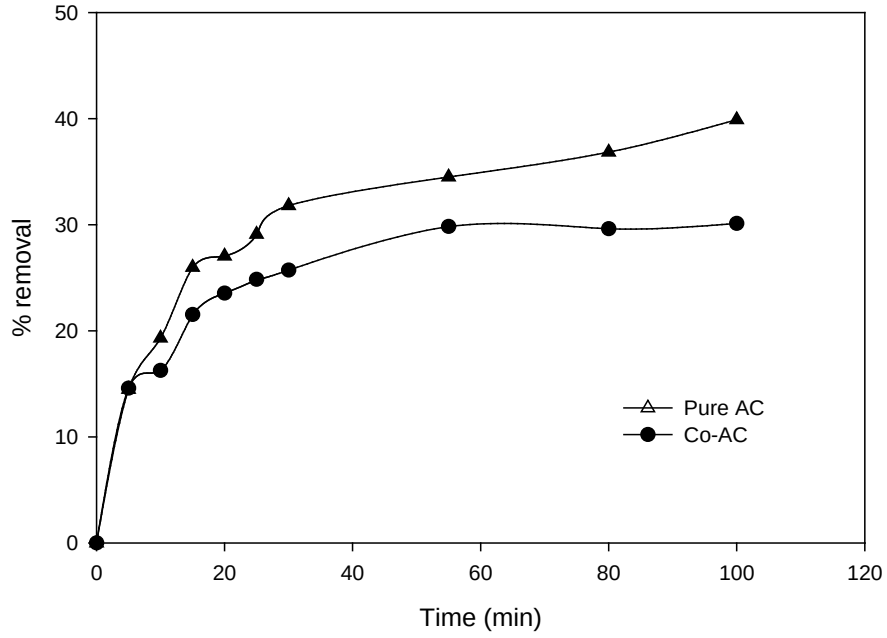

Figure 5.8-5 Adsorption kinetic of Co-AC and pure AC [C_{ph} – 25 ppm, 0.2 g/l catalyst, 25 ^{o}C]

5.8.3 Catalytic activity of cobalt-activated carbon

Several preliminary experiments to assess the potential of Co-AC catalysts for the oxidation of phenol in the presence of PMS oxidant were conducted and the activity is compared with that of pure activated carbon. As seen from Figure 5.8-6, the control experiment of phenol oxidation performed in the presence of PMS without the addition of catalyst results in insignificant change in the phenol concentration,

suggesting that PMS is incapable of undergoing self cleavage to generate any sulphate radical. The oxidation experiment carried out in the presence of PMS and AC results in the extent of phenol removal, similar to that of phenol adsorption using pure AC, suggesting the incapability of pure AC to generate any active sulphate radical for phenol oxidation and the phenol removal mechanism follows only adsorption. Finally the experiment carried out in the presence of Co-AC with PMS shows extremely fast reduction in the phenol concentration and achieving complete removal of phenol within 30 min.

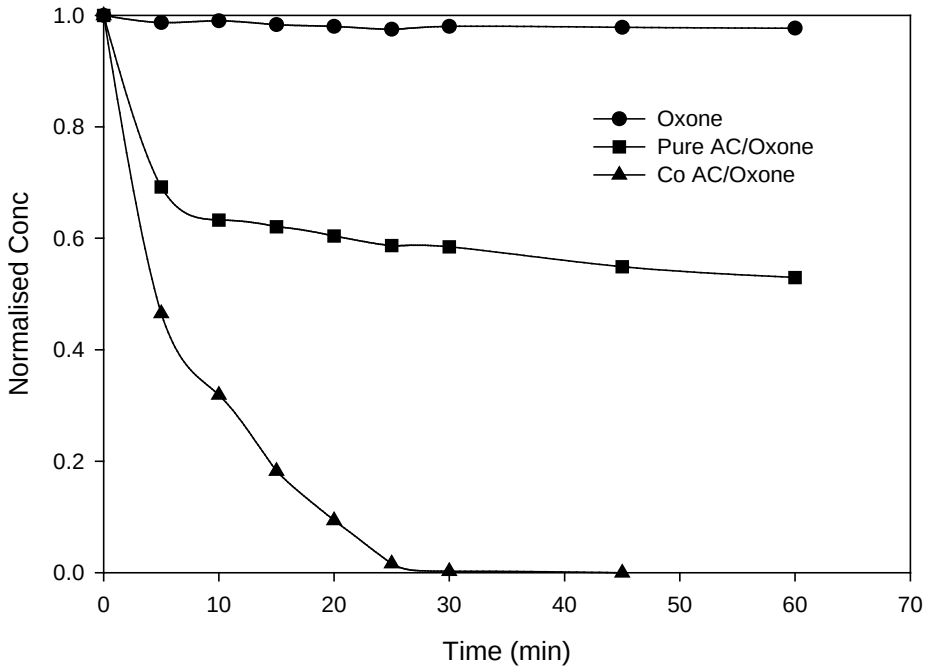

Figure 5.8-6 Preliminary test of catalytic oxidation of phenol using Co-AC and pure AC [C_{ph} – 25 ppm, 0.2 g/l catalyst, 25 ^{o}C].

The extent of phenol removal in the presence of both AC and Co-AC was correlated with the amount of TOC removal from the solution as seen from Figure 5.8-7 (insert). The test in AC-PMS system showed almost 45% removal of TOC, which is similar to the extent of phenol adsorption on the solid. During the same test, almost 49% loss of oxidant was measured (Figure 5.8-7). In the case of combined adsorption and reaction in the presence of Co-AC/PMS system, almost 80% TOC was removed from the solution. The removal of TOC is in agreement with the catalytic reaction taking place; however the total TOC removal was lesser than the corresponding extent of phenol removal, implying the presence of reaction intermediates in the solution. The

presence of intermediates was also confirmed during the HPLC analysis, but the quantification of the released intermediate was not attempted here. As seen from the oxidant concentration profile (Figure 5.8-7), the loss of oxidant in AC/PMS system suggests the possible interaction of AC with oxone resulting in decomposition of the oxidant without any generation of any active sulphate radical. There is a possibility of reaction of PMS with the function groups present on AC as per reaction below

$$AC + HSO_5^- \rightarrow AC - H + SO_5^- \qquad \text{Equation 5.8-1}$$

$$AC + HSO_5^- \rightarrow AC + HSO_5^{\bullet} \qquad \text{Equation 5.8-2}$$

The activity of peroxymonosulphate radical $(HSO_5^{\bullet})$ for oxidation of organic contaminants is minimal. Lastly, in the case of Co-AC based system, around 70% oxidant was found to be consumed for the generation of active sulphate radical resulting in phenol oxidation.

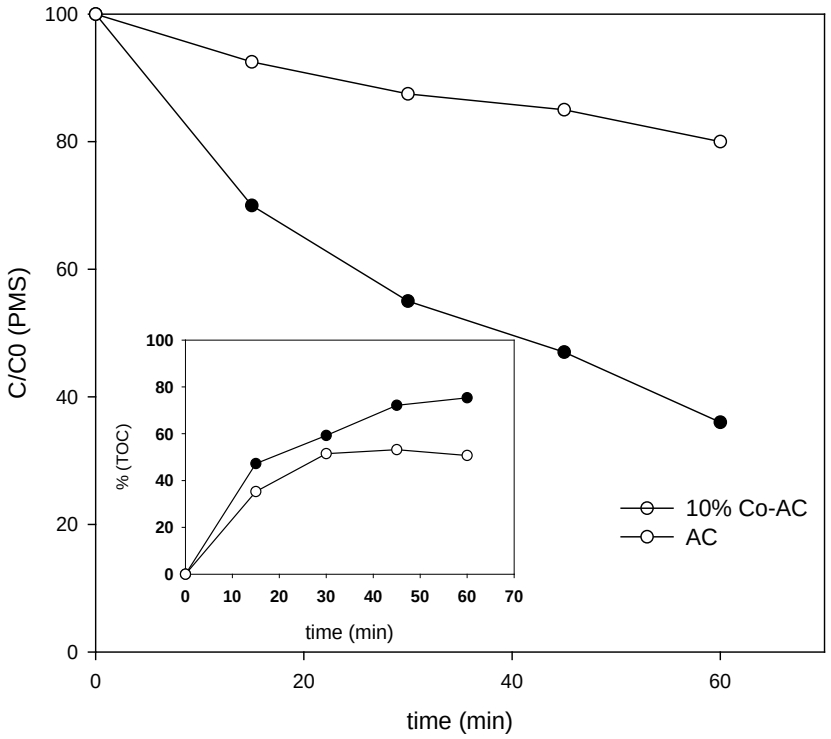

Figure 5.8-7 Oxone consumption in the presence of Co-AC and pure AC. [C_{ph} – 25 ppm, 0.2 g/l catalyst, 25 ^{o}C, 2g/l oxone]. Insert Figure showing the extent of TOC removal.

5.8.4 Effects of reaction parameters for phenol degradation using Co-AC catalyst

In order to study the reaction kinetics, several experiments were carried out at different feed concentrations of phenol. As seen in Figure 5.8-8, the extent of oxidation was found to decrease with the increase in the feed concentration with almost 80% phenol removal at the end of 3 hrs for the maximum feed concentration of 100 ppm. In order to estimate the rate kinetic parameters a general pseudo first order phenolic decay was assumed in the present system.

$$V\frac{dC_{ph}}{dt} = -\left(k_{app}C_{ph}\right)W \qquad \text{Equation 5.8-3}$$

Where, k_{app} is the apparent first order decay rate of phenol, V is the volume of the batch, W is the weight of the catalyst and C_{ph} is the concentration of phenol at any instant time, t.

The apparent rate constant considered in the given case is the global rate constant comprising of several intermediate steps of adsorption oxidation and desorption. The concentration profile of phenol degradation can thus be represented as follows.

$$C_{ph} = C_{ph0}\exp\left(-k_{app}\frac{W}{V}t\right) \qquad \text{Equation 5.8-4}$$

The concentration data were fitted to the above derived concentration profile as seen in Figure 5.8-8 insert. The apparent rate constant was observed to decrease with the increase in the feed concentration having other parameters fixed. Rate constant data are shown in Table 5.8-1.

Table 5.8-1 Rate constant of phenol degradation at different feed concentration

Feed Concentration	Rate constant *10^{-4} (min^{-1})
25 ppm	5.85
50 ppm	2.35
75 ppm	1.5
100 ppm	0.75

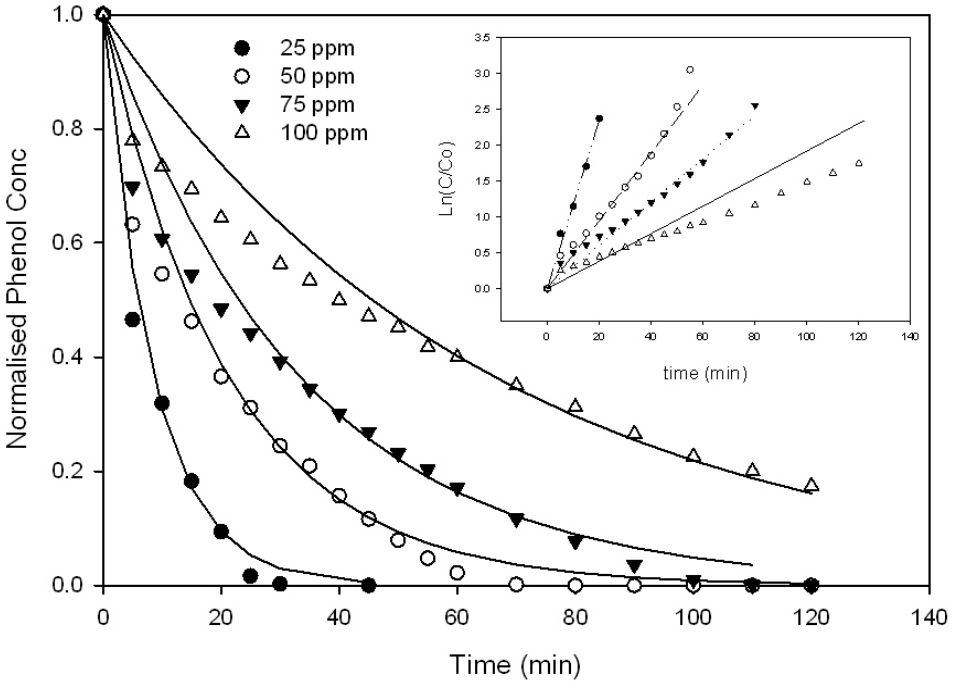

Figure 5.8-8 Phenol degradation kinetic in the presence of Co-AC and oxone [2g/l oxone, 0.2 g/l catalyst, 25 ^{o}C]

Effect of cobalt loading in AC

The effect of cobalt loading on the rate of phenol oxidation is shown in Figure 5.8-9. Higher amount of cobalt loading provides additional sites for generation of active sulphate radical thereby enhancing the rate of reaction. The increase in the cobalt loading from 2.5% Co/g of AC to 5% Co/g of AC resulted in almost doubling of the rate constant; however the further increase to 10% Co/g of AC, showed a comparatively smaller improvement in the extent of reaction. The increase in the cobalt loading would enhance the rate of activation of the PMS to generate the active sulphate radical, resulting in an increase in the rate of phenol removal. However, the high amount of cobalt loading would reduce the extent of phenol adsorption, thus the extent of phenol degradation is capped by the extent of PMS and phenol getting adsorbed onto the surface.

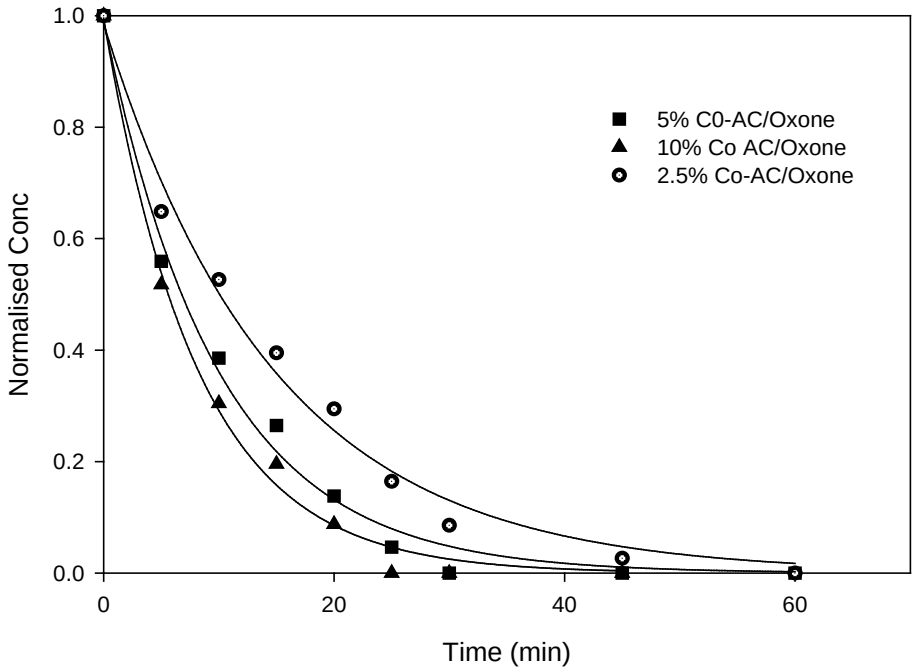

Figure 5.8-9 Phenol degradation kinetic in the presence of Co-AC catalyst having different cobalt loading. [C_{ph} – 25 ppm, 2g/l oxone, 0.2 g/l catalyst, 25 ^{o}C]

Effect of catalyst and oxidant amount on the reaction kinetics

Another alternative to enhance the amount of cobalt in the reaction mixture is by increasing the catalyst amount in the solution. In order to evaluate the effect of catalyst on the rate kinetics, several experiments were performed by varying the amount of catalyst from 0.05 to 0.2 g/L, with the results shown in Figure 5.8-10. Unlike the effect of increment cobalt loading, there was a significant improvement in the rate of reaction upon increasing the amount of catalyst. The incremental addition of catalyst would increase the additional adsorption sites and also provide extra catalyst for activation of peroxymonosulphate, thereby favorably influencing the rate of degradation. The change in the rate constant was observed to be increasing linearly with the increase in the catalyst amount. A similar trend was observed on increasing the amount of oxidant in the reaction. Within the given range of oxidant employed, i.e. 0.5 to 2 g/L as observed in Figure 5.8-11, the rate of reaction is observed to improve with enhancement of the initial rate as much as 3 times for 1 g PMS when compared with 0.25 g of PMS.

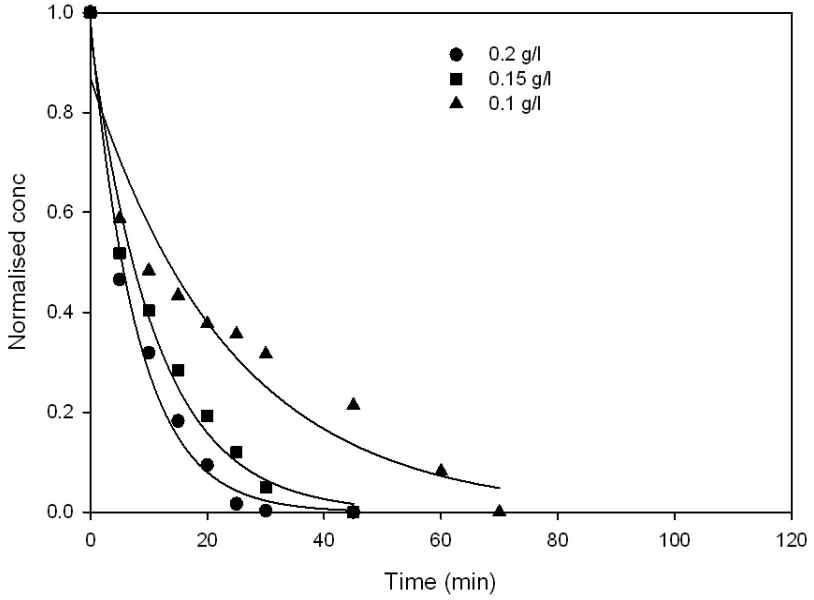

Figure 5.8-10 Phenol degradation at different *catalyst* loading [C_{ph} – 25 ppm, 2 g/l oxone, 25 ^{o}C]

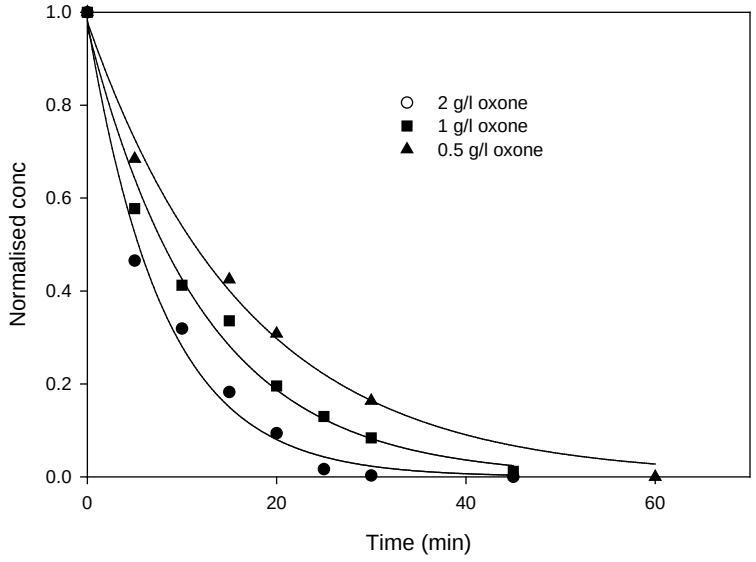

Figure 5.8-11 Phenol degradation at different oxidant amount [C_{ph} – 25 ppm, 0.2 g/l catalyst, 25 ^{o}C]

Effect of reaction temperature

The reaction temperature would play a contradicting role in the case of reaction rate and the adsorption equilibrium. It is likely that increasing the temperature would result in an enhancement in the rate of reaction; nonetheless, the adsorption process being an exothermic process, the increase in the temperature would result in the reduction in the amount of adsorption. In order to evaluate the temperature effect, the reaction was conducted at 3 different temperatures viz 25, 40 and 50 ºC and the results are shown in Figure 5.8-12. It is observed that the rate of reaction increases significantly with the rise in temperature with complete oxidation of phenol being observed within 5 min at 50 ºC, implying that the reaction is the dominating mechanism for the phenol disappearance rate. The dependence of the kinetic constant on the reaction temperature shown in Figure 5.8-12 implies an Arrhenius behavior on of the rate constant on the reaction temperature. The value of the activation energy for the given case of phenol oxidation was estimated at 59.7 kJ/mol.

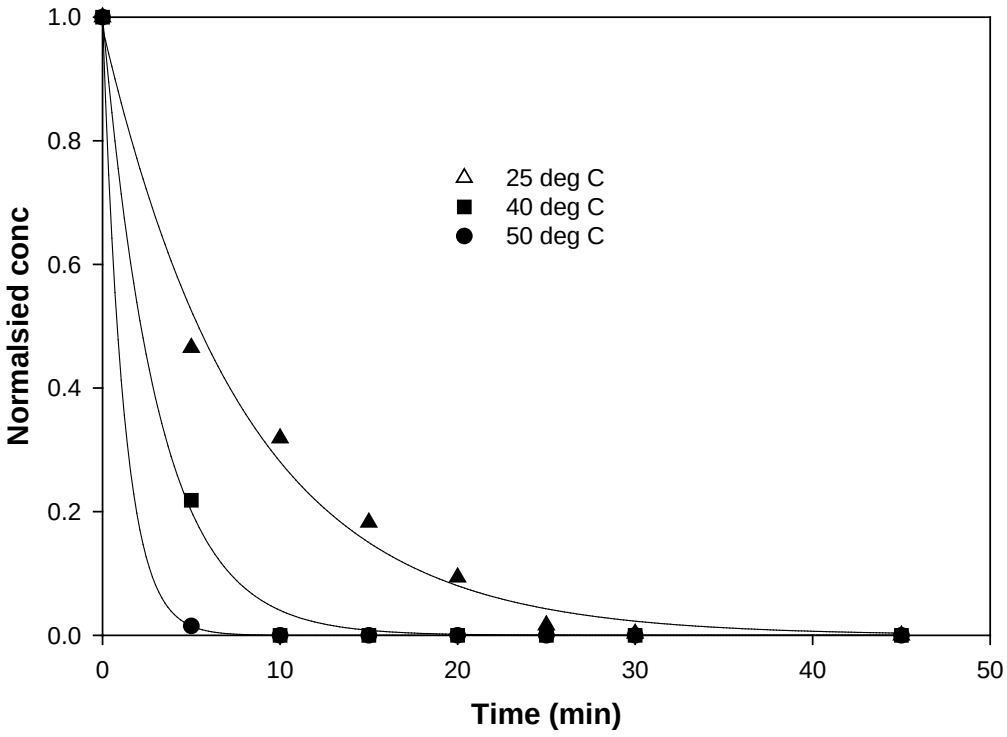

Figure 5.8-12 Phenol degradation at different temperature. [C_{ph} – 25 ppm, 0.2 g/l catalyst, 2 g/l oxone]

5.8.5 Leaching of cobalt and reusability of catalyst

For heterogeneous phenolic oxidation by using Co-AC, it is essential to examine the catalytic efficiency of the spent catalyst. After each reaction, the catalyst was recovered from the reaction mixture by filtration through 0.5 micron filter and washed with distilled water several times to remove any organic component adsorbed on the surface. The acquired catalyst was reused for the oxidation of phenol and the results are shown in Figure 5.8-13.

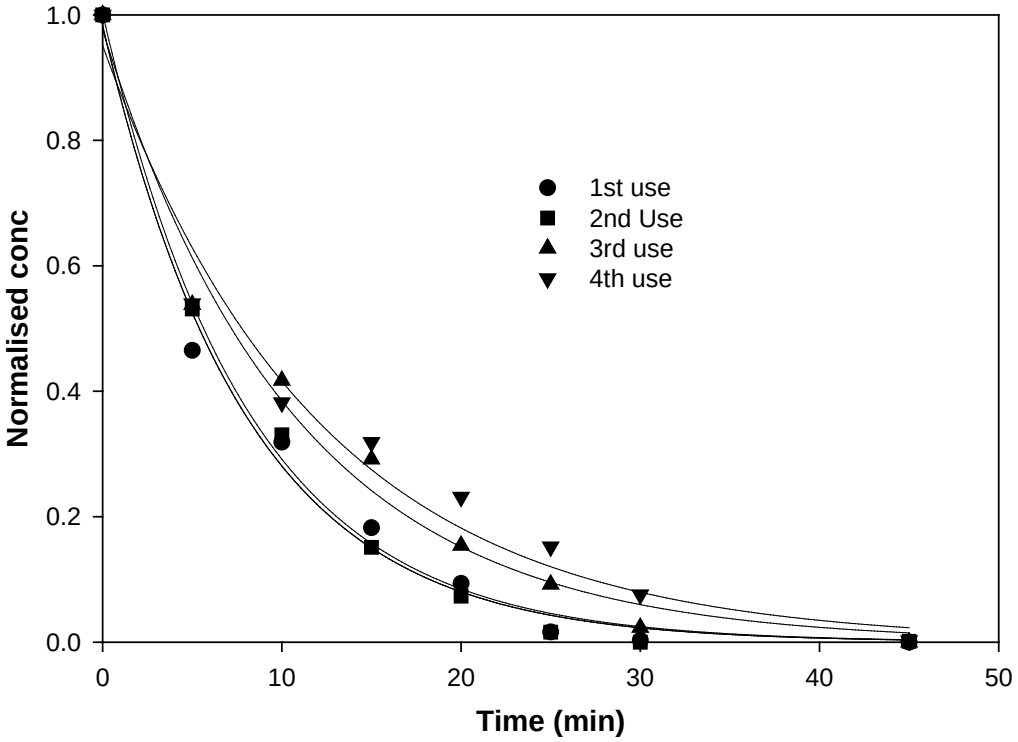

Figure 5.8-13 Degradation of phenol in multiple use of Co-AC catalyst. [C_{ph} – 25 ppm, 2g/l oxone, 0.2 g/l catalyst, 25 ^{o}C]

As seen from Figure 5.8-13, the catalyst activity remained unaffected even after 4th use. The rate of phenol oxidation remained similar in the 1st and 2nd use while decreased slightly in the 3rd and 4th use, suggesting that a small amount of cobalt is probably leached from the carbon catalysts.

Thermo gravimetric analysis (TGA) was carried out in order to determine the relative amount of cobalt leached from the carbon samples. A small amount of samples obtained after each regeneration experiment was burnt under air to form ash and

cobalt oxide slag. The amount of slag left was correlated to the amount of cobalt leaching. Figure 5.8-14 shows the TGA results of the 4 samples. A reference carbon without impregnating with any cobalt was also analyzed to estimate the weight of ash left from pure AC.

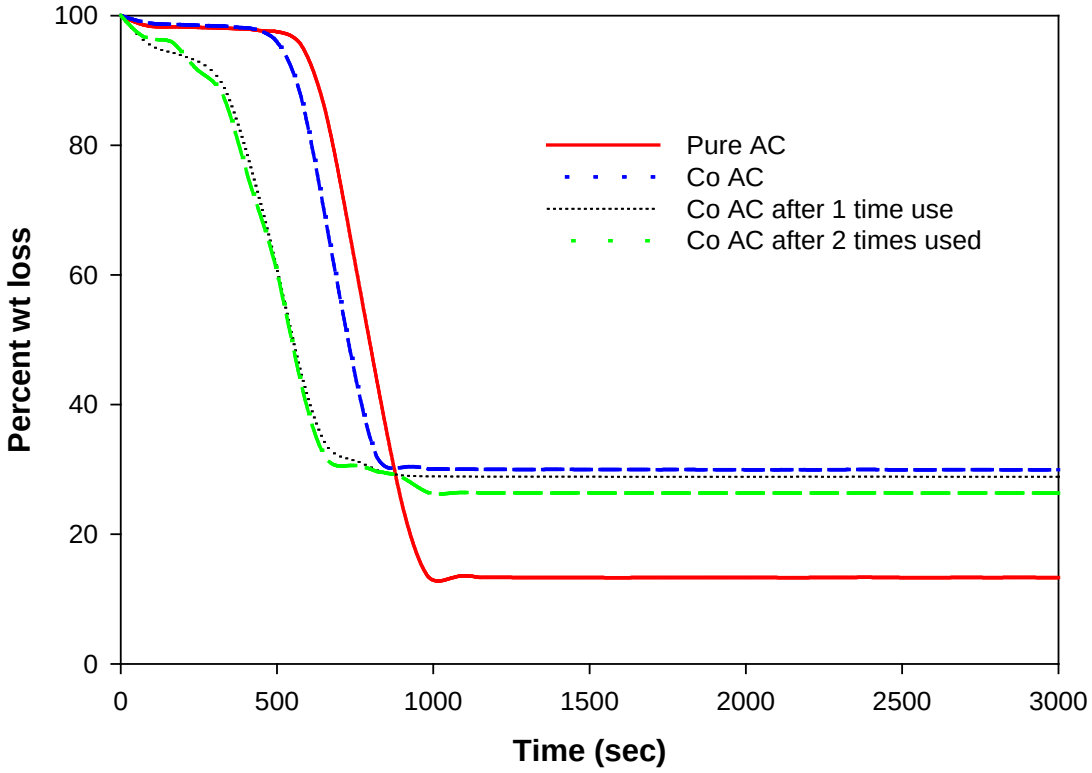

Figure 5.8-14 Weight loss of Co-AC to examine the amount of cobalt loss from catalyst

As seen from the figure, complete burning of pure AC resulted in almost 90% weight loss thereby indicating the ash content of almost 10% by weight. Complete burning of Co-AC resulted in approximately 70% loss in the original weight. The leftover slag would consist of almost 10% by weight of ash and remaining 20% Co-oxide present in the sample which would contain approximately 14.1% cobalt (metal) as seen from Table 5.8-2. The weight loss of 1st and 2nd time reused samples were found to be very similar to that of the Co-AC sample suggesting that very small amount of cobalt oxide was leached from the sample and the reaction proceeded under the heterogeneous mode.

Table 5.8-2 Results of Co-AC tests in different runs.

Test No.	Rate constant (min^{-1})	R^2	Co wt%
CoAC 1st use	0.125	0.991	14.1
CoAC 2nd use	0.123	0.996	13.9
CoAC 3rd use	0.0930	0.986	12.14
CoAC 4th use	0.0827	0.975	-

5.9 Conclusion

Part A

The catalysts prepared by loading cobalt in SBA-15 and silica have been found to have a reasonable capacity to retain cobalt in the form of cobalt oxide and acted as a catalyst for activation of peroxymonosulphate to generate active sulphate radical for phenol oxidation. The rate of phenol oxidation was found to be better in the case of amorphous silica supported catalyst but counters the true heterogeneous activity due to excessive cobalt leaching. The in-situ loading of cobalt in SBA-15 based catalyst resulted in stronger bonding with the cobalt oxide crystallite indicating the stability of the catalyst with respect to the cobalt leaching. The leaching of cobalt metals from the catalyst surface hindered the multiple usage of the catalyst. In order to enhance the catalyst-support bonds, several different metal precursors were used. Co-silica prepared using Co-nitrate showed a strong bond between the support and the catalyst due to the easier removal of the nitrate species during the heat treatment. The catalyst stability and the rate of reaction were observed to be inversely related, since reaction proceeds via homogeneous mode in the catalyst which has no cobalt leaching.

Part B

Co-AC exhibits high activity for phenol oxidative decomposition with sulphate radicals. Co-AC also exhibits adsorption for phenol, favoring the catalytic reaction by trapping the contaminant and finally oxidizing it. Several factors such as phenol concentration, catalyst loading, radical concentration and temperature were found to influence the decomposition rate and efficiency. The initial degradation rate of the

pollutant was correlated to the first order kinetics with the linear dependence of the rate constant on the initial concentration. High loading of catalyst, temperature and radical concentration promote phenol decomposition. Co-AC also shows good catalytic activity after regeneration and less Co leaching, making it as a promising heterogeneous catalyst for organic oxidation in sulphate radicals.

5.10 Reference

1. Sheppard, D.A., C.F. Maitland, and C.E. Buckley, *Preliminary results of hydrogen adsorption and SAXS modeling of mesoporous silica: MCM-41.* Journal of Alloys and Compounds, 2005. **404**: p. 405-408.

2. Xu, X., et al., Preparation and characterization of novel CO2 “molecular basket” adsorbents based on polymer-modified mesoporous molecular sieve MCM-41. Microporous and mesoporous materials, 2003. **62**(1-2): p. 29-45.

3. Reddy, K.M., B. Wei, and C. Song, Mesoporous molecular sieve MCM-41 supported Co–Mo catalyst for hydrodesulfurization of petroleum resids. Catalysis Today, 1998. **43**(3-4): p. 261-272.

4. Wu, Q., et al., *Copper/MCM-41 as catalyst for the wet oxidation of phenol.* Applied Catalysis B, Environmental, 2001. **32**(3): p. 151-156.

5. Zhao, D., et al., Triblock copolymer syntheses of mesoporous silica with periodic 50 to 300 angstrom pores. Science, 1998. **279**(5350): p. 548.

6. Yang, C., et al., Highly dispersed metal nanoparticles in functionalized SBA-15. Chem. Mater, 2003. **15**(1): p. 275-280.

7. Mart nez, A., et al., Fischer–Tropsch synthesis of hydrocarbons over mesoporous Co/SBA-15 catalysts: the influence of metal loading, cobalt precursor, and promoters. Journal of Catalysis, 2003. **220**(2): p. 486-499.

8. Liu, A.M., et al., A new class of hybrid mesoporous materials with functionalized organic monolayers for selective adsorption of heavy metal ions. Chemical Communications, 2000. **2000**(13): p. 1145-1146.

9. Pandya, P.H., et al., Studies on the activity and stability of immobilized -amylase in ordered mesoporous silicas. Microporous and mesoporous materials, 2005. **77**(1): p. 67-77.

10. Yiu, H.H.P. and P.A. Wright, *Enzymes supported on ordered mesoporous solids: a special case of an inorganic–organic hybrid.* Journal of Materials Chemistry, 2005. **15**(35-36): p. 3690-3700.

11. Yan, A.X., X.W. Li, and Y.H. Ye, *Recent progress on immobilization of enzymes on molecular sieves for reactions in organic solvents.* Applied biochemistry and biotechnology, 2002. **101**(2): p. 113-129.

12. Jun, S., et al., Synthesis of new, nanoporous carbon with hexagonally ordered mesostructure. J. Am. Chem. Soc, 2000. **122**(43): p. 10712-10713.

13. Ohtsuka, Y., et al., Fischer- Tropsch Synthesis with Cobalt Catalysts Supported on Mesoporous Silica for Efficient Production of Diesel Fuel Fraction. Energy Fuels, 2003. **17**(4): p. 804-809.

14. Shin, E.W., et al., Phosphate adsorption on aluminum-impregnated mesoporous silicates: surface structure and behavior of adsorbents. ENVIRONMENTAL SCIENCE AND TECHNOLOGY-WASHINGTON DC-, 2004. **38**(3): p. 912-917.

15. Jasra, P. and B. Bhatt, Studies on the activity and stability of immobilized alpha-amylase in ordered mesoporous silicas. Microporous and mesoporous materials, 2005. **77**(1).

16. Xia, F., et al., Photocatalytic degradation of dyes over cobalt doped mesoporous SBA-15 under sunlight. Dyes and Pigments, 2008. **76**(1): p. 76-81.

17. Yang, Q., et al., Heterogeneous activation of peroxymonosulfate by supported cobalt catalysts for the degradation of 2, 4-dichlorophenol in water: The effect of support, cobalt precursor, and UV radiation. Applied Catalysis B, Environmental, 2008. **77**(3-4): p. 300-307.

18. Ramirez, J.H., et al., Azo-dye Orange II degradation by heterogeneous Fenton-like reaction using carbon-Fe catalysts. Applied Catalysis B, Environmental, 2007. **75**(3-4): p. 312-323.

19. Zazo, J.A., et al., *Catalytic wet peroxide oxidation of phenol with a Fe/active carbon catalyst.* Applied Catalysis B, Environmental, 2006. **65**(3-4): p. 261-268.

20. Georgi, A. and F.D. Kopinke, Interaction of adsorption and catalytic reactions in water decontamination processes Part I. Oxidation of organic contaminants with hydrogen peroxide catalyzed by activated carbon. Applied Catalysis B, Environmental, 2005. **58**(1-2): p. 9-18.

6

6 – Photocatalytic oxidation using zinc oxide and sulphate radicals

Abstract

This chapter has been divided into two parts. The first part focuses on the phenol degradation carried out using artificial solar radiation under the presence of zinc oxide and TiO_2 along with sulfate radical generated via peroxydisulphate. As compared to TiO_2, ZnO shows better activity under visible light condition; however it faces a drawback of catalyst dissolution at acidic pH condition. The kinetics of phenol oxidation follows the first order rate model. Several parameters influencing the reaction rate were also investigated including power intensity, phenol concentration, ZnO and persulphate concentrations. It is shown that stronger light intensity will increase phenol oxidation. An optimal concentration of ZnO and persulphate will be required for the maximum degradation of phenol.

The second part is an extension of the first part and mostly focuses on investigating the combined photocatalytic and photochemical oxidation under the influence of low power UV radiation. Photochemical and photo-catalytic reactions and the synergetic effect of their combination were investigated using various oxidants and ZnO. Three different oxidants viz peroxymonosulphate (PMS), peroxydisulphate (PDS) and hydrogen peroxide (H_2O_2) were employed to generate active sulphate/hydroxyl radicals for oxidation. It was found that homogeneous photo-chemical oxidation of phenol using PMS, PDS and H_2O_2 exhibited much better performance than heterogeneous photo-catalytic oxidation on UV/ZnO. The combination of photo-chemical and photo-catalytic oxidation by combining UV/oxidant with ZnO at low UV radiation showed a different degradation trend depending on the oxidant. Due to strong blockage and scattering of UV radiation, the presence of ZnO in UV/PDS and UV/H_2O_2 resulted in a reduction in the extent of photo-chemical phenol degradation.

However, UV//PMS/ZnO showed higher rate of oxidation of phenol as compared to photo-chemical oxidation of UV/PMS, which was mainly attributed to the self chemical reaction between ZnO and PMS. The phenol degradation in the UV/PMS/ZnO followed the first order kinetics while the phenol degradation resulted from the sulphate radical generated due to the dark chemical reaction between ZnO/PMS followed zero order kinetics.

Part A: Photo-catalytic oxidation of phenolic pollutants using zinc oxide and sulphate radical in the presence of artificial solar light

6.1 Introduction

In the last few decades there have been extensive developments in the area of photocatalytic reactions especially for the treatment of wastewater containing highly toxic and refractory chemicals. Pollutants like phenol, cresols and several other strong acids fail to degrade in the conventional primary and secondary wastewater treatment units, making it essential to implement tertiary treatment techniques, mostly advanced oxidation processes such as thermal oxidation, chemical oxidation, wet air oxidation etc. Among the various techniques for tertiary treatments, photocatalytic oxidation has also been successful in treatment of several organic pollutants. Various compounds such as chlorophenols, nitrophenols, trichloroethylene, and toluene have been reported to be completely degraded in both UV and photocatalyst/UV systems [1-3]. Acids like salicyclic and t-cinnamic acids, dyes, and various biocalcitrant pesticides could also be successfully treated under photocatalytic system [4, 5]. There has also been a marked rise in research involving photocatalytic degradation of actual industrial effluents and mixed pollutants [6-9].

In general, photolysis includes irradiating pollutants with UV radiation to generate active hydroxyl radicals from water to successfully oxidize the pollutants. In order to further enhance the degradation efficiency, different semiconductors such as TiO_2 and ZnO as catalysts have been employed. These semiconductors absorb UV radiation more efficiently than the pollutants to generate active hydroxyl radicals. To date, TiO_2 has been the most extensively used photocatalyst. Studies have also been done using ZnO, ZrO_2, SrO_2, CdS etc [10]. As an alternative to TiO_2, ZnO has been reported as an effective catalyst, which has a band gap of 3.2 eV. It has been tested for the oxidation of dyes, phenolic compounds and also for the treatment of groundwater pollutants [11-14].

In further developments of photocatalytic efficiency, it has been observed that addition of small quantities of oxidants such as hydrogen peroxide results in enhanced formation of hydroxyl radicals. The combination of oxidants with a photocatalyst has the capability of oxidizing several highly refractory compounds.

Apart from H_2O_2 and O_3, persulphate (PDS) and peroxymonosulphate (PMS) are also important oxidants producing sulphate radicals, which have caused an increasing attention in recent years. However, few studies have been reported in using sulphate radicals for photocatalytic oxidation of water contaminants and most of the work was focused on TiO_2 catalysts [15-18] under UV radiation.

Little work has been conducted on the effect of sulphate radicals with ZnO on photocatalysis activity in the presence of UV-Vis radiation. In the current study, we conducted a detailed investigation of photocatalytic degradation of some phenolic compounds in the presence of ZnO and PDS under artificial solar radiation. The experiments were focused on studying the influence of various reaction parameters, light bandwidth, lamp power, catalyst loading and oxidant concentration on the reaction rate. A comparison between ZnO and TiO_2 on catalytic degradation was also performed. Phenol was selected as a model contaminant as it is the most common waste product occurring in the waste stream of chemical, petrochemical, pharmaceutical, wood and coal processing units. It is also an intermediate product of several high molecular compounds and is found to be quite recalcitrant for the secondary treatment unit.

6.2 Experimental

6.2.1 Reagents

Zinc oxide (ZnO), [particle size 1-2 micron and surface area 7.5 m^2/g] obtained from B.D.H (Australia) was used as such without further treatment. TiO_2, Degussa P25 [surface area 55.5 m^2/g] was obtained from Degussa, Germany. Pure potassium persulphate ($K_2S_2O_8$, PDS) was used as an oxidant sourced from Aldrich. Phenolic compounds including phenol, dichlorophenol and trichlorophenol obtained from Aldrich were used to prepare stock solutions by dissolving them in water to obtain a solution of 5000 ppm and then the solutions were stored in dark until used. Pure methanol (99.5%) was used as a quenching agent to stop the reaction for analysis of phenolic compounds using a HPLC. Sodium nitrite was used as a quenching agent for total organic content (TOC) measurement.

6.2.2 Photocatalytic reactor and photocatalytic testings

A 1 liter Pyrex glass reactor with a circular base and a jacket was used in the study as a photo reactor. The reactor was placed on a magnetic stirring plate for a constant

mixing at 400 rpm. The reactor was irradiated with a 330 W Xenon lamp, placed in Oriel 66905 lamp housing and powered by Newport 69911 lamp power supply as shown in Figure 6.2-1. This Xenon lamp (model 6259) was used as it emits the light of continuous band from UV to visible range, similar to solar radiation. The lamp housing was equipped with Oriel Filter 6227, having a water cell (path length 10 cm) to filter unwanted infrared radiations. The filter cell has front and back windows of fused silica capable of transmitting radiation from the wavelength range of 200 to 800 nm. The cell also has an external jacket through which cooling water was circulated to control the radiation temperature. Cooling water was also circulated through the reactor jacket to maintain the temperature of reaction. In testing of different light bandwidth on reaction, varying filters were employed to obtain the specific range of light radiation.

Figure 6.2-1 Experimental setup for the photo catalytic reaction.

For each run, a 500 ml phenolic solution at predetermined concentration was prepared by diluting the stock solution (5000 ppm) with deionized water. Before the start of experiments a fixed amount of oxidant, PDS, was added into the phenolic solution and stirred till it was well dissolved. Persulphate is known to be activated thermally; hence the temperature was controlled at 25 ºC for all the experiments. The experiment was started by the addition of a fixed amount of photocatalyst and switching on the lamp. During the reaction, 0.5 ml of sample was withdrawn at fixed

time intervals from the external tube. The sample was quenched by adding excess methanol, and analyzed using a HPLC. The HPLC unit consisted of isocratic pumps from Varian with a UV-Vis detector. The sample was transported using a 40% acetonitrile-water solution. The separation was obtained through a C-18 column and detected at wavelength of 270 nm. The experiments to study the phenol reaction rate at various concentrations were run in triplicates to find the variance, all the experiments done further were duplicated and the mean values were reported. Apart from phenol oxidation kinetics of other phenolic compounds like dichlorophenol (DCP) and trichlorophenol (TCP) were also investigated. The initial concentration of those contaminants was maintained at the same molar concentration of 0.266 mM. For few tests, total organic content (TOC) was also determined using a Shimadzu TOC-5000 CE analyzer. For the measurement of TOC, 5 ml sample was extracted at an interval of 1 h and quenched with 5 ml of 3 M sodium nitrite and then analyzed on the TOC analyzer.

6.3 Results and Discussion

6.3.1 Influence of light wavelength on the photo activity

The artificial solar light used in the current study emits the radiation from 275 to 800 nm. Prior to carrying out the oxidation reaction, the light spectrum emitted by the lamp was measured. Two different filters were used to obtain the light having different wavelength. The spectra obtained from the lamp were measured by a UV-vis detector and the results are shown in Figure 6.3-1. The Xenon lamp without any attached filter emits a light radiation ranging from 300 to 800 nm, which comprises of visible and UV-A band. This spectral is similar to that obtained from solar radiation which also has a small amount (approx 5%) UV radiation. Attaching filter 1 tends to completely absorb the UV radiation and allows only visible light to pass though whereas filter 2 prevents the visible radiation and allows the passage of UV-A radiation band. A proper investigation using both the filters helps in identifying the correct wavelength band responsible for the oxidation reaction.

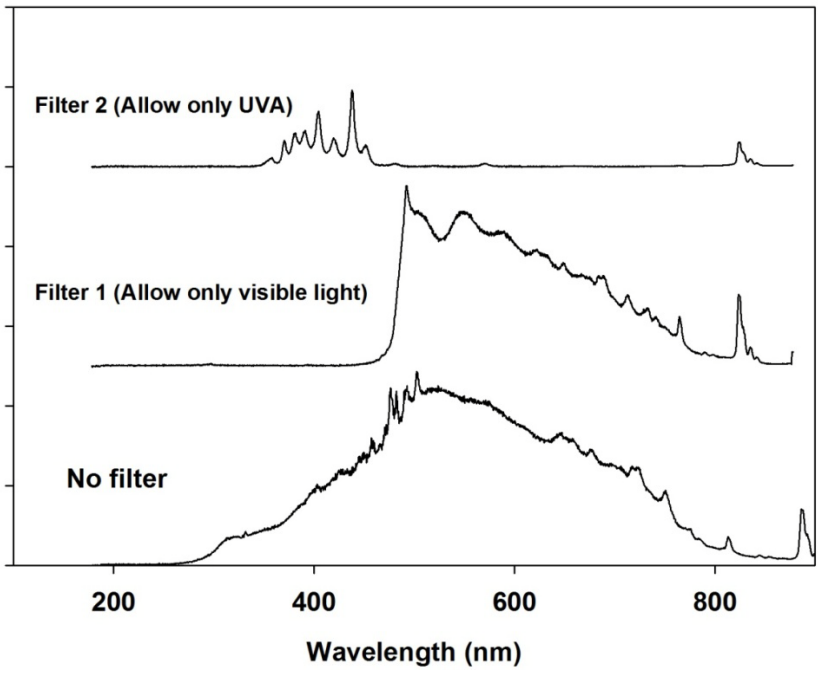

Figure 6.3-1: Light Spectrum observed from the lamp after installing the filters.

A series of preliminary experiments of phenol degradation were performed in the presence of either ZnO or persulphate in order to identify the influence of different light band on the oxidation. As seen in Figure 6.3-2, both ZnO and PDS show a minimal activity in the presence of visible radiation obtained by using filter 1. In the presence of near UV (UVA) radiation obtained using filter 2, PDS is found to be still inactive whereas ZnO shows a considerable activity with 40% reduction in phenol concentration after 150 min. However, under UV-vis light phenol degradation is obtained with both ZnO and PDS individually. After 150 min, phenol degradation reaches 70% for both ZnO and PDS. This suggests that ZnO shows the photocatalyst effect in both UV and UV-vis light, causing catalytic reaction. In contrast, PDS is insensitive to both UV-A band and visible band obtained using filter 1 & 2. The activity of PDS under UV-vis light (without any filter) can be attributed to the small extent of UV radiation emitted below 300 nm, which was cutoff while using both the filters. The intensities of light measured by UVA and visible probes are as shown in Table 6.3-1.

Table 6.3-1: Light Intensities measured at the lamp using different filters

	Intensity measured by UVA probe (W/m^2)	Intensity measured by visible probe (W/m^2)
Filter 1	2.7e-3	413
Filter 2	135.9e-3	222
No Filter	320e-3	543

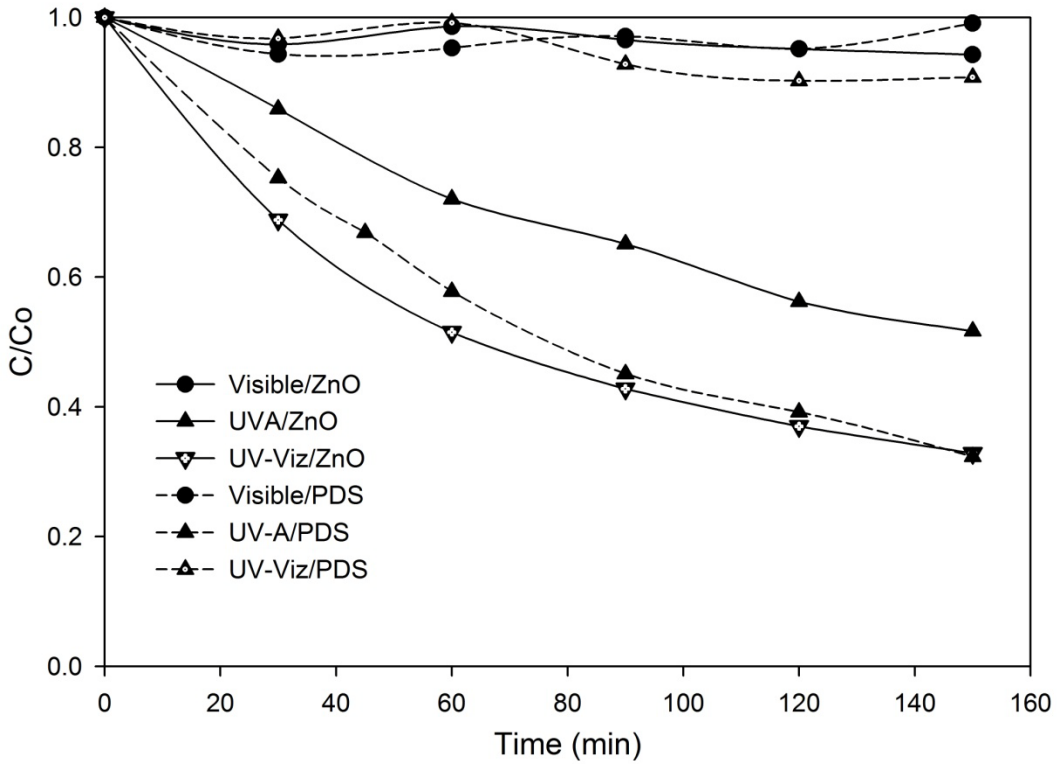

Figure 6.3-2 Effect of light band on photocatalytic degradation of phenol with ZnO and persulphate. Reaction conditions: $[C_{phenol}]_0$=25 ppm, ZnO = 0.4 g/L, persulphate = 2 g/L, power=330 W.

6.3.2 Phenol degradation under different photocatalyst

It is well known that TiO_2 is an effective photocatalyst, however, TiO_2 is only sensitive to UV light and it usually shows a negligible activity under visible light. A comparative study of TiO_2 and ZnO for phenol photo oxidation under UV-vis light was conducted. As observed from Figure 6.3-3, the activity of TiO_2 under UV-vis radiation is

significantly lower than that of ZnO. The observation was same regardless of the presence of oxidant along with the catalyst, suggesting that ZnO have a higher light absorption or quantum efficiency as compared to TiO_2 in the given spectrum. A similar observation has been reported previously for the photo degradation of 2-phenyl phenol [13]. The higher phenol removal with ZnO as compared to TiO_2 could also be attributed to the photo decomposition of ZnO into Zn^{2+} and H_2O_2 due to low pH (approx -5 to 5.5). The photodecomposition also results in generation of intermediate oxygen radical thereby causing oxidation of phenol in the solution [19]. The effect of photo decomposition of ZnO is more evident from Figure 6.3-3, wherein the rate of oxidation of phenol in the presence of ZnO tends to become constant after a certain period of time due to the decrease in the amount of ZnO in contrast to the TiO_2 based oxidation. It is also seen that the photocatalytic oxidation of phenol with the assistance of peroxydisulphate to the catalyst is much faster when compared to the oxidation in the presence of photo catalyst alone. This is mainly due to the electron scavenging effect by the oxidant thereby preventing the electron hole recombination on the surface of photo catalyst resulting in the generation of active sulphate radical which aids in phenol oxidation [20].

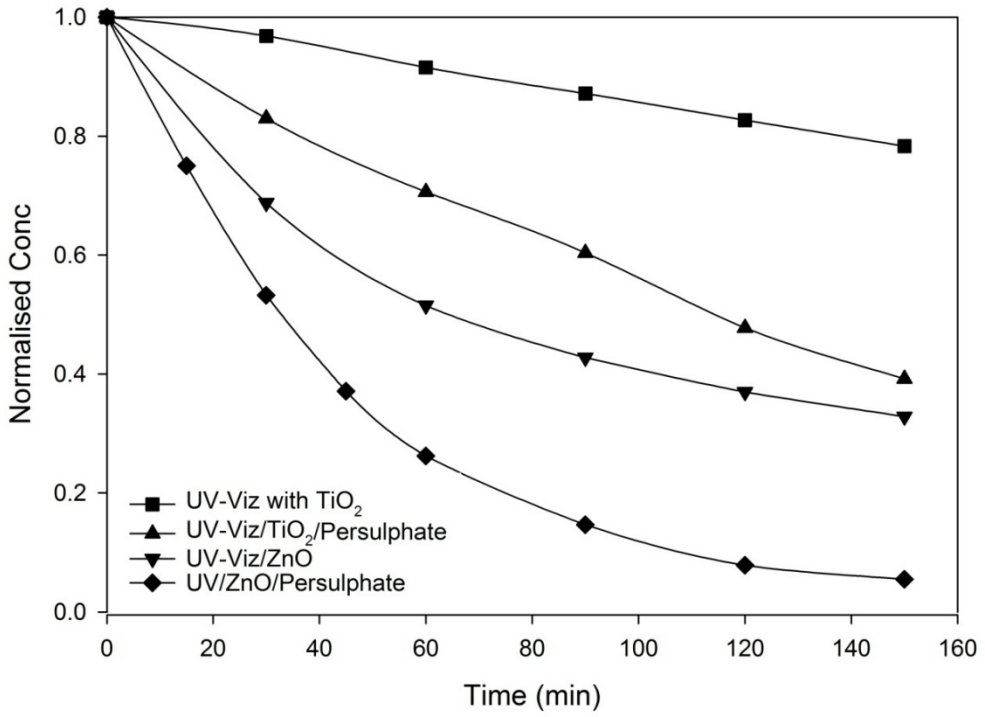

Figure 6.3-3 Comparison of ZnO and TiO_2 on photocatalytic oxidation of phenol, Reaction conditions: $[C_{phenol}]_0$=25 ppm, ZnO or TiO_2 = 0.4 g/L, Persulphate = 2 g/l

Figure 6.3-4 shows a comparison of phenol degradation under varying conditions using ZnO as a photocatalyst. The control experiment of phenol photolysis reveals a much slower reaction rate with only 5% degradation at 200 min. Phenol has a maximum UV absorbance at approximate 270 nm, suggesting an extremely weak absorbance of direct UV radiation arising from the Xenon lamp as shown in Figure 6.3-1. A similar control experiment of phenol with ZnO in the dark also showed a negligible change in the concentration, suggesting a minimal adsorption capacity of ZnO particles for phenol. However, irradiating phenol in ZnO suspension with UV-vis light resulted in phenol degradation and a complete oxidation of phenol was achieved within 5 h. Photo oxidation of phenol using PDS and UV-vis light also presents a fast degradation in a similar rate as ZnO/UV-vis. For ZnO/PDS/UV-vis, the oxidation rate was much faster than the above two cases and a complete oxidation of phenol was achieved in about 2 h, suggesting the combined effect of homogeneous and heterogeneous photocatalytic oxidation induced by PDS and ZnO, respectively.

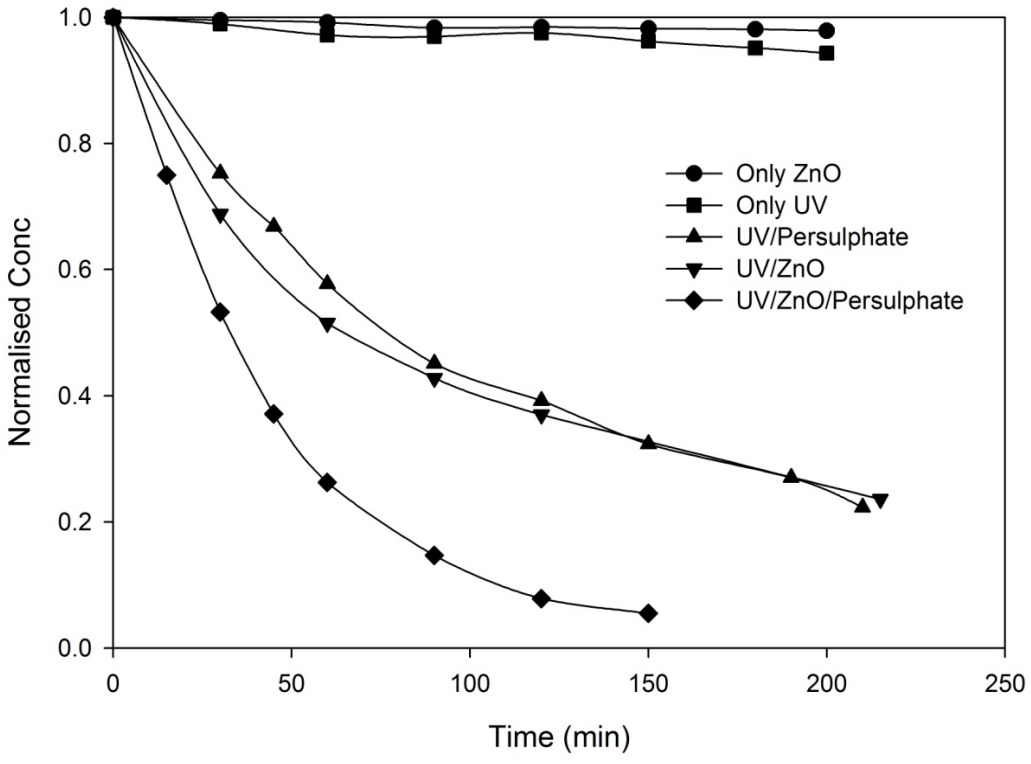

Figure 6.3-4 Photocatalytic oxidation of phenol under various reaction conditions. Reaction conditions: $[C_{phenol}]_0$=25 ppm, ZnO = 0.4 g/L, persulphate = 2 g/l, power =330 W.

Semiconductors are known to absorb the energy from UV radiation, resulting in the transfer of electrons from their valence band to conduction band. This brings about the formation of holes ($ZnO_{surf} \cdot h^+$) in the valence band and free electrons ($ZnO_{surf} . e^-$) in the conduction band on catalyst surface. The high oxidizing capacity of the holes aids in direct oxidation of phenolic contaminants as per reactions 6.3-1

$$ZnO_{surf}\, h^+ + C_6H_5OH \rightarrow C_6H_5OH^{\bullet +} + ZnO_{surf} \qquad \text{Equation 6.3-1}$$

Apart from directly reacting with phenol, the valence band holes ($ZnO_{surf} . h^+$) are also capable of oxidizing water molecules to generate hydroxyl radicals which will in turn oxidize the contaminants [21]. Additionally, the conduction band electrons ($ZnO_{surf} . e^-$) also play a vital role by donating electrons to the molecular oxygen in water, which in turn reacts to form hydroxyl radicals in a series of steps as shown in Equation 6.3-2 below.

$$O_2 + ZnO_{surf}\, e^- \longrightarrow O_2^{\bullet -} + H_2O \longrightarrow H_2O_2 \longrightarrow OH^{\bullet} \qquad \text{Equation 6.3-2}$$

The oxidation of phenol under UV/PDS system is due to the formation of active radicals from PDS. Under the influence of UV radiation (approx~250 nm), PDS is known to undergo a direct photo dissociation to generate sulphate radicals following Equation 6.3-3, which is known to have a high oxidation potential of 2.6 eV [22].

$$S_2O_8^{2-} + h\upsilon \longrightarrow SO_4^{\bullet} + SO_4^{-} \qquad \text{Equation 6.3-3}$$

The similar rate of phenol photo-degradation under UV-vis/ZnO and UV-vis/PDS suggests a quantitatively equivalent active radical formation under the heterogeneous UV-vis/ZnO system and homogeneous UV-vis/PDS system.

Further addition of an oxidant to UV-vis/ZnO system, the reaction will be enhanced by several folds. PDS can react with the freely available electrons, following the similar mechanism on TiO_2 surface [23] to generate active sulphate radicals shown in reactions 6.3-4 and 6.3-5.

$$S_2O_8^{2-} + ZnO_{surf}\,e^- \longrightarrow SO_4^{\bullet-} + SO_4^{2-} + ZnO_{surf}$$ Equation6.3-4

$$SO_4^{\bullet-} + C_6H_5OH \rightarrow C_6H_5OH - SO_4^{\bullet-} \xrightarrow{-SO_4^{2-}} C_6H_5OH^{\bullet+}$$ Equation 6.3-5

As seen in Figure 6.3-4 in the combined UV-vis/ZnO/PDS system, almost complete degradation of phenol (0.266 mM or 25 ppm) was achieved in 2 h after addition of 3.75 mM of PDS.

6.3.3 The kinetics of phenol oxidation in ZnO/PDS/light system

Phenol degradation in the catalytic photoreaction, without any oxidant, occurs by the heterogeneous reaction on the catalyst surface as briefly discussed above. Primarily, a part of phenol is oxidized by direct reaction of phenol with the active holes on the catalyst (ZnO) surface, thereby forming intermediates which could further react to generate end products. The reaction mechanism of this step has been well described by the Langmuir-Hinshelwood kinetics, wherein the phenol molecules are initially adsorbed on the catalyst surface and further react following the first order reaction. The kinetic model is given by Eq.6.3-6.

$$-\frac{dC_{phenol}}{dt} = \frac{kKC_{phenol}}{1 + KC_{phenol}}$$ Equation 6.3-6

Where k is the rate constant and K is the equilibrium adsorption constant.

However, on addition of sulphate based oxidant (PDS) the majority of phenol oxidation occurs in the homogeneous phase due to the reaction with the sulphate radicals as given in reaction 6.3-5. These sulphate radicals are generated either from the reaction of PDS with active ZnO (Eq.6.3-4) or by the direct activation of PDS under UV-vis radiation (Eq.6.3-3).

Figure 6.3-5 shows the degradation profiles of phenol at different initial concentrations in ZnO/PDS/UV-vis system. In the given scenario, wherein the concentration of PDS is several times higher than that of phenol, the phenol degradation can be assumed to follow a pseudo first order reaction as shown in Eq.6.3-7.

$$-\frac{dC_{phenol}}{dt} = k_{app}C_{phenol}$$ Equation 6.3-7

Where, k_{app} represents the apparent pseudo first order reaction rate constant.

On integrating the above equation, Eq.6.3-8 is obtained.

$$\ln\left(\frac{C_{phenol}}{C_{phenol,0}}\right) = -k_{app}t \qquad \text{Equation 6.3-8}$$

The plot of $\ln(C_{phenol}/C_{phenol,\,0})$ with time gives a straight line, as shown in Figure 6.3-5 (insert figure), further confirming the first order degradation of phenol. The rate constants are presented in

Table 6.3-2. The above calculated apparent rate constant of the reaction is assumed to be dependent on various reaction parameters such as oxidant and catalyst concentrations and intensity of incident radiation.

Table 6.3-2 Kinetic parameter of photocatalytic oxidation of phenol.

Initial Phenol Concentration	Apparent Rate constant ($mg.l^{-1}min^{-1}$)
12.5 ppm (0.132 mM)	0.0566
25 ppm (0.265 mM)	0.0207
37.5 ppm (0.398 mM)	0.0127

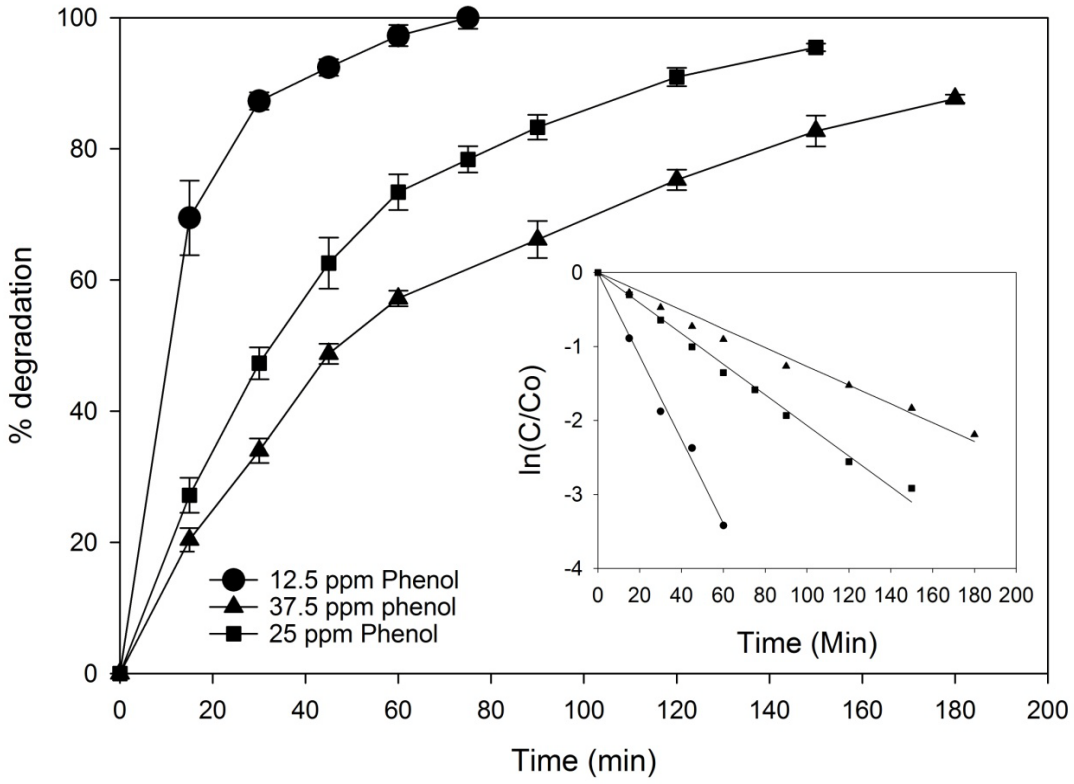

Figure 6.3-5 Degradation efficiency of phenol at varying phenol concentrations. Reaction conditions: ZnO = 0.4 g/L, Persulphate = 2 g/l, power =330 W.

6.3.4 Effect of oxidant concentration

Oxidant concentration will affect the rate of photocatalytic oxidation. To evaluate such an effect, experiments were performed at different concentrations in the range of (1 to 11 mM) at a fixed concentration of contaminant, catalyst and lamp power. It was ensured that the amount of persulphate added was kept below its maximum solubility in water. The clear solution obtained after addition of various amounts of persulphate also ensured the similar amount of light transmissivity into the solution. As shown in Figure 6.3-6, addition of persulphate from 0.18 to 7.4 mM produced an appreciable enhancement of reaction rate; however, further addition of the oxidant resulted in a negligible change in the reaction rate, suggesting a minimal effect of oxidant variation above 14.7 mM. The negligible effect of the oxidant could be due to the presence of excess amount of sulphate radicals as compared to the phenol molecules, which tends to follow the pseudo first order reaction rate.

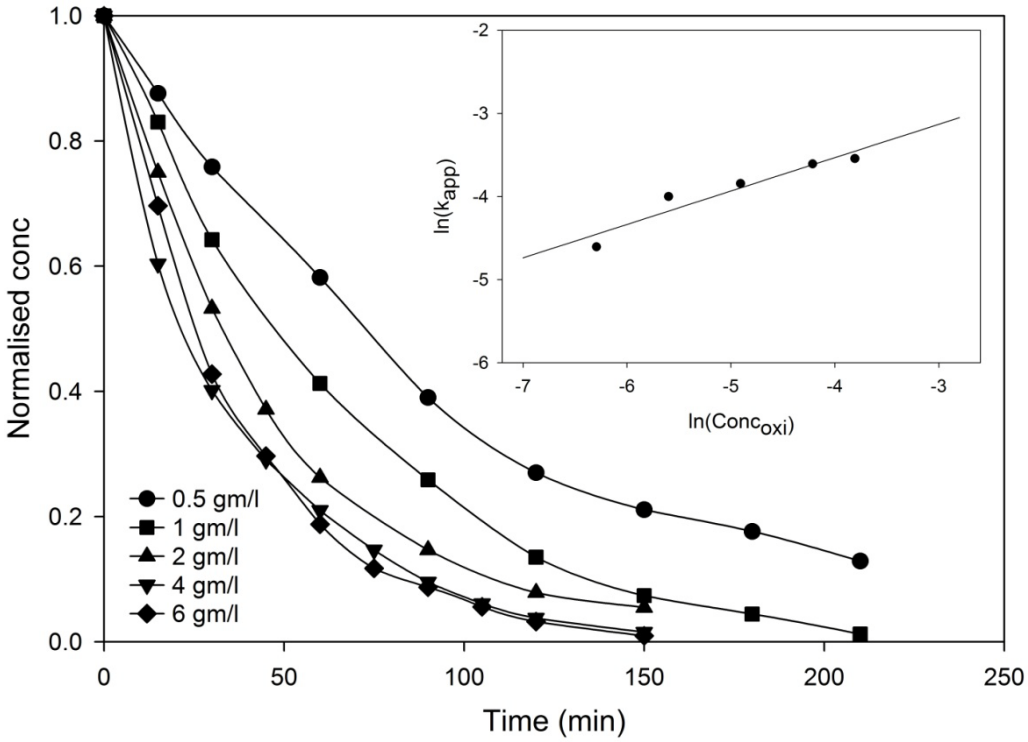

Figure 6.3-6. Effect of persulphate concentration on photocatalytic oxidation of phenol, $[C_{phenol}]_0$=25 ppm, ZnO = 0.4 g/L, power =330 W.

Additionally, excess sulphate radical is also known to abstract the free conduction band electrons of the photocatalyst as per Equation 6.3-9, which could induce consumption of sulphate radicals at higher concentration of the oxidant.

$$SO_4^{\bullet -} + ZnO_{surf}\, e^- \longrightarrow SO_4^{2-} + ZnO_{surf} \qquad \text{Equation 6.3-9}$$

The apparent rate constant of the reaction is correlated to initial oxidant concentration by a simple power law as follows.

$$k_{app} = k_{oxi}\left(C_{oxi}\right)^n \qquad \text{Equation 6.3-10}$$

Where, k_{oxi} is the proportionality constant, C_{oxi} is the oxidant concentration (mM) and n is the order. The proportionality rate constant and the order were then estimated as 0.145 and 0.4, respectively.

6.3.5 Effect of catalyst loading

The amount of catalyst affects the reaction rate by providing the surface for the adsorption as well as generating oxidative valence band holes and electrons. To determine the effect of catalyst loading on the reaction rate, several experiments were also conducted at catalyst loading from 0.2 to 1 g/l. As observed in

Figure 6.3-7, the increase in catalyst amount shows a significant rise in the rate of oxidation. For ZnO loading of 0.2 g/l, the oxidation efficiency of phenol will achieve 95% at 4 h while a complete oxidation will be reached within 3 h for 0.4 g/l or within 2 h at higher amount of catalyst loading. However, there is an insignificant difference in the rate of oxidation between the catalyst amount of 0.8 and 1 g/l, suggesting a minimal effect of additional catalyst to the oxidation. In contrast to accelerating the rate of reaction resulted from the addition of excess catalyst, it can possibly cause a negative effect by reducing the transmittivity of light due to the formation of a milky solution, suggesting the need of an optimal amount of catalyst to balance the benefit of enhanced production of the active radicals and the light transmissivity. In this investigation, it is seen that ZnO loading at 0.8 g/l will be the optimal for phenol oxidation. Similar results were reported by Augustina et al [24] in their work on treatment of winery wastewater with TiO_2.

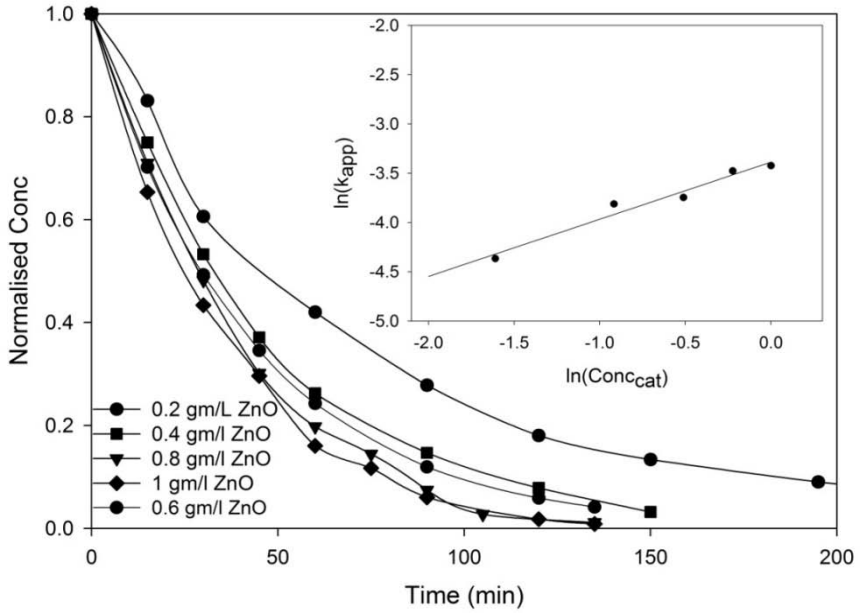

Figure 6.3-7 Effect of ZnO concentration on photocatalytic oxidation of phenol, $[C_{phenol}]_0$=25 ppm, Persulphate = 2 g/l, power =330 W.

Applying the power law to the apparent rate constant predicts the relationship between the rate constant and the catalyst concentration and yields an order value (n) as 0.58. The higher value of 'n' for the catalyst as compared to the oxidant suggests the dominance of the catalyst amount on the rate of reaction when compared to the effect of oxidant.

6.3.6 Effect of light intensity

Light intensity plays an important role in activating the suspended photocatalysts. It has been observed that both ZnO and PDS tend to absorb UV-vis radiation independently and induce phenol oxidation. Dissociation of PDS under UV-vis radiation to produce sulphate radical helps in a quicker oxidation of phenol. Active sulphate radicals can also react with water to generate hydroxyl radicals for oxidation. However, it has also been suggested that addition of particulate ZnO tends to result in light scattering which can reduce the direct activation of persulphate from the radiation. It is further understood that using a high power lamp to generate high intensity radiation would overcome the barrier. Thus further tests on the effect of light intensity were carried out by changing the lamp power from 160 to 330 watts and the results are shown in Figure 6.3-8. It is observed that the rate of oxidation is indeed favored by the increase in lamp power with 95% conversion being obtained within 3 h using the lamp power of 330 W as opposed to 4 h while using the lamp power of 160 W.

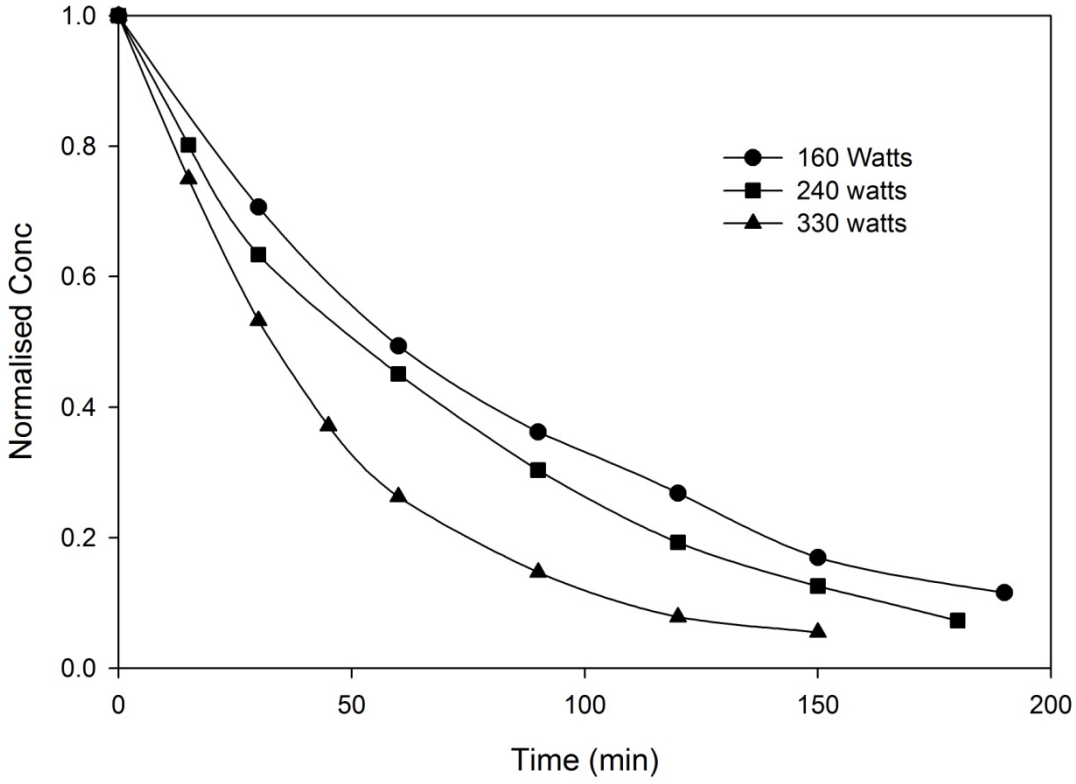

Figure 6.3-8. Effect of light intensity on photocatalytic oxidation of phenol, Reaction conditions: $[C_{phenol}]_0$=25 ppm, ZnO = 0.4 g/L, Persulphate = 2 g/l

6.3.7 Degradation of other phenolic contaminants

The photocatalytic oxidation technique was further employed to study the oxidation of other halogenated compounds such as dichlorophenol (DCP) and trichlorophenol (TCP). DCP and TCP are under the list of drinking water pollutants compiled by USEPA. For comparison, same concentration of phenol, DCP and TCP at 0.266 mM solution was treated in the presence of UV-vis/ZnO/PDS. Degradation of any of these compounds under solar simulator alone was found to be negligible as none of these compounds absorbs the light in the available wavelength. As seen in Figure 6.3-9, for the similar initial molar concentration the rate of oxidation of phenol was considerably higher than that of DCP and TCP. Similarly, the rate of oxidation was found to be higher for DCP as compared to TCP. The slower rate of disappearance of DCP and TCP suggests that the sulphate radical generated are more effective on the degradation of the intermediate compounds as compared to the parent compounds. This was further confirmed with the TOC analysis which shows that in spite of lesser

degradation of TCP and DCP, the total organic carbon removal was fairly similar around 30% after 3 h.

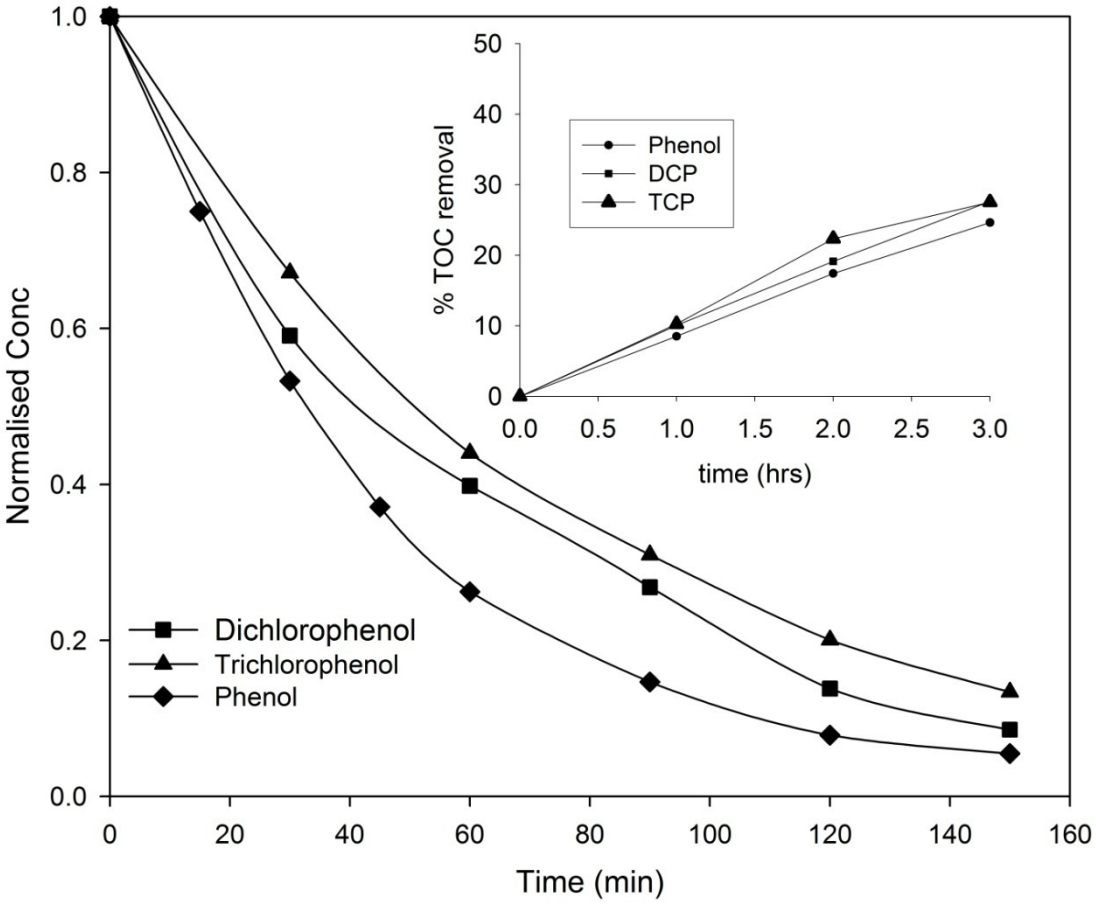

Figure 6.3-9. Photocatalytic degradation of Phenol, DCP and TCP Reaction conditions: $[C_{phenol}]_0$=25 ppm, $[C_{DCP}]_0$ = 44 ppm, $[C_{TCP}]_0$ = 52 ppm, ZnO = 0.4 g/L, Persulphate = 2 g/l

Part B

Non synergetic effect of photo-catalytic and photochemical oxidation when using Low powered UV radiation

6.4 Introduction

In the earlier part of this chapter we discussed about the photocatalytic activity of ZnO for degradation of phenol in aqueous solution. ZnO was found as an efficient photo-catalyst even for visible light irradiation. In order to make photocatalytic oxidation more efficient, addition of electron scavengers such as persulphate was tested. These electron scavengers perform a dual task of scavenging the electron to improve the photo-catalyst efficiency and producing the active oxygen or peroxide radical for photo-chemical oxidation of the contaminants. It was even observed from Figure 6.3-4 that the rate of phenol oxidation in the presence of Light/ZnO/persulphate was better than ZnO or persulphate alone. Thus the combination of photochemical oxidation due to Persulphate and photocatalytic oxidation due to ZnO was observed to be synergetic.

To date there has been a common consensus that addition of an oxidant as an electron quenching agent is beneficial for enhancing the rate of reaction, which may not be necessarily true. The synergy of photo-chemical reaction arising from the oxidants and the photo catalytic reaction would depend on several factors. In the current study, we compared the photo-chemical oxidation of phenol under UV/Oxidant such as PMS, PDS and H_2O_2 and photo-catalytic oxidation under UV/ZnO system in the presence of low powered UV light to oxidize phenolic contaminants in water were compared. The synergetic effect of combination of photo-chemical and photo-catalytic oxidation was examined. Experiments were also carried out in the absence of light to understand the direct chemical reaction between ZnO and the PMS for phenol oxidation.

6.5 Experimental

6.5.1 Reagents

Zinc oxide (ZnO, Dp = 1-2 µm, S_{BET}= 7.5 m^2/g) obtained from B.D.H (Australia) was used as such without further treatment. Pure potassium persulphate ($K_2S_2O_8$, PDS),

peroxymonosulphate (PMS), and H_2O_2 (30%) were obtained from Aldrich. Phenol obtained from Aldrich was used to prepare a stock solution with 5000 ppm and then the solution was stored in dark until used. Pure methanol (99.5%) was used as a quenching agent to stop the reaction for analysis of phenolic compounds using a HPLC.

6.5.2 Reactor setup and photo-degradation testing

A one-liter reactor with a circular base and a jacket was used in the study. The reactor was placed on a magnetic stirring plate with constant mixing at 400 rpm. The whole system was kept in a laminar flow chamber fitted with a germicidal UV-C lamp of 30 watts. The reactor position was fixed at 20 cm below the UV lamp in all experiments. In spite of the lamp not being in the axial position with respect to the reactor, preliminary experiments confirmed a positive influence of the UV radiation on the experiment. The intensity of the radiation was measured using a UV probe and a light meter. A syringe was attached to the reactor outlet to withdraw samples at fixed intervals during 6 h runs. In each test, 500 ml of 25 ppm phenol solution was prepared by diluting the stock solution with deionized water. Before the start of the experiment a fixed amount of oxidant was added to the reaction solution and stirred until dissolved. The experiment was started by the addition of a fixed amount of photocatalyst and UV exposure. A sample of 0.5 ml was withdrawn at fixed intervals using a filter syringe. Samples were quenched by adding excess methanol and analyzed using a HPLC. A similar procedure was used for dark reactions in the absence of UV light.

6.6 Results and Discussion

6.6.1 Photolytic and photocatalytic degradation of phenol with PDS

Preliminary experiments were carried out to observe phenol degradation under different reaction conditions. As seen in Figure 6.6-1, a control experiment with only ZnO in solution showed a negligible change in phenol concentration after 5 h, indicating no significant surface adsorption of phenol on the photocatalyst particles. Another control experiment carried out under UV radiation for photolytic decomposition of phenol showed a minor 10% reduction in phenol concentration resulted from the direct absorption of UV radiation by phenol. The reaction carried out in the presence of ZnO under photo-catalytic UV irradiation showed a significant

degradation of phenol of around 55% within 5 h, suggesting the high oxidation capacity of the active holes formed on the catalyst surface induced by UV radiation.

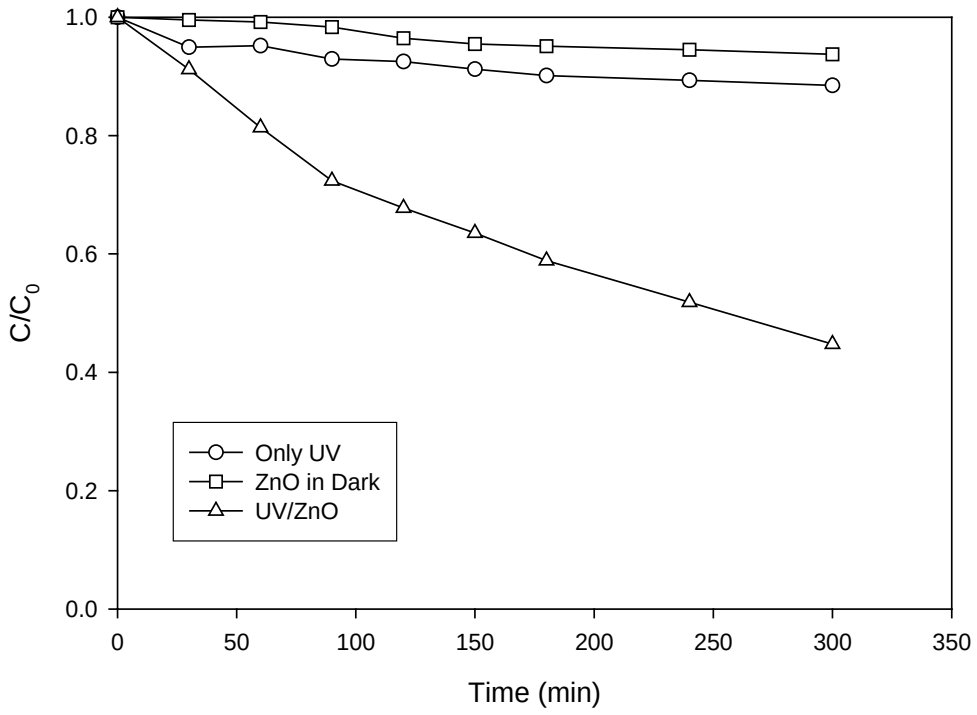

Figure 6.6-1 : Preliminary test of phenol oxidation under UV and ZnO

Figure 6.6-2 shows the dynamic variation of phenol concentration under photo-chemical reaction (UV/PDS) and the effect of adding of ZnO into the photo-chemical/ photo-catalytic system. Under UV/PDS, phenol degradation rate was high and complete phenol removal was obtained within 5 h. However, on addition of 0.2 g/l of ZnO into the reaction mixture, the rate of phenol degradation is found to decrease, showing just 60% degradation within the time span of 5 h. Furthermore, increasing the amount of the photo catalyst further suppresses the rate of phenol degradation, indicating the non-synergetic effect resulted from the combination of photo-chemical and photo-catalytic oxidation. Interestingly, it was observed that the degradation rate of phenol in the presence of 0.2 g/l of ZnO as seen from Figure 6.6-2 follows similarly to the degradation of phenol in the presence of 0.2g/l of ZnO as shown in Figure 6.6-1, thus suggesting that upon adding ZnO to the photo-chemical reaction system, the reaction proceeds mainly due to the photo catalytic reaction and the effect of PDS is completely suppressed.

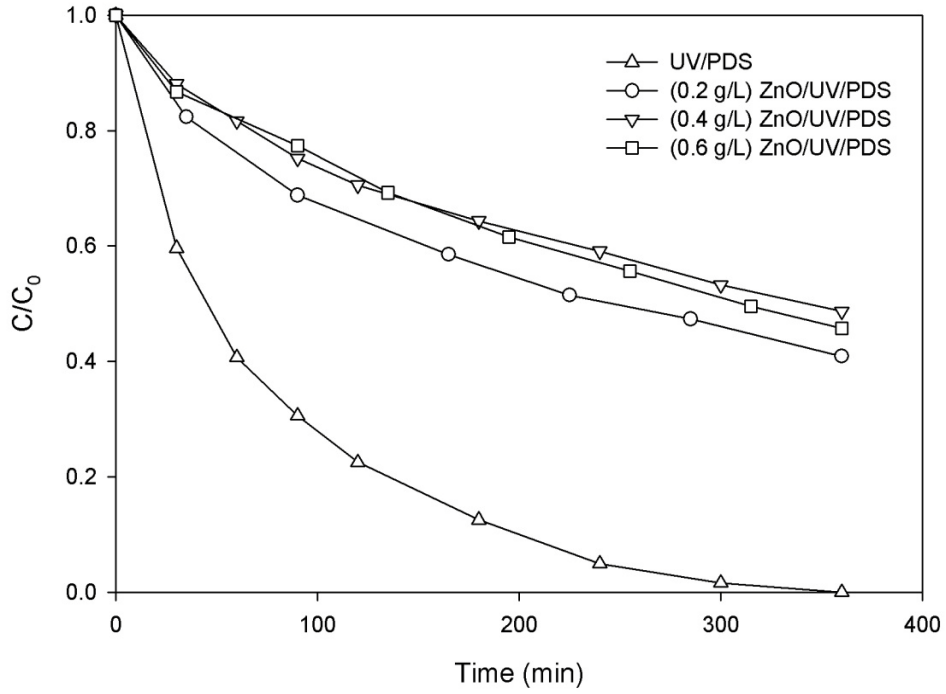

Figure 6.6-2 Phenol oxidation with combination of low power UV/ZnO/PDS at different amount of ZnO [PDS= 7.4 x10^{-3} M]

Under UV radiation, PDS disintegrates to generate active sulphate radicals (Equation 6.6-1), which have oxidation potential of 2.4 eV, thus capable of oxidizing the contaminants in water.

$$S_2O_8^{2-} + h\upsilon \longrightarrow SO_4^{\bullet} + SO_4^{-}$$ Equation 6.6-1

The results from Figure 6.6-1 and Figure 6.6-2 suggest that under the given conditions, homogeneous oxidation of phenol is much more efficient than the heterogeneous oxidation with ZnO. In the combination system (UV/ZnO/PDS), the rate of oxidation was similar to that of the photo-catalytic oxidation using UV/ZnO. The decreased rate of phenol degradation in the current study using the combined UV/PDS/ZnO system suggests that the photo-chemical oxidation of phenol occurring by the direct absorption of UV radiation by the oxidant is completely suppressed upon adding the photocatalyst. A contradicting observation, however, has been previously reported in the literature. Dhanalakshmi et al. [17] investigated phenol degradation by the coupling of PDS with TiO_2 and obtained a significant enhancement in the rate of phenol oxidation by adding PDS along with TiO_2 using a

UV lamp source of 250 W. Barakat et al. [25] studied the photo-catalytic oxidation of phenol and monochlorophenol in aqueous suspensions of commercial TiO_2 rutile and found enhanced photo-catalytic oxidation rates in a UV/TiO_2/H_2O_2 system compared to either UV/TiO_2 or UV/H_2O_2 alone under a UV irradiation of 260 W/m^2. A similar observation was also reported for the oxidation of an organophosphorous pesticide with TiO_2 and H_2O_2 at UV power of 100-450 W [26, 27].

Interestingly in all the reported cases a high powered UV lamp source was utilized for carrying out the experiments. In a distinctive study Wang et al. [28] reported a non-synergetic combination of H_2O_2 with TiO_2 for 2-chlorobiphenyl degradation carried out in the UV irradiation of 19 W/m^2. It has been claimed that the chemical sorption of the oxidant on the TiO_2 surface could result in significant scavenging of the active holes along with quenching of OH radicals formed on the TiO_2 surface to decrease the reaction rate. A similar effect cannot be ruled out in the current case of the UV/ZnO/PDS system. However, in the earlier part of this chapter using a high-power UV light (500 W), the rate of phenol degradation was enhanced considerably by the combination of photo-chemical and photo-catalytic oxidation, thereby implying that the scavenging of the oxidative valance band holes by the oxidant is not the controlling factor for the decrease in oxidation rate. The reduction in the degradation rate under the UV/ZnO/PDS system is the result of the opacity caused by addition of ZnO, which could block the low-power UV radiation (intensity~2.8 W/m^2) from penetrating the reaction mixture to induce photo-chemical reaction. Further, it is deduced that a synergistic effect by combining UV/ZnO/PDS would be observed only beyond a certain threshold of light intensity, at which the light is capable to penetrate the opacity caused by small dispersed ZnO particles. Additionally, the increased amount of ZnO in the UV/PDS/ZnO system, showing a reduced degradation rate even in comparison to heterogeneous UV/ZnO, implies the opacity effect can prevail over the photo-chemical and photo-catalytic oxidation of phenol.

6.6.2 Photocatalytic degradation of phenol with PMS

Similar to PDS, PMS is known to undergo degradation upon UV irradiation to generate sulfate and hydroxyl radicals thereby aiding in the photo-chemical oxidation of phenol (Equation 6.6-2).

$HSO_5^- + h\gamma \rightarrow OH\bullet + SO_4\bullet^-$ Equation 6.6-2

Figure 6.6-3 depicts the kinetic degradation of phenol under various reaction conditions. With UV/PMS, phenol degradation was almost 60% in 5 h, which is higher than the photo-catalytic UV/ZnO oxidation. The combination of UV/PMS with ZnO resulted in an enhancement of the degradation rate to almost 80% phenol degradation within 5 h, thereby suggesting a synergistic effect with UV/ZnO/PMS, contrary to the UV/ZnO/PDS results. Furthermore, increasing the concentration of ZnO in the solution increased the degradation rate with almost 100% degradation of phenol at 0.6 g/L of ZnO.

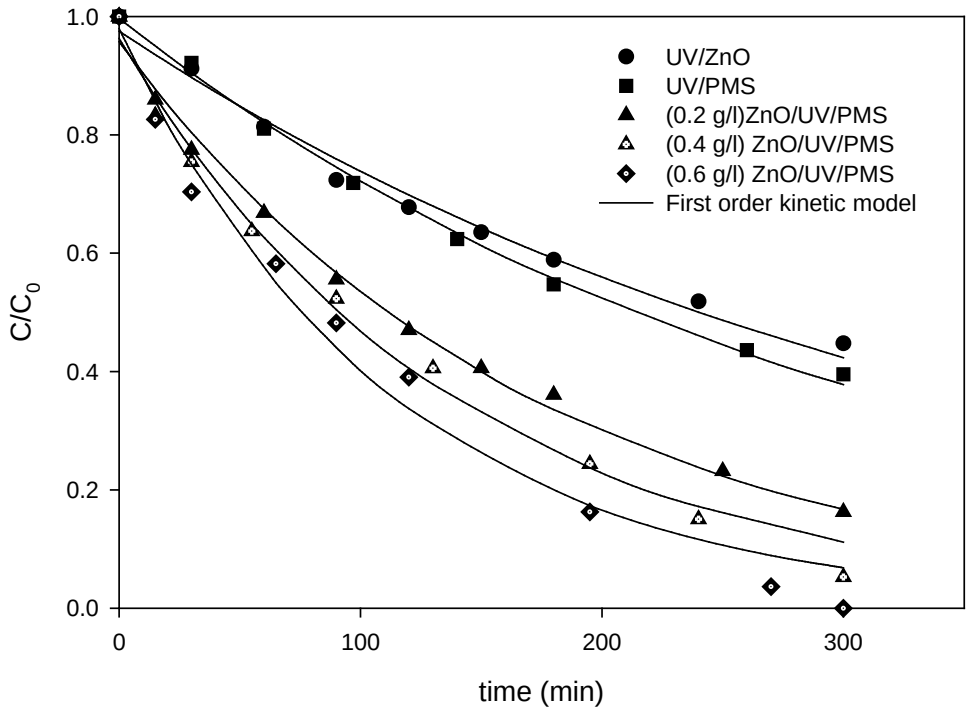

Figure 6.6-3 Phenol oxidation with combination of low power UV/ZnO/PMS for different amount of ZnO [PMS=6.51 x10^{-3} M]

The enhanced phenol degradation in the UV/PMS/ZnO system compared to the UV/PMS system suggests that the contribution of photo-chemical oxidation was still significant in the degradation unlike the combination of PDS with ZnO. For UV/ZnO/PMS, it was observed that some ZnO particles dissolved in the solution during the reaction process, which made the reaction mixture more transparent and allowed sufficient transmission of UV light to induce photo-chemical oxidation with PMS.

Apart from photo-chemical and photo-catalytic reactions taking place in the UV/PMS/ZnO system, a series of additional reactions were found to be taking place due to the direct reaction of ZnO with PMS, which may also cause the dissolution of ZnO. In-order to investigate the effect of ZnO dissolution and its possible influence on phenol degradation several experiments were performed with ZnO and PMS under the absence of UV radiation. As seen from Figure 6.6-4, phenol degradation was also observed in the presence of ZnO with PMS even in the absence of UV radiation. Furthermore, the rate of degradation increased with the increase in the concentration of ZnO. The control experiment conducted in the absence of ZnO showed negligible phenol degradation.

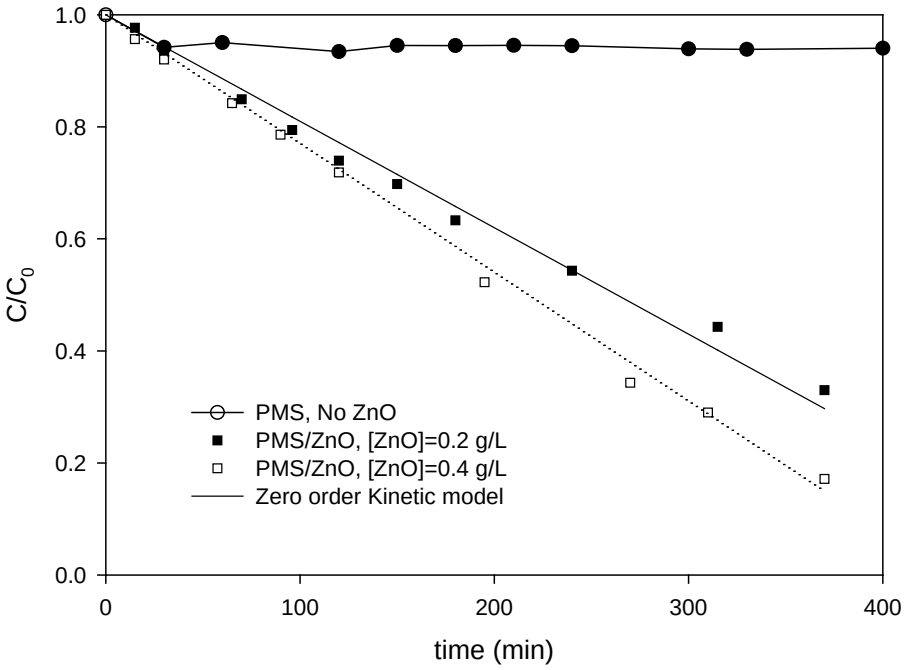

Figure 6.6-4: Phenol oxidation under dark ZnO/PMS [PMS=6.51 x10^{-3} M]

Previous investigations have found that PMS can be activated by transition metals to produce sulphate radicals which can then degrade organic compounds in water. Similarly, in the current case, the PMS is activated by ZnO to generate active hydroxyl and sulphate radicals as per equation 6.6-3

$$ZnO + HSO_5^- \rightarrow Zn^{2+} + OH\bullet + SO_5\bullet^-$$ Equation 6.6-3

The rate of phenol degradation was found to follow zero-order kinetics, thus implying that the phenol oxidation rate is controlled by the generation of active sulphate/hydroxyl radical rather than by the reaction with phenol itself. The rate constant of phenol degradation based on zero order is given in Table 6.6-1. It is shown that the rate of phenol photo degradation is enhanced at increased ZnO loading. However such an enhancement of the reaction results in the loss of photocatalyst.

Table 6.6-1 Rate constant of phenol degradation in PMS and ZnO.

Amount of ZnO (g)	Rate constant (mg/L.min)
0.2	0.0018
0.4	0.0023

Given the series of reactions taking place in UV/PMS/ZnO, the photo-catalytic oxidation of phenol in the UV/PMS/ZnO system would generally occur following these mechanisms:

1) homogeneous photo-chemical oxidation by UV/PMS and sulphate radicals generated from the interaction of PMS with conduction band electrons,
2) heterogeneous photo-catalytic oxidation from UV/ZnO,
3) Direct chemical reaction between ZnO and PMS to generate active sulphate or hydroxyl radicals.

Figure 6.6-5 shows the effect of PMS concentration on photo-catalytic phenol oxidation in UV/ZnO/PMS. The incremental addition of PMS from 1.85 to 7.4 mM resulted in increased phenol degradation by reaching a maximum of 100% within 6 h. Further addition of PMS, however, reduced the extent of phenol oxidation efficiency. This can be attributed to two factors. One is the dissolution of ZnO with PMS causing the reduction in oxidation rate. The other factor is the self-quenching of sulphate and hydroxyl radicals by PMS (Equation 6.6-5 & 6.6-5). It is known that $SO_5^{\bullet -}$ exhibits lower oxidation rates than $SO_4^{\bullet -}$. Previous investigations also have found that higher PMS in metal/PMS systems would reduce organic degradation in water [26]. Therefore, an optimum amount of PMS/ZnO is important and required for the synergistic behaviour in the UV/ZnO/PMS photo-catalytic oxidation of contaminants.

$HSO_5^- + SO_4^{\bullet -} \rightarrow SO_5^{\bullet -} + SO_4^{2-} + H^+$ Equation 6.6-4

$HSO_5^- + OH^{\bullet} \rightarrow SO_5^{\bullet -} + H_2O$ Equation 6.6-5

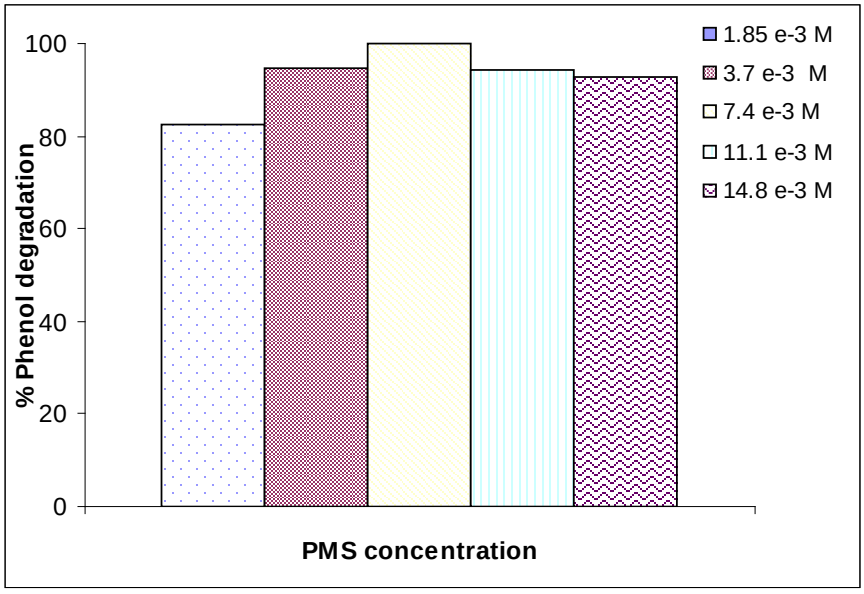

Figure 6.6-5 Phenol oxidation efficiency under UV/ZnO/PMS for a fixed reaction time of 5 h and different concentration of PMS [ZnO = 0.4 g/L]

6.6.3 Photocatalytic degradation of phenol with H_2O_2

Figure 6.6-6 shows the dynamic variation of phenol degradation in H_2O_2, UV/H_2O_2 and UV/ZnO/H_2O_2 systems. H_2O_2 at dark condition did not show significant phenol degradation. With the assistance of UV, phenol degradation was much stronger and phenol degradation could reach 100% in 5 h. However, the rate of phenol degradation with UV/ZnO/H_2O_2 was reduced in comparison to UV/H_2O_2. The more ZnO in solution, the lower the phenol degradation was. This observation was similar to that of photocatalytic oxidation of phenol with UV/ZnO/PDS. The reduced phenol degradation could still be attributed to well dispersion of ZnO into the solution making the solution turning milky and preventing UV radiation to penetrate inside. Therefore, for UV/ZnO/H_2O_2, it is also suggested that the synergetic combination of UV/ZnO with UV/H_2O_2 would be realized by employing a lamp with intensity above a minimum threshold.

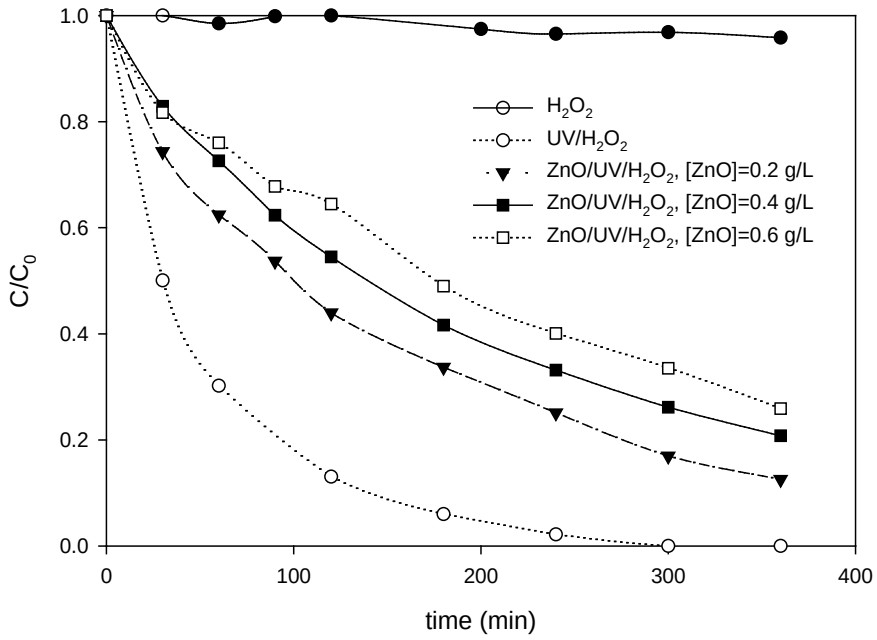

Figure 6.6-6: Phenol oxidation with combination of low power UV/ZnO/H_2O_2 at different amount of ZnO [H_2O_2=6.68 x10^{-3} M]

With regard to the effect of H_2O_2 concentration on photocatalytic oxidation of phenol in UV/ZnO/H_2O_2 (Figure 6.6-7), the increase in H_2O_2 concentration resulted in a substantial increase in phenol oxidation rate to a maximum limit. Further high concentration of H_2O_2 actually reduced phenol oxidation efficiency. This is due to quenching of the active hydroxyl radicals by H_2O_2 (Eq. 6.6-5), similar to the quench of sulphate radicals. Many investigations have reported the quench effect of excess H_2O_2 in advanced oxidation processes of organic compounds [28, 29].

$H_2O_2 + OH\bullet \rightarrow HO_2\bullet + H_2O$ Equation 6.6-6

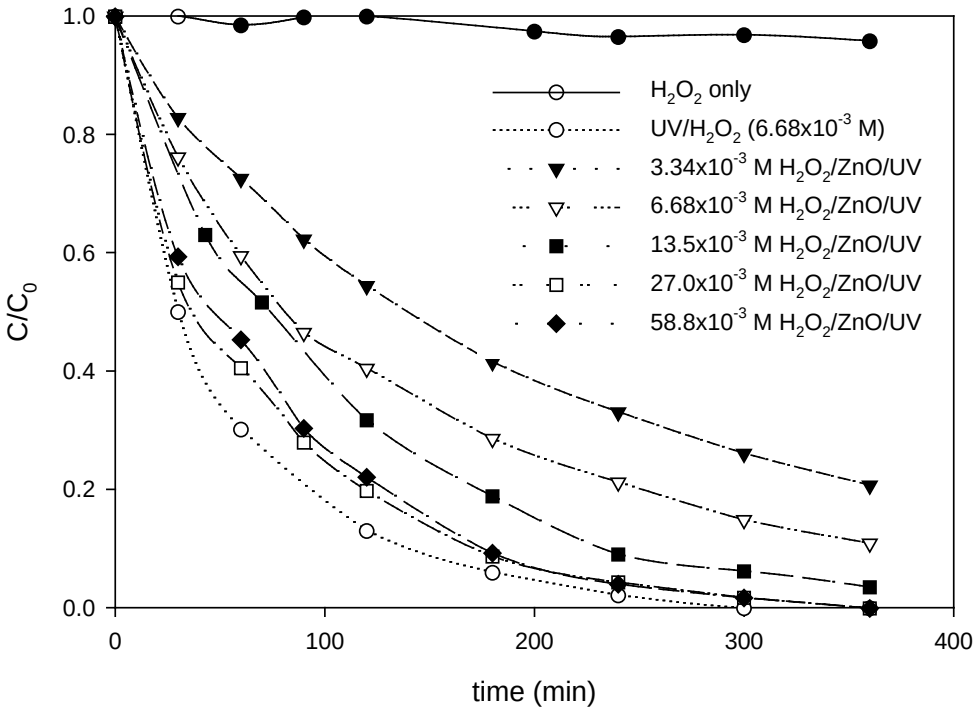

Figure 6.6-7: Phenol oxidation with combination of low power UV/ZnO/H_2O_2 at different concentration of H_2O_2 [ZnO= 0.4 g/L]

6.7 Conclusions

Part A

Photocatalyst ZnO exhibits higher activity than TiO_2 for the photocatalytic and photo oxidation of phenolic contaminants under UV-vis light. Addition of sulphate based oxidant, PDS, can remarkably enhance the rate of phenol oxidation. Moreover, under UV-vis radiation, the combination of UV-vis/ZnO/PDS is more efficient as compared to UV-vis/PDS or UV-vis/ZnO system. The amount of ZnO and PDS in solution will influence the oxidation rate and the maximum degradation of phenol can be achieved at optimum loading while excess ZnO and PDS will have a negligible effect. The reaction rate is also enhanced with the increase in light intensity. The overall degradation of phenol follows the first order reaction. For other chlorophenols such as DCP and TCP, photocatalytic oxidation rate is less than phenol, giving an order of phenol > DCP > TCP.

Part B

ZnO is a promising photocatalyst as an alternative to TiO_2 and shows effective oxidation of phenol under low powered UV radiation. Three oxidants, PMS, PDS and H_2O_2, are also effective in photo degradation of phenolic pollutants and exhibited higher activity than heterogeneous UV/ZnO. However, the combination of UV/ZnO with UV/oxidant can produce different synergetic effects on photocatalytic oxidation depending on the oxidant and UV power strength. Under low-power UV radiation, a reduction in photocatalytic oxidation of phenol due to the blockage and scattering of UV radiation by ZnO particles could be observed. The addition of PDS in UV/ZnO would increase phenol degradation as compared to UV/ZnO, but the activity was lower if compared with UV/PDS. On the other hand, under high powered UV light, UV/ZnO/PDS showed an enhanced photocatalytic oxidation of phenol compared with UV/PDS. The synergetic effect could be observed only after a certain threshold of light intensity was reached. A similar observation was found with the combination of UV/ZnO with UV/H_2O_2. While in the case of PMS based system, the combination of UV/ZnO and UV/PMS showed a higher reaction rate compared with UV/PMS even at low UV power. This was found to be due to the partial dissolution of ZnO during the reaction thereby allowing better transmission of UV radiation. Additionally the reaction of ZnO with PMS resulted in the generation of active radicals, which also helped in enhancing the rate of phenol degradation. Kinetic studies showed that photocatalytic oxidation of phenol followed the first order kinetics while the catalytic oxidation of phenol in ZnO/PMS followed zero order kinetics.

6.8 References

1. Wang, K.H., et al., *Photocatalytic degradation of 2-chloro and 2-nitrophenol by titanium dioxide suspensions in aqueous solution.* Applied Catalysis B, Environmental, 1999. **21**(1): p. 1-8.

2. Luo, Y. and D.F. Ollis, *Heterogeneous Photocatalytic Oxidation of Trichloroethylene and Toluene Mixtures in Air: Kinetic Promotion and Inhibition, Time-Dependent Catalyst Activity.* Journal of Catalysis, 1996. **163**(1): p. 1-11.

3. Crittenden, J.C., et al., *Photocatalytic oxidation of chlorinated hydrocarbons in water.* Water Research, 1997. **31**(3): p. 429-438.

4. Farré, M.J., et al., *Degradation of some biorecalcitrant pesticides by homogeneous and heterogeneous photocatalytic ozonation.* Chemosphere, 2005. **58**(8): p. 1127-1133.

5. Ranjit, K.T., et al., *Lanthanide Oxide Doped Titanium Dioxide Photocatalysts: Effective Photocatalysts for the Enhanced Degradation of Salicylic Acid and t-Cinnamic Acid.* Journal of Catalysis, 2001. **204**(2): p. 305-313.

6. Gomes de Moraes, S., R. Sanches Freire, and N. Durán, *Degradation and toxicity reduction of textile effluent by combined photocatalytic and ozonation processes.* Chemosphere, 2000. **40**(4): p. 369-373.

7. Peralta-Zamora, P., et al., *Evaluation of ZnO, TiO2 and supported ZnO on the photoassisted remediation of black liquor, cellulose and textile mill effluents.* Chemosphere, 1998. **36**(9): p. 2119-2133.

8. Beltrán, F.J., M. González, and J.F. González, *Industrial wastewater advanced oxidation. Part 1. UV radiation in the presence and absence of hydrogen peroxide.* Water Research, 1997. **31**(10): p. 2405-2414.

9. Beltrán, F.J., J.M. Encinar, and J.F. González, *Industrial wastewater advanced oxidation. Part 2. Ozone combined with hydrogen peroxide or UV radiation.* Water Research, 1997. **31**(10): p. 2415-2428.

10. Serpone, N., et al., *Exploiting the interparticle electron transfer process in the photocatalysed oxidation of phenol, 2-chlorophenol and pentachlorophenol: chemical evidence for electron and hole transfer between coupled semiconductors.* Journal of Photochemistry & Photobiology, A: Chemistry, 1995. **85**(3): p. 247-255.

11. Villasen8or, J., P. Reyes, and G. Pecchi, *Photodegradation of Pentachlorophenol on ZnO.* J. Chem. T echnol. Biotechnol, 1998. **72**: p. 105È110.

12. Akyol, A., H.C. Yatmaz, and M. Bayramoglu, *Photocatalytic decolorization of Remazol Red RR in aqueous ZnO suspensions.* Applied Catalysis B, Environmental, 2004. **54**(1): p. 19-24.

13. Khodja, A.A., et al., *Photocatalytic degradation of 2-phenylphenol on TiO2 and ZnO in aqueous suspensions.* Journal of Photochemistry & Photobiology, A: Chemistry, 2001. **141**(2-3): p. 231-239.

14. Khalil, L.B., W.E. Mourad, and M.W. Rophael, *Photocatalytic reduction of environmental pollutant Cr (VI) over some semiconductors under UV/visible light illumination.* Applied Catalysis B, Environmental, 1998. **17**(3): p. 267-273.

15. Yang, Q.J., et al., *Heterogeneous activation of peroxymonosulfate by supported cobalt catalysts for the degradation of 2,4-dichlorophenol in water: The effect of support, cobalt precursor, and UV radiation.* Applied Catalysis B-Environmental, 2008. **77**(3-4): p. 300-307.

16. Malato, S., et al., *Enhancement of the rate of solar photocatalytic mineralization of organic pollutants by inorganic oxidizing species.* Applied Catalysis B, Environmental, 1998. **17**(4): p. 347-356.

17. Dhanalakshmi, K.B., et al., *Photocatalytic degradation of phenol over TiO2 powder: The influence of peroxomonosulphate and peroxodisulphate on the reaction rate.* Solar Energy Materials and Solar Cells, 2008. **92**(4): p. 457-463.

18. Yang, Q.J., H. Choi, and D.D. Dionysiou, *Nanocrystalline cobalt oxide immobilized on titanium dioxide nanoparticles for the heterogeneous activation of peroxymonosulfate.* Applied Catalysis B-Environmental, 2007. **74**(1-2): p. 170-178.

19. Fujishima, A., et al., *Mechanism of the Current Doubling Effect. I. The ZnO Photoanode in Aqueous Solution of Sodium Formate.* Bulletin of the Chemical Society of Japan, 1981. **54**(6): p. 1671-1674.

20. Bekbolet, M. and I. Balcioglu, *Photocatalytic degradation kinetics of humic acid in aqueous TiO2 dispersions: the influence of hydrogen peroxide and bicarbonate ion.* Water Science and Technology, 1996. **34**(9): p. 73-80.

21. Matthews, R.W. and S.R. McEvoy, *Photocatalytic degradation of phenol in the presence of near-UV illuminated titanium dioxide.* J. Photochem. Photobiol. A : Chem, 1992. **64**: p. 231-246.

22. Dogliotti, L. and E. Hayon, *Flash photolysis of per[oxydi]sulfate ions in aqueous solutions. The sulfate and ozonide radical anions.* The Journal of Physical Chemistry, 1967. **71**(8): p. 2511-2516.

23. Madhavan, J., et al., *Peroxomonosulphate, an efficient oxidant for the photocatalysed degradation of a textile dye, acid red 88.* Solar Energy Materials and Solar Cells, 2006. **90**(13): p. 1875-1887.

24. Agustina, T.E., H.M. Ang, and V.K. Pareek, *Treatment of winery wastewater using a photocatalytic/photolytic reactor.* Chemical Engineering Journal, 2008. **135**(1-2): p. 151-156.

25. Barakat, M.A., J.M. Tseng, and C.P. Huang, *Hydrogen peroxide-assisted photocatalytic oxidation of phenolic compounds.* Applied Catalysis B-Environmental, 2005. **59**(1-2): p. 99-104.

26. Madhavan, J., et al., *Kinetic studies on visible light-assisted degradation of acid red 88 in presence of metal-ion coupled oxone reagent.* Applied Catalysis B-Environmental, 2008. **83**(1-2): p. 8-14.

27. Doong, R.A. and W.H. Chang, *Photoassisted titanium dioxide mediated degradation of organophosphorus pesticides by hydrogen peroxide.* Journal of Photochemistry and Photobiology a-Chemistry, 1997. **107**(1-3): p. 239-244.

28. Wang, Y. and C.-S. Hong, *Effect of hydrogen peroxide, periodate and persulfate on photocatalysis of 2-chlorobiphenyl in aqueous TiO2 suspensions.* Water Research, 1999. **33**(9): p. 2031-2036.

29. Wang, S., *A Comparative study of Fenton and Fenton-like reaction kinetics in decolourisation of wastewater.* Dyes and Pigments, 2008. **76**(3): p. 714-720.

7

7 – Modelling and Simulation of “REACTIVE ADSORBER” to Mimic the Permeable Reactive Barrier

Abstract

The chapter describes the practical application of combined adsorption and oxidation technique for the remediation of groundwater using PRB. Alternatively, the combined adsorption and oxidation technique can be utilized for the treatment of industrial waste using a novel unit termed here as “Reactive Adsorber”. The unit operates under simultaneous adsorption and oxidation mode, thereby allowing the column to be used for a longer period before a complete regeneration. This chapter discusses the detailed modeling of the column to study the dynamics of contaminant flow and to predict the breakthrough curves of the adsorbent bed. The model was validated against the simple adsorption data reported in the literature. The current model was utilized without incorporating the reaction term, and the results were found to be in good agreement. The effects of several parameters such as catalyst concentration, the ratio of oxidation to catalyst deactivation, porosity and diffusivity on breakthrough curve were studied. The model developed may be helpful in the design and analysis of reactive bed adsorber for treating aqueous wastes. In addition, it can also be readily extended to the treatment of multicomponent waste streams.

7.1 Introduction

Ground water contamination is a relatively new problem to the list of environmental issues and has grabbed the world attention significantly in the last few years. There are reports suggesting serious problems associated with Australian inland water. Also, experience from Europe and North America suggests that groundwater pollution in Australia will become a more serious issue in the future. The current and the only major technique for ground water treatment in based on "**Pump and Treat Method**". Unfortunately this method is insufficient to cater the need of ground water decontamination from both economics and sustainability.

Permeable Reactive Barrier (PRB) is the most recent innovation in ground water treatment technologies. This is an in-situ remediation technique, where the contaminant plume in the groundwater gets treated as it permeates through the reactive wall installed within the aquifer. In the broadest sense, "*A PRB is a continuous, in situ permeable treatment zone designed to intercept and remediate a contaminant plume. The treatment zone may be created directly using a reactive material such as iron or indirectly using the material designed to simulate secondary process, such as by adding carbon substrate and nutrients to enhance chemical or microbial activity. In this way, contaminant treatment may occur through physical, chemical or biological process*" [(Barriers et al.)].

The following Figure 7.1-1 gives a pictorial representation of the PRB system, where the groundwater flowing through the barrier gets treated.

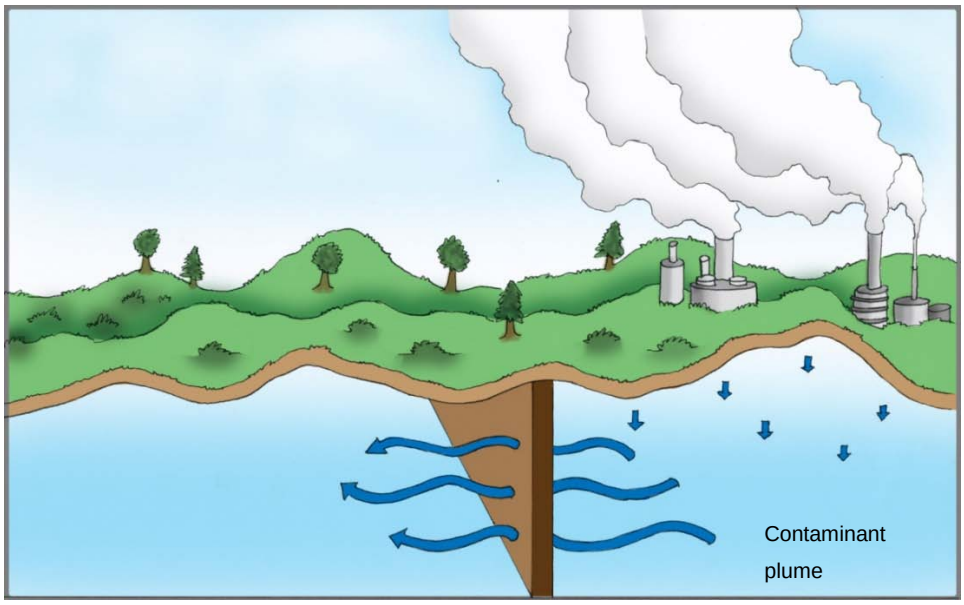

Figure 7.1-1: Permeable Reactive Barrier installed subsurface

It is important to note that the PRB only blocks the movement of the contaminants and does not affect the flow of water. The reactive walls are designed to be more permeable than the aquifer region and thus imparting minimal resistance to the flow of water. The major design parameters for the installation are the bed area and bed thickness. The area of the PRB is dependent on the plume size which is estimated by carrying out the groundwater flow modeling using programs such as 'MODFLOW'; however it is beyond the scope of this work. The chapter is focused on understanding the parameters affecting the bed thickness which in turn affects the bed life.

7.2 Combined adsorptive oxidation technique in PRB

The earlier chapters have described the synthesis of several supported cobalt catalysts capable of adsorbing and oxidizing the adsorbed contaminants in the presence of oxidants. One of important applications of such a technique is the PRB. The PRB wall fabricated with the developed supported catalyst can act as a medium to trap the pollutants as the groundwater flows past the wall. A solution of oxidant (1-2 molar oxone) is pumped into the barrier wall which, in the presence of cobalt catalyst within the barrier wall, would generate active sulphate radical and oxidize the adsorbed contaminants. The major advantage of this technique is that the contaminants are initially adsorbed and thus a well calculated amount of oxidant can be pumped into the barrier wall. Additionally, the cobalt catalyst is well immobilized

into the wall and hence is prevented from getting into the groundwater. After a predefined period (depending on the PRB life as per the design), the barrier wall can be digged out of the aquifer and the barrier material can be regenerated or dumped safely into the secured landfill.

One of the most significant factors affecting the performance life of the PRB bed is the bed thickness. A simple column study is proposed to be carried out in order to estimate the performance of the PRB. The column height is theoretically equivalent to the PRB bed thickness given other parameters such as pollutant concentration in the plume, plume dimensions etc are uniform. The column proposed here to mimic the PRB can also be used as a system to treat the industrial waste water by combined Adsorption and Oxidation. This novel unit is termed as “REACTIVE ADSORBER”. The system as shown in Figure 7.2-1 is utilized to separate the pollutants from wastewater and oxidized them to harmless components. Various investigations have been done earlier to achieve the similar objective but in different ways. Doocey et al. (2004) utilized ferrous impregnated zeolite in a column to carry out combined adsorption and Fenton oxidation to treat phenolic waste water using Fe Zeolite beta and 4A[1]. Similar attempts have been made by Phu et al. (2001) using Fe-ZSM5 [2]. Fe supported on activated carbon was used by Ramirez et al. (2007) for dye waste water treatment in a batch reactor [3].

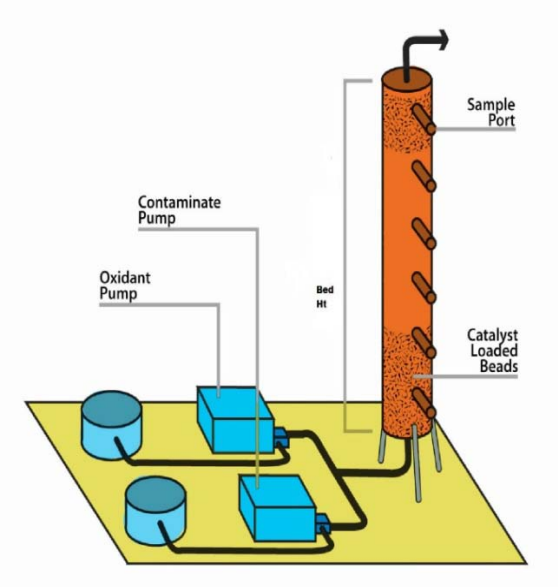

Figure 7.2-1: A column setup to mimic PRB

In spite of wide research on combined adsorption and oxidation, hardly any attempt has been made on studying the reactive adsorption column dynamics. The aim of this study is focused on the development of a model for the Reactive Adsorber and studying the effect of parameters such as catalyst concentration, particle porosity, Damkohler number, and diffusivity on the column dynamics. The work reported in this chapter is limited to the conceptual design of such a system and has been studied by mathematical modeling. It is our future interest to carry out experimental studies to further validate this model and improvise on the system for potential commercial application. Wherever possible, actual data obtained from literature was utilized for carrying out the simulation.

7.3 Physical scenario for simulation

A model was developed for describing the contaminant profile in a hypothetical reactive adsorption column. The study depicts the treatment of phenolic wastewater using the reactive adsorption bed consisting of catalyst loaded adsorbent particles. The adsorbent is selected as spherical beads of activated carbon loaded with Co^{2+} or Fe^{2+} catalyst. The stream of phenolic wastewater is mixed with the oxidant (hydrogen peroxide and/or oxone) and fed through the bottom of the column as shown in Figure 7.1-1. As the contaminant and the oxidant move through the column, they get transported in the pore of the pellet with the rate of movement governed by film transport in the surface film of pellet and diffusion inside the pellets. As the oxidant comes in contact with the catalyst, it reacts to form active hydroxyl or sulphate radicals (depending on the catalyst and the oxidant), which in turn oxidizes the available phenol to form harmless products. The end product on complete oxidation is CO_2 and water. The phenol in the pores also gets adsorbed into the adsorbent governed by the Langmuir equilibrium isotherm. The oxidation reaction taking place inside the particle is a multi-step reaction. Several different reaction mechanisms have been proposed involving around 15-20 reaction steps [4]. However for the sake of simplicity in the modeling, the first order degradation kinetics with respect to the contaminant concentration and the first order kinetics with respect to the catalyst concentration are assumed. For future application of the model, any reaction rate can be plugged into the model equations.

The reaction taking place in the presence of Fe^{2+} ion and hydrogen peroxide can be represented as below.

$$H_2O_2 + Fe^{2+} \longrightarrow OH^{\cdot} + OH^{-} + Fe^{3+}$$ Equation 7.3-1

$$\text{Phenol} + OH^{\cdot} \longrightarrow \text{Oxidized Products}$$ Equation 7.3-2

The reaction taking place in the presence of Co^{2+} ion and peroxymonosulphate (oxone) can be represented as below.

$$HSO_5^{-} + Co^{2+} \longrightarrow OH^{-} + SO_4^{\bullet} + Co^{3+}$$ Equation 7.3-3

$$\text{Phenol} + SO_4^{\bullet} \longrightarrow \text{Oxidized Products}$$ Equation 7.3-4

7.4 Mathematical model

Based on the above described physical scenario, a representative mathematical model was formulated. To simplify the mathematical calculations several assumptions were made as follows:

1) The fluid velocity through the bed is assumed to be constant.
2) The column operates under isothermal condition.
3) The adsorbent particles are assumed to be spherical and uniformly distributed into the column.
4) The reaction of the phenol degradation is assumed to be of the first order.
5) The reactions are assumed to reach completion, and thus reaction intermediates are neglected. This assumption is made to reduce the complexities involved into the model and reduce the computational time. However, the model can be easily modified to incorporate the intermediates generated during the process.
6) The reaction takes place inside the pellet and no reaction is assumed to be taking place in the bulk liquid outside the pellet.
7) The catalyst is homogeneously distributed in the adsorbent pellets
8) Catalyst leaching is assumed to be negligible.

Assuming that at time *t*=0, a step input of contaminant A with contaminant concentration C_A and oxidant with concentration C_B is given to the column.

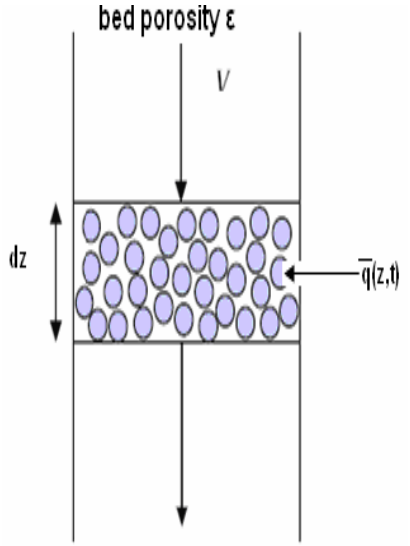

The flow dynamics of the contaminant and the oxidant in the column is computed by the mass balance in a small section as shown in 7.4-1 using equations 7.4-1 and 7.4-2. The direction of the flow is adjusted as per the sign convention.

7.4-1: A section of "Reactive Adsorber"

$$-\varepsilon D_{l1}\frac{\partial^2 C_{b1}}{\partial Z^2}+V\frac{\partial C_{b1}}{\partial Z}+\varepsilon\frac{\partial C_{b1}}{\partial t}+\frac{\partial Q_{b1}}{\partial t}=0 \qquad \text{Equation 7.4-1}$$

$$-\varepsilon D_{l2}\frac{\partial^2 C_{b2}}{\partial Z^2}+V\frac{\partial C_{b2}}{\partial Z}+\varepsilon\frac{\partial C_{b2}}{\partial t}+\frac{\partial Q_{b2}}{\partial t}=0 \qquad \text{Equation 7.4-2}$$

C_{b1} and C_{b2} are the concentrations of contaminant (phenol) and oxidant (oxone or H_2O_2) in the bulk liquid phase respectively. 'V' is the velocity of the flow of the pollutant and oxidant stream respectively and finally Q_{b1} and Q_{b2} are the masses of the pollutant and oxidant lost in the small section of the column due to the penetration inside the pellets.

The first term in equations 7.4-1 and 7.4-2 defines the flow due to axial dispersion; the second term defines the flow due to convection, and the next two terms define the mass transfer of the pollutant/oxidant in the pellet and accumulation term, respectively.

Prior to getting inside the pellet, the contaminant and oxidant have to diffuse through the stagnant film boundary around the pellet as seen in Figure 7.4-2.

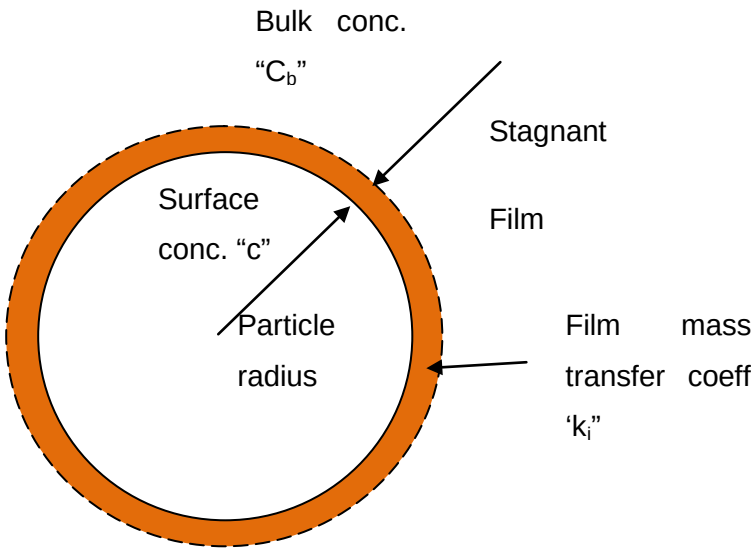

Figure 7.4-2: A thin liquid film on a single particle inside the column

The rate of mass transfer of the molecules across the film can be expressed as the product of a mass transfer coefficient, a concentration differential (C_{bulk}-$c_{surface}$), the contact area and the total number of pellets present in the small section dz.

As per the Fick's law, the rate of mass transfer in the film can be given as

$$\frac{dQ_{b1}}{dt} = k_{fA1}\left(C_{b1} - c_p\Big|_{R=R_0}\right) * 4\Pi Rp^2 * Total.no.of.pellets$$

Equation 7.4-3

The total number of pellets can be given as

$$Total.no.of.pellets = \frac{A\Delta z(1-\varepsilon)}{\frac{4}{3}\Pi R_p^{\ 2}}$$

Equation 7.4-4

A similar equation would represent the film transport of oxidant.

Mass Balance on the single pellet

The contaminant and oxidant on the pellet surface get transported through the pellet by diffusion through the pores as per Figure 7.4-3

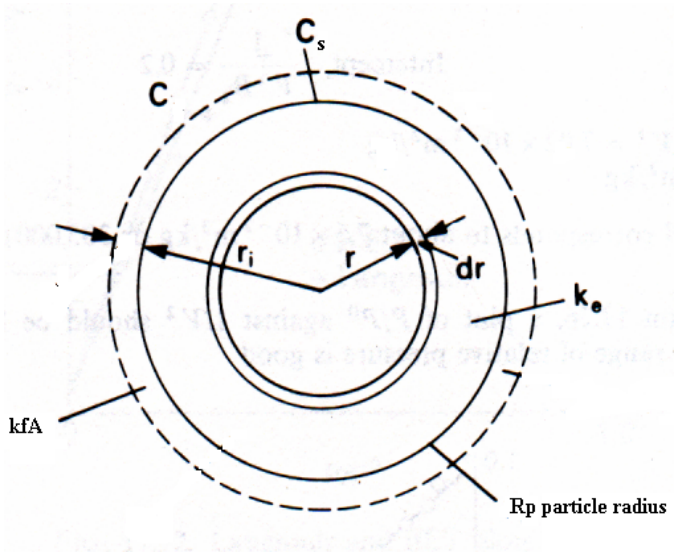

Figure 7.4-3: Elemental section in the single pellet particle

The water in the pores is assumed to be stagnant. The diffusion transport of the organic contaminant and the oxidant in the pellet is defined by equation 7.4-5,

$$D_{pi}\frac{\partial^2 C_{p_i}}{\partial R^2}+D_{pi}\frac{2}{R}\frac{\partial C_{p_i}}{\partial R}-\frac{(1-\varepsilon_p)}{\varepsilon_p}\rho_p\frac{\partial Q_{p_i}}{\partial t}-\frac{\partial C_{p_i}}{\partial t}=0 \qquad \text{Equation 7.4-5}$$

The first two terms represent the diffusion flux into the pellet, the third and fourth terms define the rate of accumulation in the solid and in the liquid phases, respectively. Where i=1 is the contaminant and i=2 is the oxidant concentration.

The rate of accumulation in the solid can be related by equation 7.4-6 using the chain rule under the assumption of instantaneous adsorption as well as the reaction taking place in the solid phase.

$$\frac{\partial Q_{p_1}}{\partial t}=\frac{dQ_{p_1}}{dC_{p_1}}\frac{\partial C_{p_1}}{\partial t}-k_1 Q_{pi} Q_{rad} \qquad \text{Equation 7.4-6}$$

The second term on the right is the rate of phenol degradation with the rate constant k_1. Q_{rad} is the concentration of the active radical generated by the reaction of the oxidant with the catalyst as per the following equation obtained from the mass accumulation of the oxidant in the pellet

$$\frac{\partial Q_{p2}}{\partial t} = \frac{dQ_{p_2}}{dC_{p_2}} \frac{\partial C_{p_2}}{\partial t} - k_2 Q_{p2} C_{cat} \qquad \text{Equation 7.4-7}$$

The contaminant concentration in the solid is expressed in terms of the liquid phase concentration by a Langmuir equilibrium relationship given by equation 7.4-8

$$Q_{p_i} = \frac{q_{mi} b_i C_{p_i}}{(1 + b_i C_{p_i})} \qquad \text{Equation 7.4-8}$$

The abovementioned equations can be written in terms of the dimensionless quantities defined in Table 7.4-1.

Table 7.4-1 Dimensionless quantities

$c_{b\,i} = \frac{Cb_i}{C_0}$; $c_{p_i} = \frac{Cp_i}{C_0}$; $q_{p_i} = \frac{Q_{p_i}}{C_0}$	$Pe_{Li} = \frac{vL}{D_{li}}$; $B_i = \frac{k_i R_p}{\varepsilon_p D_{pi}}$; $\eta_i = \frac{\varepsilon_p D_{p_i} L}{Rp^2 v}$
$\tau = \frac{vt}{L}$; $r = \frac{R}{R_p}$; $z = \frac{Z}{L}$	$\xi_i = \frac{3B_i \eta_i (1-\varepsilon)}{\varepsilon}$; $D_{a\,i} = \frac{Lka_i}{v}$

Using the dimensionless quantities and combining equations 7.4-1 and 7.4-2, the following basic transport equations are obtained.

$$-(1/Pe_{li}) \frac{\partial^2 c_{bi}}{\partial z^2} + \frac{\partial c_{bi}}{\partial z} + \frac{\partial c_{bi}}{\partial \tau} + \xi_i \left(c_{bi} - c_{pi,r=1}\right) = 0 \qquad \text{Equation 7.4-9}$$

$$\eta_i \frac{\partial^2 c_{pi}}{\partial r^2} + \eta_i \frac{2}{r} \frac{\partial c_{pi}}{\partial r} - \varepsilon_p D_{ai} c_{pi} c_{pj} C_0 - (1-\varepsilon_p) \rho_p \frac{\partial q_{pi}}{\partial \tau} - \varepsilon_p \frac{\partial c_{pi}}{\partial \tau} = 0 \qquad \text{Equation 7.4-10}$$

$$\frac{\partial q_{pi}}{\partial \tau} = \frac{dq_{pi}}{dc_{pi}} \frac{\partial c_{pi}}{\partial \tau}$$ Equation 7.4-11

$$\frac{dq_{pi}}{dc_{pi}} = \frac{q_{mi} b_i}{(1 + b_i c_{pi} C_0)^2}$$ Equation 7.4-12

The initial and boundary conditions are given as follows:

<u>For the transport in the column</u>

Initial Condition

c_{bi} = 1 (z = 0)

c_{bi} = 0 (z > 0)

Boundary condition

$\frac{\partial c_{bi}}{\partial z} = Pe_{li}(c_{bi} - 1)$ z = 0

$\frac{\partial c_{bi}}{\partial z}$ =0 z = 1

<u>For the transport in the pellet</u>

Initial Condition

c_{pi} = 0

q_{pi} = 0

Boundary condition

$\frac{\partial c_{bi}}{\partial z} = 0$ r = 0

$\frac{\partial c_{pi}}{\partial r} = b_i (c_{bi} - c_{pi}\big|_{r=1})$ r = 1

The constants D_p, k, and D_l are calculated from the following correlations for the phenol-water-hydrogen peroxide system.

$$D_p = Dm / tau$$ Equation 7.4-13

$$k = 2.0 + (1.1 Sc^{0.333} \mathrm{Re}^{0.6}) Dm / 2Rp$$ Equation 7.4-14

$$D_l = \left(\gamma_1 + \frac{\gamma_2 \mathrm{Re}\, Sc}{\varepsilon} \right) Dm$$ Equation 7.4-15

7.5 Discretization of the equation and computation

The set of equations 7.4-9 to 12 are solved simultaneously to evaluate the concentration profiles in pellet and column. These equations defined are non linear

partial differential equations (PDE), which were discretized to Ordinary Differential Equations (ODE's) using a Finite Difference technique, an example shown below:

$$\frac{d^2C}{dz^2} = \frac{C_{i+1} - 2C_i + C_{i-1}}{delZ^2} \qquad \text{Equation 7.5-1}$$

$$\frac{dC}{dz} = \frac{C_{i+1} - C_{i-1}}{2 * delZ} \qquad \text{Equation 7.5-2}$$

The ODE's were further solved using the ODE solver in MATLAB to obtain the required solution. The algorithm for the solution of the above mentioned equations can be given as

1. Create a matrix of C_i and c_j and set it to zeros. (Initial condition)
2. Calculate matrix of C_i using the boundary conditions at the bottom of the column
3. Calculate matrix of c_j using the boundary conditions for the pellet at the bottom of the column.
4. Calculate new value of C at time t_0+h, where h is the time increment.
5. Repeat the steps 2 and 3.
6. Continue till the end of the time is reached.

7.6 Solving the memory allocation limitation

The discretized ordinary differential equation resulting from the Partial differential equation would run into thousands in order to get a converged solution. This not only affects the computational time required but sometime may lead to memory allocation limitation due to extremely large variable matrix generated in the calculation. A similar situation was encountered in the current algorithm.

In the current system, a MATLAB toolbox (ODE15s) was used in-order to solve the ordinary differential equations generated using the Finite difference technique over the model equations. During the computational process, the inbuilt function (ODE-15s) computes a Jacobian matrix of the ODE set generated by the algorithm, which becomes exceptionally large in the case of very fine division of the column.

In order to counter this issue, a sub program was written to generate a self created Jacobian matrix was coded and the spare of that matrix was then clubbed on to the ODE 15s solver.

$$J = \begin{bmatrix} \frac{dy_1}{dx_1} & \dots & \dots. & \dots.. & \frac{dy_n}{dx_1} \\ \dots. & \dots & \dots & \dots. & .. \\ \dots & \dots & \dots & \dots. & .. \\ \dots & \dots & \dots & \dots. & .. \\ .\frac{dy_m}{dx_1} & \dots & \dots & \dots & \frac{dy_m}{dx_n} \end{bmatrix}$$

$$\begin{bmatrix} 1 & 1 & 0 & 0 & 0 & 0 & 0 & 0 & 0 & \dots \\ 1 & 1 & 1 & 0 & 0 & 0 & 0 & 0 & 0 & \dots \\ 0 & 1 & 1 & 1 & 0 & 0 & 0 & 0 & 0 & \dots \\ 0 & 0 & 1 & 1 & 1 & 0 & 0 & 0 & 0 & \dots \\ 0 & 0 & 0 & 1 & 1 & 1 & 0 & 0 & 0 & \dots \\ 0 & 0 & 0 & 0 & 1 & 1 & 1 & 0 & 0 & \dots \\ 0 & 0 & 0 & 0 & 0 & 1 & 1 & 1 & 0 & \dots \\ 0 & 0 & 0 & 0 & 0 & 0 & 1 & 1 & 1 & \dots \\ 0 & 0 & 0 & 0 & 0 & 0 & 0 & 1 & 1 & \dots \\ 0 & 0 & 0 & 0 & 0 & 0 & 0 & 0 & 1 & \dots \\ 0 & 0 & 0 & 0 & 0 & 0 & 0 & 0 & 0 & \dots \\ 0 & 0 & 0 & 0 & 0 & 0 & 0 & 0 & 0 & \dots \\ \dots & \dots & \dots & \dots & \dots & \dots & \dots & \dots & \dots & \end{bmatrix}$$

Figure 7.6-1 Jacobian Matrix

In the self created Jacobian matrix it was observed that a large number of matrix variable were zeros as seen in the figure above. This resulted in significantly reducing the computational time as well as the memory requirement.

7.7 Results and discussion

7.7.1 Model Validation

The model and the codes were validated with the adsorption breakthrough data reported by T.Gu [6]. Since the results reported by T.Gu were purely for the adsorption effect and without any reaction, the Damkohler number in the current program was set to zero to nullify the effect of the reaction. The breakthrough curve was obtained for these parameters as shown in Figure 7.7-1, which matches very well with results reported by T Gu [6]. The concentration profile in the column is shown in Figure 7.7-2, which is a set of several breakthrough curves at different axial positions of the bed. The development of concentration profiles in the pellet with respect to time is shown in Figure 7.7-3.

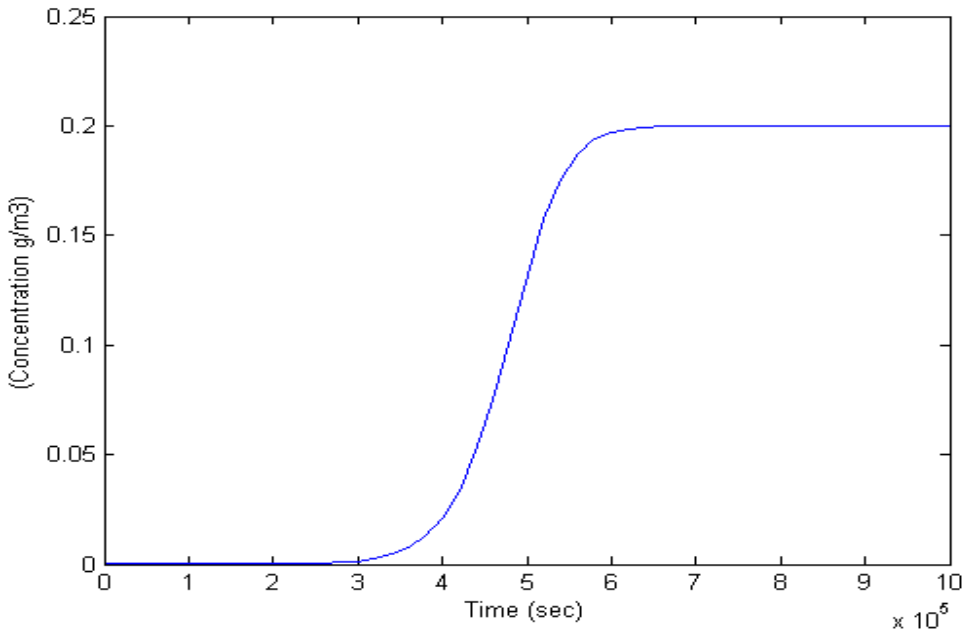

Figure 7.7-1: Breakthrough Curve from literature data [6]

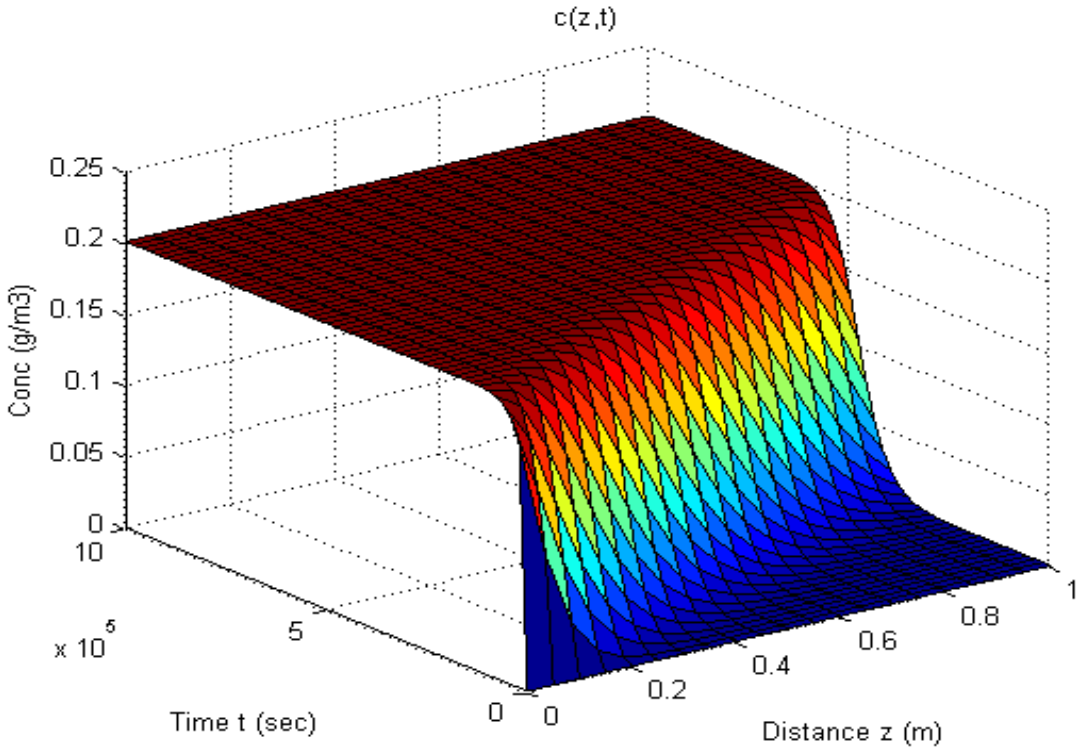

Figure 7.7-2: Column profile of contaminant.

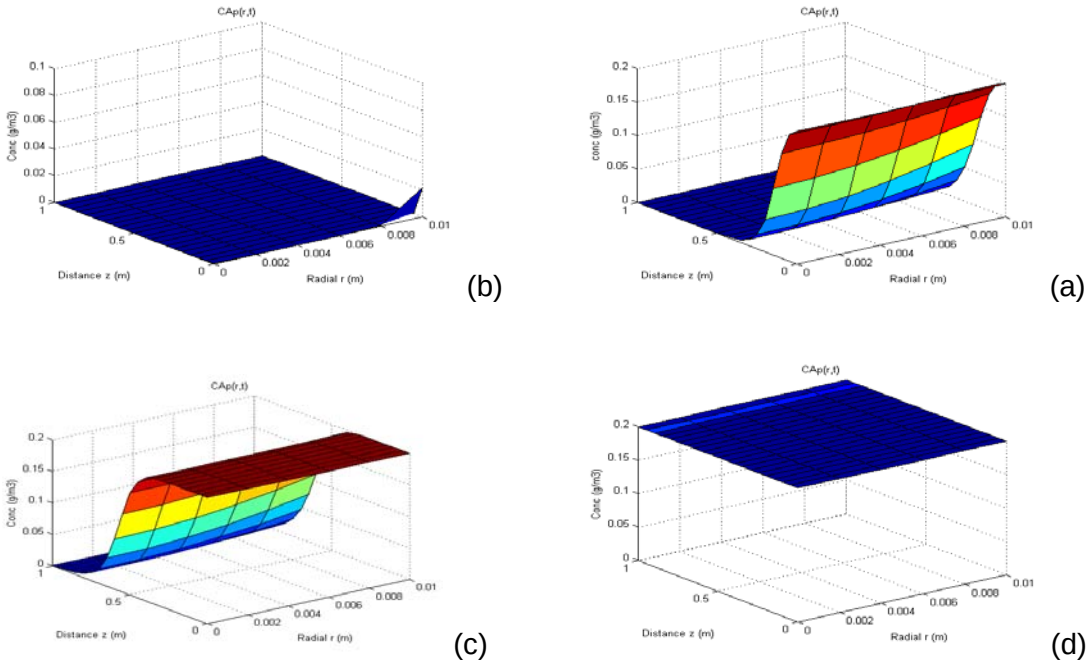

Figure 7.7-3: Pellet profile of contaminant at different times a) 100 s b) 1000 s, c) 10000 s d) 100000 s

7.7.2 Simulation of the Reactive Adsorber

For the described reactive adsorber model, the constants are calculated using equations 7.4-10 – 7.4-12. The column design parameters taken in the simulation are shown in Table 7-7-1. The effects of major factors influencing reactivity of the contaminant in the column such as catalyst concentration, particle porosity, Damkohler number and diffusivity are also studied.

Table 7.7-1 Parameters used in simulation

L, m	1
R_p, m	0.01
Superficial velocity, m/s	1×10^{-5}
b_i (Phenol) Bed Porosity, m^3/g	0.083
Dispersion coefficient (Phenol) , m^2/s	2.509×10^{-7}
Dispersion coefficient (H_2O_2) , m^2/s	2.513×10^{-7}
Density of pellet, gm/cc	0.4

7.7.3 Effect of Catalyst Concentration

The catalyst concentration in this study was varied from 0.2 to 2 mg/g of pellet. For the reactive adsorber, it can be seen from Figure 7.7-4, that including an oxidation reaction in the adsorption column tends to increase the breakthrough time. It can be easily interpreted that, contaminant oxidation works as *in situ* regeneration of the column, thereby increasing the shelf-life of the bed. Increase in the concentration of the catalyst amount in the pellet further helps in increasing the breakthrough time in spite of catalyst getting consumed with time, which suggests that the rate of reaction is sufficiently high enough to degrade the available contaminants, regardless of reduction in the amount of catalyst. The variation in the active catalyst concentration in the pellet with respect to time for an initial catalyst concentration of 1.4 mg/g of pellet is observed in Figure 7.7-5.

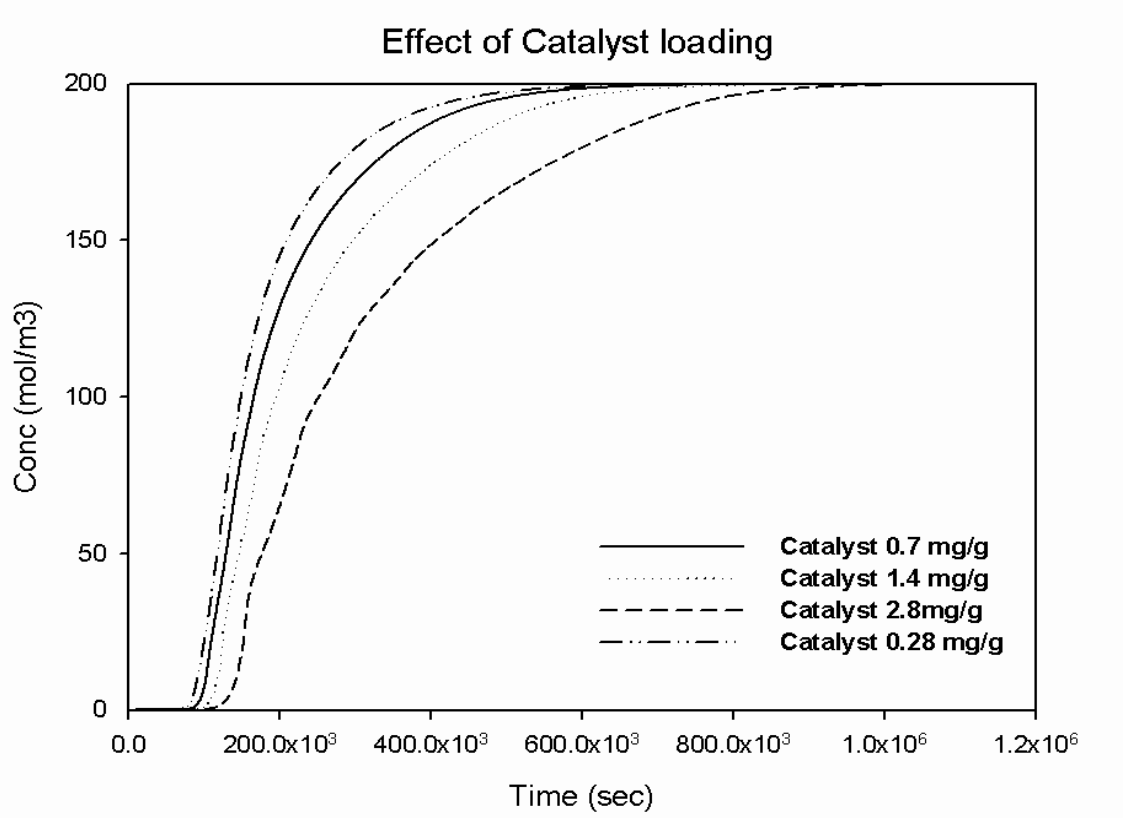

Figure 7.7-4: Effect of catalyst amount on the column breakthrough performance

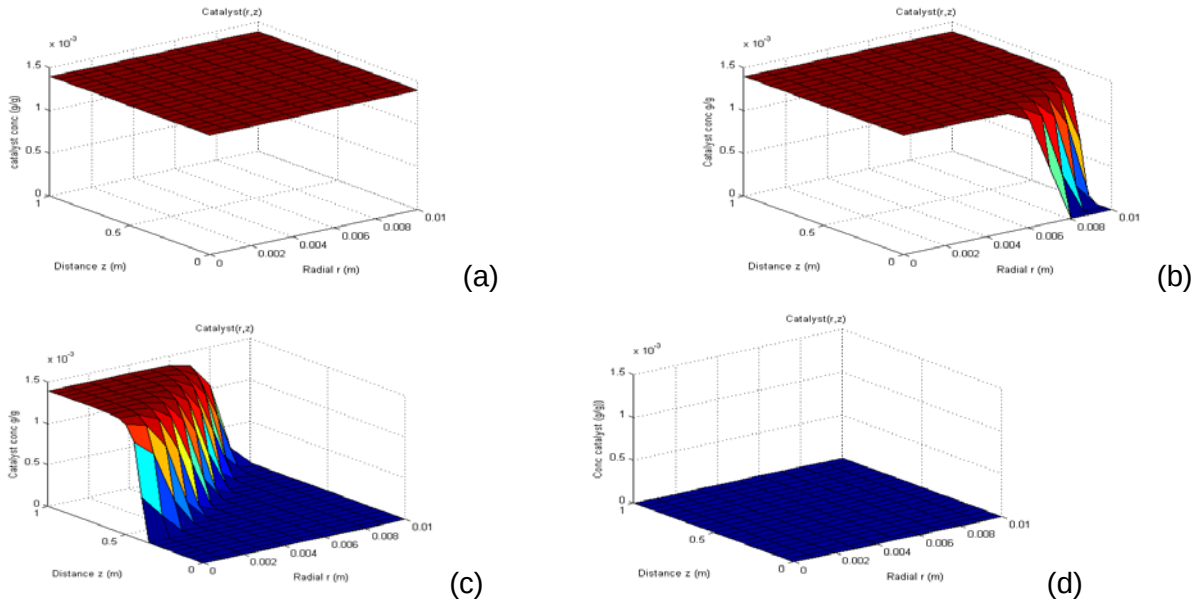

Figure 7.7-5: Pellet profile of catalyst at different time periods: a) 100sec b) 1000 sec, c) 10000 sec d) 100000 sec

7.7.4 Effect of Particle Porosity

The particle porosity ε_p varies in the range from 0 to 1, representing an impervious to completely porous particle. The simulation was carried out at three different porosities ε_p = 0.4, 0.5 and 0.6, as shown in Figure 7.7-6. The change in the porosity affects the availability of the catalyst and contaminant for the reaction. As observed in this figure an increase in the porosity increases the breakthrough time, apparently, the observed change is relatively much smaller as compared to other factors.

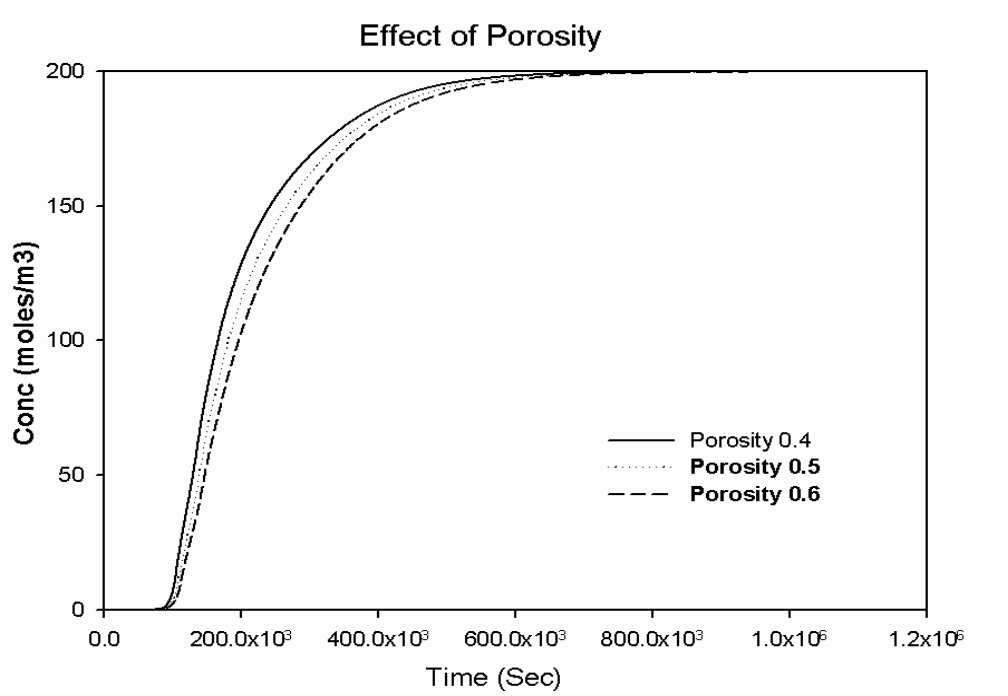

Figure 7.7-6 Effect of particle porosity on the column breakthrough performance

7.7.5 Effect of reaction rate constant (Damkohler Number)

Reaction rate constant is the most important factor describing the reactivity of the given reaction. The dimensionless constant, "Damkohler number" which represents the ratio of characteristic reaction time to the stoichiometric time, incorporates the rate constant factor. In the current analysis, second order reaction rates for phenol oxidation and catalyst deactivation are assumed. Moreover, it is assumed that the rate of deactivation of catalyst is the same as the rate of reaction of oxidant with the catalyst. Also since the phenol reacts with an active radical, OH, its rate is assumed to be much higher. The Damkohler number for the rate of phenol oxidation and the rate of catalyst deactivation was varied from 10–10^5. As observed in Figure 7.7-7, as the Damkohler number increases, the breakthrough time increases. Also, if the ratio of Damkohler number for catalyst deactivation and phenol oxidation remains fixed, there is no change in the breakthrough profile, as evidenced from results 1 and 3 in Figure 7.7-7. Although, the current reaction rate is a simplified assumption, yet the rate expression can be modified in the model depending on the rate constants obtained experimentally.

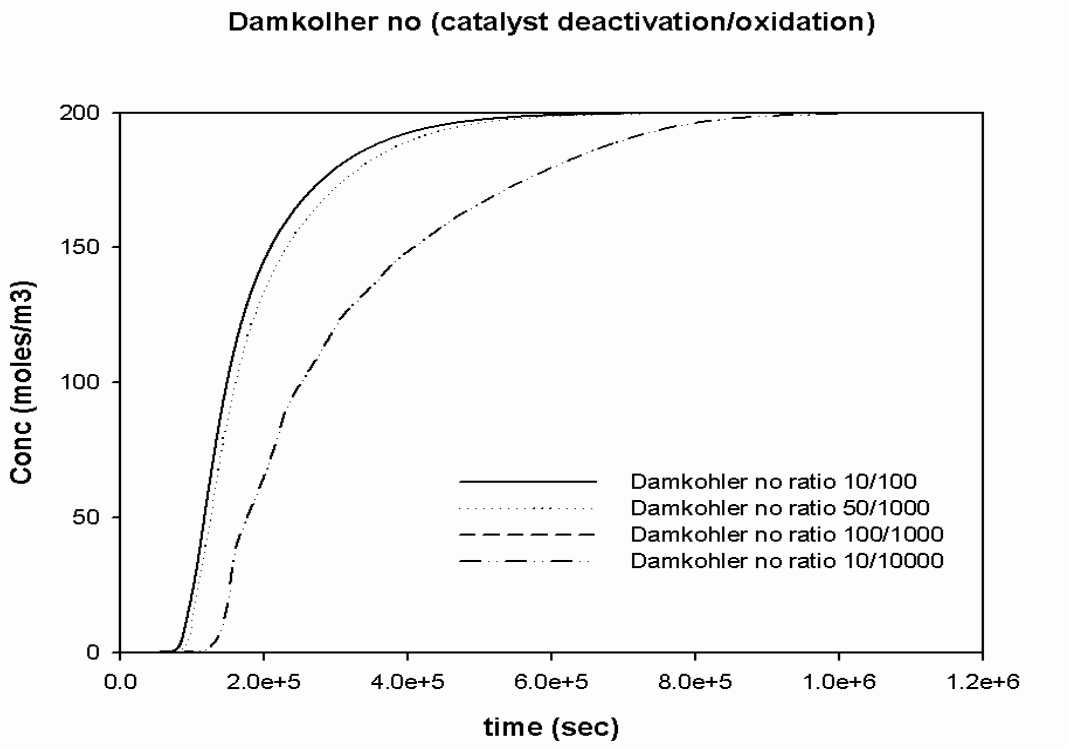

Figure 7.7-7: Effect of reaction rate constant (Damkohler no) on the breakthrough performance of the column

7.7.6 Effect of Diffusivity

The diffusivity determines the rate of movement of contaminants and the oxidants inside the pellet, making the reactants available for the reaction. The diffusivity in the model was varied by changing the tortousity factor. Tortousity factor of any adsorbent is determined by the size of pores and the interconnection between the pore channels. The tortousity factor was varied from 2.5 to 20, with 10 being for activated carbon. Figure 7.7-8 shows that for a constant mass transfer coefficient, constant particle size and a fixed ratio of Damkohler number, the concentration profile changes significantly on varying the tortousity factor, suggesting the imperative effect of intra particle diffusion. For tau = 2.5, the breakthrough time was the shortest, and increases as the diffusivity increases.

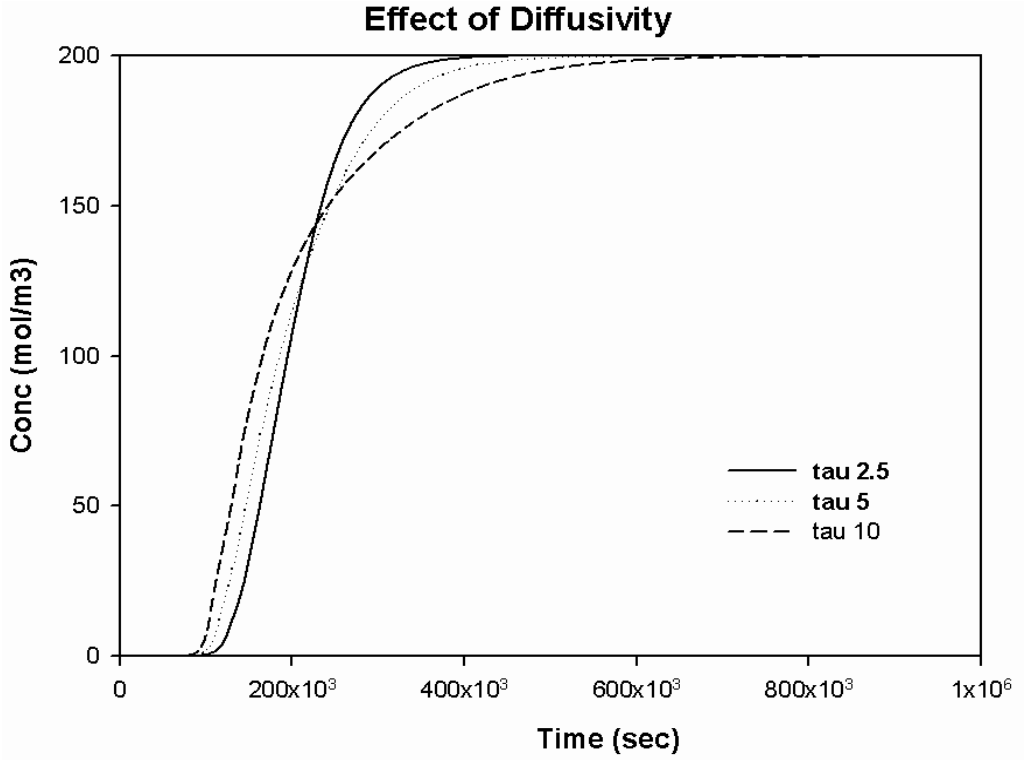

Figure 7.7-8: Effect of diffusivity on the breakthrough performance of the column

7.8 Conclusion

From the simulated performance of the reactive adsorber, it can be concluded that, combining a reaction system with an adsorption bed increases the breakthrough time of the column, and hence provides a cost effective alternative to the conventional system in which the bed is regenerated separately. A major challenge in the current research is the synthesis of homogeneously distributed catalyst in the adsorbent like activated carbon and zeolite. The breakthrough time is highly dependent on the rate of reaction, which needs to be well defined. In this study, a general second order rate of reaction was assumed for the ease of mathematical calculation, however, it is widely accepted that the rate of oxidation is much more complex, and demands further research. The further work can be directed to have a set of experimental data for both identifying the rate of reaction and obtaining the breakthrough curve to critically verify the simulation performance.

7.9 Abbreviations

C_b Concentration in the bulk phase of the column, mol/m^3

Z Length of the column, m

u Interstitial velocity, m/s

v Superficial Velocity, v= u/ε, , m/s

t Column run time, s

k Mass transfer coefficient, m/s

R_p Particle radius, m

C_p Concentration in the particle pore, mol/m^3

D_l Axial Dispersion coefficient, m^2/s

D_p Pore diffusivity, m^2/s

q_m Langmuir Constant

b Langmuir Constant

Pe_l Peclet number

B Biot number

D_a Damkohler number

D_m Molecular Diffusivity

Tau Tortousity Factor

Re Reynolds number

Sc Schmidt number

Greek letters

ε Bulk porosity of the column

ε_p Particle porosity

η Dimensionless constant

ξ Dimensionless constant

γ_1 γ_2 Constants to calculate axial dispersion, $\gamma_1 = 0.45+0.55\varepsilon$, $\gamma_2 = 0.5$

7.10 References

1. Doocey DJ, Sharratt PN, Cundy CS, and Plaisted RJ (2004), "Zeolite-mediated Advanced Oxidation of Model Chlorinated Phenolic Aqueous Waste Part 2: Solid Phase Catalysis", *Process Safety and Environmental Protection/Official Journal of the European Federation of Chemical Engineering: Part B*, **82**(B5):359-364.

2. Phu NH, Hoa TTK, Tan NV, Thang HV, and Ha PL (2001), “Characterization and activity of Fe-ZSM-5 catalysts for the total oxidation of phenol in aqueous solutions”, *Applied Catalysis B, Environmental*, **34**(4):267-275.
3. Ramirez JH, Maldonado-Hódar FJ, Pérez-Cadenas AF, Moreno-Castilla C, Costa CA, and Madeira LM (2007), “Azo-dye Orange II degradation by heterogeneous Fenton-like reaction using carbon-Fe catalysts”, *Applied Catalysis B, Environmental*, **75**(3-4):312-323.
4. Kang N, Lee DS, and Yoon J (2002), “Kinetic modeling of Fenton oxidation of phenol and monochlorophenols”, *Chemosphere*, 47(9): 915-924.
5. Georgi A and Kopinke FD (2005), “Interaction of adsorption and catalytic reactions in water decontamination processes Part I. Oxidation of organic contaminants with hydrogen peroxide catalyzed by activated carbon”, *Applied Catalysis B, Environmental*, **58**(1-2):9-18.
6. Gu T, (1995), “Mathematical Modeling and Scale-Up of Liquid Chromatography”, Springer Verlag, Berlin-New york.

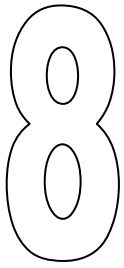

8 –Conclusion and Future Work

8.1 Concluding remarks

The major aims and objectives outlined in the introduction of this thesis have been satisfactorily achieved. Three different types of cobalt catalysts supported on zeolite, silica and activated carbon have been synthesized, characterized and tested for heterogeneous adsorption and advanced oxidation of phenol. The photo-catalytic degradation of phenolic contaminants in the presence of sulphate radical in conjunction with ZnO has also been investigated. Finally a mathematical model to mimic a PRB was proposed and the effect of process parameters were analyzed using that model. The major conclusions are stated below.

8.1.1 Cobalt exchanged zeolite catalysts

1) Three different types of zeolite (Zeolite A, Zeolite X and ZSM-5) have been selected and exchanged with cobalt ion using cobalt chloride as a precursor. The crystallinity of zeolite A almost completely collapsed after ion exchange whereas it partially collapsed for Zeolite X. Among all the three types of support, ZSM-5 retained its crystalline structure after cobalt exchange due to its highest silica content. The stability of the supports for liquid-phase catalytic reaction in the presence of oxone also varied with the silica content. Zeolite A having the least silica in the structure was found to be the least stable and then Zeolite X while ZSM-5 showed the most stability.
2) Phenol degradation was carried out using Co-ZSM-5 catalyst in the presence of oxone. The reaction rate was observed to follow the zero order kinetics with the rate of reaction increasing linearly with the amount of catalyst. On the other hand the rate constant increased with the increase in oxidant amount until a constant plateau was reached. The rate of reaction increased exponentially following the Arrhenius law.

8.1.2 SBA-15 and silica supported cobalt catalysts

1) The phenol degradation rate was observed to be very slow in the case of cobalt exchanged zeolite catalyst probably due to the limitation in the quantitative loading of cobalt by ion-exchange technique. A much higher loading was achieved in the case of cobalt loading by impregnation on silica support or by in-situ loading on SBA-15. In the present study, 5% cobalt was loaded into SBA-15 and amorphous silica. The in-situ loading of cobalt in SBA-15 resulted in stronger bonding with the cobalt oxide crystallites indicating the stability of the catalyst with respect to the cobalt leaching.

Compared to Co-SBA-15, the Co-silica showed a higher rate of reaction. The high amount of cobalt leaching in Co-silica based catalyst suggests the combination of heterogeneous and homogeneous reaction between cobalt and oxone to generate the sulphate radical.

2) Co-silica prepared using Co-nitrate precursor showed a strong bonding between the support and the catalyst due to the easier removal of nitrate species during the heat treatment. The catalyst stability and the rate of reaction were observed to be inversely related, since the reaction proceeds via homogeneous mode in the catalyst which has no cobalt leaching. Although the catalyst which has cobalt leaching showed enhanced rate of reaction, such a catalyst is harmful to the environment due to high toxicity of cobalt ion.

8.1.3 Activated carbon supported cobalt catalysts

1) A novel Co-carbon catalyst was synthesized and investigated for combined adsorption and oxidation of phenolic waste water. The catalyst showed a high rate of phenol degradation following a pseudo first order kinetics with the rate constant (0.125 min^{-1}) at 25 ^{0}C.
2) The degradation of phenol was dependent on the process variables such as contaminant feed concentration, catalyst amount, oxidant amount and temperature. The rate of reaction was observed to be linearly dependent on the phenol feed concentration, catalyst amount and the oxidant amount in the given range and exponentially dependent on the temperature.
3) 3 different catalysts were synthesized with varying cobalt loadings viz 2.5, 5 and 10% cobalt by weight. It was observed that the rate of reaction increased significantly by increasing the cobalt content from 2.5 to 5%, however further increase in the cobalt loading yielded much lesser enhancement in the reaction rate. A higher amount of cobalt loading enhances the rate of reaction of oxone with cobalt to generate sulphate radical, however, diminishes the rate of phenol adsorption possibly due to the reduction in catalyst surface area and pore blocking.
4) In comparison to the silica catalyst, the catalyst prepared from activated carbon showed enhanced rate of reaction which can be attributed to the fact that phenol removal is assisted by the adsorption in the carbon adsorbent. The phenol removal in Co-Silica is mainly due to the heterogeneous reaction of phenol and there is hardly any accumulation of phenol in the catalyst.

8.1.4 Photocatalytic phenol degradation under artificial solar radiation

1) Photo degradation of phenolic wastewater was carried out in a 1 litre glass reactor under the artificial solar radiation to estimate the photocatalytic activity of ZnO under solar radiation. The kinetic data indicated the first order decay of phenol with the rate constant observed as 0.0207 min^{-1} for the phenol feed concentration of 25 ppm.
2) The phenol degradation was also conducted using TiO_2 and ZnO photocatalysts. Under the solar type radiation, ZnO showed better activity as compared to TiO_2. The higher rate of phenol degradation using ZnO is attributed to the photodecomposition of ZnO in water resulting in generation of H_2O_2 which can then produce OH^* radical for phenol oxidation. However, the enhanced rate of phenol degradation comes at the cost of ZnO loss in the process
3) The contaminant degradation was dependent on the process variables such as feed concentration, photocatalyst loading, oxidant loading, temperature and lamp power. The dependence of reaction rate on all of these parameters was analyzed mathematically. The degradation rate was observed to be linearly dependent on the contaminant feed concentration, catalyst and oxidant amount and exponentially dependent on the reaction temperature.

8.1.5 Comparison of photochemical and photocatalytic degradation and the synergy of their combination

1) The comparison was conducted between photocatalytic oxidation and photochemical oxidation of phenol using ZnO as a photocatalyst and three different oxidants such as, Hydrogen Peroxide, Peroxydisulphate (PDS) and Peroxymonosulphate (PMS) under a low power UV radiation. The combination of ZnO with PDS or H_2O_2 showed a non-synergetic behavior with the rate of phenol degradation getting reduced with the combination of ZnO with oxidant as compared to the phenol degradation with oxidant alone. At low power UV radiation, the light scattering resulted from addition of ZnO compromise conversion.
2) The combination of ZnO with PMS showed a synergetic behavior with the rate of phenol degradation getting enhanced with the combination of ZnO with PMS. A direct reaction was observed between ZnO and PMS resulting in generation of additional sulphate radical leading enhanced degradation of phenol. However, it comes at the cost of loss of ZnO catalyst during the reaction.

8.1.6 Modelling and simulation of novel “Reactive Adsorber”

1) A reactive adsorber design is proposed employing combined adsorption and oxidation technique and simulated using MATALB. From the simulated performance of the reactive adsorber, it can be concluded that, combining a reaction system with an adsorption bed increases the breakthrough time of the column, and hence provides a cost effective alternative to the conventional system in which the bed is regenerated separately.
2) Several design parameters for the reactive adsorber were simulated. Increasing the particle porosity increases the breakthrough time of the column thus extending the life of the column. The particle porosity can be enhanced by improving the catalyst synthesis technique. Similarly improving the rate of reaction would further increase the break-through time. The rate of reaction is dependent on several factors such as oxidant amount, the catalyst loading, temperature etc. Finally the diffusivity affects the breakthrough profile controlled by the pollutant flow rate.

8.2 Scope for future work

The study deals with the development of upcoming technology on combined adsorption and oxidation and thus demands a greater amount of study before it can be brought to the commercial scale. A few of the potential work to be carried out is outlined below

1) **Validation of the proposed adsorption model using other adsorbents:** In the current work, a new empirical multi-component adsorption model was proposed. This model was based on the observation of multi-component adsorption on activated carbon as the adsorbent. Similar study can be carried out using other adsorbents such as Zeolites. Additionally, the similar study on activated carbon having different properties can be done.
2) **Synthesis of other metal supported catalysts**: In the current thesis the focus was to explore the potential of cobalt impregnated catalyst with peroxymonosulphate oxidant for organic degradation. However, further research needs to be done to investigate the potential of several other supported metals such as silver, iron and ruthenium etc to carry out organic degradation.
3) **Investigation of optimum light intensity for combined photochemical and photo-catalytic oxidation**: In the current study we have observed the two extreme ends where the combination of photochemical and photo-catalytic efficiency is non synergetic at low lamp power while synergetic at high lamp power. For commercial

application of the combined photochemical and photo-catalytic oxidation it is imperative to investigate the effect of lamp power and determine the transition lamp power (intensity) with respect to the amount of photo catalyst and oxidant added to the system. It would be more useful if a mathematical model is proposed to correlate the light intensity with the amount of photo-catalyst and oxidant.

4) **Column test for combined adsorption and oxidation**: A mathematical model has been proposed in this thesis and the simulations were carried out to investigate the effect of process parameters. However, the model needs to be validated with the actual column test prior to giving some solid justifications to take this technology to pilot scale and finally to the industrial scale. We have attempted a few column test but encountered several problems such as extremely high pressure drop in the bed packing, leaking in the column, high diffusion resistance, poor control of pH, cobalt leaching from the catalyst etc. A well organized column design is required prior to carrying out the test.

Appendices

Appendix A

Derivation of Modified Butler and Ockrent Theory

Assuming η is the refinement of the interaction factor b. This can be considered as the factor affecting the movement or the adsorption of molecules onto the surface. Desorption is generally dependent only on the amount of molecules adsorbed and seldom gets affected by the type and concentration in the liquid phase. Thus, assuming that the rate of adsorption depends on the concentration of the adsorbate, the fraction of unoccupied surface and finally the extent of interaction between the adsorbate molecules, the rate of adsorption suggested by Butler and Ockrent can be modified as

$$r_{a_1} = \eta_1 k_a c_1 (1 - \theta_1 - \theta_2) \qquad \text{Equation A1}$$

(Assuming γ as total adsorption in the adsorbent for a given component)

And the rate of desorption can be written as

$$r_{d_1} = k_d (\theta_1) \qquad \text{Equation A2}$$

This at equilibrium becomes

$$\eta_1 b_1 c_1 (1 - \theta_1 - \theta_2) = (\theta_1) \textbf{ component 1} \qquad \text{Equation A 3}$$

$$\eta_2 b_2 c_2 (1 - \theta_1 - \theta_2) = (\theta_2) \text{ component 2} \qquad \text{Equation A 4}$$

(where $b = k_a/k_d$)

On further solving the above two equations simultaneously the modified Butler and Ockrent model is obtained.

Appendix B

Additional results of multicomponent adsorption system

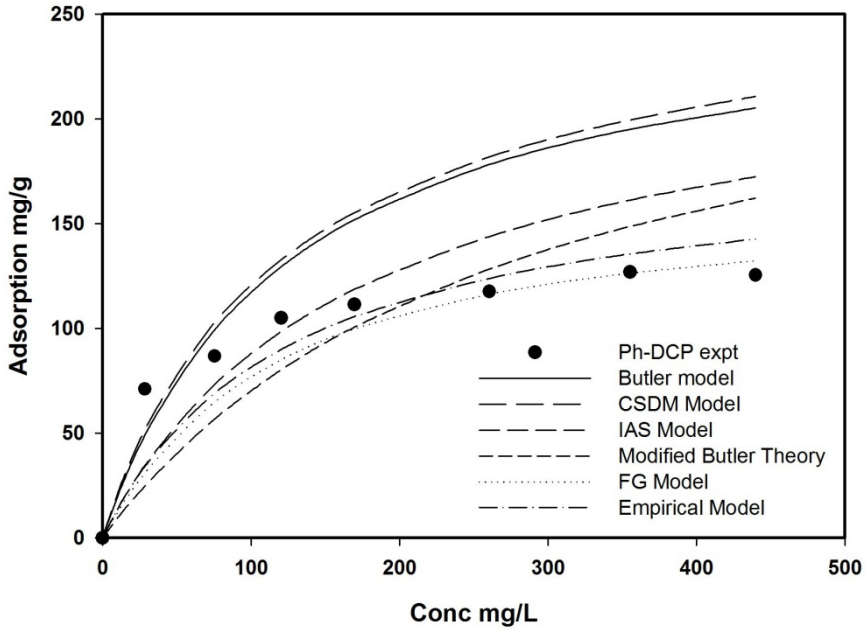

S1: Modeling of adsorption of Phenol in presence of DCP following the experimental test scheme 1

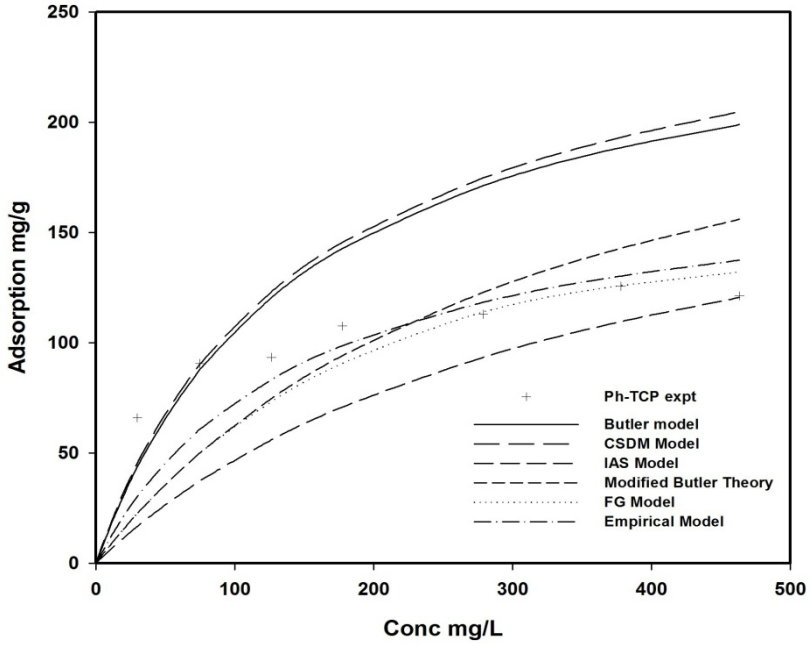

S2: Modeling of adsorption of Phenol in presence of TCP following the experimental test scheme 1

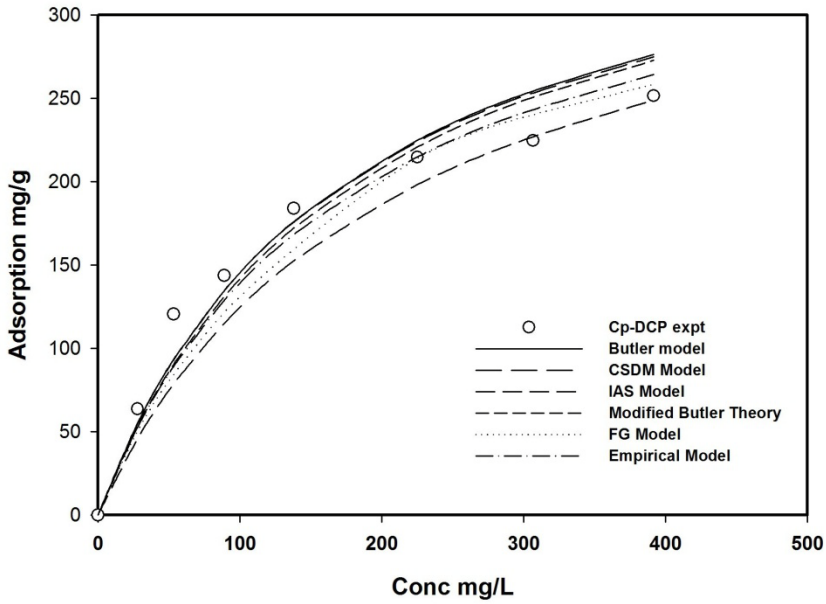

S3: Modeling of adsorption of CP in presence of DCP following the experimental test scheme 1

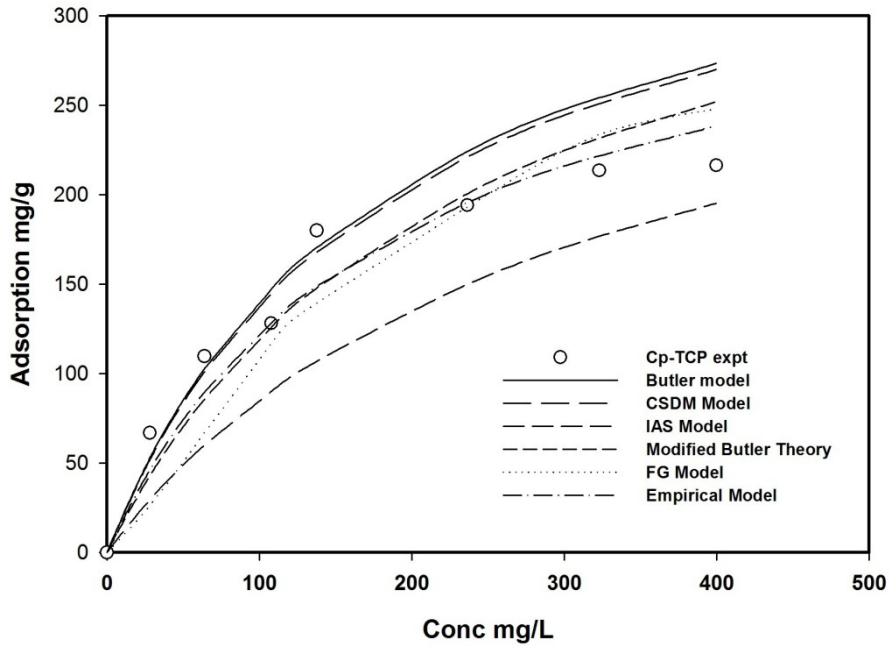

S4: Modeling of adsorption of CP in presence of TCP following the experimental test scheme 1